Depositional environment of the Upper Cretaceous oil shales in the Negev Desert, Israel: Geochemical constraints based on trace elements and stable isotopes

Zur Erlangung des akademischen Grades eines
Doktors *der* Naturwissenschaften
(*Dr. rer. nat.*)

von der
Fakultät für Bauingenieur-, Geo- und Umweltwissenschaften
des Karlsruher Instituts für Technologie (KIT)

genehmigte

DISSERTATION

von

Diplom Geologe Peter Illner

Tag der mündlichen Prüfung:	16.07.2014
Referent:	Prof. Dr. T. Neumann
Korreferent:	Prof. Dr. W. Püttmann
Karlsruhe	Juni 2014

Erklärung über die Erstellung der Dissertation

Hiermit erkläre ich, dass ich die vorliegende Dissertation selbstständig verfasst, keine anderen als die angegebenen Quellen und Hilfsmittel benutzt, alle wörtlichen und sinngemäßen Entlehnungen deutlich als solche gekennzeichnet und die Grundsätze des Karlsruher Instituts für Technologie (ehemals Universität Karlsruhe TH) zur Sicherung guter wissenschaftlicher Praxis in ihrer aktuell gültigen Fassung beachtet habe.

Karlsruhe im Juni 2014

Für Dina

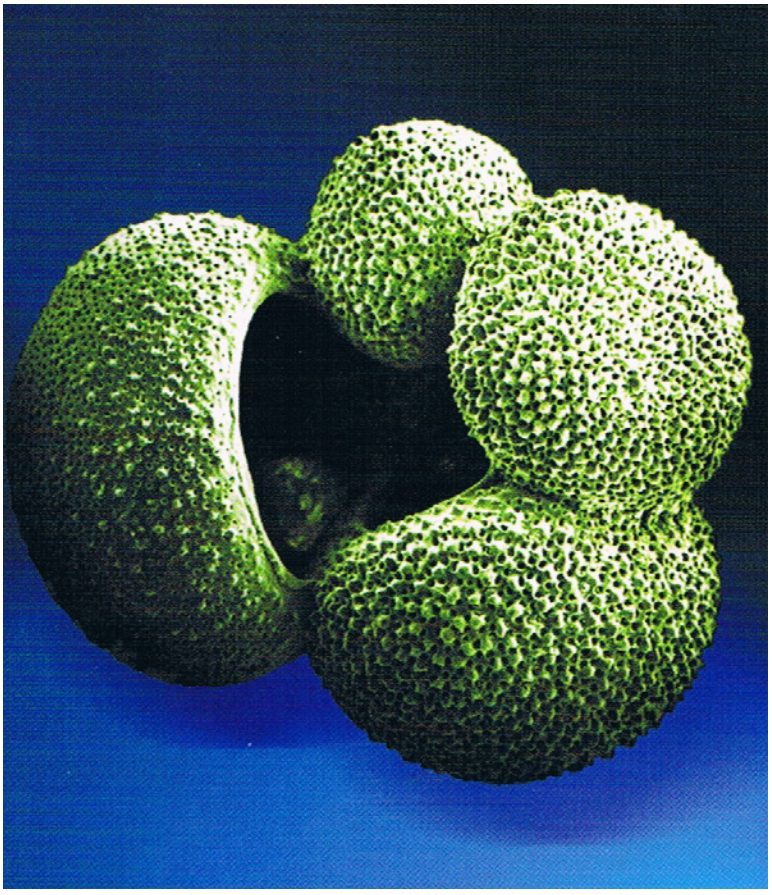

Scanning electronic microscope image of marine calcifying organisms. The foraminifer Globigerina bulloides (diameter 400 micro meter).

Depositional environment of the Upper Cretaceous oil shales in the Negev Desert, Israel: Geochemical constraints based on trace elements and stabile isotopes

Zur Erlangung des akademischen Grades eines
Doktors *der* Naturwissenschaften
(*Dr. rer. nat.*)

von der
Fakultät für Bauingenieur-, Geo- und Umweltwissenschaften
des Karlsruher Instituts für Technologie (KIT)

eingereichte

DISSERTATION

von

Diplom Geologe Peter Illner

Tag der mündlichen Prüfung:	16.07.2014
Referent:	Prof. Dr. T. Neumann
Korreferent:	Prof. Dr. W. Püttmann
Karlsruhe	Juni 2014

Erklärung über die Erstellung der Dissertation

Hiermit erkläre ich, dass ich die vorliegende Dissertation selbstständig verfasst, keine anderen als die angegebenen Quellen und Hilfsmittel benutzt, alle wörtlichen und sinngemäßen Entlehnungen deutlich als solche gekennzeichnet und die Grundsätze des Karlsruher Instituts für Technologie (ehemals Universität Karlsruhe TH) zur Sicherung guter wissenschaftlicher Praxis in ihrer aktuell gültigen Fassung beachtet habe.

Karlsruhe im Juni 2014

Für Dina

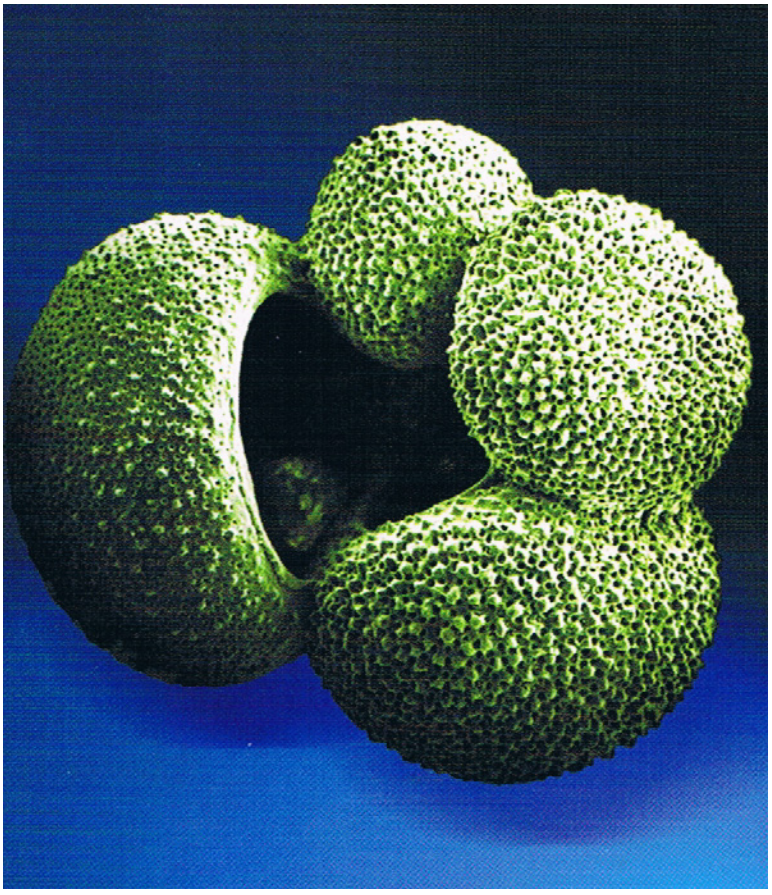

Scanning electronic microscope image of marine calcifying organisms. The foraminifer Globigerina bulloides (diameter 400 micro meter).

Kurzfassung

Die vorliegende Dissertation ist Teil eines bi-nationalen Gemeinschaftsprojektes. Beteiligte Projektpartner waren die Ben-Gurion Universität Beer Sheeba (Mikropaläontologie), die Johann Wolfgang von Goethe Universität Frankfurt (Organische Geochemie) sowie das Institut für Mineralogie und Geochemie des KIT.

Im Mittelpunkt der Arbeit standen Ölschieferablagerungen in der Negev Wüste in Israel. Sogenannte Schwarzschiefer (black shales)- oder Ölschiefer (oil shales) sind seit mehr als 50 Jahren von großem wissenschaftlichem Interesse. In der Hauptsache bestehen Schwarzschiefer aus Siliziklastika und sind zum großen Teil in siliziklastisch dominierten und unter eisen nicht limitierten Umweltbedingungen entstanden. Im Gegensatz dazu zeichnen sich Ölschiefer durch einen höhreren Anteil an organischem Kohlenstoff und Schwefel aus und bilden sich vorwiegend in karbonatreich- und eisenlimitierten Ablagerungsräumen. Der hohe Anteil von organischem Kohlenstoff verbunden mit Konzentrationen an Spurenelementen und die spezifische Zusammensetzung der Organik machen diese Sedimente attraktiv für anorganisch – organisch geochemische Fragestellungen.

Auch hinsichtlich einer möglichen kommerziellen Nutzung zur Gewinnung von fossilen Brennstoffen rücken diese Ablagerungen immer mehr in den Fokus von Wirtschaft und Wissenschaft. Für die nahe Zukunft wird prognostiziert, dass sowohl Schwarz- als auch Ölschiefer als unkonventionelle Ressourcen eine wichtige Energiequelle darstellen können. Öl- und Schwarzschiefer haben sich im Verlauf der Erdgeschichte in einer großen Vielfalt in verschiedenen Sedimentationsräumen gebildet. Insbesondere in Küstengebieten, welche von küstenparallelen Winden und dem Auftrieb von kaltem, sauerstoff- und nährstoffreichem Tiefenwasser beeinflusst sind, kann es unter bestimmten Voraussetzungen zur Bildung dieser organikreichen Sedimenten kommen.

Dies geschah zum Beispiel vor ca. 20 Mio. Jahren am Südrand der Tethys, wo organikreiche Karbonate als Folge eines hochproduktiven Auftriebssystems kombiniert mit geringem terrigenem Eintrag entstanden

sind. Im Untersuchungsgebiet dieser Arbeit, in Israel, wurden diese Sedimente als Ölschiefer abgelagert und weisen eine charakteristische Wechselfolge von Chert, organikreichen Karbonaten und Phosphoriten (Si - C - P- Sedimente) auf. Diese Schichten werden als Ghareb Formation bezeichnet und liegen, mit einer Mächtigkeit von ca. 40 m, in der südlichen Negev Wüste. Die Ghareb Formation markiert einen wichtigen Abschnitt in der Oberkreide. So wird anhand von mikropaläontologischen Untersuchungen, der israelischen Kollegen geschlussfolgert, dass sich mit dem Übergang vom Campan zum Maastricht ein signifikanter Wechsel in der Dynamik des oberkretazischen *upwelling-systems* vollzogen haben könnte.

Das wichtigste Ziel des Gesamtprojektes bestand darin, ein tieferes Verständnis für die komplexen Wechselwirkungen von Salinität, Primärproduktion, Anoxia und der natürlichen Sulfurisierung organischer Materie in den untersuchten Sedimenten zu erhalten und dadurch neue Einblicke in die Entstehung der hoch-organikreichen Ablagerungen am Übergang Campan-Maastricht zu erhalten. Dazu wurde in den einzelnen Teilprojekten eine umfassende biostratigraphische und organisch bzw. anorganisch-geochemische Charakterisierung dieser israelischen Ölschiefer-Serie der Negev Wüste durchgeführt.

Der Fokus der vorliegenden Dissertation lag dabei auf der Analyse der Haupt- und Spurenelemente sowie der Schwefelisotopie der Sedimente und der Spurenelementzusammensetzung der im Sediment eingeschlossenen Foraminiferen. Ziel war es, basierend auf diesen Untersuchungen und mit Hilfe von daraus abgeleiteten anorganisch-geochemischen Proxies das Ablagerungsmilieu der Sedimente zu rekonstruieren und in Übereinstimmung mit der biostratigraphischen Einteilung zu bringen. Zusätzlich sollte gezeigt werden, wie sich mit Hilfe geochemischer Methoden auch geringe Veränderungen im Sauerstoffgehalt, in der Produktivität des Auftriebsgebietes und im terrigenen Eintrag nachweisen lassen. Dazu wurden die geochemischen Ergebnisse mit Hilfe einer multivariaten statistischen Analyse mit den biostratigraphischen Resultaten des israelischen Projektpartners kombiniert. Durch diese Verknüpfung sollte ein neues Ablagerungsmodell der geochemischen Evolution des Sedimentationsraumes entwickelt werden. Dies umfasst insbesondere eine neue Interpretation hinsichtlich der Erhaltung der Organik, der

Wassermassenzirkulation, der Herkunft des Sedimentmaterials sowie der Änderungen des Meeresspiegels und der Redoxbedingungen.

Als geochemische Proxies wurden das Nickel/Vanadium Verhältnis, der Urangehalt, die Eisen-Schwefel-Kohlenstoff-Systematik sowie die Schwefelisotopie des Sulfats, Sulfids und des organischen Schwefels angewendet. Außerdem wurde der Spurenelementgehalt in benthischen wie auch planktischen Foraminiferen bestimmt. So gestattet die Bestimmung von Spurenelementen in den Foraminiferen-schalen, Rückschlüsse auf die Änderung der Umweltbedingungen am Übergang Campan- Maastricht. Mit Hilfe der δ^{34}S-Isotopie ist es möglich zwischen oxidierenden- und reduzierenden Bedingungen zum Zeitpunkt der Frühdiagenese zu unterscheiden, sowie den Einfluss der Spätdiagenese auf das Sediment zu beschreiben. Die Anwendung einer Multi-Proxy-Analyse in Kombination mit multivariater Statistik erlaubt es, den Einfluss der Spätdiagenese auf die Zusammensetzung der Spurenelemente im Sediment wie auch auf die Schalen von Foraminiferen zu erfassen.

Die Kombination aus sedimentologischen, biostratigraphischen sowie anorganisch-organisch geochemischen Untersuchungen wurde an einem Profil in einem Steinbruch in Mishor Rotem in der südlichen Negev (31°04’51.82"N; 35°10’02.85"E) vorgenommen. Dieser Aufschluss ist Teil eines der größten Ölschiefervorkommen in der Negev Wüste. Hauptkriterien für die Auswahl des Profils waren die geringe thermischen Reife des Sedimentes sowie die hervorragende Erhaltung der Foraminiferen. Insgesamt wurden 266 Proben in einem Intervall von 10 - 20 cm auf einer Profillänge von ca. 50 m genommen. Die Probenentnahme vor Ort wurde von den israelischen Kollegen durchgeführt.

An der Basis des Profils befindet sich eine 5 m mächtige Phosphorit-Lage (Mishash-Formation). Die darauf folgenden 42 m geben einen vollständigen Überblick über die Ölschiefer der Ghareb Formation. Die hangenden Mergel der Ghareb Formation (3 m) schließen das Profil nach oben hin ab. Da der Schwerpunkt der Dissertation auf den Ölschiefer lag, wurden hier die meisten Proben (n=218) entnommen. Von den Phosphorite wurden 24 und von den Mergeln 18 Proben genommen. Die Geochemie wurde mittels ED-XRF an allen Proben bestimmt. Weitere Parameter wie

Hauptelementzusammensetzung (WD-XRF), Gesamtschwefel (CSA), Schwefelisotope (IR-MS), Dithionat lösliches Eisen (ICP-OES) und Mineralogie (XRD) der Sedimente sowie die Analyse der Spurenelemente in den Foraminiferenschalen (ICP-MS) wurden an 39 ausgewählten Proben charakterisiert.

Die Hauptbestandteile der Ölschiefer sind Kalzit, Quarz, Opal, organischer Kohlenstoff (Kerogen) und Tonmineralien (Kaolinit, Illit, Montmorillonit). Als Nebenbestandteile sind vorwiegend Dolomit, Gips/Anhydrit, Muskovit, Feldspat, Apatit und Goethit anzutreffen. Ein markantes Merkmal ist der für Ölschiefer außergewöhnlich niedrige Gehalt an Pyrit von ca. 1 Gew-%. Die bevorzugte Anreicherung von Kupfer, Nickel, Zink, Chrom aber auch Arsen und die gleichzeitige Korrelation zu Schwefel und organischen Kohlenstoff (C_{org}) im Sedimentprofil zeigt an, dass die unteren Lagen der Ölschiefer in einem reduzierenden Milieu entstanden sind. Durch ihre abnehmende Konzentration, sowie die abnehmende Korrelation zu Schwefel und C_{org} und gleichzeitigem Anstieg in der Elementkonzentration an Silizium, Eisen- und Aluminium , grenzen sich die hangenden Einheiten der Ölschiefer durch eine zunehmend offenere und sauerstoffreichere Umgebung ab.

Dieses Ergebnis wird durch die Anwendung der Faktoranalyse bestätigt, welche die Haupt- und Spurenelementkonzentrationen des Gesamtsedimentes umfasste. Als Ergebnis wurde ein Zweifaktorenmodell erstellt, welches 84% der Gesamtvarianz des Datensatzes für die Ölschiefer erklärt. Die Kombination aus chalcophilen Elementen und deren Korrelation zum Schwefel und C_{org}, wird als Faktor interpretiert, der den Grad der Sauerstoffverfügbarkeit im Sediment anzeigt. Der andere Faktor, welcher identifiziert wurde, zeigt gegensinnige Faktorenladungen zwischen den Elementen Calcium und Silizium, Aluminium und Eisen und wurde als gegenseitige Wechselwirkung zwischen terrigenem Eintrag und biogener Karbonatproduktion (Foraminiferen) interpretiert.

Des Weiteren können basierend auf den multivariaten statistischen Auswertungen Paläoindikatoren definiert werden, mit deren Hilfe Veränderungen in Bezug auf Änderungen in der Wassermassenzirkulation im Ablagerungsraum beschrieben werden können. Ein Beispiel hierfür ist die

Anwendung des rsMo/TOC[1] Verhältnisses als Proxy für die Zirkulation der Wassermassen. Unter der Voraussetzung, dass die Molybdän-Konzentration im Sediment von der Konzentration an gelöstem Molybdän im Meerwasser und der Menge an Organik im Sediment abhängt, existiert unter hoch reduzierenden/sulfidischen Verhältnissen eine positive Korrelation des Molybdäns mit dem organischen Kohlenstoff. Eine Änderung im Anstieg der Korrelationsgeraden beim Übergang von der Mishash-Formation (rsMo/TOC = 8) zur Ghareb Formation (rsMo/TOC ~ 1) stützt die Annahme, dass der passive Kontinentalrand in eine Becken- und Schwellenfazies untergliedert war. Diese Interpretation wird durch die ermittelte Änderung in der benthischen wie auch planktischen Faunenvergesellschaftung des israelischen Projektpartners bestätigt. Diese zeigen ebenfalls an, dass der Übergang von den Phosphoriten zu den Ölschiefern mit einem grundlegenden Wechsel in der Wasserzirkulation verbunden war.

Die δ^{34}S-Muster des Pyrit- Schwefels im Sedimentprofil können ebenfalls für einen Nachweis der Wassermassenzirkulation benutzt werden. Die Ergebnisse zeigen ungewöhnlich schwere δ^{34}S-Werte zwischen -24‰ und -16‰ an der Basis der Ölschiefer. Diese relativ schwere Schwefelisotopie des Pyrits kann sich bei sehr geringer Wasserzirkulation in der oberen Wassersäule bei gleichzeitig extrem geringem terrigenem Eintrag bilden. Ein rezentes Beispiel hierfür ist der Framvaren Fjord in Norwegen, aus dem ebenfalls schwere syngenetische Schwefelisotope des Pyrits in der oberen Wassersäule beschrieben worden sind (Sælen et al., 1993). Im Gegensatz dazu weisen die oberen Ölschieferschichten des in dieser Arbeit untersuchten Profils mit -42‰ bis -30‰ eine vergleichsweise leichte δ^{34}S-Signatur in Form von syngenetischem Pyrit auf. Die Ergebnisse werden dahingehend interpretiert, dass die oberen Ölschiefer in einem sauerstoffreicheren, offenen System und unter Eisen- wie auch Sulfat-reichen Bedingungen abgelagert wurden.

Weiterhin lassen sich organometallische Komplexe als Paläoindikator für die Charakterisierung des Ablagerungsraumes nutzen. Das geochemische Milieu für die Bildung organometallischer Komplexe hängt sowohl vom Eh- als auch vom pH-Wert sowie der Rate an bakterieller Sulfatreduktion ab. In

[1] rs = Anstieg der Korrelationsgerade (regression slope)

Rohölen wie auch Öl- und Schwarzschiefern sind vor allem Nickel und Vanadium in organometallischen Komplexen gebunden (Porphyrine, Vanabine). Aus diesem Grund lässt sich das Ni/V-Verhältnis als Paläoindikator nutzen. So wird ein niedriges Ni/V-Verhältnis als bevorzugter Einbau von Vanadium (Porphyrin) über Nickel in Kerogen sowie Algen als marine Quelle für die Nährstoffmineralisation in der Wassersäule interpretiert. Die Ni/V-Verhältnisse dieser Arbeit deuten darauf hin, dass die Erhaltung des Porphyrins bevorzugt auf den hangenden Part der Ölschiefer beschränkt ist. Der Übergang von den liegenden Ölschiefern (hohes Ni/V) zum Hangenden kann als signifikanter Wechsel von einem salinar dominierten Ablagerungsmilieu zu einem marin (Karbonat) dominiertem Sedimentationsregime (niedriges Ni/V) interpretiert werden. Damit werden die Interpretationen der Frankfurter Arbeitsgruppe bestätigt, welche die Anwesenheit von (thiolane(3-methyl-5-(3,7,11-trimethyldodecyl)-thiolane) als Indikator für ein salinares Ablagerungsmilieu interpretiert haben (mdl. Mttlg. Wilhelm Püttmann, 2010).

Änderungen im Verhältnis von relativ immobilen Elementen die an verwitterungsresistente Schwermineralien gebunden sind, wie Titan und Zirkon, ermöglichen Aussagen über den Reifegrad des abgelagerten Materials. Die Verteilung des Zr-Ti-Al_2O_3-Verhältnisses im Sedimentprofil zeigt an, dass sich im Ablagerungszeitraum die Zusammensetzung der angelieferten Sedimente allmählich geändert hat. An der Basis dominiert die klastische, schwermineralreiche Komponente wohingegen zum Top hin eine Verschiebung zu einem tonreicheren Material stattfand.

Spätdiagenese im Sediment ist ein wichtiger Aspekt der bei der Diskussion der geochemischen Ergebnisse keinesfalls vernachlässigt werden darf. Solche Prozesse verändern die Sedimentzusammensetzung nach der Ablagerung und führen zu einer signifikanten Verfälschung und letztendlich zur Auslöschung primärer Umweltsignale. Diese Art von Veränderungen können beispielsweise durch die Analyse des $\delta^{34}S_{Sulfat}$ sowie der $\delta^{18}O$-Werte in benthischen und planktischen Foraminiferenschalen erfasst werden. Es konnte mehrfach gezeigt werden, dass die $\delta^{34}S_{sulfat}$-Werte zeitlichen Schwankungen unterliegen. Für die Oberkreide wird ein $\delta^{34}S_{sulfat}$ -Referenzwert von ~ 17‰ angenommen (Claypool et al., 1980; Strauss, 1997). Im Gegensatz dazu sind die $\delta^{34}S_{sulfat}$-Signale in den Sedimenten der Ghareb Formation

ungewöhnlich leicht mit Werten von -20‰ bis -3‰. Diese Signale spiegeln somit nicht die ursprüngliche Meerwasserzusammensetzung der Oberkreide hinsichtlich $\delta^{34}S_{sulfat}$ wider. Stattdessen konnte zum ersten Mal gezeigt werden, dass die leichten $\delta^{34}S_{sulfat}$-Signale einem Mischsignal aus der Oxidation des Pyrits im Sediment und dem des Sulfats des ursprünglichen Meerwasserwertes entsprechen. Die Ursache für die Verfälschung ist in der Penetration des Profils mit meteorischem Wasser zu suchen.

Die $\delta^{18}O$-Werte in benthischen- und planktischen Foraminiferen unterstützen diese Schlussfolgerungen. Die Werte schwanken zwischen -7‰ und -3‰ und sind damit deutlich leichter als vergleichbare $\delta^{18}O$-Werte in der Oberkreide (-2,5 bis -1‰) (Friedrich, 2005). Aufgrund der starken Veränderung des Isotopensignals, kann dieses nicht mehr als Indikator für Paläotemperaturen verwendet werden. Ein $\delta^{18}O$-Werte von ~ -10‰ ist typisch für rezente meteorische Wässer in niederen Breitengraden aber vermutlich auch in der Oberkreide. Daher kann angenommen werden, dass eine Penetration von meteorischen Wässern zu einer gleichmäßigen Veränderung des Isotopensignals geführt hat (Faure and Mensing, 2005; Amiot et al., 2004).

Mit der Bestimmung der Mg/Ca- und Sr/Ca- Verhältnisse in benthischen wie auch planktischen Foraminiferenschalen können Rückschlüsse über die Paläo-Wassertemperatur sowie über die Schwankungen des Meerwasserspiegels gezogen werden. So zeigen die in dieser Arbeit bestimmten Mg/Ca-Verhältnisse der benthischen wie auch der planktischen Foraminiferen einen Temperaturunterschied zwischen Boden- und Oberflächenwasser von ca. 4°C an. Das Sr/Ca- Verhältnis in benthischen Foraminiferen zeigt ähnliche Schwankungen wie die Meeresspiegelkurve zur Zeit des Übergangs am Campan- Maastricht (Haq, 2014).

Zusammenfassend lässt sich sagen, dass auf Basis des geochemischen Multiparameteransatzes und der statistischen multivariaten Analyse Paläoindikatoren ermittelt werden konnten. Mit deren Hilfe können die Umweltbedingungen am Übergang vom Campan zum Maastricht rekonstruiert werden. Daraus ergibt sich ein neues konzeptionelles Ablagerungsmodell, welches den Unterschied im Gehalt an organischer Materie und die Spurenelementvariabilität erklären kann. Wichtige Parameter sind dabei das Zusammenwirken

von Meeresspiegelanstieg, extrem geringem sedimentären Eintrag sowie der Rückgang in der Wassermassenzirkulation bei gleichzeitiger Erhöhung der Primärproduktion durch Remobilisierung von Phosphor aus den liegenden Phosphoriten. Die Summe aller Faktoren führte zur Ablagerung der organikreichen Karbonate an der Basis der Ölschiefer. Die einsetzende Sulfurisierung (Vulkanisierung) der Organik erklärt die außerordentlich gute Konservierung des hohen organischen Kohlenstoffgehaltes. Die beginnende Regression verursacht eine Erhöhung des Sauerstoffgehaltes in der Wassersäule infolge des Rückzugs der *Oxygen-Minimum-Zone* (OMZ). Daraus resultiert eine abrupte Abnahme im organischen Kohlenstoffgehalt und die Rückkehr der benthischen wie auch der planktischen Foraminiferen. Am Meeresboden bildeten sich periodisch sauerstoffreiche Bedingungen aus an die sich das benthische Leben anpassen konnte. Die Rückkehr gekielter Foraminiferen bei 33 mbsf, welche als Paläoindikator für sauerstoffreiches Oberflächenwasser benutzt werden, unterstützt diese These.

Als Ursache für die unterschiedlichen geochemischen Milieus während der Sedimentation des Ölschiefers zur Zeit des Campan-Maastrichts kann das Ablaufen eines kompletten Transgressions- und Regressionszyklus angeführt werden. Der Übergang von den unteren Ölschiefern zu den hangenden Einheiten (33 mbsf) zeigt eine komplette Neuausrichtung des Paläoumfeldes an. Dies ist verbunden mit Änderungen der Sedimentationsrate, der Sedimentzusammensetzung, des $\delta^{34}S_{pyrit}$, des C_{org}-Gehaltes, des Sulfurisierungsgrades und der Rückkehr der benthischen und planktischen Foraminiferen. Eine erneute Trangression am Übergang zu den hangenden Mergeln führte schließlich zur Überflutung und zur Entstehung offen mariner Verhältnisse.

.

Abstract

A binational team of palaeontologists (Ben-Gurion University, Beer Sheva, Israel), organic geochemists (Johann- Wolfgang v. Goethe University, Frankfurt, Germany) and professionals in inorganic geochemistry (Institute of Mineralogy and Geochemistry, KIT, Germany), has conducted a series of analyses to reveal new insights into the palaeontology, palaeoclimate and geochemistry of the Upper Cretaceous along the southern coast of the Tethyan Ocean.

Since more than a decade, organic rich deposits, commonly known as black shale, oil shale, and sapropelite, have inspired scientists around the world. The factors, which caused such accumulations are not only of commercial interest, but also specifically for related topics in palaeoclimate, such as oil shales (OS), formed throughout the Earth´s history in a wide variety of marine, lacustrine, and continental environments. In nearshore marine settings, the deposition of organic rich sediments is related to a massive increase in primary production because of the wind-driven upwelling of nutrient-rich water towards the ocean surface.

Organic rich deposits during a time span of more than 20 Ma in the Upper Cretaceous are part of a major upwelling system at the former southern coast of the Tethyan Ocean. In Israel, the Late Cretaceous organic rich carbonates, locally termed as “oil shales,” cover a patchy area and are mostly associated with silica (chert) - phosphorite and anomalously high substances of organic matter (Si-P-C). In the southern Negev, Israel, the accumulation of a 40 m thick oil shale sequence during the latest Campanian marks a major change in the dynamics of the Late Cretaceous southern Tethys upwelling system (Ashckenazi-Polivoda et al., 2011).

The part of the Institute of Mineralogy and Geochemistry, Karlsruhe, within the binational project, was to focus on analyses on the inorganic geochemistry of these samples, with the goal to achieve a high-resolution general lithogeochemical characterisation of the section.

In the course of the thesis, it is shown how subtle changes in bottom-water aeration, surface water productivity, and terrigeneous vs. bioclastic input, are reflected in the geochemistry and foraminiferal assemblages of the sediments. Lastly, the results were merged into a new conceptual geochemical model about the evolution of the high organic carbonates along the Southern Tethyan coast.

To achieve this, we combined high-resolution sedimentological, biostratigraphical and inorganic geochemical analyses on a profile of one of the largest oil shale reservoirs in southern Israel. The reservoir is located in an open quarry (Mishor Rotem) in the central Negev desert and represents the transition from the Mishash formation (Campanian) to the Ghareb Formation (Maastrichtian). For a better understanding of the palaeoenvironmental changes on a profile, extracted samples were split for inorganic, organic and biostratigraphical analyses.

The quarry was originally considered representative because the sampled material and foraminiferal assemblages were fresh and unaltered, with a low thermal maturity and well-preserved fossils (Ashckenazi-Polivoda et al., 2011). About 250 samples were taken in 10 and 20 cm intervals from a 50 m sequence which includes the upper part of the Phosphate Member (PM) of the Mishash formation, as well as the complete Oil Shale Member (OSM), and the base of the Marl Member (MM) of the Ghareb formation. The chemical composition of selected bulk sediment samples and of foraminifera tests were analysed by means of different high resolution techniques (ED-, WD- XRF, ICP-MS, ICP- OES, HR-ICP-MS). Results obtained by means of ED- and WD-XRF were used for multivariate statistical analyses. This method groups related variables, and thus geochemically coherent groups, into a limited number of factors that account for a substantial proportion of the variance of the data.

Principal component analysis of major and trace elements concentrations of the studied sequence allows distinguishing between two factors. The two-factor model explains 84% of the variance contained in the initial data set, with high factor loadings. Based on the geochemical characteristics of the parameters, the factors have been interpreted to represent the degree of water oxygenation (Factor 1) and the input of the bioclastic versus terrigeneous detrital components into the sediment (Factor 2). The Israeli co-partner used

similar statistical techniques that are based on the vertical distribution pattern of foraminiferal assemblages. Statistical results defining a high-resolution palaeoenvironmental scheme, which summarise five planktic (P-Type) and benthic (B-Type) foraminiferal assemblages. Due to productivity reasons of surface water and favourable bottom-water aeration, those assemblages flourished effectively.

In order to disclose the environmental factors, which controlled the deposition of the oil shales of the Ghareb fm., the chemostratigraphic data evaluated by means of factor analysis and the resulted factor scores were matched with the biostratigraphic interpretation prepared by the Israeli co-partner. Summating all notions, it seems like the statistical analysis of micropalaeontology and inorganic composition of the sediments lead to an identical conclusion about the palaeoenvironment. This will be briefly shown below.

The pattern, which occurred in the bulk inorganic sediment chemistry and organic carbon, coincides with gradual upward changes, in benthic and planktic foraminiferal community, within the profile. This is in accordance to the Israeli project partner, their results implying a gradual shift from eutrophic to mesotrophic and strong anoxic to dysoxic conditions (Ashckenazi-Polivoda et al., 2011). This, in return, corresponds with own results, implying a gradual shift from calcareous, bioclastic sedimentation in a strong anoxic environment, towards the top of the oil shale profile to more aerated conditions and simultaneously to more detrital input. A more detailed discussion about the indication of factors that show how the palaeoenvironment has been changed is given by the application of several inorganic proxies.

All results from the high-resolution inorganic geochemistry reveal that the oil shale deposits show a division into two different geochemical main units, which is termed as Lower Oil Shale unit at the base and the overlying Upper Oil Shale unit. The cross plot between uranium and phosphor gave some insights into the geochemical history of these two parts. In terms of differences in the redox potential, both the units Lower Oil Shale (LOS I, II) and Upper Oil Shale horizon differ significantly, thus concluding that LOS were deposited under highly anoxic/sulphidic conditions at the sediment/water interface. In the contrary, regarding the oxygen content in the sediment, the Upper Oil Shale unit displayed upward oscillating conditions. This might be caused due to a bioturbated sedimentation regime with periods of a

higher oxygen concentration in the pore water. Further conclusions about the seawater chemistry are given by using a cross plot between the bulk sediment concentration of Mo and the amount of total organic carbon (TOC).

The molybdenum concentration in the sediment depends on the concentration of dissolved Mo in the seawater itself and the level of organic carbon in the sediment (Algeo and Lyons, 2006). In times of highly reducing/euxinic conditions molybdenum correlates well with the organic carbon concentration in the sediment. A calculation of the $rsMo/C_{org}$ ratio therefore leads directly to the Mo concentration in seawater. Deviations in the regression slope (rs) can be used to reveal information about the bottom water renewal time (τ_{DW}). There is a low concentration of dissolved Mo as a result of limited water circulation. Hence, the application of this proxy yields a $rsMo/C_{org} \sim 8$ for the PM, whereas for the OSM only a $rsMo/C_{org} \sim 1$ exist. This is interpreted in terms of a drastic change in the deepwater renewal time at the Campanian-Maastrichtian transition. Micropalaeontological results from the Israeli partner support the above mentioned notion, and reveal a drastic change in the foraminiferal assemblage composition, which is further interpreted in terms of a massive change in the water mass circulation along the former Tethyan coast.

Similar results from the pyrite sulphur isotopy support this, not merely the results from chemical determination of bond sulphur tell, that at the base of the OSM more than 90% of sulphur is bond onto to organic matter. Subsequently, based on wet chemical analysis and sulphur isotopy, a shift from a more sulphate-limiting system at the base of the OSM to more aerated conditions towards the top of the profile can be seen. This is in strong accordance to sulphur isotope signatures ($\delta^{34}S_{sulphide}$), which show extremely heavy values at the base to lighter and more strongly fractionated values at the top of the profile. Such super-heavy $\delta^{34}S_{sulphide}$ values from -16‰ to -24‰ were interpreted as a result of a massive reduction in the water mass circulation at the base of the OSM (Sælen et al., 1993). Another possible explanation for the above mentioned notions arises from an installation of a chemocline close to the bottom, which is sufficient to prevent a thermal water mass stratification. Furthermore, this perhaps signifies a formation of

syngenetic pyrites formed in the upper water column ore above the sediment/water interface. Unlike the Lower Oil Shale, the Upper Oil Shale horizon was influenced by more aerated conditions due to a retreat of the Oxygen-Minimum-Zone (OMZ) from the inner passive continental margin, thus allowing bioturbation at the sediment/water interface. These findings are corroborated due to a light isotopic sulphide composition from -30‰ to -42‰ and a higher degree in fractionation (33‰ to 60‰). This corresponds with the rsMo/C_{org}, and micropalaeontogical results by the Israeli partner. Their outcomes imply a re-occurrence of the benthic and planktic foraminifera assemblage composition at the transition from the LOS toward the Upper Oil Shale unit.

In order to identify in which marine settings the deposition of organic rich sediments took place, a well-established proxy for determining the source of marine organic matter is given by the application of the Ni/V relationship. Own results show a Ni/V ratio of < 0.5 in the Lower Oil Shale, due to the preferred incorporation of vanadium into the porphyrin, instead of nickel. On the contrary, a higher Ni/V ratio of > 1 is observed in the Upper Oil Shale horizon, which might be explained by the low input and preservation of porphyrin in to an environment that changes from a saline (non-marine?) to marine carbonate (non-siliciclastic) environment. Furthermore, based on the results, it was concluded that a gradual shift from a restricted water circulation to a more open marine condition towards the deposition of the MM took place. The German partner from the University Frankfurt, probably support the above mentioned notions due to the detection of several sulphur containing compounds (thiolane(3-methyl-5-(3,7,11-trimethyldodecyl)-thiolane), which belong to the aromatic hydrocarbon fraction. These results may suggest a deposition of hydrocarbons in sediments, which were deposited under hyper-saline and euxinic conditions (pers. com. Wilhelm Püttmann, 2010).

In pursuit of the project, a main goal was to answer the question whether the sedimentary input has changed significantly. The transition from the underlying PM to the LOS reveals a distinctive change in the sediment composition. The results obtained by applying a ternary diagram (Zr – Ti – Al_2O_3) indicate a change in the transport mode and point to a gradual change in the sedimentary composition of the

delivered material. During the transition from the LOS, being a clastic component, a gradual change to sediments containing more clay mineral is observed from base to top of the profile. Such distinct changes might be explained due to sea-level changes which is shown by Haq (2014). Consequently, a change in the sea level leads to a complete reorganisation in the transport route/length and delivery method of the deposited sediments.

The preservation of the foraminiferal assemblage can also be used to reveal a late diagenetic statement. This can be shown exemplary by the analysis of the $^{18}O/^{16}O$ ratios from benthic and planktic foraminifera, obtained by our Israeli partner, which show light $\delta^{18}O$-values of about ~ -7‰. In addition, the analysis of sulphur isotopes reveal isotopic light values of $^{34}S_{sulphate,}$ interpreted as a massive penetration of meteoric water which has led to an oxidation of pyrite and light $\delta^{34}S_{sulphate}$ values between -3‰ and -20‰. Therefore, both results support the theory, that the profile is affected by weathering processes that significantly alter the original chemical composition of the deposited sediment and enclosed foraminifer's shells.

Due to their occurrence on the seabed as well as in the water column, both benthic as well as planktic foraminifera are excellent markers for changes in palaeo-seawater chemistry. An analysis was performed, to acquire new insights into the palaeoxygenation of the environment. For this purpose, a cleaning procedure was used, which is based on previous works of Boyle (1981), Boyle and Keigwin (1985), Elderfield et al. (1996), Hastings et al. (1996) and has been refined by Meudt (2004). Some elements, such as Mo, As, and U, are enriched in organic-rich anoxic waters and should be a signal for an enrichment of redox-sensitive elements in the respective tests. Typically in times of high productivity (high biomass production), which are expressed by depletion of micronutrient (Ni, Cu, Zn, Cd) in seawater, lower minor elements concentrations in foraminifer's shells occurs. The interpretation of these results reveals that both benthic and planktic foraminifera match the pore water milieu and cannot be used for interpretations in the palaeoenvironment.

Acknowledgments

This thesis could not have been finished without the knowledge, generous help, and skills of many people who helped me during this period of my life. The following lines are dedicated to those people as a way to express my gratitude.

The first person I wish to thank is my academic advisor, to Dr. Zsolt Berner! This work would still be incomplete without his great knowledge, advice and supervision, and incredible patience in each stage of this thesis. I am more grateful to him than he knows! My gratitude is also dedicated to my second scientific advisor, Prof. Dr. T. Neumann and Prof. Dr. W. Püttmann. I wish to thank them both too for their support and the possibility to participate in conferences, as well as their kind support, patience and supervision in finalising this thesis.

Thanks to all my friends and colleagues from the Institute of Mineralogy and Geochemistry, who offered help and guidance throughout this time. Special thanks to C. Haug, Gesine Preuß, Beate Oetzel, Claudia Mössner, and Pirimze Kelashivilli, for their support and critical supervision during my lab work. I would also like to thank my colleagues and friends in my office, Alex und Jan. During these two years you always made time to assist me, when I needed your help. In particular, I would like to thank Alex, who spent a lot of his private time to improve this thesis.

I received further guidance in my academic life from my advisors at the Ben-Gurion University, Beer Sheva, Dr Sigal Abramovich and Prof. Dr Shimon Feinstein. Both contributed similarly and aided me with their incredible hospitality, support, and knowledge, during my two stays at the department there. This important part of my academic life would not have been possible without their financial support during my stays. I thoroughly enjoyed the time in Dr Sigal Abramovich's laboratory, where I conducted my palaeontological preparations for this project. Special thanks also go to Dr Sarit Ashckenazi-Polivoda, especially for her guidance and support in selecting samples for the biogeochemical analysis. Furthermore, I thank Ari Meilijson, Libby Ron, Menahem Weinbaum-Hefetz and Gily Markado from the

micropalaeontological lab, for their encouragement and for their generousity in sharing their knowledge, patience and thoughts with me. I hope that we will be able to expand our collaboration in the near future.

Last but not least, I would like to thank my family, my girlfriend Dina and Trucky, who continuously offered their support, advice and patience during my time as a PhD candidate. The successful realisation of this thesis would be no longer imaginable today, without my family.

This research was supported by GIF – The German-Israeli Foundation for Scientific Research and Development, grant no. 956-38.8/2007, and by Israeli Ministry of Infrastructure, grant no. 27-17-005 and the Helmholtz- Association (GRACE) in Karlsruhe.

List of content

List of figures

List of tables

List of formulas

List of abbreviations

Fig.: Graph, Figure

bent.: Benthic

CF: Occurence of foraminifera assemblage in Campanian - Maastrichtian

CSA: Carbon/Sulphur-Analysis

DSDP: Deep Sea Drilling Project

ED-XRF: Energy dispersive X- ray fluorescence

HR: High-Resolution

ICP: Inductiv Coupled Plasma

ka: thousand years

LA: Laser Ablation

Ma: billion years

MS: Mass Spectrometry

ODP: Ocean Drilling Project

OES: Optical Emission Spectrometry

p: statistical signifikance (p-niveau, mostly $p>0.05$)

p.a.: pro analysi

plankt.: Planktic

r: Pearson correlation coefficient

®: Registered trademark

SEM: Scatter electron microscopy

Stbw: Standard deviation

Tab.: Table

VPDB: Vienna Pee Dee Belemnite

WD-XRF: Wavelength Dispersive (X-ray fluorescence analyses)

XRD: X-Ray Diffractometry

°C: Degree Celsius

‰: permille

wt. %: weight percent

1. Objectives

The main objective of the inorganic part of this project is by analysing trace elements, stable isotopes and their relationship to foraminiferal assemblages, to establish factors that controlling the accumulation, distribution, and preservation of the organic matter.

It was originally concluded, that the chosen profile exhibit thermal inmature and well-preserved sediments, including foraminifera. However, preliminary analysis exhibit isotopic values in $^{18}O_{benthic+planktic}$ foraminifera that show lighter values, which expected. By this fact, an additional goal arises from that to get more precise conclusion about the extent of late diagenetic influence on bulk sediment and foraminifera.

To achieve these goals, in course of this project we have used well established proxies (e.g. V/Ni, U, Fe-S-C systematics and $\delta^{34}S$) and by determination of selected trace elements in foraminifera to get more conclusions about a high resolution stratigraphy and subtle changes in to the pore water and overlying water column. Subsequently, obtained $\delta^{34}S$ was also used, to distinguish between oxidizing conditions (sulphate) and reducing conditions (sulphide) at time of diagenesis.

In order to minimize effects from late diagenetic stage, that change the composition of trace elements in test`s of foraminifera and bulk sediment as well, I applied a multi-proxy analyses in combining with a multi-variant statistical analyses.

In a last step, the ascertained high-resolution proxies merged into a conceptual geochemical deposition model, which explains the evolution of the upwelling sequence during the transition from Campanian to Maastrichtian time.

2. State of the research

Organic rich rocks (oil shale/black shale) are in many ways an interesting object in marine and geological research (Dyni, 2003). One of the reasons is that these rocks represent anoxic events that are temporally and spatially widespread throughout the earth's history. Another significant aspect is the increasing economic importance of oil and gas resources, which is promoting the acquisition of new knowledge on their formation. Based on their different types of accumulation, these rocks provide a wealth of information about past environments and unique ecosystems: *"They range in age from Cambrian to Tertiary and were formed in a variety of marine, continental, and lacustrine depositional environments thousands of square kilometres and reach thicknesses of 700 or more meters"* (Dyni, 2003). One of the most important factors of oil shale deposits is their widespread distribution around the world – some 600 deposits in more than 30 countries are known. These identified resources contain shale oil of almost 500 billion tonnes, or approximately 3.2 trillion barrels (http://iei-energy.com/).

Organic-carbon-rich rocks, commonly termed as "black shales," consist of dark grey to black, laminated, carbonaceous mud rocks characterised by an impoverished benthic fauna, or devoid of metazoan life (Shpirt et al. 2007, Arthur and Sageman, 1994). The amount of organic carbon in black shale never exceeds 15 wt. % (Füchtbauer and Müller, 1988). Unlike black shales, oil shales are broadly defined as fine-grained sediments that contain a significant amount of organic matter, generally more than 10 wt. %, in form of hydrocarbons (oil and gas) (Dyni, 2004, 2003; Füchtbauer and Müller, 1988). According to Neuendorf et al. (2005), black shale can be defined as:

"… a dark, thinly laminated carbonaceous shale, exceptionally rich in organic matter (5 % or more carbon content) and sulphide (esp. iron sulphide, usually pyrite), and more commonly containing unusual concentrations of certain trace elements (U, V, Cu, Ni)."

Whereas oil shale is defined as: "… a kerogen-bearing, finely laminated brown or black sedimentary rock that will yield liquid or gaseous hydrocarbons on distillation." (Neuendorf et al., 2005). The debate about the correct definitions for these kinds of rocks is still underway. In order to avoid misleading

interpretations, we follow both definitions by Neuendorf et al. (2005), which state that black shale usually contains appreciable amounts of trace elements, whereas oil shale is broadly defined as yielding liquid hydrocarbons on distillation. According to Minster and Miknis (1994), Gvirtzman et al. (1989), Reiss et al. (1985), Spiro et al. (1983) and Shahar (1968), we prefer using the traditional term of our Israeli project partner „Oil shale – organic rich carbonates“.

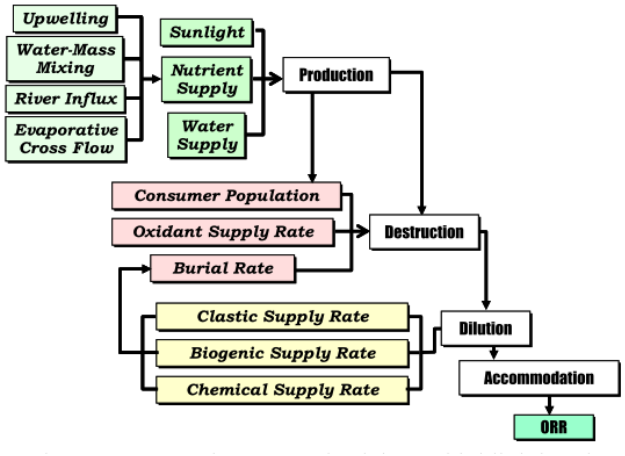

Fig.1 Factors controlling the accumulation of organic-rich rocks (ORR) (Passey et al., 2010)

As shown in fig. 1, the deposition of both (black and oil shales) requires a supply of organic matter and conditions that are conducive for the preservation of organic material (**Production**). These conditions include the depletion of dissolved oxygen in the water overlying the sediment/water interface (**Destruction - Dilution**), and the subsequent **accommodation** of organic matter on the seafloor, which will finally result in the deposition of organic-rich rocks (**ORR**) (Passey et al., 2010).

Based on the composition of marine vs. terrestrial organic matter, mineral content, soluble OM (bitumen), and insoluble OM (kerogen), attempts were made to classify different types of organic-rich rocks (Cook and Sherwood, 1991; Hutton, 1987). Based on the classification scheme of Hutton (1991, 1987), which is shown in fig. 2 (next page), oil shales can be categorised in three groups, comprising humic coals, bitumen-impregnated rocks, and oil shales. Depending on their environment of deposition Dyni (2004), oil shales can be further classified in terms of terrestrial, lacustrine, and marine origin. Lipid-rich organic matter is the main source for all types of oil shales, but a main difference between these arises from the different composition of the lipid-rich organic matter. For example, in terrestrial organic matter lipids are mostly made up of resin spores, waxy cuticles, and the corky tissue of roots

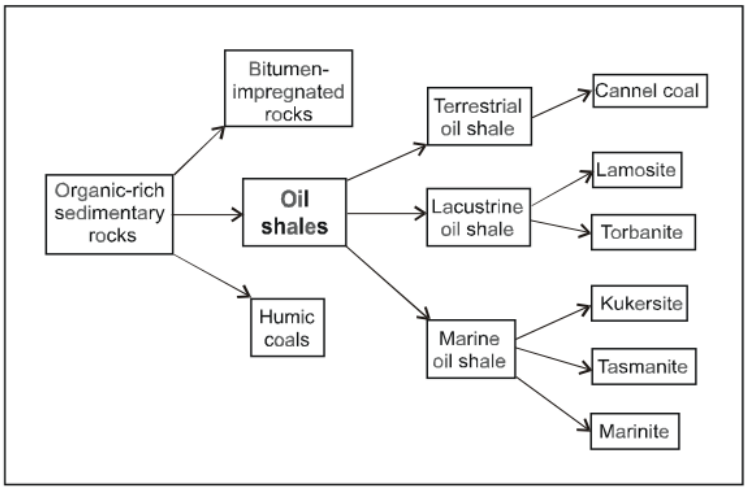

Fig.2 Classification of oil shales (Hutton, 1987)

and stems of vascular terrestrial plants that are generally found in coal-forming swamps and bogs (Dyni, 2004, 2003).

In contrast, in lacustrine oil shales, the constituting lipid-rich organic matter is derived from algae that live in saline, brackish lakes (Dyni, 2004, 2003). In oil shales from marine origin, the lipid-rich organic matter is derived from marine algae such as dinoflagellata and acritarchs (Dyni, 2004, 2003). From preliminary investigations, the type of organic matter in the research area is known (C/N ratio and $\delta^{13}C$), and they are mainly derived from marine algae (Schneider-Mor et al. 2012). Therefore, we will mainly focus on marine oil shales (kukersite, tasmanite, and marinite) in this project. These terms refer to the different locations, where these types of organic rich sediments have been initially described.

2.1. The palaeooceanography of upwelling systems

Important areas of marine organic rich rock accumulation are high productivity systems that are mostly located on the western margins of the continents. Such areas are also known for extraordinarily high accumulation rates for carbonates, phosphates, and silica (Giraudeau et al. 2000; Obrien et al. 1981); Obrien and Veeh, 1980).

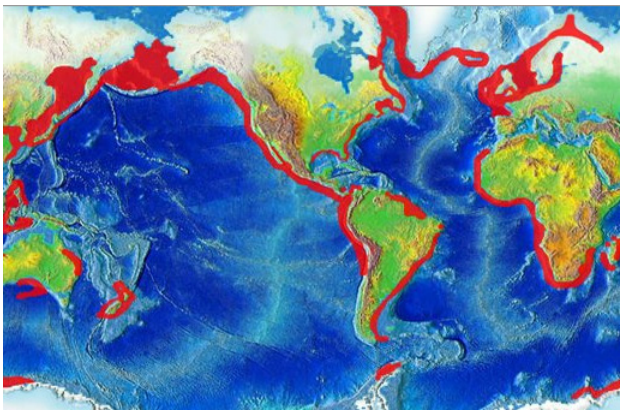

Fig.3 Areas of recent upwelling (EBCS) in the world, red lines (http://oceanservice.noaa.gov)

Today, eastern bondary current systems (EBCS) are developed along the eastern margins of both the Pacific and Atlantic Oceans (Doney et al. 2012; Stewart, 2007). Recent EBCS are characterized by high primary production due to sustained nutrient input by vertical water circulation (Marchesiello, 2009). Approximately, 25% of the annual marine fish catches come from there, despite upwelling's cover only 5% of world`s ocean (Mann and Lazier, 2006). The main factors that affect the strength of organic matter accumulation in upwelling systems are: wind stress (monsoonal winds, passat winds), changes in the composition of intermediate waters between 200 and 500 m water depth (e.g. caused by freshwater input), and changes in the strength of upwelled water. Additional factors are related to changes in the expansion of the oxygen minimum zone (OMZ), circulation of advected bottom water and the input of detrital material by rivers and winds. Recent studies confirmed these notions and found some additional oceanographic factors that influence the primary production (Gilly et al. 2013, 2011; Marchesiello, 2009; Rossi, 2008; Gruber, 2006; Kuypers, 2005). For example, the upper bondaries of the OMZ[2] can have major effect on the vertical distribution of planktonic organisms and therefore on their contribution to the sediments.

[2] midwater ocean layer with reduced oxygen concentrations in the world`s ocean (<20-40µmol kg^{-1}), typically at depths of 100–1.000 m; these result from a confluence of upwelling, high primary productivity, stratification, and minimal mixing acting on "old" seawater Levin and Sibuet (2012); Gilly et al. (2013)

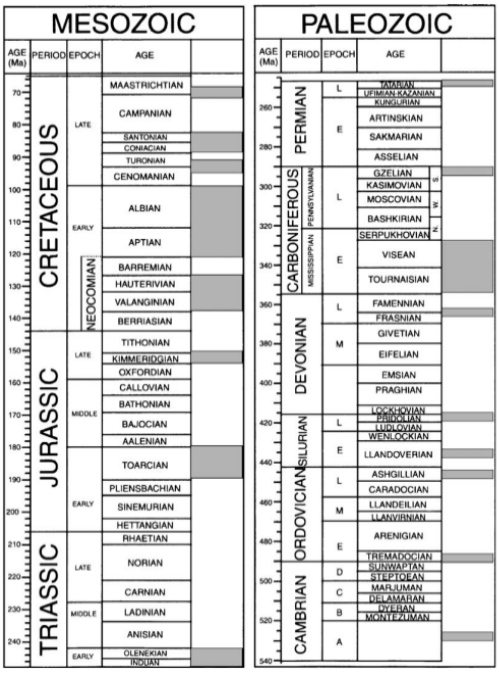

Fig.4 Occurrence of black shales across the Mesozoic and Palaeozoic time modified after Negri et al. (2006)

Arthur and Schlanger (1979) introduced the concept of Oceanic Anoxic Events (OAE), which is defined as a globally lowered oxygen level below the limit in the world`s oceans. Totman Parrish and Curtis (1982) used basic principles of atmospheric circulation models to reconstruct oceanic circulation patterns from the past. The authors showed a high statistical correlation between the occurrence of upwelling zones and organic rich rocks, especially in Triassic, middle Early Cretaceous to Late Cretaceous age (fig. 4). Obviously, the Cretaceous period is the most known time regarding the accumulation of organic rich rocks.

Recently, some attempts have been made to explain the formation of black shales. Lately, Gilly et al. (2013) argues that primary production is the main cause of organic matter accumulation, because a higher surface productivity creates more organic detritus that can be consumed by microbial communities. Concerning the organic matter accumulation, (Challands et al. 2009), summarised several models:

(1) the runoff model (Bjerrum et al. 2006; Beckmann et al. 2005a) has been proposed tropical latitudes and under a warm climate, when the continental runoff increased the transport of nutrients and lead to an increase in productivity and organic carbon export

(2) the upwelling model (e.g. Pope and Steffen, 2003; Summerhayes et al. 1992; Totman Parrish and Curtis, 1982) is most suitable for mid- to high latitudes with well-developed trade wind zones and possibly best applicable for the studied case here

(3) the transgressive model (Leggett, 1980) explains the organic rich accumulation as a function of the expansion of the deep ocean oxygen minimum zone during a rising sea level, enhancing the OC preservation in high productivity near-shore environments

(4) the productivity model (e.g. Brumsack, 2006; Calvert and Pedersen, 1993; Demaison and Moore, 1980; Arthur and Schlanger, 1979) stating that the main factor for organic matter accumulation is a high surface productivity and subsequently a high degradation rate of organic matter, which leads to an oxygen-deficit in both surface- and bottom water and thereby to the preservation of organic matter (OM)

(5) the stagnation model developed by Tyson (1991), Stein (1990) and Reiss et al. (1985) proposed that widespread anoxic bottom water conditions were the result of restricted water circulation and/or related to high flux of organic matter from phytoplankton

In summary, in all these models organic matter accumulation is a consequence of an oxygen deficit in the water column or the sediment/water interface. This is caused by high surface productivity and promotes a high accumulation rate and preservation of organic matter. However, Zonneveld et al. (2010) demonstrated in his review that additional factors influence the preservation of organic matter. This includes the amount and the type of mineral ballast and both the flux rate, composition and preservation of OM that is produced in the upper water column and subsequently delivered down to the seafloor.

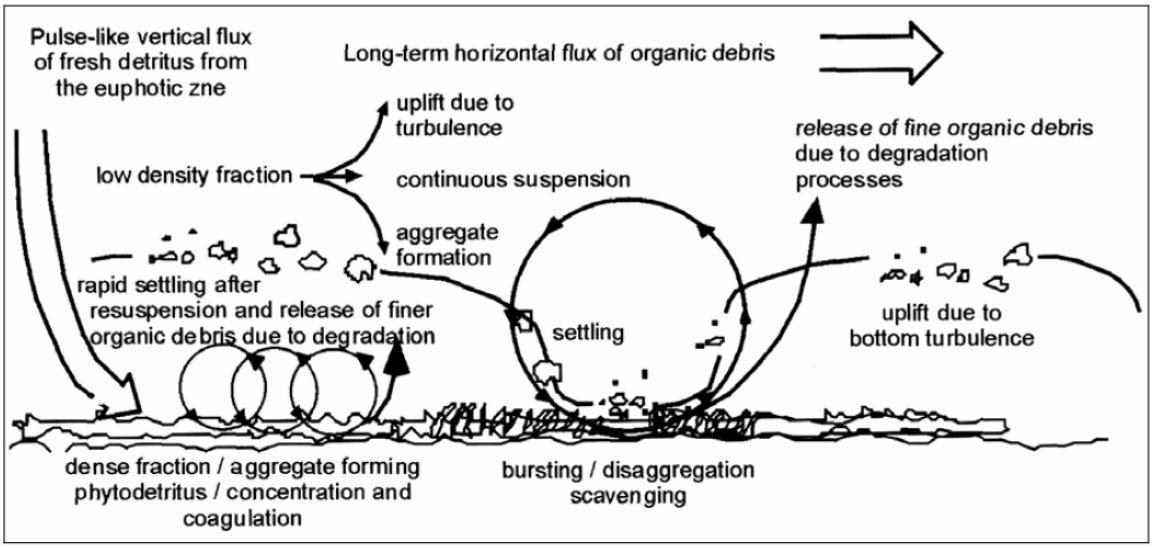

Fig.5 Schematic model of a resuspension loop of aggregated particles, modified after Thomsen et al., (2002)

Besides the mineral ballast, small refractory particles, including coccolithophorida, diatoms (opal) are too small for sinking. To enhance the sinking velocities, these particles will be incorporated in pellets or marine snow aggregates. For example, Inthorn et al. (2006), Thomsen et al. (2002) and Littke (1993) differ between distinct types of mineral ballast[3] and transport to calculate the difference in sinking velocities (fig. 5). This distinction is important for understanding the degradation potential of the OM, which varies in cases of terrestrial or marine organic sources due to their different composition. Moreover, terrestrial OM can alter before entering the marine realm. For example, particles that are transported in suspension undergo repeated sedimentation followed by aggregation/disaggregation and scavenging which, in further (repeated) steps, leads to the release of finer organic debris. These processes of lateral suspension and transport have a significant effect on the quality and the preservation of organic matter (Thomsen et al., 2002).

[3] Different types and sizes of mineral ballast: terrigeneous organoclasts (100-10µm), quartz grains (10µm), fecal pellets (1mm), according to Littke (1993).

2.2. Modern major upwelling systems

One major objective for reconstructing ancient upwelling systems is to compare its main oceanographic, faunal and geochemical features to those of modern ones. In the course of the following lines, the author will introduce some of the features that determine the formation of upwelling systems and discuss their formation.

Distinguishing different oceanographic conditions

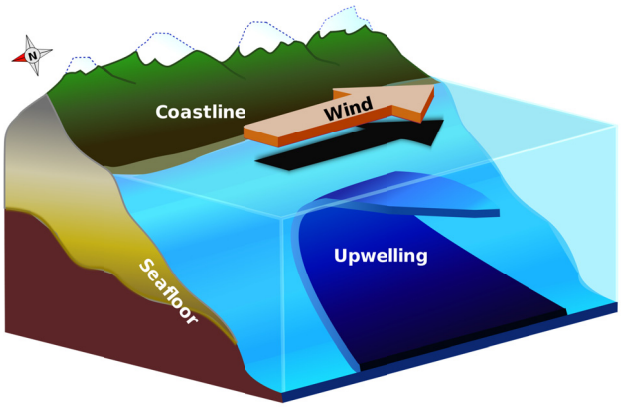

Fig.6 Surface waters are replaced by cold, nutrient-rich water that has up-welled from below (http://oceanexplorer.noaa.gov)

Oxygen-Minimum Zone

Three originators that cause an upwelling are Ekman transport, Coriolis effect and wind currents (Bakun, 1990). The strength of a wind current determines the intensity of the upwelling water, as shown in fig. 6 (Tomczak and Godfrey, 2003). It has been shown that upwelling water is nutrient- and O_2-rich, and stimulates the bioproductivity in the surface water which is expressed in high concentrations of chlorophyll-a (Thiede and Suess, 1983).

The stimulation of surface productivity is a result of a complex interplay between sunlight, temperature, salinity, and dissolved nutrients. The concentration of dissolved oxygen in the ocean varies greatly both in depth and along the surface (Stramma et al., 2012). Direct consequences of this process are phytoplankton blooms resulting in thermal stratification of the water column and the formation of an oxygen-minimum zone (OMZ) below the euphotic zone (Stramma et al. 2012; Keeling et al. 2010; Paulmier and Ruiz-Pino, 2009).

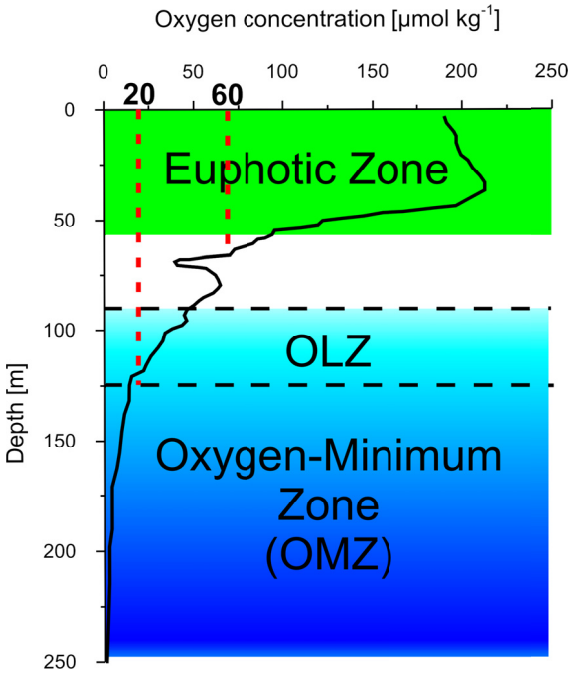

Fig.7 Water mass stratification in the world`s oceans; trend line shows a characteristic profile for dissolved oxygen in the water column for the eastern tropical North Pacific region. Different colours indicating depth of (1) Euphotic zone (2) oxygen limited zone - OLZ (3) oxygen minimum zone – OMZ, modified after Gilly et al. (2013)

Such areas in the world`s oceans (Pacific, Indian-Atlantic ocean) are well defined due to a decline in the oxygen content in the upper water column and their decreasing trend towards the bottom. They range in depth from 100 – 900 m. As shown in fig. 7, within this layer the oxygen threshold in an OMZ is defined as < 20 µmol kg^{-1} (Paulmier and Ruiz-Pino, 2009). All recent upwelling systems are affected by the installation of a permanent OMZ. This zone impinges the sediment in different depths that range, for example at the California margin, from ~500 up to 2000 m (Thunell et al. 1994; Shiller, 1983), Arabian Sea (150 - 3200 m), (Cowie, 2005; Nagender Nath et al. 1997), Namibian/ Benguela margin (200 - 400 m), (Emeis and Morse, 1993), Peru (50 - 600 m) (Muñoz et al. 2004).

Upwelling cell

Widespread phenomenon of Eastern Boundary Currents (EBC) is the installation of upwelling cells. For example, seven different cells are occurring off the Namibian coast. These cells are producing 0.35 Gt carbon per year (Campillo-Campbell and Gordoa, 2004; Carr, 2003). Similar observations are reported from the Peruvian upwelling system, in which occurring upwelling cells (plumes about 100-300 km diameter) are restricted to a patchy area of cells located at 100-300 km off the Peruvian/Chilean coast (Acha et al., 2004). Numerous reports state that these upwelling cells are accompanied by filaments that

can be described as narrow bands of cold water in vicinity to the coast. Their principal feature is to bring cold-water currents closer off the upwelling coasts (Tomczak and Godfrey, 2003).

Eddies and filaments

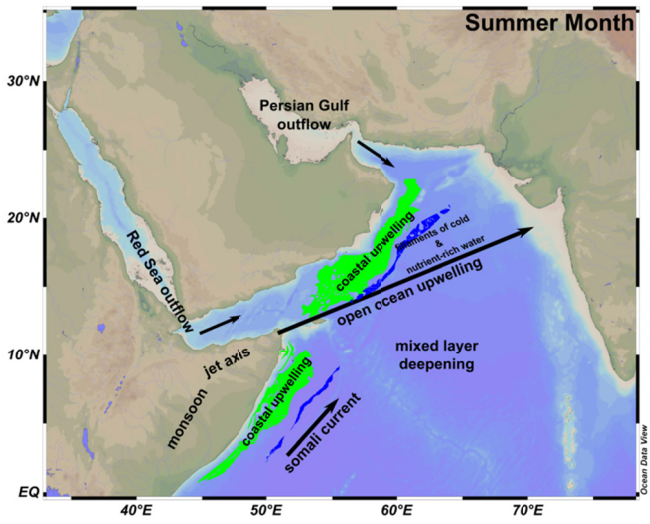

Fig.8 The Arabian Sea including the Omar margin at the Arabian coast, modified after Tomczak and Godfrey, (2003) and Luther et al. (1990). Note blue stripes are filaments

A so-called quasi-stationary front close to the position of the shelf-break often occurs. These oceanographic boundaries between the coastal upwelling and the oceanic basin regime are frequently marked by jet currents, eddies and filaments directed alongside the coast. Such filaments are observed in regions of major upwelling in Peru/Chile (Acha et al. 2004), Namibia/ Benguela (Tomczak and Godfrey, 2003) and the Arabian Sea. As shown in fig. 8, within this region both the Findlater Jet Axis and the filaments transport cold and nutrient rich water (Brock and McClain, 1992).

As mentioned above, another feature that is in still controversial debate is by so- called eddies which are defined as ephemeral meso scale surface counter clockwise circulation of water masses. It is thought that such phenomenon might lead to loss of nitrogen from the near surface water off the coast (Gruber et al., 2011). In terms of the Peruvian system these eddies develop alongside the coast and decay in a time span within few days or weeks (Acha et al., 2004). In opposite to the eddies that are observed in the Benguela current, this one transport water from the Indian Ocean in to the Atlantic Ocean, their life time spans about many years. Their “main task” is to contribute to recirculation of North Atlantic Deep Water (Tomczak and Godfrey, 2003).

Faunal distribution of calcareous and siliceous organism

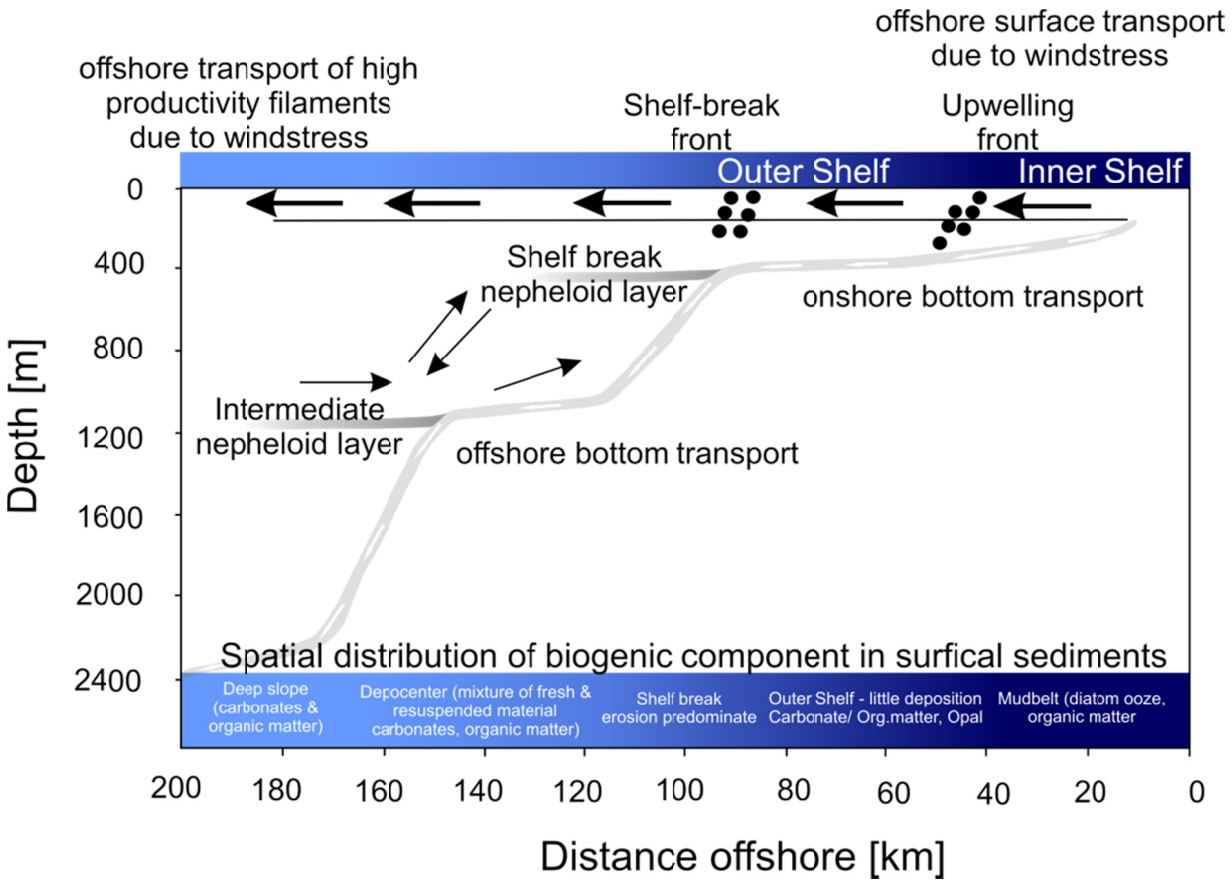

Fig.9 A cross-section in a recent upwelling system, modified after Inthorn et al., (2006), and Giraudeau et al., (2000)

One of the first aspects that should be viewed is the faunal distribution of some calcareous and siliceous organisms, which are responsible for the major organic flux in the euphotic zone. Figure 9 shows an example for the faunal distribution in the surface water of the recent Namibian upwelling system (Walvis Bay).

The Walvis Bay is exemplary for other upwelling areas despite some minor differences to other upwelling areas. Giraudeau et al. (2000) explores the phenomenon of the distinct contribution of biogenic components (carbonates, opal, and organic matter) to the total biogenic flux. In upwelling areas coccolithophores and planktic foraminifera are the main contributors to calcareous sedimentation at the

outer shelf regions, whereas diatoms compose the dominant component that controls the sedimentation onto the inner shelf area. Coccolithophorida prefer to inhabitate mesotrophic[4] and oligotrophic water masses (outer shelf), in contrast to diatoms that live preferentially in eutrophic inshore water. These diverse habitats are separated by differences in the influence of water masses, bottom topography, and additional topographic factors like the location of the shelf breakfront. In turn, the shelf breakfront determines the location of the upwelling cell and therefore the nutrient availability. This notion is confirmed by Schiebel et al. (2004), and (Thomsen et al. 2002), at the Oman margin. In addition, both authors stressed that the major part of the biogenic flux and bulk sediments is resuspended material from the outer shelf area (see also section 6 for a detailed discussion). Hence, we find a similar sequence of carbonate-, opal and phosphor-rich sedimentation (Ca-Si-P) in ancient analogues (for example Cretaceous Levante Basin).

Geochemistry of surface sediments: example California Margin

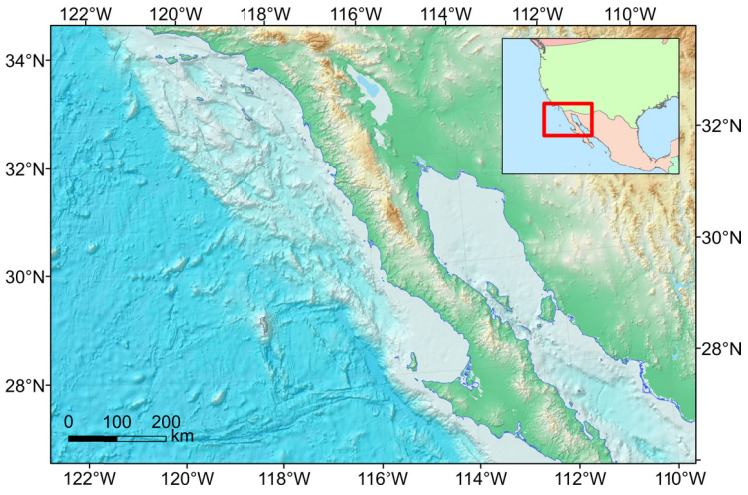

Fig. 10 The Southern Continent Californian Borderland margin as part of the California upwelling region (map is drawn with ARCGIS).

One of the northernmost upwelling sites in the world is in the northern Pacific region. Part of this system includes the region around the California margin and the coast of Oregon (~ 2000 km alongside), fig.10. The region is an example for an upwelling system that shows a complex interplay of seasonal upwelling, ocean currents, and trade

[4] It common to differentiate between distinct stages in terms of the nutrient availability in water masses: oligo-, meso-, eutrophic systems in which the most limiting factor is the phosphate content.

winds in combination with aeolian and fluviatile input. Within this area, seasonal wind patterns that occur in winter cause an enhanced surface productivity. Unlike during the summer months, when the winds are prevailing from the south and trigger a monsoonal climate with increased rainfall and reduced primary productivity (Barron et al., 2004). The opal production in early autumn coincides with a stronger upwelling, which initiates an anoxia in the water column, a condition that has led to the most rapid accumulation of biogenic sediments in the world (Barron et al., 2004). The water below sill depth (475m) is generally low in oxygen and shows evidence of nitrate reduction (Shiller, 1983). The OMZ at the California margin ranges in depth from ~500 up to 2000 m. Moreover, the southern California Borderland margin is separated by a series of sills, which hamper the water mass circulation followed by a restricted circulation, and high carbon flux induces almost anoxic conditions (Tomczak and Godfrey, 2003; Pinet, 1992).

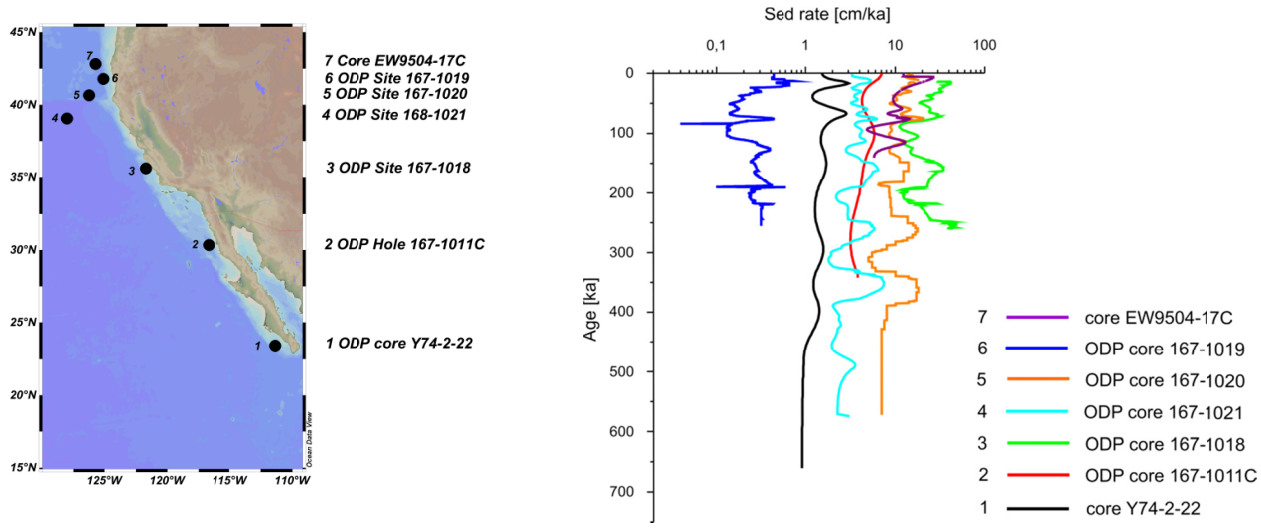

Fig.11 ODP sites for sedimentation rate along the Californian continental margin, data source and modified after Lyle et al. (2000), note the use of a logarithmic scale for sedimentation rate

With respect to the California margin, several authors have examined the sedimentation rates in this zone in detail. Lyle et al. (2000, 1992), fig. 11, analysed the sedimentation rate on five Leg 167 drill sites and three piston cores.

They report different sedimentation rates up to 5 - 50 cm/ka within this area (Hovan et al. 2000; Lyle et al. 2000). Similarly, Barron et al. (2004) re-evaluated the sedimentation rate for the last 150 ka and calculated an average rate ~100 cm/ka.

Irino and Pedersen, (2000) analysed the minor and trace elements, to track sediment source and pathways, by using Q-mode factor analysis, north of the Santa Barbara Basin, Site 1017. Results of this study reveal that a mafic complex in the mainland (Fransican Complex), acts as the main source for detrital input into the continental margin, which may enhance the bioproductivity at the Californian shelf.

Phytoplankton assimilate major and trace elements from the seawater (Coale and Bruland, 1988). The phytoplankton is grazed by zooplankton and the trace elements are integrated into the zooplankton biomass. A study by Rentería-Cano et al. (2010), in this region, concluded four clusters in which major and trace elements contribute to the zooplankton biomass: These include firstly - redox sensitive metals (Cr, Cu, Mo, As), secondly - trace metals from terrigeneous origin (mostly REE), thirdly - biologically active trace metals (Fe, Sr, Ba, Zn, Br, Zr) and lastly - major elements (Na, Ca).

A special role is played by U, Mo, V, and Cd as proxies for anoxia and productivity (Dean, 2007; McManus et al. 2006; Zheng et al. 2002; La Lanza-Espino and Soto, 1999; Brumsack, 1989). On transects at the Oregon coast, Zheng et al. (2002) measured the diffusive flux of uranium into the sediment in pore water. Results primarily suggest a separation in slope and deep sediments and a strong coupling between the authigenic enrichment of U, which is higher in slope sediment than in the deeper sites. This is a result of bioturbation in slope sediments, which leads to a remobilisation of authigenic U, and subsequently an upward diffusion into an oxidizing zone. Moreover, due to a lack of connection between the organic-

carbon flux and pore water condition, it is apparent that the U reduction is mediated by bacteria, (McManus et al. 2006; Zheng et al. 2002; Lovley, 1991).

Ishiwatari et al. (2000) analysed the organic carbon (4 wt. %), and total sulphur content, which ranges between 0 - 1.78 wt. %, at the Northern Californian margin (34.3°N). Finally, (Volkov, 1984) and (Rozanov et al. 1976) report about sediments from the Southern Gulf of California with an average C_{org} content of 3.25 - 9 wt. %.

Fe-S-C systematic

In this section, a few cases will be considered to exemplify to what extent the Fe-S-C system can be used to describe the degree of anoxia in upwelling regions.

Despite some limitations, several authors have used the degree of pyritisation (DOP) in combination with Fe-S-C system to recognise the extent of anoxia in organic rich sediments (Rickard, 2012; Schultz, 2004; Werne et al. 2002; Emeis and Morse, 1993; Hatch and Leventhal, 1992).

Originally, the assumption was made that all S_{pyrite}, formed in normal marine sediments with an overlying oxic water column, show a linear relationship between C_{org}-S_{pyrite} (C/S- value) with a positive intercept. In addition, this can be used empirically, to separate between anoxic and euxinic conditions by a positive intercept of C/S ratio of 2.8 ± 0.8. (Hatch and Leventhal, 1992).

For the Benguela upwelling system (Walvis Ridge), (Emeis and Morse, 1993) found an average C/S ratio of 4.45 that is atypical for marine sediments. Similar ratios were found by (Emeis and Morse, 1993) in the Peru and Oman upwelling areas. In the same area, much higher C/S ~ 20 values were reported by Inthorn et al. (2006).

Several authors analysed the iron-sulphur-carbon system in the Peruvian upwelling system, for example (Lückge et al. 1996), sites 679-681, (Emeis and Morse, 1993,1990), and Peru margin, sites 680 and 688,

(Emeis and Morse, 1990, Volkov, 1984). Elevated C/S ratios are 6.8 (site 688) and 5.7 (site 680), respectively. These exceed the expected values in normal marine conditions.

On three DSDP sites (722, 723 724[5]), a C/S ratio is reported from the Oman margin that deviates from the usual C/S ratio in normal marine sediments (~2.8). Obtained C/S values show huge differences depending on their location at the shelf area. In this context, ODP site 722, shows a C/S ratio ~4, whereas on site 723, values are up to 48 and show large variances (1.5-48). Similar values are reported by (Seifert and Michaelis, 1991) on site 724. The observed values do not deviate significantly from the average value around 30. Emeis and Morse (1993) interpret such unusual values in terms of limits in the degradation of organic matter and postulate a non-iron limited system. Schenau et al. (2002) suggest that the iron is still available for pyrite formation, based on the DOP values (0.6-0.9). The obtained C/S values alternate between organic–rich vs. organic-poor layers (4-13.2). This suggests neither a sulphate limited system nor an accumulation of less reactive organic matter.

Based in a degree of pyritisation (DOP) close to 0.4, Emeis and Morse, (1993) conclude a non-iron limited system for pyrite formation at the DSDP Hole 735B. Brüchert et al. (2000), found similar DOP results ~0.4 at three boreholes at the DSDP site 1084. Based on the Fe-S-C relationship, Borchers et al. (2005) assumed that a complete pyritisation takes place at the sediment/seawater interface .

From these studies, the conclusion can be drawn that C/S-ratios may be inappropriate as palaeoenvironmental indicators within these areas. Further details have been discussed elsewhere (Rickard, 2012; Morse and Berner, 1995; Emeis and Morse, 1993; Emeis et al. 1991).

[5] Site 722 is located far away from the outer shelf (2038m water depth – below the OMZ) about 150km, site 723 inner shelf (800m water depth – within the OMZ) area to the Omar coast, 724 continental slope

2.3. The palaeooceanography and climate of the Upper Cretaceous upwelling system of the southern Tethys

The late Santonian to Maastrichtian sediments in Israel contain a sequence of organic rich carbonates (syn. oil shales), phosphates, and cherts-porcelanites, so called (C-P-Si). This sequence was deposited mainly in approximately 30 synclinal basins, formed by the gentle folding of the Syrian Arc system (Krenkel, 1924). In the current study, the focus was led on the oil shale occurrence in an open quarry in the Mishor Rotem area, Negev (southern Israel), where we had direct access to freshly exposed rocks. This area was described as residing within the inner-shelf of the Southern Tethyan margins (Soudry et al. 2006; Hoek et al. 1996; Eshet et al. 1994; Almogi-Labin and Bein, 1993; Eshet et al. 1992). During the Late Cretaceous, the oceanic Tethyan domain was situated within the intertropical belt (fig.12), a few hundred kilometres above the Gondwana shoreline, at ~12°N (Gilles S. Odin, 2001; Camoin et al. 1993; Dercourt et al. 1993). Following the breakup of the Pangaean continent, in the Late Cretaceous, a vast area of shallow

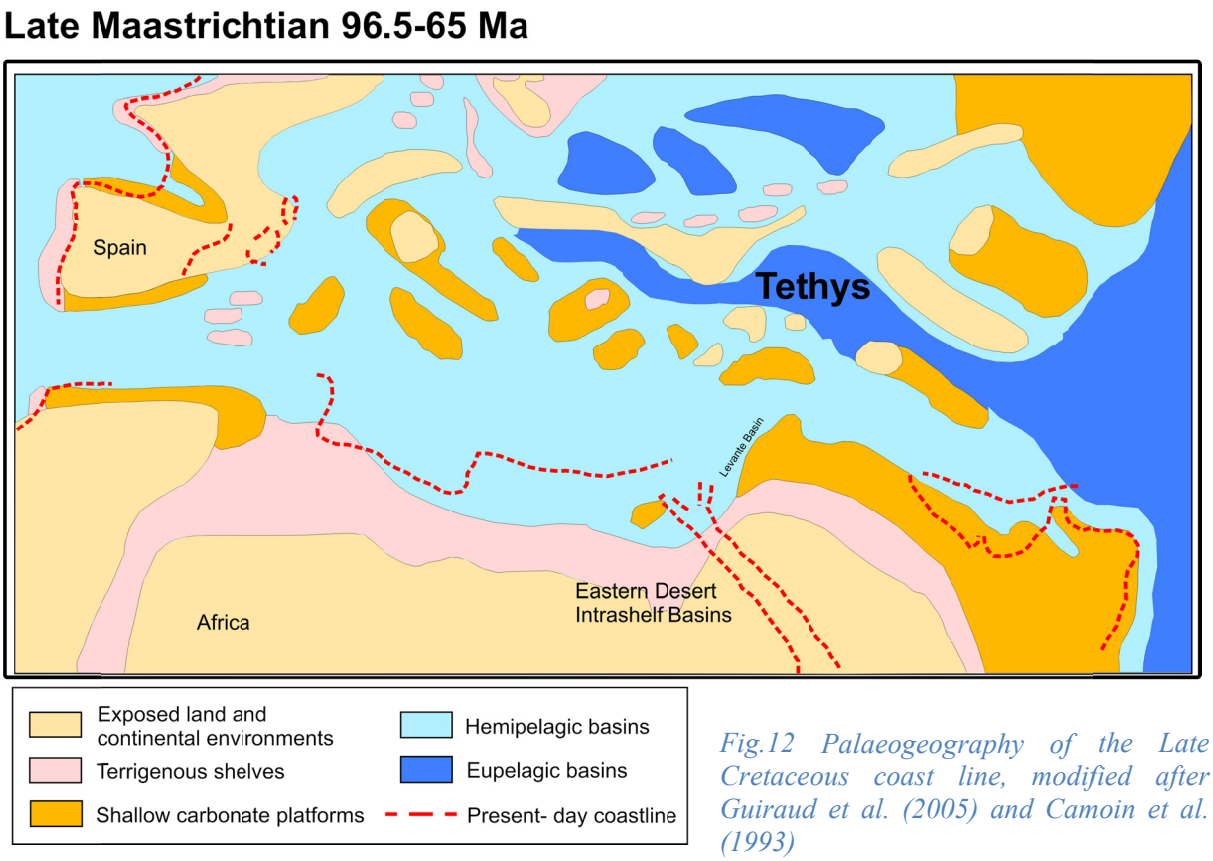

Fig.12 Palaeogeography of the Late Cretaceous coast line, modified after Guiraud et al. (2005) and Camoin et al. (1993)

epicontinental seas covered the global continental margins (Hay, 2008), including the northern African margin that led to the development of the Arabian platform (Guiraud and Bosworth, 1999; Gvirtzman et al. 1989). In Israel, different oceanographic, tectonic (Syrian Arch) and eustatic conditions during the Santonian-Maastrichtian interval have led to the deposition of the high productivity sediments, namely cherts, porcelanites and phosphates of the Mishash Fm., as well as organic rich carbonates (OSM) and overlying marls of the Ghareb Fm. (Gvirtzman et al. 1989; Reiss et al. 1985; Totman Parrish and Curtis, 1982).

Beyond the Syrian Arc to the south, the Mishash Formation becomes more uniform, predominantly of pelagic chalk interbedded with chert-porcelanite horizons and some continent-derived clastics (Almogi-Labin et al., 2012). The organic content ($C_{org.}$ average 15%) with enrichment of trace elements reflects an upwelling system (Ashckenazi-Polivoda et al., 2011, 2010; Edelman-Furstenberg, 2009, Almogi-Labin and Bein, 1993; Gvirtzman et al., 1989). On the basis of lithological and faunal analysis, the Negev area was described as the more proximal location relative to the more distal depositional basins situated in central Israel (Ashckenazi-Polivoda et al., 2011; Abramovich et al., 2010; Edelman-Furstenberg, 2009; Almogi-Labin and Bein, 1993). These distal locations (for example, the Shefela basin) contain almost exclusively oil shale deposits without the chert-phosphate-porcelanites lithology appearing in the proximal areas.

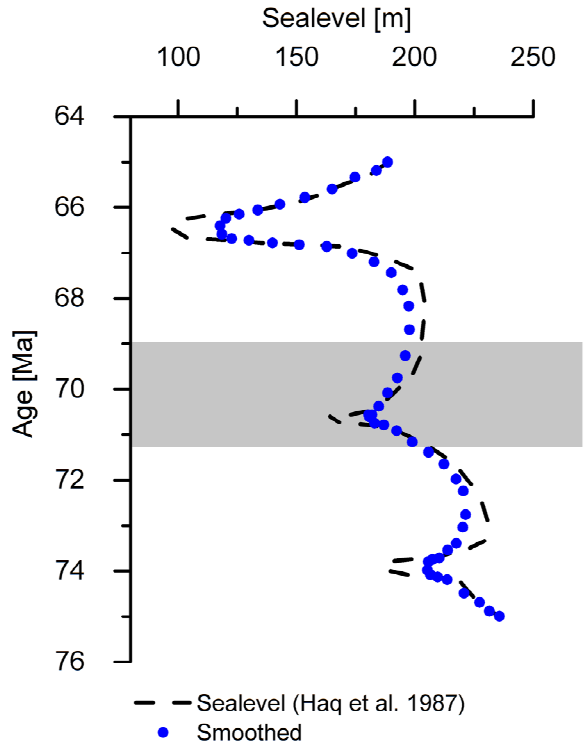

Fig.13 Sea level curve from Haq et al. (1987), which show three major sea-level changes from 75–74, 72–71, and 69–68 Ma. Redrawn after Barrera and Savin, (1999). The grey bar shows the time interval of interest Campanian - Maastrichtian

The Late Cretaceous is known as a time of dynamic climatic and oceanographic changes, reflected inter alia by different modes in the transport mechanisms of oceanic water masses. Numerous studies of climatically sensitive palaeontological data indicate much higher temperatures and a reduced equator to pole gradient during Cretaceous time (Stoll and Schrag, 2000). By using $\delta^{18}O$ to reconstruct palaeo-temperatures in the Late Cretaceous, studies show major drops in the palaeo-temperature during the younger decade, (e.g. Keller et al. 2004; Abramovich et al., 2003; MacLeod et al. 2001; Barrera and Savin, 1999; Li and Keller, 1999). Simultaneously, in the Late Cretaceous, three major sea-level changes from 75–74, 72–71, and 69–68 Ma are evident, fig. 13, (Haq et al., 1987). There is still an on-going debate whether the observed trend represents a long-term cooling or marks only a transient glacial episode: "*Little is known about the causes, was this a continuous or a stepwise event"?* (Voigt et al., 2010). Two different hypotheses about the reason for the oxygen isotopic shift have been made. Firstly, by interpreting this phenomenon in terms of changes in intermediate to deep water circulation (Friedrich et al., 2008; Barrera and Savin, 1999; Li and Keller, 1999). Secondly, other authors explain this through a temporal build-up of ephemeral ice sheets in Antarctica (Bornemann et al., 2008). Some of the first authors who recognised this problem and did not exclude the possibility of the existence of an (ephemeral) ice shield, were Huber et al. (2002) and Barrera and Savin, (1999). Unlike Haq et al. (1987), who merely noted several changes in the sea-level. Continuously, Barrera and Savin, (1999) could show that a long-term cooling event in the intermediate

and surface water masses took place, with the help of records of $\delta^{18}O$ in planktic and benthic foraminifera including different sites in the North- , South Atlantic, Indic and Tropical Pacific Ocean. Even more, the long-term trend (Friedrich et al. 2012; Barrera and Savin, 1999) has been interrupted by three events with positive isotopic incursion (short-term cooling events). A first excursion in the oxygen isotopes in a time interval between 71 - 69.5 Ma has been observed, and a second interruption in the long-term trend in the period between 68 - 67.5 Ma, and finally a last excursion is terminated approx. 65.78 - 65.57 Ma. Similar events have been recorded in the Southern Atlantic, tropical Pacific, and Indian Ocean – these worldwide observations confirm major sea-level changes, which suggest the existence of ephemeral ice-sheets during the Late Cretaceous time (Miller et al., 2003; Friedrich et al., 2012; Koch and Friedrich, 2012; Miller et al., 2003; Barrera and Savin, 1999). Finally, the transition from the Campanian-Maastrichtian is marked by a drastic change in stable isotope excursions (in both $\delta^{13}C$ and $\delta^{18}O$) which can be interpreted as major drops in the sea level. Recently, this event is termed as Campanian-Maastrichtian Boundary Event (CMBE); (Voigt et al., 2012).

In summation, the time interval between the Campanian and Maastrichtian (71-70 Ma) is marked by rapidly decreasing temperatures, a fall in sea-level, and changes in the seawater circulation (Friedrich et al., 2012; Koch and Friedrich, 2012; MacLeod et al., 2011)

Which factors lead to the development of a stable major upwelling system on the Southern Tethyan margin?

In general, it is accepted that these rocks in the Southern Negev relate to a stable upwelling system over 20 Ma. years (Ashckenazi-Polivoda et al., 2011). The most intense upwelling phase occurred during the middle-late Campanian (Soudry et al., 2006). Subsequently, in this time interval the palaeo oceanographic setting has been changed in the late Maastrichtian to more open marine conditions, (Almogi-Labin and Bein, 1993; Bein et al., 1990). Atmospheric condition is one of the most important factors that have a significant effect on the development of an upwelling system. During the Late Cretaceous time interval, the prevailing trade winds direction was from NE – SW, with a stable high pressure system around the

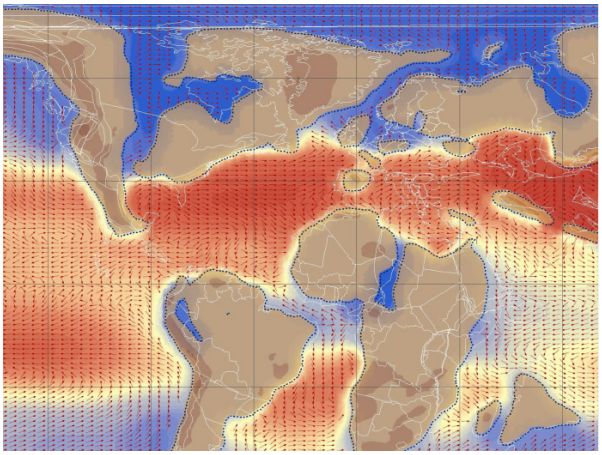

Fig.14 Surface currents in the Late Cretaceous time (www.scotese.com). Blue area is represented by cold water, red shaded area mark warm, intermediate water mass circulation

northern hemisphere (Soudry et al. 2006; Totman Parrish and Curtis, 1982), thus having led to the development of a stable upwelling system on the Southern Tethyan shelf margin.

As a consequence, Soudry et al. (2006) proposed that the massive accumulation of organic rich sediments is a result of persistent upwelling circulation, recycling dissolved phosphorous from intermediate Tethyan waters and distributing it to the photic zone. Moreover, the author proposed that a major source of intermediate Tethys waters during the Late Cretaceous was probably the North Pacific Ocean. As shown in fig. 14, from ε_{Nd} data Soudry et al. (2006), and based on literature data (Stille et al. 1996; Stille, 1992), it is conclusive that two distinct sources of intermediate seawater led to the accumulation of organic-rich sediments at the southern Tethyan coast. Firstly, a so-called "Tethyan current" flowing in the eastern Mediterranean sea, and secondly, an "Atlantic current" which promotes the accumulation of phosphates at the West African coast during the Late Campanian time. In support of this notion, MacLeod et al. (2011) used ε_{Nd} analyses to demonstrate fluctuations in circulation patterns in the North Atlantic. His data suggest that changes in the deep-water circulation, south of the Demara Rise, were responsible for climate effects at the Campanian-Maastrichtian transition in the northern Atlantic.

Nevertheless, based on palaeo-geographic reconstructions, it is apparent that the on-going breakup of Pangaea in the Cretaceous time has led to the formation of a great wide shelf area. The covered shelf areas are not comparable to those of modern day areas (Almogi-Labin et al., 2012).

2.4. Geochemical tools and proxies used in palaeoenvironmental reconstruction

In order to evaluate how anoxia may change the geochemistry of the pore waters of superficial sediment and the overlying bottom waters, proxies may help to differentiate between anoxic, dysoxic and oxic stages.

Sulphur-Iron Systematics

In past years, several approaches have been developed to recognise and distinguish among anoxic-sulphidic and iron-rich or iron-limited systems (Tribovillard et al., 2006; Lyons and Severmann, 2006; Lyons et al., 2003b; Raiswell and Canfield, 1996; Berner and Raiswell, 1984). Total organic carbon (TOC) – S – Fe relationships is an important tool in reconstructing depositional environments, to describe the degree of oxygenation, both within the sediment/water interface and the water column (Schultz, 2004; Emeis and Morse, 1993; Hatch and Leventhal, 1992; Berner and Raiswell, 1983; Leventhal, 1983). Furthermore, the occurrence of reduced sulphur (TRS: total reduced sulphur) in sediments is of interest, as pyrite and iron mono-sulphides or organic sulphur are a consequence of microbial sulphate reducing bacteria (SRB) decomposing organic matter. This, in turn, results in the release of sulphide ions in the

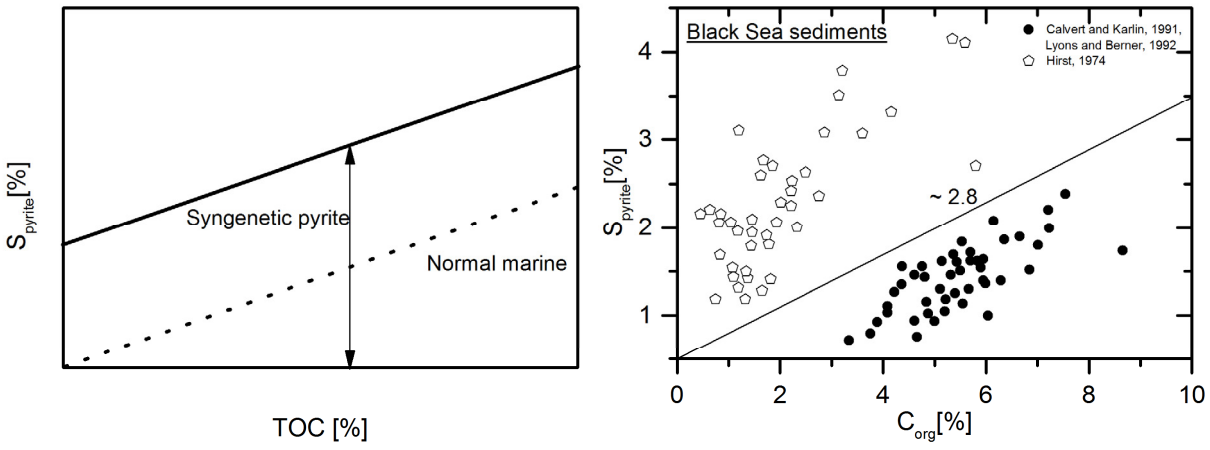

Fig.15 Left: represents an idealised plot resulting from the formation of iron-limited syngenetic pyrite, while the right graphic represents an S_{pyrite}/C_{org} plot of Black Sea sediments, also shown is the normal Holocene marine sediment ratio of 2.8, modified after Rickard, (2012), Raiswell and Berner, (1985) and Berner and Raiswell, (1983)

pore-water, followed by its reaction with dissolved iron (II). The amount of pyrite formed diagenetically is limited by availability of one or more of these compounds. It is assumed, that in normal marine sediments, the C/S ratio is controlled by the amount of microbiologically degradable organic carbon. In oxic normal marine sediments an empirical regression slope of about 2.8 between the total reduced sulphur and the amount of organic matter (C_{org}) is observed (Leventhal, 1987; Berner and Raiswell, 1984), see also section 2.3 and fig. 15 (previous page). Freshwater sediments show high > 10 C/S ratios, because within this environment, pyrite formation is limited by low sulphate concentrations in the pore water. In a euxinic environment (e.g. Black Sea, Cariaco Basin), a low C/S ratio (< 2.8) usually occurs. Such ratio is explained due to the occurrence of sulphide in the anoxic waters and the formation of pyrite in the water column, as well as the diffusion of H_2S into the sediment. Under these conditions, the availability of reactive iron is the limiting factor in pyrite formation. Researchers seem to agree that in normal marine environments the organic carbon reservoir is the main limiting factor in pyrite formation (Werne et al., 2002; Lyons and Berner, 1992; Emeis and Morse, 1990).

Proxies in distinhishing environments (Stable Isotopes (O, C, S))

Oxygen

To reconstruct past ocean temperature, the oxygen isotope signal of the benthic and planktic foraminifera can be used. Planktic foraminifera adapt the temperatures in the upper water column (sea surface temperature - SST); whereas benthic foraminifera are recorders for reconstruction of the global ice signal and temperature at the seafloor (bottom water temperature – BWT).

Two of the first geochemical proxies, which were routinely measured in foraminifera, are the ^{18}O and ^{13}C (Katz et al., 2010). Foraminifera are made of calcitic tests and are widely distributed in recent and ancient world oceans. Additionally, benthic foraminifera can be also used to track the deep-water source regions (Katz et al., 2010). Since fractionation typically occurs in the magnitudes parts per thousand or per ten

thousand, the measured isotope ratio is normalised against a standard and example delta notation as indicated.

This is expressed by the following term (eq.1):

Equation 1

$$\delta^{18}O_{\text{Sample}} = \left(\frac{{}^{18}O/{}^{16}O_{\text{Sample}}}{{}^{18}O/{}^{16}O_{\text{Standard}}} - 1 \right) \cdot 1000 \text{ ‰} \qquad \textit{Eq. 1}$$

The $\delta^{18}O$ of the calcitic organism shells is interpreted in terms of seawater-temperature, which can be determined by the following empirical equation (eq. 2).

Equation 2

$$T°C = 16.5 - 4.3 \left({}^{18}\delta O_c - {}^{18}\delta Ow\right) + 0.14 \left({}^{18}\delta O_c - {}^{18}\delta O_w\right)^2 \qquad \textit{Eq. 2}$$

In this equation $^{18}O_c$ reflects the foraminifera isotopic composition of calcite tests, whereas $^{18}O_w$ is the isotopic composition of the ambient seawater and pore water. Additionally, the isotopic composition of the seawater $^{18}O_w$ is a function of: (1) global ice volume and (2) river-water input and evaporation/precipitation (Katz et al., 2010; Hoefs, 2009). For example, a salinity greater than 3.5‰ in the ocean seawater, leads to higher ^{18}O values, as a result of the evaporation that leads to a depletion of ^{18}O in the vapour phase. During glacial periods, a great amount of water is stored in continental ice-caps or sea-ice, this ice is depleted in ^{18}O (Hoefs, 2009). In summation, a change in δO_w causes a simultaneous change in δO_c. Additionally, an increase of up to 1°C in seawater temperature (δO_w) leads to a decrease in (δO_c), of approximately 0.23 ‰ (Katz et al., 2010). Other authors Miller et al. (2008), Pekar et al. (2002), and Fairbanks and Matthews, (1978) used this relationship to estimate sea-level changes in the Eocene-Oligocene time. They found an empirical calibration of an average sea-level change of 0.10 to 0.12‰/10 m (Katz et al., 2010). For example, Barrera and Savin, (1999) used this approach to reconstruct temperature differences in the SST and the BWT in the time interval between 75 - 65Ma.

Sulphur

The sulphur isotopic composition of sedimentary sulphides has been widely applied to distinguish environments with high or low rates of bacterial sulphate reduction. In order to investigate variation in the oxygenation state and biogeochemistry of marine sediments, sulphur isotopy may provide information about (1) activity of sulphate reducing bacteria (SRB) (2) water column stratification (3) sedimentation rate via open/close system conditions (4) extent of water column anoxia.

Culture experiments with dissolved sulphate have shown that microbial sulphate reducing bacteria lead to a strong fractionation of the sulphur isotopes, with a strong depletion of ^{34}S in the produced hydrogen sulphide (Sweeney and Kaplan, 1980).

Our knowledge about the seawater value in Phanerozoic time is based on the premise that the sulphate value represents the seawater from which it originates (Strauss, 1997). According to this, the seawater value has been significantly changed from values as high as +30‰ (Cambrian) to lowest values during the Permian (ca. +10‰) and modern values at around +21‰ (Claypool et al., 1980). The different reservoirs of sulphur (seawater sulphate, sedimentary pyrite, organic matter, etc.) are characterised by variations in their $\delta^{34}S$ values (Baioumy, 2010; Bottrell and Coulson, 2003). The most important pathway, which affects the $\delta^{34}S$ of sulphur, is the reduction of (seawater) sulphate by bacteria and its fixation as pyrite in muds. Oxidative weathering of pyrite (mainly from shales) and its return to the sea as sulphate, as well as crystallisation of sulphate minerals in form of evaporites (mainly gypsum or anhydrite), is by far less important. The availability of reactive iron and decomposable organic matter, as well as sedimentation rate and the chemocline position, are important variables which affect the $\delta^{34}S$ values in sedimentary systems (Böttcher et al., 2000).

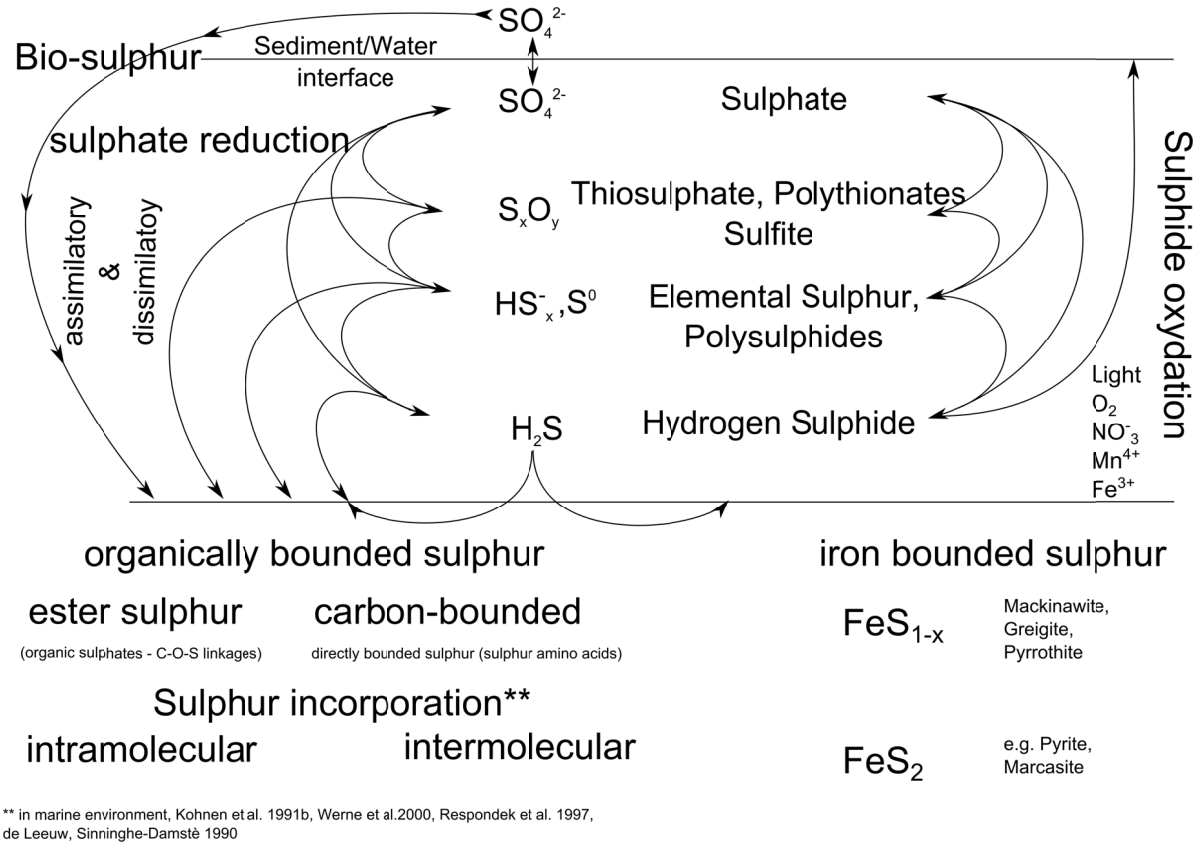

Fig. 16 Pathways for sulphur disproportionation in marine environment, modified after Werne et al. (2004), Canfield, (2001),and Fossing et al. (1995)

In marine anoxic and sulphidic environments, sulphate-reducing bacteria (SRB) reduce sulphate to sulphide. The change between open and closed system (e.g. by bioturbation) is the "classical" way to explain the occurrence of relatively high δ^{34}S-values in reduced sulphur species. High sedimentation rates or restricted water circulation conditions might result in restricted or closed to semi closed conditions, at which the pore-water sulphate and sulphide are not able to diffuse freely through the sediments. This leads to relatively heavy isotopic $\delta^{34}S_{pyrite}$ values of about -20‰ and smaller degrees in fractionation (Werne et al., 2003; Wijsman et al., 2001b). Therefore, small differences in isotopic composition between seawater sulphate and pyrite are indicative for closed or semi-closed systems of sulphate supply (Wijsman et al., 2001b). Compared to this, somewhat larger fractionations are associated with open systems conditions, with unlimited diffusion of seawater sulphate into the sediment.

Very high fractionations during bacterial sulphate reduction, leading to very strongly depleted H_2S, are lately explained by partial reoxidation followed by disproportionation of sulphur species with intermediate oxidation state, like thiosulphate, S°, etc. (Jørgensen, 1990), as shown in fig. 16. Sulphide (H_2S) can freely diffuse upwards through the sediment to the anoxic/oxic water interface to be reoxidised, in repetitive cycles (up to 90% of all H_2S). Common oxidants involved are oxygen, NO_3^-, Fe (III) or Mn (IV).

In addition, the activity of some specialised sulphide oxidising bacteria can be considered (*Beggioata spp.)* (Fossing, 1990). Sediments open to the supply of oxidants, repetitive cycles of sulphate reduction, oxidation and disproportionation, have been suggested to result in progressively lighter isotopic sulphur, of over 50 - 60‰ lighter if compared to the initial seawater sulphate (Canfield, 1994; Canfield and Thamdrup, 1994).

In general, large fractionation rates are often associated with open systems or small extensions with sulphate reduction in restricted systems. Small differences in isotopic composition between seawater sulphate and pyrite are an indicator for closed or semi-closed systems of sulphur (Wijsman et al., 2001b). Pyrite oxidation and reoxidation of HS^- can also lead to thiosulphates (Jørgensen, 1990).

Dissimilatory bacterial reductions from sulphate reducing bacteria lead to the accumulation of reduced sulphur (H_2S) in bottom water or pore water. Mostly, this is accompanied by the simultaneous formation of iron sulphides (if the system is not iron limited) and organic sulphur (Brüchert and Pratt, 1996). Because the pool of reactive iron is more susceptible for sulphurisation than organic matter (Raiswell and Canfield, 2012), a part of the sulphur can be incorporated into the organic matter, in an iron limited system (Werne et al., 2004).

In very special cases, e.g., the Namibia upwelling system, the H_2S circulates freely in dense unconsolidated diatomaceous ooze, and the concentration of H_2S can exceed 18 mmol/l (while normal H_2S concentrations in pore water seldom exceed 5 mmol/l). When changes in the atmospheric and oceanographic pressure fields occur, the gas can erupt from the bottom and will be released to the

overlying sediment/water interface. Such outgassing events within this area have been described by Monteiro and Roychoudhury, (2005), Emeis et al. (2004), Weeks et al. (2004), and from the St. Helena Bay/South Africa (Monteiro et al., 2008).

Carbon isotopy

Stable isotope composition of foraminifera ($\delta^{18}O$, $\delta^{13}C$) is one of the most used tools in tracing changes in the water column stratification, detecting changes in sea surface temperatures and variations in the primary production (Friedrich et al. 2012; Wilson et al., 2002). Recently, it is common to differ between two main approaches that include firstly, the use of $\delta^{13}C$ values of benthic and planktic foraminifera, which provide information on the carbon cycle of the ocean and changes in organic matter fluxes (Friedrich and Erbacher, 2006), and secondly, the use of $\delta^{13}C_{org}$ depends on the metabolic pathway that uses algae or plants (C3, C4). Their isotopic signature is very typical; therefore, conclusions about the composition and changes in the organic matter composition can be drawn.

The isotopic composition of carbon in marine matter adapts to variations in the ocean productivity, the concentration of CO_2 in surface water, the input of continental derived material (plant tissues), and the occurrece of diagenesis (Maslin and Swann, 2006).

The use of $\delta^{13}C_{org}$ as a proxy for organic matter source is devoted to the fact that each photosynthetic activity in the photic zone lowers the concentration of dissolved inorganic carbon (DIC) in the water column. All carbon that is stored in plants shows depletion, in relation to the PDB[6], resulting in negative (lighter) values. The degree of fractionation in C depends on the metabolic process in plants. Plants and algae prefer ^{12}C over ^{13}C for photosynthesis, due to the light values in ^{13}C of all organic matter (Maslin and Swann, 2006, Faure and Mensing, 2005). Organisms preferentially take up light ^{12}C, and have a $\delta^{13}C$ signature of about −25‰, depending on their metabolic pathway. For example, in upwelling areas, the

[6] reference standard value for carbon isotope ratio

organic matter reaches the seafloor, where it escapes from the euphotic zone as particle organic matter (POC), becomes oxidized, and underlies respiration by forming dissolved organic matter (DIC).

Because of the export of nutrients from the water surface down to the bottom, in upwelling areas, the upwelled water is enriched in $^{13}C_{org}$ values up to -25‰. Consequently, organic matter, including kerogen, petroleum, coal, and gas, adapts highly negative values too.

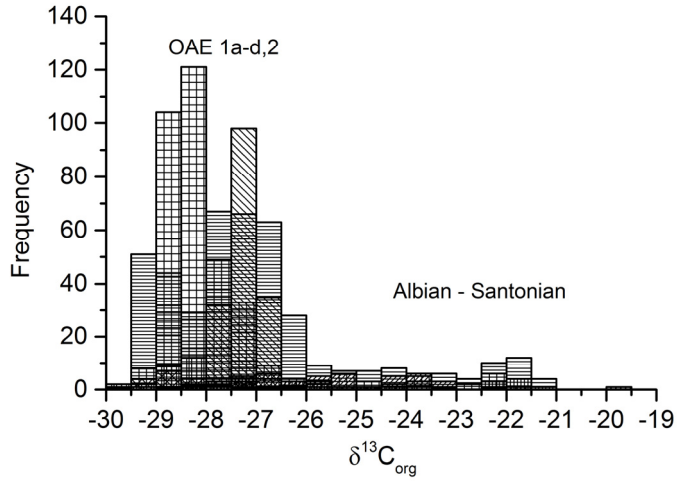

Fig.17 $\delta^{13}C_{org}$ in Upper Cretaceous time, preferentially in Oceanic Anoxic Event (OAE), that signifies an enrichment of light carbon isotopes, reference data are taken from (Beckmann et al., 2005b; Arnaboldi and Meyers, 2006; Dumitrescu and Brassell, 2006; Meyers, 2006; Friedrich et al., 2008; Sinninghe Damsté et al., 2008).

However as shown in fig. 17, the isotopic composition of organic matter in the Cretaceous time was discovered to range from -28‰ to -25‰ (Dean et al. 1986). Lightest ^{13}C enrichment in the earth`s history is often reported from Oceanic Anoxic Event (OAE). Such events have been repeatedly interpreted for the Cretaceous time in terms of a fast deposition (burial) of marine organic matter (algae).

Another goal arises from the use of carbon isotopy in calcite forming organisms. One of the best documented markers for differences in palaeoproductivity, is the difference between the change in $\delta^{13}C$ values in benthic and planktic foraminifera, obtained from the surface and the sub-surface/bottom water (Katz et al. 2010; Fischer and Wefer, 1999; Wefer, 1985).

The modern isotopic organic carbon composition of dissolved organic carbon in seawater is around 0‰ (Hoefs, 2009). Whereas the isotopic carbon composition in marine calcite forming organisms is around +2‰ to +3‰ (Maslin and Swann, 2006). It is noteworthy that the $^{13}C_b$, in benthic foraminifera, track the concentration of dissolved organic carbon in the pore water, whereas the $^{13}C_p$, in planktic foraminifera, is

used as a tracer for the surface productivity (Mackensen, 2008; Fischer and Wefer, 1999). However, differences in the isotopic carbon composition, between the surface and bottom water, can be used to track differences in the biological productivity (organic matter flux) in the ocean. This is due to the surface water being enriched with ^{13}C (more positive values), whereas the bottom water shows depletion in ^{13}C (more negative values). Consequently, the difference in the isotopic organic carbon composition between planktic and benthic foraminifera can be used to calculate the organic carbon transport from the surface to the bottom (Fischer and Wefer, 1999).

In order to evaluate surface water productivity, two or more planktic foraminiferal species that live in different depth and habitats can be used. So for example in the NW Arabian Sea, differences in the isotopic carbon composition of planktic foraminiferal species (*Globigerinoides ruber and Globigerinoides bulloides*) were used. These species live in different water depths, therefore displaying variation in the surface water productivity or the strength in the upwelled water, which are mainly controlled by the monsoon system (Peeters et al., 2002; Ganssen and Sarnthein, 1983).

Continuously, shifts in the isotopic carbon composition of marine carbonate organisms is similarly interpreted in terms of the buried organic carbon (Hoefs, 2009). As is shown in fig. 18, based on these considerations, (Friedrich et al. 2012), estimated positive $\delta^{13}C_{benthic}$ values (~6‰) in the Cretaceous time for different locations. Such exceptionally high values are explained due to the massive accumulation of organic rich sediments (black shales) during this time slice. Nevertheless, the data sets also display a continuously declining trend towards lighter values ~ 1‰ to the Maastrichtian time. For the research area, the early Maastrichtian time (shaded area) is represented by a cooling event. This is due to the rapidly decreasing trend in the bottom water temperature and an abrupt change in the organic matter accumulation. Such a rapid trend could be due to a reorganisation of the ocean current, caused by the opening of the Equatorial Atlantic Gateway (EAG) between Africa and South America (Friedrich et al., 2012). These data sets also contain estimates of the bottom water temperature $^{18}O_{benthic}$, as mentioned in

the previous section. The incorporation of oxygen into shells of foraminifera depends on the temperature and salinity of the surrounding water.

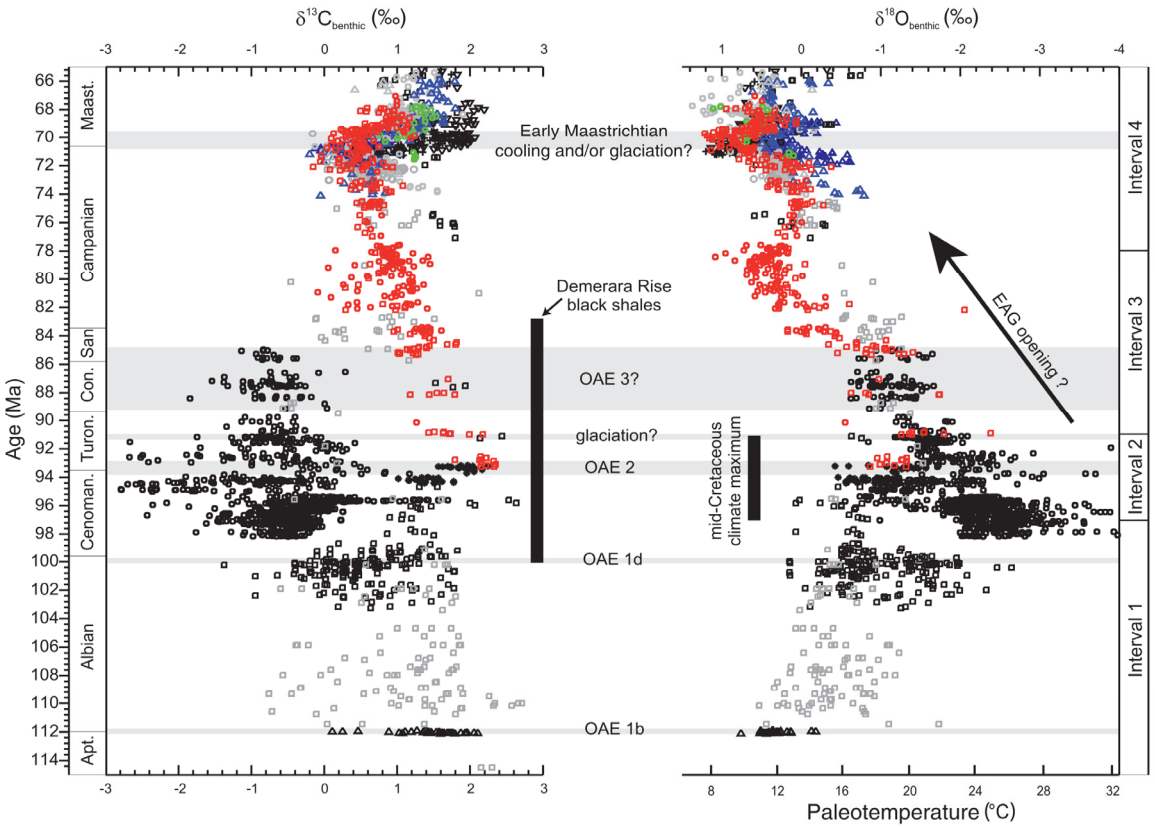

Fig.18 Stable oxygen and carbon isotope compilation of benthic foraminifera for 115–65 Ma. Black - North Atlantic Ocean, grey - high southern latitudes, red - Pacific Ocean, blue - subtropical South Atlantic Ocean, green - Indian Ocean. OAE - oceanic anoxic event; EAG - Equatorial Atlantic Gateway (Friedrich et al., 2012).

Trace elements in foraminifera, proxy for palaeothermometry- productivity, ph- value and salinity in seawater

Despite some limitation and unresolved problems, the use of Mg/Ca as an empirical proxy for palaeothermometry is widely accepted. More recently, numerous papers on the Mg/Ca relationship of planktic and benthic foraminifera have been published. Some example for this topic are the recent research work that was originally published by Branson et al. (2013), Griffiths et al. (2013), Fhlaithearta et al. (2010) and Hoogakker et al. (2009).

Former research that based on the work of Oomori et al. (1987) and on thermodynamic principles, Lea et al. (1999) predicted an increasing incorporation of Mg with increasing temperatures of about 3% per °C in foraminifera tests. However, cultured species of planktonic foraminifera (*Globigerina bulloides* and *Orbulina universa)* show an increase in the amount of incorporated Mg of up to 8 - 10% per °C. This range of values is consistent with results from marine sediments (Anand et al. 2003; Lea et al., 1999; Nürnberg et al., 1996).

Additionally, parameters which might affect the Mg/Ca control in the foraminifera shells are the pH and the salinity. Newer studies dealt with the influence of the pH on the calcification rate of foraminifera tests and on the incorporation of Mg and Sr. Allison et al. (2011) and Kisakürek et al. (2008) used cultured benthic calcitic foraminifera *Elphidium Williamsoni* to investigate the influence of pH (in a range from 7.8 - 8.3) on the incorporation of these trace elements. However, their results do not seem to be statistically significant. Unlike Russell et al. (2004), who found a Mg/Ca content in planktic foraminifera which is dependent on the pH (pH <8.2), Mg/Ca decreases by 7 ± 5% (*Orbulina universa*) and 16± 6% (*Globigerina bulloides*) per 0.1 unit increase in pH. Based on these results, the author concluded that above a pH of 8.2, no significant changes in the Mg/Ca composition were observed.

Hoogakker et al. (2009) and Ferguson et al. (2008) report a high Mg/Ca content in highly saline water from the Red Sea (7-13 mmol/mol) and the Mediterranean Sea (4-7mmol/mol). The authors conclude that this anomalously high content cannot be due to the incorporation of Mg in foraminifera tests, but this might be a secondary signal for the high Mg-calcite precipitation from $CaCO_3$ supersaturated interstitial water (this will be discussed in section 6.2 Mg-content in foraminifera).

Regarding the Mg content in tests of the low oxygen tolerating species *Bolivina spp*., Douglas and Staines-Urias, (2007) reports that the shell Mg/Ca composition differs between dead and living species. Living species show a higher amount in Mg/Ca than the dead one, and there is no trend to the temperature observable. These examples might show the controversial views about the use of Mg/Ca content as proxy for palaeothermometry.

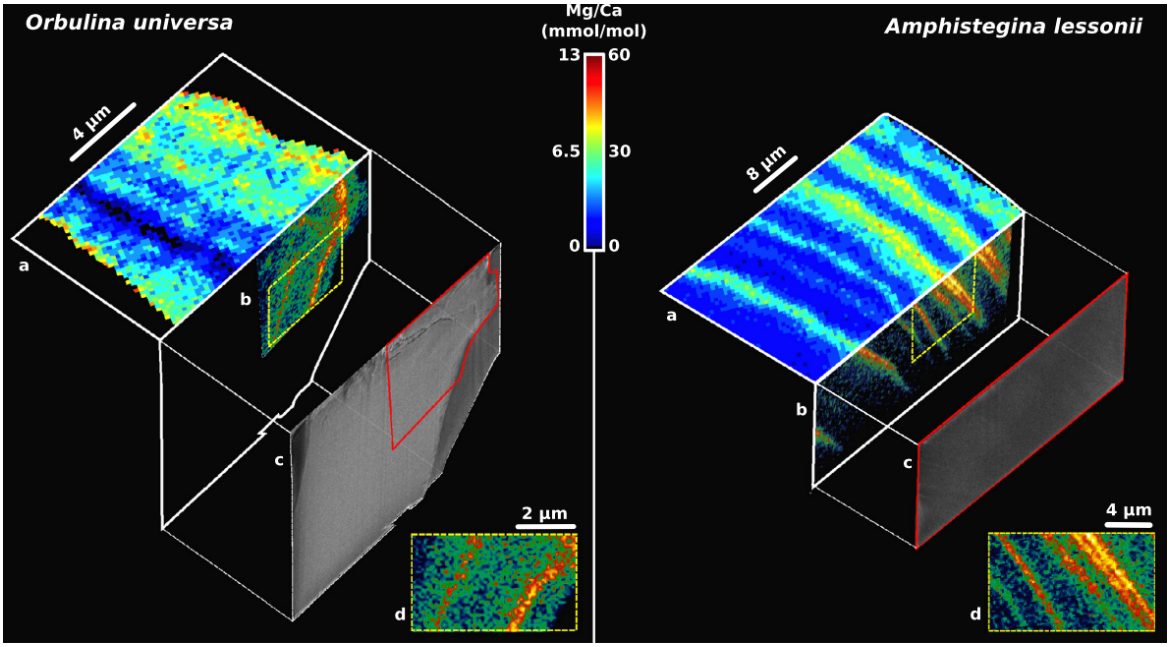

Fig. 19 The distribution of Mg in foraminifera. Electron microprobe maps of the samples reveal patterns of Mg/Ca banding within such bands, modified after (Branson et al. 2013)

In recent years there is an increasing wealth of evidence which suggests that one of the main factors which affect the Mg/Ca content in foraminiferal calcite is organic matter and bacteria. The latter is also known as "vital-effect" (biological control) (Ferguson et al., 2008; Lea et al., 1999; Mucci et al., 1985). However, one of the fundamental questions, namely the incorporation mode of Mg in foraminifera is still unresolved (Branson et al., 2013). In the last years, it has become more and more obvious that the incorporation of Mg goes hand in hand with elevated concentrations of organic molecules, sulphur, and trace elements (Erez, 2003).

New applications, for example, using Near-Edge X-ray Absorption Fine Structure Spectroscopy (NEXAFS) (Branson et al. 2013), electron microprobe mapping (Sadekov and Eggins, 2005) and particularly laser ablation – LA - ICP-MS (Eggins et al. 2004, 2003), confirm this notion and extend the common view about the use of Mg/Ca ratio for the palaeothermometry.

As shown in fig. 19, micro analytical investigations by LA - ICPMS have revealed bands of high and low Mg in tests of planktic and benthic species. Such bands of high Mg content dramatically exceed the amount of Mg, which is known to be incorporated by calcifying foraminifera (Branson et al., 2013; Eggins

et al., 2004, 2003). These results indicate that on band (high Mg) or off band (low Mg) alternations in Mg content are driven by the temperature and the kinetics of calcite growth (Branson et al., 2013). Such high-resolution investigations may be important to differentiate between distinct lifetimes of foraminifera and habitats in which they live.

In recent years, it has becomes more evident, that trace element incorporation in foraminifera tests is an important tool differentiate between different environments in which foraminifera live. Unfortunately, the exact mechanism in their incorporation is still unknown. Nevertheless, empirical research gives some insight in their behaviour in calcitic organism and conclusions concerning their life habitat.

To reach conclusions about the CO_3^{2-} saturation state in ocean water, Russell et al. (2004, 1994) used U/Ca content in tests of cultured planktic foraminiferal species (*Globigerina bulloiodes and Orbulina universa)* that note a correlation between the U/Ca content in cultured foraminifera species; U/Ca decrease exponentially with increasing seawater CO_3^{2-}content. This U content is explained by the incorporation of uranyl complexes or the reduced U adsorption at higher CO_3^{2-} seawater concentrations on the foraminifera shells.

The element copper has a strong affinity to organic compounds and therefore, it should not be surprising that incorporation takes place at high concentrations of organic matter in the sediment. Lead shows some similarity to copper. Thus, so far, the elements Cd, Ba, Zn are commonly used as proxy for palaeoproductivity, because they show a nutrient-type behaviour (Katz et al., 2010; Lea, 1999; Dehairs et al., 1980). For example, the Ba content is mostly connected to the decaying organic matter and to the release from phytoplankton (Dehairs et al., 1980).

However, the incorporation of Cd, Zn and Ba in calcite foraminifera tests is reported by Rosenthal et al. (1997), Boyle et al. (1995) and (Boyle, 1981). The incorporation of cadmium in foraminifera shells is independently of seawater temperature but varies in the degree of calcite saturation (Marchitto, 2004). Initially, it was assumed that Zn can be used as a trace of past seawater circulation, because zinc exhibits a

ten-fold difference between deep water in the North Atlantic and North Pacific (Katz et al., 2010). Otherwise zinc is sensitive to the degree of carbonate saturation state and therefore might be used as a proxy for deep ocean carbonate chemistry in benthic foraminifera (Bryan and Marchitto, 2010).

Clay mineralogy – a tool for determining changes in the weathering mode

Fluctuations in the abundance of clay minerals are a result of the combined effect of climatic factors, sea-level changes, and variations in source area as well as in transport mechanisms (Mallinson et al., 2003; Lamy et al., 1999; Deconinck and Chamley, 1995). Detrital smectite generally forms during continental weathering, whereas authigenic smectite results from alterations of volcanic glass and the transformation of feldspar to muscovite (Anderson, 2009; Mallinson et al., 2003; Deconinck and Chamley, 1995; Moore and Reynolds, 1989; Birkeland, 1984).

Moreover, the occurrence of kaolinite indicates high rates of chemical weathering under humid and warm climatic conditions (Bolle and Adatte, 2001; Chamley, 1989; Birkeland, 1984). Illite may be representative for colder, more arid climates, dominated by physical weathering, but may also be derived from an alteration of biotite under warmer and wetter conditions (Birkeland, 1984).

Aeolian/ Fluviatile input: Si/Al, Ti/Al, Zr/Al - detrital proxy.

These relationships are commonly interpreted and used to decipher between aeolian and fluviatile input. Their potential to discern between these two different kinds of mechanisms can be assessed by applying SEM to detect changes in grain size and shape (Calvert and Pedersen, 2007; Sageman and Lyons, 2003). So, for example, the use of the Si/Al relationship reflects the excess of silicon against aluminosilicates; nonetheless, silicon can be of detrital origin or biogeneous origin.

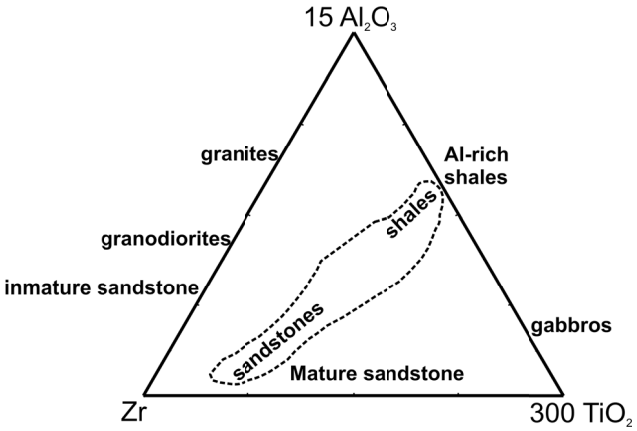

Fig.20 The ternary diagram display sorting-related trends in the Al - Ti - Zr relationship (oxides are expressed as weight percentage and Zr as ppm; Al_2O_3 is weighted by a factor 15 and TiO_2 by a factor 300 in order to centre the sedimentary cloud). Typical minerals are rutile, zircon, and ilmenite. The content of these minerals varies in response to the degree of weathering (leaching process) (modified after Garcia et al. (1994))

Changes in the sediment composition: ternary plot Zr, TiO_2, Al_2O_3

In weathering products, Al shows enrichment in micas and clays or in residual feldspars, whereas Ti is mostly hosted in mafic minerals (pyroxenes or amphiboles, and ilmenite) and partly felsic minerals, for example rutile. Additionally, Zr is mostly hosted in the mineral zircon ($ZrSiO_4$). During the transport of these elements, their composition underlies no modification. Subsequently, this leads to the accumulation of immobile elements, such as Al, Ti and Zr. However, (Hayashi et al., 1997; Garcia et al., 1994) could show that there is no significant deviation of the Al_2O_3/TiO_2 ratio in shales/sandstones relative to that in their parent rocks. The material will be sorted according to the hydraulic properties of the host material (Zr/Ti bearing minerals). Felsic or mafic rocks, or immature volcanic rocks, will plot into different fields in this diagram (Khider and McQueen, 2005; Garcia et al., 1994) (fig. 20). The application of this relationship is shown in section 5.1.

Trace element proxy to detect changes in the oxygenation state of marine sediment

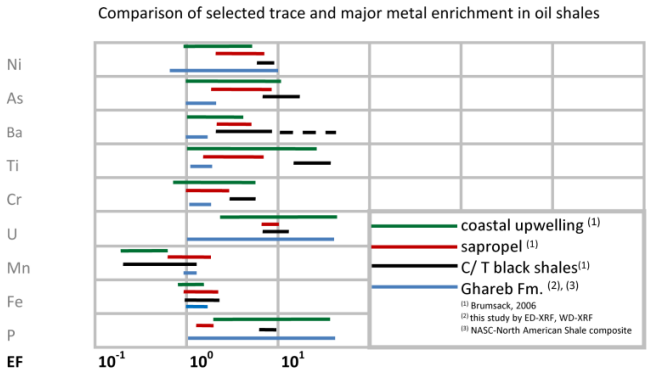

Fig.21 Graph shows the comparison of selected minor and trace elements in relation to their setting - modified after Brumsack (2006)

Figure 21 shows a comparison of the enrichment factors (EF) of major and trace elements in different marine settings as well as the research area. Obviously, their EF displays some differences in relation to their depositional setting. Many trace elements follow different pathways on the way down the sediment. Trace elements in seawater can exist in a variety of physical and chemical forms. The simplest physical distinction is particulate (metals adsorbed onto particle surfaces) versus dissolved forms (soluble complexes and colloidal forms), (Bruland and Lohan, 2004; Bruland et al. 2001). The concentration of trace elements in seawater range from ~10^{-6}mol*kg^{-1} - 10^{-15}mol*kg^{-1} (Henderson and Henderson, 2009; Bruland and Lohan, 2004; Wedepohl, 1969-1972; Turekian, 1968). Their chemical behaviour in the seawater is in first order influenced by three processes: (1) complexation, (2) biological assimilation, which requires the biological uptake on the cell surface and (3) adsorption on the surface sites of suspended particles (Bruland and Lohan, 2004). Based on these three processes, Tribovillard et al. (2006), Bruland and Lohan, (2004), and Mongenot et al. (1996) and other authors, grouped trace elements in four categories (conservative-type-, nutrient-type-, scavenged-type-, hybrid-type distribution) depending on their distribution in the seawater.

A first approach to detect changes in the state of oxygenation at the seafloor was the analyses of trace elements that change their valence state in distinct environments. Sources for authigenic trace elements (Cd, Ag) are organic matter, whereas the seawater itself act as the main source for Mo, and U. In turn, other elements fall between these two categorizes and show a nutrient type behaviour amongst these are

Cu Cr, V, Ni, , Zn, Co (Calvert and Pedersen, 2007; Tribovillard et al. 2006; Piper, 1994). On the one hand Cr, V, and U occur in oxic environments as soluble species. On the other hand, in an anoxic surrounding they are able to change their valence state to lower valence and high insoluble species. In the presence of H_2S some elements (chalcophile elements, like Ag, Cu, Ni, Zn, Cd), are precipitated by forming insoluble sulphides (Huerta-Diaz and Morse, 1992, 1990). The combined use of U, Mo, and V, allows deciphering between anoxic-suboxic conditions.

Uranium

Uranium in seawater is present mainly as U(VI) in the conservative form of uranyl ions that bind to carbonate ions, forming $UO_2(CO_3)_3^{4-}$ (Tribovillard et al., 2006). The major source of uranium is the seawater itself; it contains up to 0.0033 ppm U (Turekian, 1968). Borchers et al. (2005), reported from the Namibian diatom ooze an average U content of 30µg/g. Variations in the uranium concentration of sediment with time are controlled directly by the uranium content of the source material settling from the water column and indirectly by the organic content of this material and the sedimentation rate (Klinkhammer and Palmer, 1991; Crusius and Thomson, 2000; Anderson et al., 1989; Anderson, 1987). On the other hand McManus et al. (2005) and Zheng et al. (2002) reported, that in an reducing environment, uranium can be removed from the overlying water column by forming organo-metallic ligands and humic acid. In pore water, the removal of uranium is induced by bacteria by the reduction from soluble U^{6+} to less soluble U^{4+} (Boonchayaanant et al., 2009; Sani et al. 2004; Lovley and Phillips, 1992; Lovley et al., 1991). Consequently, in terms of a normal alkalinity of seawater and pH ranges, the reduction of uranium takes place under conditions, which are similar to those of Fe^{3+} to Fe^{2+} (Chaillou et al., 2008; McManus et al., 2005).

Vanadium/Nickel

Nickel (Ni^{2+}) and vanadium (VO^{2+}) are often found in mixed tetradentates, humate complexes, and tetrapyrole (organometallic) complexes. The latter one show highest thermal stability (Lewan and

Maynard, 1982). Vanadium and nickel are the most abundant trace elements in crude oil, in thermally inmature rocks and in buried sediments (Louda and Baker, 1981; Hodgson et al., 1968). They occur preferentially as (organometallic) porphyrin complexes, which originate from chlorophyll degradation (Killops and Killops, 2005; Barwise, 1990; Lewan, 1984; Lewan and Maynard, 1982). Under anaerobic conditions these tetrapyrole complexes and the organic matter show a high preservation grade and a high resistance against weathering and microbial degradation (Davis and Gibbs, 1975). A systematic enrichment of nickel over vanadium has been observed in different crude oils, organic rich sediments and in shales. On basis of the work of Lewan, (1984), many other authors have used the Ni/V cross plots to define the source rock or the environment. For example Barwise, (1990) could show in crude oils a systematic variation in nickel – vanadium content, which is in close relation to source rock typ and the deposition environement. Their interpretation of this relationship in terms of a definition over the palaeoenvironment based on the premise that there is an change in the input of the porphyrin- precursor of chlorophylls to the organic matter that is mainly derived from marine algae and bacteria. Differences in the relation between Ni and V can be used to distinguish between marine or non – marine sourced oils (Barwise, 1990).

Molybdenum/C_{org}

Because of its redox sensitive behaviour, molybdenum is strongly enriched in organic rich sediments deposited under oxygen-depleted conditions (Algeo and Lyons, 2006). There is a vast literature about the geochemical behaviour of Mo and its use as a proxy for palaeoredox conditions (Algeo and Lyons, 2006; Siebert et al., 2003; Zheng et al., 2000; Morford and Emerson, 1999; Helz et al., 1996; Calvert and Pedersen, 1993; Emerson and Huested, 1991). Two main specifications exist, firstly oxic conditions favour the occurrence of unreactive molybdate oxyanions MO_4^{2-}(Algeo and Lyons, 2006). Secondly, in anoxic environments the organic detritus and Mn/Fe oxyhydroxides are able to scavenge Mo (OM act as a simply carrier for iron and other trace elements) and its deposition in the sediment (Tribovillard et al. 2004). Along a redox gradient from the bottom water, Mo diffuses into the reducing sediment, where it

precipitates (Emerson and Huested, 1991). Another possibility for the fixation of Mo arises from the complexation as particle reactive thiomolybdates in marine anoxic sediments. That is explained by the longer exposure time to a critical concentration (switch point 11μM S^{2-}) of H_2S, this promotes the scavenging of Mo by humic materials and iron-rich phases (Zheng et al. 2000; Helz et al., 1996).

The Mo/C_{org} ratio and the slope of the regression line show different values in silled basin environments. Algeo and Lyons (2006) used these differences in the slope of regression line to define this as a palaeo-redox proxy. Their approach is based on the premise that in anoxic silled basins the slope of the regression line depends on the water mass circulation pattern. It is thought that in environments with restricted water mass circulation, and in absence of an adequate re-supply the concentration of dissolved Mo in the water column becomes more and more depleted (Algeo and Lyons, 2006). Such an environment is defined as restricted in respect of surface (subpycnoclinal) water renewal/depletion. Algeo and Rowe, (2011) and Algeo and Lyons, (2006) have applied cross-plots of sedimentary Mo/C_{org} to distinguish among environments with different rates of replenishment of Mo (deep-water renewal time - τ). A completely isolated water body in such basins leads to a decrease of the rsMo/TOC[7] ratio. McArthur et al., (2008) note that the implementation of this method is allowed only for (weak?) euxinic conditions. Another note concerns the validity of this method for upwelling areas. Most upwelling systems lacks topographic barriers, which usually are characterized by a highly variable hydrographic regime. Topographic barriers generally act as a bondary for oxygen deficit in the water column. Most upwelling regimes are located within open-marine systems, with no restricted water mass circulation. Based on these considerations, the deep-water renewal time off the Namibian shelf was estimated to be below one year (Algeo and Lyons, 2006). The application of this proxy will be presented in section 4.1

[7] regression slope in the relationship between molybdenum (Mo) and total organic matter (C_{org})

Degree of pyritization (DOP)

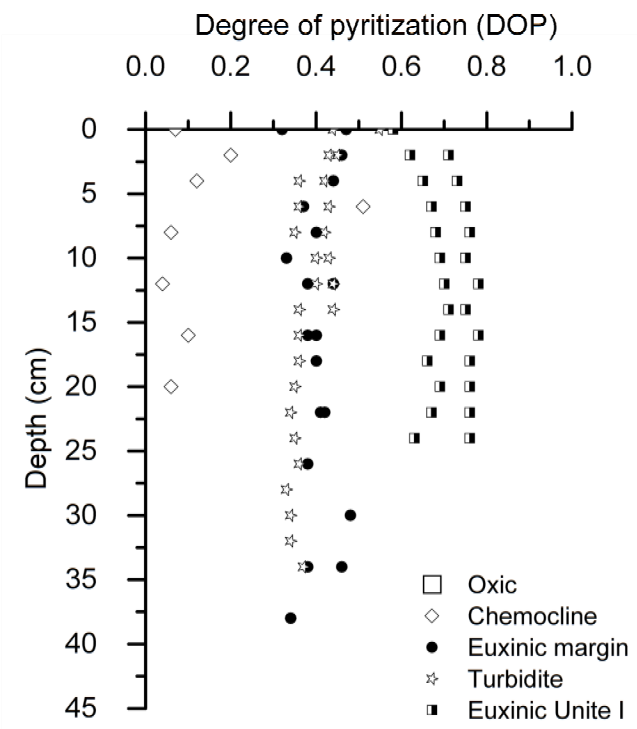

Fig.22 Degree of pyritization from Black Sea sediments- data source (Lyons and Severmann, 2006) DOP is defined as: $\frac{Fe_{pyrite}}{Fe_{pyrite}+Fe_{reactive}}$

Berner (1970) defined the DOP as a relationship between the pyrite bonded Fe, the sum of pyrite bonded Fe, and Fe which is soluble in HCl (Fe_{HR} – highly reactive iron). The degree of pyritisation (DOP) is defined as: $\frac{Fe_{pyrite}}{Fe_{pyrite}+Fe_{reactive}}$. This is one of the most reliable indicators of euxinic/sulphidic conditions in bottom-water oxygenation in organic bearing rocks, see also fig. 22 (Lyons and Severmann, 2006). Thus, the DOP represents the proportion of the original sediment`s Fe_{HR} that has been converted to pyrite (Raiswell and Canfield, 2012). Possibilities arise from the introduction of a series of proxies that deal with the amount of reactive iron (Fe_{HR}), which subsequently forms pyrite; see also Raiswell and Canfield, (2012), Lyons and Severmann, (2006) and Poulton and Canfield, (2005). Such an example is given by the use of a Fe_{HR}/Fe_T and inorganic carbon, and Fe_{HR}/Fe_T that is plotted against the DOP. This application allows the differentiation between anoxic and euxinic conditions in the bulk sediment, which is extensively discussed in section 5.3 (Shen et al., 2002; Raiswell and Canfield, 1998; Canfield et al. 1992).

Chemical constituents in pore water

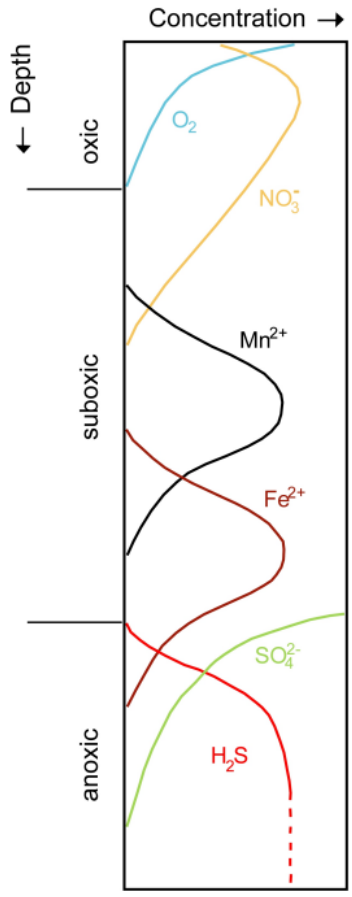

Fig.23 Schematic redox trends in the water column and pore water modified after Diener, (2012) and Rickard, (2012).

Usually, anoxic/ suboxic sediments or water columns show a stepwise decline in the oxygen concentration. In order to gain energy and maintenance their life, depending on their electron potential, microbenthic communities using electron acceptors other than oxygen (Murray and Yakushev, 2006). This is shown in in fig. 23 displaying an idealised cross section at the sediment water interface. The **oxic zone** (300 – 400µM O_2) persists until all O_2 is exhausted, and is controlled by the amount of organic carbon that is consumed by microorganism and stored in the sediment. After exhaustion of all the oxygen, in a stratified water column or undisturbed sediment, a cascade of chemical reactions is initiated. This depends on the supply of various electron acceptors in the order of their decreasing electron potential. The **suboxic** region follows below and is characterised by high dissolved manganese (10µM - 100 µM) and iron (25 nM - 10 µM) concentrations. In the **anoxic** zone S^{2-} occurs. Permanently anoxic basins are defined as environments with less than 6 - 10 $MO_{2(aq)}$, which also contain sulphide minerals in the scale between micrometre to millimetre. In the anoxic zone, the formation of pyrite can take place especially close to the interface of Fe^{2+} and H_2S curves. Within the sulphate-reducing zone the H_2S concentration ranges in micromolar units. Euxinic conditions will start at circumstances in which all measurable O_2 disappears and the onset of measurable S^{2-}.

In marine environments, bottom sediments are dominated by the occurrence of bacterial mats. Sulphate-reducer (*Thioploca spp.*) Fossing et al. (1995) and sulphide-oxidising bacteria (*Beggiatoa spp.*) (Canfield and Desmarais, 1991) usually dominate these bacterial communities. They mostly occur below the OMZ.

Such mats are either distributed in patchy areas or covering the whole bottom sediment, which is reported from the Peruvian upwelling zone (Bohlen et al. 2011; Mosch et al. 2010; McCaffrey et al. 1989), NE Arabian Sea (Erbacher and Nelskamp, 2006; Schmaljohann et al. 2001), Baja California (Fike et al. 2009), and Namibian coastal zone (Brüchert et al., 2003).

Alteration of primary signals

An accurate reconstruction of the palaeo-bottom water is hampered by the alteration of metals that are sensitive to oxygen. In order to be able draw meaningful and valid conclusions, the pristine environmental signals, carried by proxies/indicator parameters, should not be affected/changed during diagenetic or post-diagenetic processes.

Several processes affect the environment in their later stage of diagenesis. This comprises firstly the compaction by drainage dissolution or formation of sulphides according to their environment of the pore waters, and secondly, in the course of the oxidative dissolution by which sulphuric acid is created, a conversion of calcium carbonate component to gypsum ($CaSO_4 * 2H_2O$) is commonly observed. Within such a milieu, the formation of paramorphism, e.g., calcite to pyrite/anhydrite/halite may also occur. Upon the oxidation of pyrite, oxide residues in form of diffuse russet areas, and partially rounded particles of FeOOH, remain in the sediment. A further dissolution of the carbonate component by stagnant pore waters, because of the higher solubility of aragonite, leads to a preferred loss of aragonite from the sediment. This might lead to the formation and precipitation of a calcitic matrix. Further consequences are (1) reduction of pore volumina and grain growth, (2) transformation of aragonite to high magnesium calcite – low magnesium calcite, and (3) growth of idiomorphic calcite and dolomite.

According to the processes described above, samples should display diffuse organic matter (OM) in a dark brown and black colouration matrix, rather than well shaped black/dark brown particles (Riboulleau et al., 2003). Regarding certain trace element compositions, those are sensitive to the exposure of oxygen (chalcophile elements). All these processes significantly alter the composition of sediments. Upon further

diagenesis, it is important to note that the authigenic formation of minerals is the most substantial process that changes the pristine diagenetic signal.

An example of how alteration affects the sediment composition, during several stages of diagenesis, is given in equation 3, which shows the authigenic formation of opal, muscovite/illite (Madsen et al., 2010; Anderson, 2009; Noe-Nygaard and Surlyk, 1985; Spiro and Rozenson, 1982). Which includes the transformation of metastable phases into a stable phase: opal-A → opal-CT → quartz/cherts.

Equation 3

$$\frac{3}{2}KAlSi_3O_8(s) + H^+ \rightarrow \frac{1}{2}KAl_3Si_3O_{10}(OH_2)(s) + SiO_2(aq.) + K^+ \quad Eq.\ 3$$

K-feldspare muscovite opal CT

Apart from this, diagenesis also leads to the dolomitisation, as commonly observed in carbonate-rich, bio-siliceous deposits, which might start from a decomposition of organic matter by microbial attack. Such a process leads to an increase of pH, a dissolution of carbonates, lowering of SO_4^{2-} in pore water, and a subsequent release of Ca^{2+}, Mg^{2+}, CO_3^{2-}, resulting in the precipitation of dolomite (Roberts et al., 2013; Bontognali, et al., 2010; Wang et al., 2009; Wright and Wacey, 2005; Wright, 1999; Vasconcelos and McKenzie, 1997; Vasconcelos et al., 1995).

3. Material and Methods

3.1. Lithostratigraphy of the Mishor Rotem Section

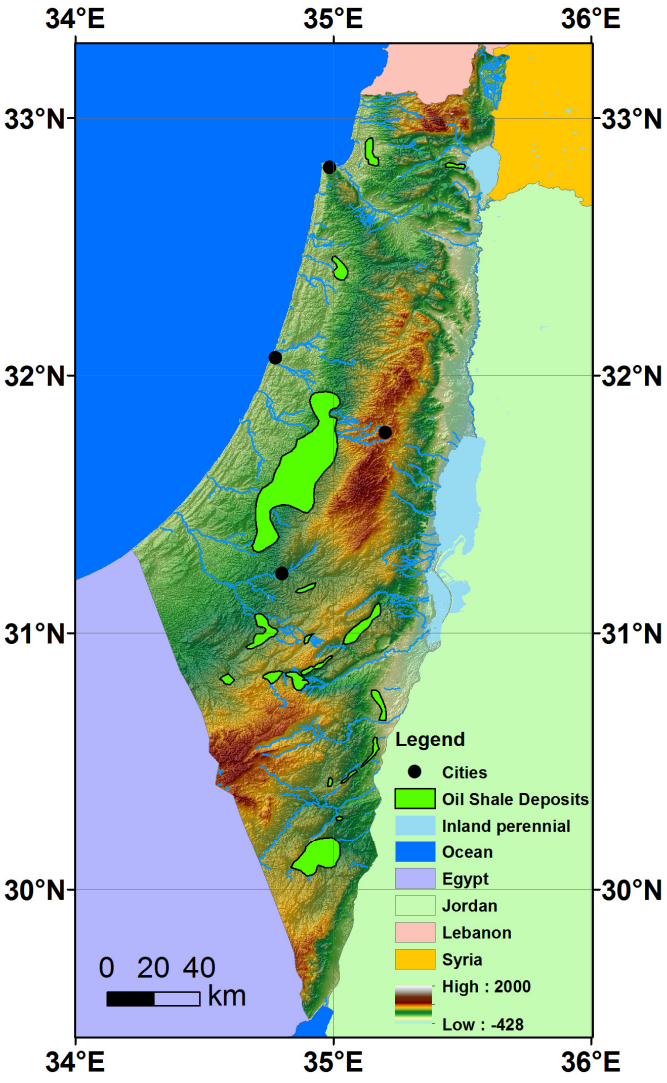

Fig.24 Overview of the Israeli oil shale resources modified after Minster, (2009)

The largest oil shale deposits in Israel can be found in the Shefela basin, with estimated reserves that contain roughly 150 billion barrels of oil (60% of the Saudi reserves), of which 40 billion barrels are situated within the Israeli area (http://iei-energy.com).

Nevertheless, Late Cretaceous deposition in southern Israel took place in tectonic controlled northeast trending shelf basins, as shown in fig. 24 (Almogi-Labin and Bein, 1993). The oil shales were deposited over a time interval of approximately 12.2 Ma (Gradstein, 1999). Sediment deposits, which are well exposed in the Mishor Rotem quarry, represent the transition from the Mishash formation to the Ghareb formation. The section spans a time interval from the Upper Campanian to the Lower Maastrichtian and covers a time slice of up to 1.42 Ma, with a sedimentation rate of approx. 2.4 cm/ka (Ashckenazi-Polivoda et al., 2011). From base to top, three units can be distinguished. These comprise of a phosphorite layer at the base (Mishash fm.), followed by the organic-rich chalks, and the Marl Member (MM) at the top. The top of the Phosphorite

Member (PM) (top of the Mishash fm.), consists of fluor-apatite and a low TOC content, in a 1 - 4 wt. % range. Fish skeletons, oval phosphates, and gypsum occur, and bone fragments, peloides and fecal pellets, are the main constitutens of this sequence (Soudry et al. 2006). A condensed layer of a ca. 0.9 m thick horizon marks the transition from the Mishash fm. to the Ghareb fm. Within this unit dolomite (20 wt. %), fluorapatite (45 wt. %) and calcite (30 wt. %) can be found, and the TOC content drops below 2 wt. % (Bein et al. 1990). Moreover, no foraminiferal assemblages are placed within this horizon (Ashckenazi-Polivoda et al., 2011). The Ghareb fm. starts with a monotonous section of dark-grey colour. This unit, termed as Oil Shale Member (OSM), is composed of organic-rich carbonates – carbonate rich mudstone with an average carbonate content of 50 - 75 wt. %. At the base, the organic matter content rises fast up to 15 wt. % (Reiss et al., 1985). A sharp change in colour from dark-grey to light-yellow signifies the contact of the OSM and the Marl Member (MM), which contains well layered limestone, biomikrite, dolomitic- and phosphatic marls, with a calcite content of up to 60 - 75 wt. % (Ashckenazi-Polivoda et al., 2011; Reiss et al., 1985).

3.2. Sampling

The samples were taken from an open quarry in the Negev Desert. This area is located in the Mishor Rotem (Efe`s syncline 31°04’51.82"N; 35°10’02.85"E), which belongs to the owner Rotem Amfert Negev Ltd. However, the biggest oil shale reservoir in Israel is disclosed there (Ashckenazi-Polivoda et al. 2011; Minster, 2009). The location is a part of the ZIN basin, which has an elongated shape, is about 23 km in length, and covers an area of ca. 70 km^2, with proven reserves of several billions of m^3 (Yoffe et al. 2002). Organic matter in the Negev desert normally shows a high oxidation grade. For this reason, several of these locations are not suitable for organic geochemical, biostratigraphical analyses and analyses of stabile isotopes. One exception is disclosed in the Mishor Rotem quarry; the rocks show less thermal maturity and well preserved microfossils.

3.3. Sample preparation and analytical methods

3.3.1. Bulk samples

Mineralogical composition

The bulk mineral composition of the samples was analysed by means of X-ray diffraction (XRD) analysis (Kristalloflex D500, Siemens, Germany) at 40 kV and 25 mA in a 0 - 2θ geometry. $CuK\alpha_1$ - radiation was used at angles between 3° and 63° with an increment of 0.02°, resulting in a continuous scanning of 0.5° per minute. The detection limit is about 1 wt. %. Crystallographic identification based on 2θ–peaks was done with QualX, version 1.2, by using the American Mineralogist Crystal Structure Database for the reference peaks. The main mineral occurring in the oil shale samples is calcite. To detect further minerals, which can be masked by calcite or diluted by organic matter, the samples were treated with 3.5% peroxide and afterwards with 10% hydrochloric acid to remove organic matter and carbonate.

Chemical composition

Energy dispersive X-ray fluorescence analysis (ED-XRF)

50 to 100 g of each sediment sample were ground with a vibratory (agate) disc mill and dried at 110°C for 24h. Concentrations of trace elements (V, Cr, Ni, Cu, Zn, Ga, As, Rb, Sr, Y, Zr, Nb, Mo, Cd, Ba, La, Ce, Pb, Th, U) and some major elements (SiO_2, TiO_2, Al_2O_3, Fe_2O_{3tot}, CaO, MnO, K_2O, SO_2, P_2O_5) were determined by means of energy dispersive X-ray fluorescence (ED-XRF), using an Epsilon 5 spectrometer (PANalytical). For the analyses, spectro-cups were filled with 5 g of the powdered sample material and subsequently sealed with 6 µm Mylar film. Signal stability was monitored by measuring a variety of reference materials (AGV-1P, GXR-2, GXR-3, GXR-4, GXR-5, GXR-6, SCO-1, SDO-1P, SCO-1, SL1, SOIL V, SOIL VII). Precision varied between 1 and 3%. Whereas the accuracy varies between 1 - 3ppm, exceptionally Ba (51ppm), and V (7ppm).The detection limits range from 1 to 5 ppm, higher detection limits apply only to Cr (10 ppm) and V (50 ppm).

(WD) X-ray fluorescence analyses (Wavelength Dispersive- XRF)

To complement the element spectrum (MgO, Na_2O), additional measurements were carried out by wavelength dispersive (WD) - XRF on a selected set of samples, using a S4 Explorer WD-spectrometer (BrukerAXS, Germany). Prior to the WD-XRF analyses, exactly 0.5 g of the sample material was calcinated at 950°C to assess the loss on ignition (LOI). Fused glass discs were prepared by mixing the calcinated material with SPECTROFlux (Alfa Aesar, Germany) in a weight ratio of 1:10. Standards from certified reference materials (AGV-1, SDO, BHVO) were prepared, following to the same procedure, and run simultaneously with the samples. Accuracy was found to be within 10% of the certified values of the reference materials, while the precision was better than ±0.1 wt. %. For Si, Ti, Al, Fe, Ca, and P, the WD- and ED-XRF data correlate very well (r >0.97). Considering the higher accuracy of the WD measurements, the ED-analyses were corrected, according to the regression equation established between the two sets of analytical data.

Determination of total sulphur (S_{total})

Sulphur values were obtained by analyses with an Eltra-Element Analyser CS 2000 using a broadband non-dispersive IR cell. Samples were crushed and ground to pass through a >63 µm sieve. Approximately 250 mg were used for the sulphur determination in samples with a lower carbonat content, while 110 mg were used for samples with higher carbonate content. The method is based on sample-combustion and the measurement of the resulting gas via infrared absorption. Used standards were the Eltra cement standard 90811-13 and 90811-81, respectively. Repeated measurements indicate an analytical precision of ±2.1% (90811-81) and ±0.5% (90811-13), whereas the detection limit is 100 ppm, respectively.

Determination of highly reactive iron (Fe_{HR})

The amount of reactive iron was assessed using the dithionate method (Raiswell et al. 1994, Canfield, 1989). A buffered solution of pH 4.8 was prepared from 68.8 g/L tri-sodium citrate dihydrate ($C_6H_5Na_3O_7$* $2H_2O$) with 0.35 M acetic acid and 0.2 M sodium citrate. The extraction was carried out by treating 0.2 g of sediment with 50 ml of buffered dithionate solution for 2h, before the Fe concentration was determined. Inductively coupled plasma optical emission spectroscopy (ICP-OES) was initially used for the analysis of Fe with a Varian 715-ES instrument. Iron was measured at a wavelength of 238.204 nm. The average of three measured values was taken. The reference standard CertiPur (VWR), containing 1 g/L of Fe, was used, with the detection limit for Fe of 1 µg/L. Repeated measurements indicate an analytical precision of ±0.04% (double standard deviation).

High-resolution inductively coupled plasma mass spectrometry (HR-ICP-MS)

The element contents (Mg, Mn, Fe, Co, Ni, Cu, Zn, As, Rb, Sr, Mo, Cd, Ba, Pb, U) in foraminifera tests were performed with a double focusing single collector mass spectrometer; inductively generated plasma served as ion source (Axiom, VG Elemental, UK). All measurements were done by using a micro concentric atomiser (flow rate ~100 µL/min), a Scott-spray chamber and nickel cones. The measurements were carried out in the magnetic scanning mode, which uses both the electrostatic and magnetic influence of the ion beam.

The concentrations were calculated as the mean of three measurements from the sample. The detection limit for each selected trace element is described in section 10. The calibration standard was a High Purity Standard with a stock solution of 1000 mg/L (± 0.4%) and a dilution factor of 10. The accuracy of the measurements was calculated with a reference solution in form of certified multi-element standard within 1% HNO_3 matrix (HPS = Certified Reference Material-Trace Elements in Drinking Water, CRM-TMDW). The trace metals of the high purity standard (Promochem, HPS) were measured after calibration and after measurement of the samples. All samples were diluted in 2 ml, 1 ml respectively of 1% HNO_3

solution. The detection limit for each element can be obtained from tables 29, 30, in the appendix. The relative standard deviations (RSD) amounted to 0 - 9.43% (Zn). With regard to the precision of the double-focusing sector field SF-ICP-MS (Axiom, VG Elemental, UK), the RSD of the three sample measurements was calculated and amounted to values between 1 and 3%.

Wet chemical extraction of different bond of sulphur species

Extraction of the following five fractions of the sample has been carried out: **acid volatile sulphides (AVS)** primarily including *Fe-monosulphides, (mackinawite, pyrrothite, greigite*); **acid soluble sulphates (ASS)** including *gypsum, anhydrite*; **$CrCl_2$ reducible sulphides** (*CRS)* consisting of disulphides, mainly in form of *pyrite*; **organic sulphur** including intramolecular bonded sulphur (extracted with Thode solution); **intermolecular bonded sulphur**, removed with Eschka mixture.

Introduction to extraction techniques

A completely selective extraction of sulphur from sediments is not possible. This also counts for the extraction of monosulphides by means of $SnCl_2$ and HCl. The degree of extractability of different kinds of bonded sulphur (including monosulphides) is depending on a number of factors, such as the grain size of the material. However, because of the low concentrations, mostly below one percent in sediments and a low particle size, “traditional” techniques, for example x-ray diffractometry and the sample-examination by microscopy, are not helpful for quantifying sulphur minerals in the bulk sediments (van der Veen, 2003; Morse et al., 1987; Cornwell and Morse, 1987).

For iron sulphide digestion, several techniques have been developed, which are based on the premise that iron monosulphides dissolve in acid (mostly HCl) faster than pyrite under similar conditions. In order to quantify the concentration of total reduced sulphur (H_2S, S^0, AVS, FeS_2) in sediments, a combination of HCl+$CrCl_2$ is mostly used (Zhabina and Volkov, 1978).

The extraction steps of bonded sulphur from marine sediments are described in (Rickard and Luther, 2007; Groot, 2004; van der Veen, 2003; Cornwell and Morse, 1987). According to the cited authors, the analysed samples may contain:

Monosulphide (FeS_x; $0.9<x<1.5$; $Fe^{2+}S^{2-}$)

This group includes minerals like mackinawite, pyrrhotite, and greigite, respectively. Monosulphides are considered to be soluble in HCl, whereas pyrite (disulphide) is not (Morse et al., 1987).

Mackinawite (FeS) is a Fe(II) sulphide that occurs mainly in marine and limnic sediments, and is commonly viewed as most important precursor of pyrite. Mackinawite show a higher solubility compared to pyrite. Dissolved species can be oxidised very quickly under oxygen-rich aqueous conditions. A conversion of mackinawite to greigite and subsequently to pyrite is also possible (Rickard and Luther, 2007). Mackinawite may contain amounts of Ni, Co, and Cu (Morse et al., 1987).

Pyrrhotite (Fe_{1-x} S; $x \approx 0–0.2$) According to (Rickard, 1995), pyrrhotite comes along with pyrite and greigite in oily sediments. A treatment of the sample with HCl will lead to the formation of hydrogensulphide, if pyrrhotite is present. So pyrrothite is recognised as part of the AVS group, alongside other monosulphides. The mineral is not commonly identified in anoxic marine sediments (Cornwell and Morse, 1987).

Greigite (Fe_3S_4)

Greigite is preferably observed in recent freshwater, brackish water and marsh sediments. For example, the Baltic Sea (Böttcher and Lepland, 2000) and Framvaren Fjord (Cutter and Kluckhohn, 1999). Greigite is a lot more sustainable in lacustrine environments because of the low concentrations of dissolved sulphur species, in contrast to the marine area. The conversion of greigite to pyrite in freshwater sediments thus takes place more slowly and incompletely (van der Veen, 2003;Wilkin and Barnes, 1997). Nevertheless, greigite is also observed in marine settings, for example the Black Sea (Lewis and Landing, 1991). Newer

results indicate a greigite formation in sediments from the continental margin of Oman and the California upwelling region (Rowan et al., 2009).

As noted above, greigite is detected in the sediment as AVS by means of hot hydrochloric acid. The addition of $SnCl_2$ increases the amount of extracted greigite, but in this case poorly crystalline pyrite will partially also dissolve (Morse et al., 1987).

Iron disulphide (pyrite - cubic, FeS_2)

Annually, 5 million tons of pyrite is produced in the world's oceans. Pyrite is the most abundant iron sulphide on the surface and it is stable in the absence of oxygen (Rickard and Luther, 2007; Berner, 1970). For the formation of pyrite, in addition to sulphate, degradable organic matter and reactive iron compounds are needed (Marnette et al., 1993). Pyrite often contains traces of minor elements, especially chalcophile elements, that are used to evaluate palaeoenvironmental conditions (Pisarzowska et al. 2014; Berner et al. 2013; Huerta-Diaz and Morse, 1992).

Two mechanisms for the formation of pyrite can be distinguished: The first requires the presence of Fe(II) - ions and polysulphides (FeS – S(-II)). The second is dependent on the existence of reactive iron compounds and elemental sulphur (Rickard and Luther, 2007). These reactive iron compounds include hydroxides, oxyhydroxides (goethite / lepidokrokite - FeOOH), and oxides of hematite (Fe_2O_3) and magnetite (Fe_3O_4), placed in fresh water and seawater as detritus. By the involvement of intermediates such as mackinawite and greigite, the inorganic precipitation and bacterial formation of pyrite follows a pathway via a progressive sulphurisation, dissolution, and precipitation, by including changes in aqueous sulphur speciation (Schoonen and Barnes, 1991).

Under standard conditions, formation of pyrite follows two mechanisms that are described as the "H_2S-pathway" (Berzelius- reaction; eq. 4), and the "polysulphide pathway" – (Bunsen- reaction; eq. 5).

Equation 4

$$FeS + H_2S \rightarrow [Fe - S \rightarrow SH_2] \rightarrow FeS_2 + H_2 \quad \text{"Berzelius reaction"} \quad \text{Eq. 4}$$

Equation 5

$$FeS_{(aq)} + S^{2-}_{n\,(aq)} \rightarrow FeS_{2(S)} + S^{2-}_{n-1\,(aq)} \quad \text{"Bunsen reaction"} \quad \text{Eq. 5}$$

A rate limiting role is given by the concentration of H_2S (circumneutral conditions at pH ~7) or polysulphide concentration (alkaline conditions at pH ~8.1) (Rickard and Luther, 2007). In such an environment, the pyrite formation follows the polysulphide pathway and in this case, is about two magnitudes slower than in the H_2S one (Butler and Rickard, 2000).

In a natural environment, bacterial mediated sulphur – disproportionation plays a major role in anoxic/sulphidic environments that enhance the pyrite formation up to 10^5 times faster than inorganic precipitation can (Canfield et al. 1998).

As noted above, pyrite can be precipitated at a concentration of picomolar HS^- (less than 1 nM) and in the presence of nanomolar dissolved iron. This implies that extraordinarily low quantities of sulphur species are required to precipitate pyrite (Rickard and Luther, 2007).

Sulphate

The main source of sulphate is represented by the fluvial entry (Drews, 2010). Calcium sulphate, gypsum and anhydrite are major constitutes of carbonate sediments, whereas barite and celestine are often observed with less abundances. However, sulphate can also be adsorbed onto the surface of iron oxides or hydroxides (Chen et al., 1997). They may include additional labile organic sulphur compounds such as sulphate ester (Nriagu and Soon, 1985).

Sulphur (elemental sulphur, sulphate, poylsulphide, organic sulphur)

According to equation 6, an addition of H_2S to oxygen free water is a result of the formation of polysulphide ions through the interaction of S with HS^- (Morse et al., 1987). Subsequently, the resulting polysulphides S_n^{2-} react with H^+ to form HS^-, (Rickard and Luther, 2007). The net result is accompanied at a given pH value, whereas all total reduced sulphur (S_T) can be expressed by equation 6.

Equation 6

$$S_T = [HS_2] + [HS^-] + [S^{2-}] + [S_4^{2-}] + [HS_4^-] + [S_5^{2-}] + [S_6^{2-}] \quad \text{Eq.6}$$

Equation 6 is an example for using this term to describe dominant sulphur species in pore water at a given pH of 8 (Morse et al., 1987). The most abundant sulphide species in a natural environment are $H_2S > HS^- > HS_2^-$ (Rickard and Luther, 2007).

According to the notions above, polysulphides refer to alternating chains of sulphur atoms. They are an important part of the pore water in tidal- and marine sediments, and highly reactive and can therefore bond to both metals and organic matter compounds.

A possibility to extract polysulphides includes the extraction with acetone or carbon disulphide (CS_2). According to Henneke et al. (1997) in a wet chemical sequential extraction scheme S_8 and non- polar organic polysulphides can also be extracted.

Organic sulphur

Sulphurisation of organic matter leads to the formation of a wide variety of organic sulphur compounds in nature, especially in marine sediments. More than 1500 different compounds are currently known (Werne et al. 2004, Sinninghe Damsté and Leeuw, 1990)

Sulphur can be incorporated *intra-molecularly* into organic compounds, forming a cyclo-sulphur group such as a thiophene or thiane, or it can be incorporated *inter-molecularly*, resulting in organic compounds linked via C-S-C bonds into a macromolecular matrix.

Intramolecular S incorporation

Fig. 25 shows the intramolecular S-incorporation, which is defined as the integration of heterocyclic compounds into kerogen-bonded sulphur. They can be divided into three main constituents - (1) **thiane**, heterocyclic compounds that contain a saturated six-membered ring with five carbon atoms and one sulphur atom, (2) **thiolane**[8], the saturated analogue to (3) **thiophene** - that are all related to intra-molecular sulphur incorporation (Werne, 2000; Rospondek et al., 1997; Kohnen et al., 1991).

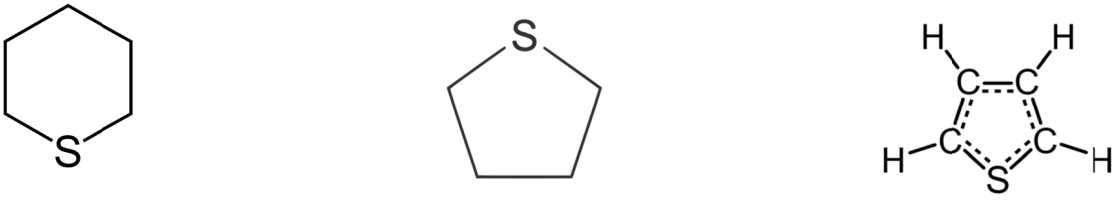

(1) Thiane ($C_5H_{10}S$) **(2) Thiolane (C_4H_8S)** **(3) Thiophene (C_4H_4S)**

Fig.25 Different heterocyclic compounds in sulphur rich kerogen

Typical for thiophenes is the incorporation into the so-called highly branched isoprenoid (HBI). The HBI components are composed of carbon skeletons of 20, 25, 30 or 35 carbon atoms. They have been reported from a wide variety of ancient and recent sedimentary settings (Jaraula et al., 2010; Werne et al., 2008; Sinninghe Damsté et al., 2007; Volkman et al., 1987).

HBIs occur predominantly as saturated hydrocarbons or in sulphurised form (Zhang et al., 2011; Köster et al., 1998). Kolonic et al. (2002) reported on pristane and phytane skeletons that have been released upon desulphurisation of samples from the largest oil shale reservoir in North Africa, the Tarfaya Basin, SW Morocco. These skeletons contain thiolane, thiophenes and thianes. The observations are comparable to those obtained from deposits in the Monterey and Duwi formations (Stankiewicz et al. 1996), and Kashpir oil shales (Riboulleau et al. 2003) and the sulphur-rich Orbagnoux deposits (Mongenot et al. 1999).

[8] Organosulphur compound with the formula $(CH_2)_4S$ - five-membered saturated heterocycle having four carbon atoms and one sulphur atom Swanston (2000).

Intermolecular S incorporation (hopanoides)

Such hopanoides are widespread in kerogen (Farrimond et al., 2003). Hopanoides are pentacyclic compounds and are based on the structure of hopanes. Their function is to improve the strength of bacteria membrane. This helps the bacteria to adapt to different environments (Madigan and Martinko, 2009). In hopanoides, the sulphur is linked to polysulphides and sulphides.

Extraction techniques

A very detailed overview about different extraction techniques is given in Rickard and Morse, (2005), van der Veen, (2003), Rice et al. (1993) and (Cornwell and Morse, 1987). There are two main approaches to recover differently bonded sulphur. This includes methods for sulphur extraction in both sequentially and non-sequentially operated methods.

In a sequential procedure, the individual forms of sulphur are extracted successively. In a parallel extraction procedure, a new sample aliquot per sulphur species is used. This enhances the probability of sample inhomogenities (van der Veen, 2003). The sequential procedure is based on a method that was originally proposed by (Zhabina and Volkov, 1978). Here, all used solutions must be purged with nitrogen or another inert gas first, to remove all of the oxygen. Different reagents can effectively convert acid-volatile sulphide (AVS), $CrCl_2$-reducible sulphide (CRS), and elemental sulphur into hydrogen sulphide (Hsieh and Shieh, 1997). Subsequently, the H_2S has to be transferred by means of an inert gas (Ar, He, N_2) into a flask containing a Cd-acetate, where sulphur is precipitated in form of CdS. An overview about the use of different extraction solutions (precipitation with Ag, Zn, Cd) is given in van der Veen, (2003), who modified the method of Zhabina and Volkov (1978).

Methodology of sulphur extraction

Fig. 26 and 27 (next page and page 75) illustrate the principle steps of the wet chemical extraction of different sulphur species. The first step involves the determination of the AVS- bonded sulphur. The sample was treated with 6M HCl. Liberated H_2S reacts with Cd-acetate to CdS. The released H_2S represents different iron sulphide species (mackinawite, greigite, pyrrothite). 5 g of dried and finely ground sample material was filled into a round-based flask. 40 ml of cadmium acetate solution and 40 ml of acetic acid, together with 60 ml monodestilled water, was added to a water-cooled glass column unit. Subsequently, a mixture of 50 ml 6M HCl and 50 ml mineralised water was injected into the bottom flask with the sample material. By heating the flask to 80°C, the released H_2S was transported by means of a N_2 gas stream into the cooled glass column, where the evolved H_2S was precipitated in form of CdS. Adhering residual CdS onto the glass wall (cooling unit) was rinsed out with acetic acid and splashed into the beaker.

In the second step of the sequential extraction procedure, the supernatant with acid soluble sulphates has to be separated from the residue, which contained all the other forms of sulphur. For this, the content of the round-based flask from the former step was filled into a 50 ml tube and was centrifuged for 8 min at 4000 rpm. The supernatant was transferred into a 500 ml plastic bottle. This procedure was repeated two more times until the supernatant became colourless. NaOH was used as buffer solution to set the pH-value at 3 - 3.5. It followed the addition of barium chloride solution, in order to precipitate barium sulphate, which was further used to identify the isotopic composition of sulphate-bonded sulphur (eq. 7).

Equation 7

$$SO_4^{2-} + Ba^{2+} + 2Cl^- \rightarrow BaSO_4\downarrow + 2Cl^- \quad \text{Eq. 7}$$

Now, the residue contains the di-sulphide (pyrite) and organically bonded sulphur. From this residue, the pyrite-sulphur (actually $CrCl_2$ – reducible sulphides: CRS) was extracted by means of a mixture of $CrCl_2$ and HCl. It was necessary to prepare a fresh $CrCl_2$ solution, which was obtained by reduction of $CrCl_3$.

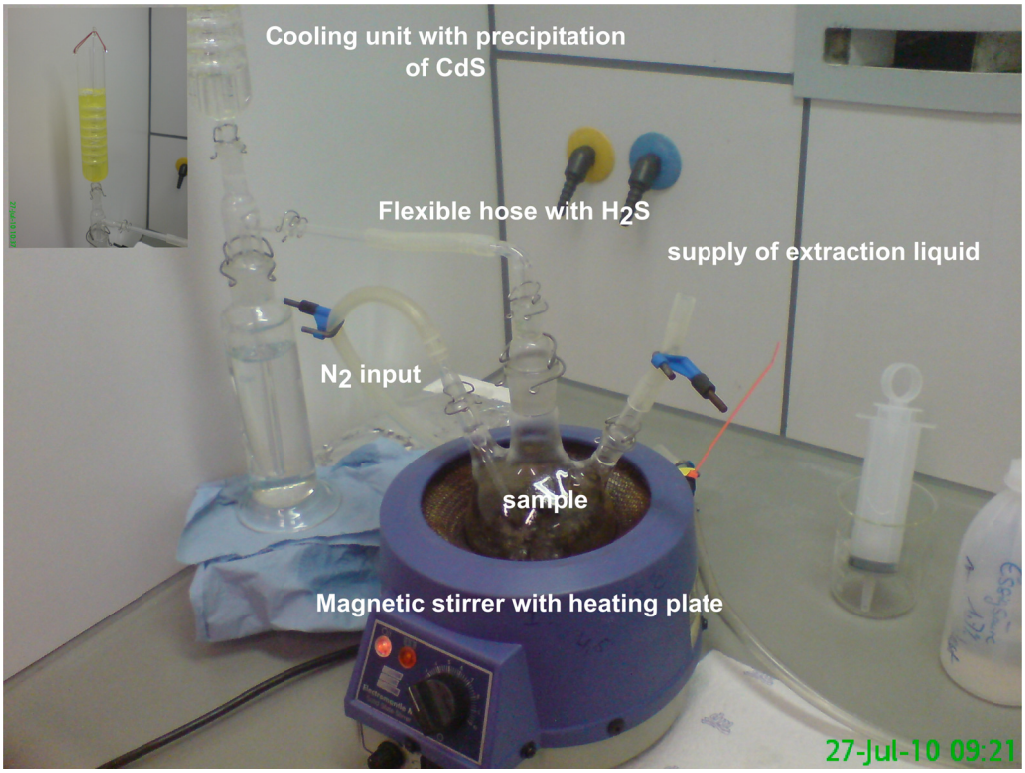

Fig.26 Extraction equipment for different kind of bond sulphur

For this, the $CrCl_3$ solution was sent through a column with amalgamated zinc. Thereby, a change from green to blue colour could be observed, indicating the reduction of chromium (III) to chromium (II), Eq. 8(van der Veen, 2003).

Equation 8

$$2CrCl_3 + Zn \rightarrow 2CrCl_2 + ZnCl_2 \qquad \text{Eq.8}$$

$$Cr^{3+} + e^- \longleftrightarrow Cr^{2+}$$

The further processing has to be done rapidly otherwise, a re-oxidation to chromium (III) takes place. Subsequently, the extraction agent was prepared. This consisted of a mixture of 65 ml $CrCl_2$ solution and 35 ml of concentrated HCl in 300 ml of demineralised water. The addition of concentrated HCl improves the conversion of $CrCl_3$ to Cr^{2+} (Hsieh and Shieh, 1997), see eq. 8. The remaining sample material from the previous step was re-introduced into the round-based flask and processed similarly to the extraction of the AVS. Equation 9 displays the chemical equation for CRS- sulphur extraction (van der Veen, 2003):

Equation 9

$$FeS_2 + 2Cr^{3+} + 8H^+ \rightarrow 4H_2S\uparrow + 2Cr^{2+} + Fe^{3+} \qquad \text{Eq. 9}$$

According to Francois, (1987) it is important to note that chromium reduction liberates some of the organic polysulphides and humic substances, but their contribution to the total amount of extracted organic sulphur is negligibly low (Canfield et al., 1986).

The residue from this step was processed with Thode solution in a similar way as described above. The Thode solution extracts organically bonded sulphur (intramolecular sulphur), and in part some of the elemental sulphur contained in the bulk sediment.

The strongly reducing Thode solution is a mixture of:

1. HJ = 500 ml (850g) d=1,7
2. H_3PO_2 = 245 ml (50%)
3. 12M HCl = 816 ml

The remaining material from the previous extraction step was treated with 100 ml of Thode solution at 80°C for about three hours. The liberated hydrogen sulphide was converted into cadmium sulphide as described above (Eq. 10).

Equation 10

$$H_2S + CdC_4H_6O_4 \rightarrow CdS + H_2C_4H_6O_4. \qquad \text{Eq.10}$$

After this step, the sample material remaining in the flask contains the organically bonded sulphur fraction.

Organically bond sulphur

The organically bonded sulphur (actually kerogen sulphur) was extracted by means of the Eschka method, according to ASTM D-3117, ISO334, ISO351. For this 1 g of the remaining sample material was mixed

with 3 g of Eschka mixture, consisting of two parts by weight of calcified MgO with one part of anhydrous Na_2CO_3. In order to prevent any lost during combustion, the sample mixture was covered with an additional amount of 2 g of Eschka powder. The platinum crucible was transferred into an oven and heated at 800°C for 6 h. During combustion, sulphur compounds in samplematerial reacted with MgO and Na_2CO_3 to form $MgSO_4$ and Na_2SO_4.

After cooling, the crucible was placed into a hot water bath (80°C) for 45 minutes to get sulphate into solution. The beaker content was filtered and the residue washed again and heated gently for 10 minutes in order to oxidize sulphite to sulphate. Finally, sulphate in solution was precipitated with $BaCl_2$ to give $BaSO_4$ which was used in isotopic measurements. In fig. 27 is shown the analytical procedure as described above.

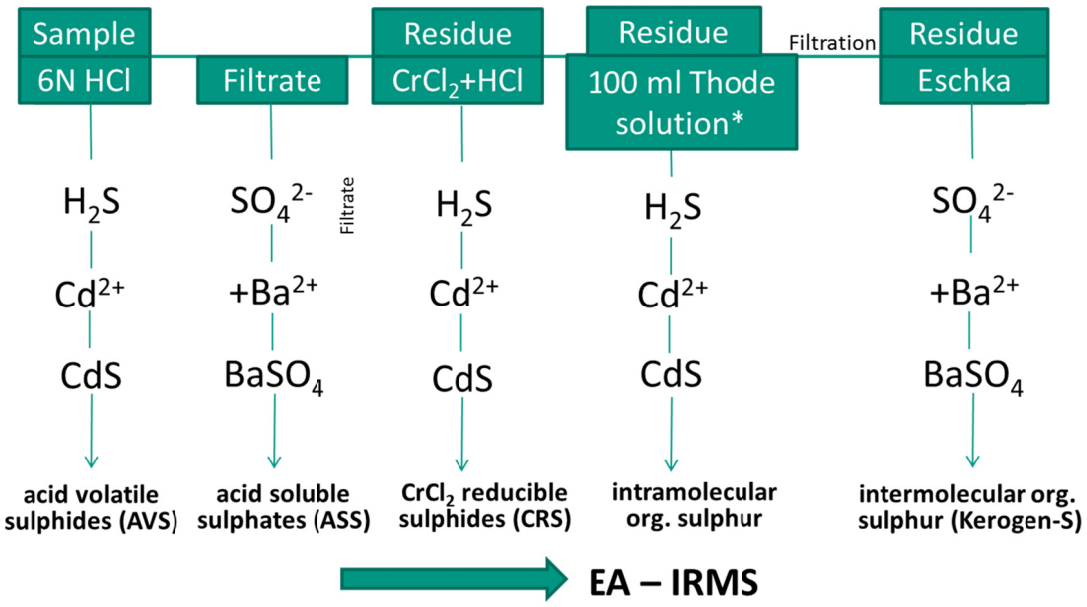

Fig.27 Analytical scheme used to separate various forms of sulphur in oil shale and associated rocks (adapted from Mayer and Krouse, 2004)

Analysis of the stable sulphur isotopes: Continuous Flow- IR-MS, (CF-IRMS)

The continuous flow mass-spectrometry (IR-IRMS) is widely used for online determination of the isotopic composition of inorganic and organic materials (Barrie and Prosser, 1996). In terms of the reduced amount of sample material needed, and high performance, the CF-IRMS is to be preferred over the classic and laser methods (heating, ablation method) (Grassineau et al., 2001).

Device description

For this work, the extracted sulphur fractions were measured for their sulphur isotope composition with a stable isotope ratio mass spectrometer (IsoPrime), coupled in continuous flow mode with an element analyser (NA1500; Carlo Erba, Milan, Italy) (EA-Py-CF-IRMS).

Analytical procedure

From each sample/standard, 300-500 µg were weighed together with ~5 mg of V_2O_5 into tin-foil capsules. The weighed sample/standard is dropped by the automatic sampler into an oxidation/reduction column, kept at 1020°C. The packing of the column in the furnace is shown in fig. 28 (Fry et al. 2002, Grassineau et al. 2001). The sulphur is oxidised to SO_2 in the reaction column. Helium acts only as a carrier to transport the gas through the column. The tungsten oxide causes the conversion of sulphur species (CdS, $BaSO_4$) into SO_3/SO_2, while copper leads to the reduction of SO_3 to SO_2 (Grassineau et al. 2001). The resulting gaseous burning products are dried using a magnesium perchlorate water trap. After passing the water trap, the gas reaches the chromatographic column where the different gaseous species are separated, while the SO_2 is transferred into the analyser of the mass spectrometer. The isotopic composition of the SO_2 from the sample is compared to the value of the reference gas.

Isotopic composition of the samples was calibrated against internationally certified standards with known isotopic composition: IAEA-S1 (Ag_2S, $\delta^{34}S$ = -0.3‰); IAEA-S2 (Ag_2S, $\delta^{34}S$ = +22.7‰ ± 0.2‰), IAEA-S3 (Ag_2S, $\delta^{34}S$ = - 32.3‰ ± 0.2‰), and NBS-127 ($BaSO_4$ $\delta^{34}S$ = +20.32‰ ± 0.4‰). Precision of the preparation and analysis, estimated from replicate analyses of standards, is generally better than ±0.2‰.

All data are expressed in standard delta notation as per mil (‰) deviation, relative to the Vienna-defined Cañon Diablo Troilite (V-CDT).

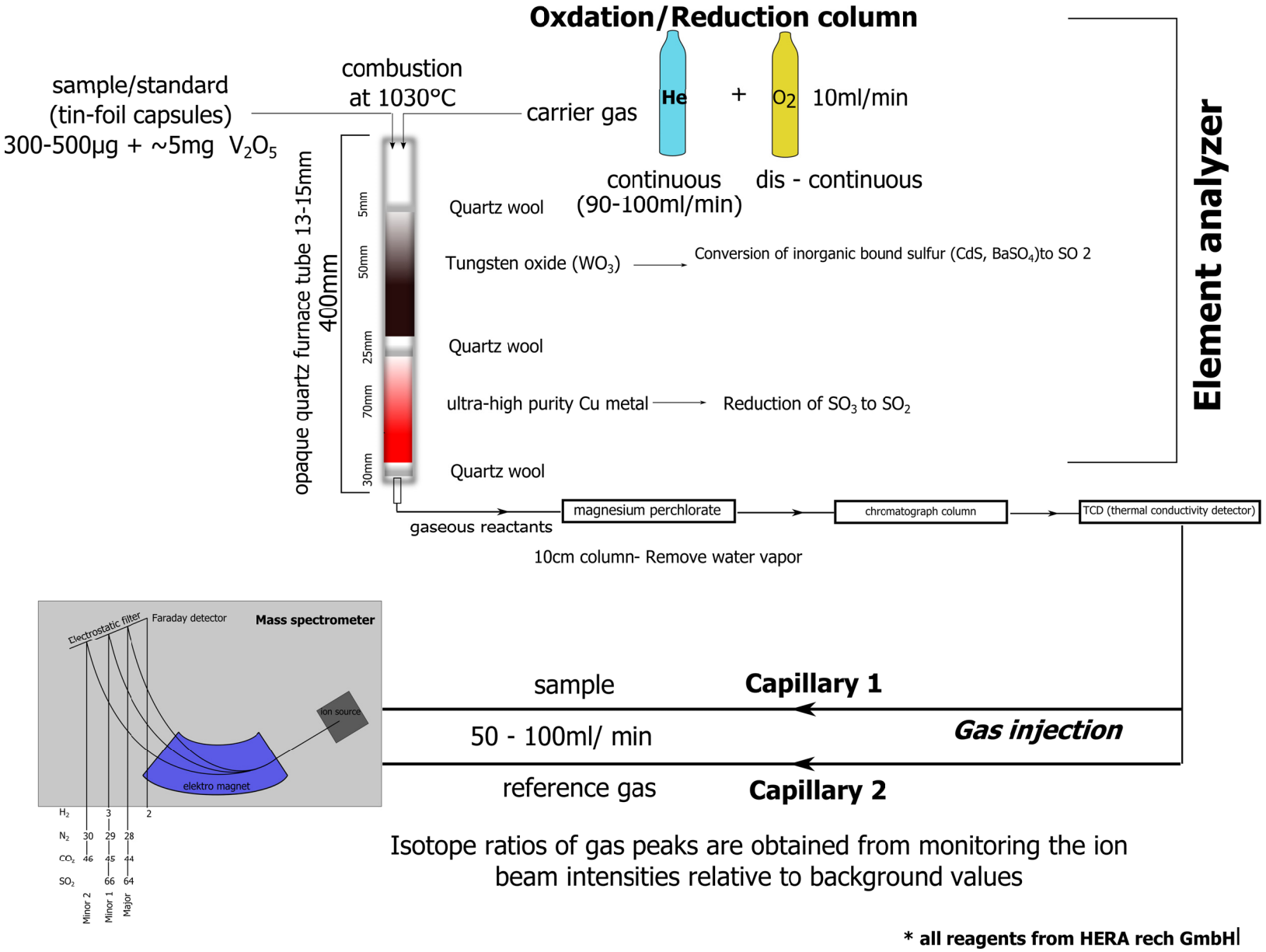

Fig.28 Schematic of the S reactor system used in analysis, mass spectrometry modified after (Olsen, 2006;. Fry et al., 2002)

3.3.2. Foraminifera

Preparation and cleaning procedure

The determination of the trace element composition of benthic (*Gavelinella*) and planktic (*Heterohelix*) foraminifera tests aimed at gaining insights about the differences in the composition of surface and bottom water, as well as on detecting temporal composition trends because of radical changes in the upwelling system and oceanic circulation in the southern Tethys during the Late Cretaceous. Methods of preparing and analysing foraminiferal samples for trace element composition vary between laboratories; there is no standardised method per se (Barker et al., 2005). A good overview about different cleaning techniques is given by (Barker et al., 2003).

Actual cleaning techniques comprise two different schemes that include firstly "oxidative cleaning technique – Mg cleaning" and secondly "reducing cleaning technique – Cd cleaning" (Pena et al., 2005). The so-called Mg-technique contains a step to remove clays (referred as C_2H_5OH), and with an oxidising agent (mostly H_2O_2) all organic matter becomes oxidised. Finally, a leaching step which involves the use of weak acid is recommend by (Barker et al., 2003; Elderfield and Ganssen, 2000). The "original" cleaning Cd-technique, which was initially introduced by Lea and Boyle, (1991), Boyle and Keigwin, (1985) and Boyle, (1981), includes an additional reduction step to remove Mn-Fe-oxyhydroxides. Additionally, this cleaning step allows the removal of all insoluble mineral phases, e.g., pyrite overgrowth (Boyle, 1981). They are typically on the surface of the foraminifera tests. The possibility of silicate coatings removal from the surface of foraminifera tests, has previously been described (Pena et al. 2005, Barker et al., 2003; Martin and Lea, 2002; Lea and Boyle, 1991; Boyle and Keigwin, 1985; Boyle, 1981).

The cleaning procedure, which was performed for this work, is based on previous works (Brown and Elderfield, 1996; Hastings and Emerson, 1996; Boyle and Keigwin, 1985; Boyle, 1981). There are existing descriptions in form of detailed laboratory guides (Meudt, 2004, Barker et al. 2003).

For the purposes of the palaeo-investigations, the specimen were broken up under the binocular microscope between two glass plates in order to free the filling of the chambers and subsequently

submitting them to the meticulous cleaning procedure. This includes the following four major steps: (i) removal of adhering clay particles with double distilled water and methanol, (ii) removal of any coatings (notably Fe- and Mn- oxyhydroxides) in a reducing environment by means of hydroxyl ammonium chloride, (iii) oxidising and removing organic impurities with H_2O_2, and (iv) etching the surface of the fragments with diluted (0.25 vol. %) HNO_3, which aims to remove any trace of impurities. Finally, the thoroughly cleaned material was dissolved in 1 ml of 1 vol. % HNO_3 and the solution was analysed with a high resolution ICP-MS, equipped with a micro-concentric nebuliser with low uptake time.

From each sample, a minimum of ~100 µg of foraminifera tests (>10 specimens) have been picked under the binocular microscope. A main selection criterion was a good preservation. This includes no visible (under magnification) dilution effects on the surface of the shells as well as no recrystallisation of calcite and inclusion of clay minerals and pyrite. In order to enlarge the surface to be analysed, we used a glass top to crush the foraminifera tests into two parts. A critical minimum for the initial weight of each analysed sample was a weight of 50 µg. Samples with less than 50 µg were analysed but not considered in the statistical analysis. The crushed samples were filled into a 1.5 ml plastic reaction tube. The following procedure includes five dissolution steps and it is described in detail below, see also fig. 29, next page.

First Step: removal of clay particle with H_2O_{bidest} and CH_3OH

This step aims to remove any occurring clay particles from the surface of the foraminifera. An amount of (~500 µl) H_2O_{bidest} was added to the reaction tube. Resulting air bubbles were removed by tapping against the reaction tube. The tube was closed and placed into an ultrasonic bath for 1-2 minutes. In order to resolve any occurring air bubbles, it was tapped against the frame several times. The tube was left in the rack for about a half minute to allow the shell fragments to settle at the bottom. By using a 1000 µl pipette, the water was carefully removed. This step was repeated once with H_2O_{bidest}, twice with 100 µl methanol (in p.a. quality) and finally three times with H_2O_{bidest} (1000 µl) to flush out the methanol repeatedly. After the third wash cycle and before storing, the samples were placed in an oven at 40° C overnight.

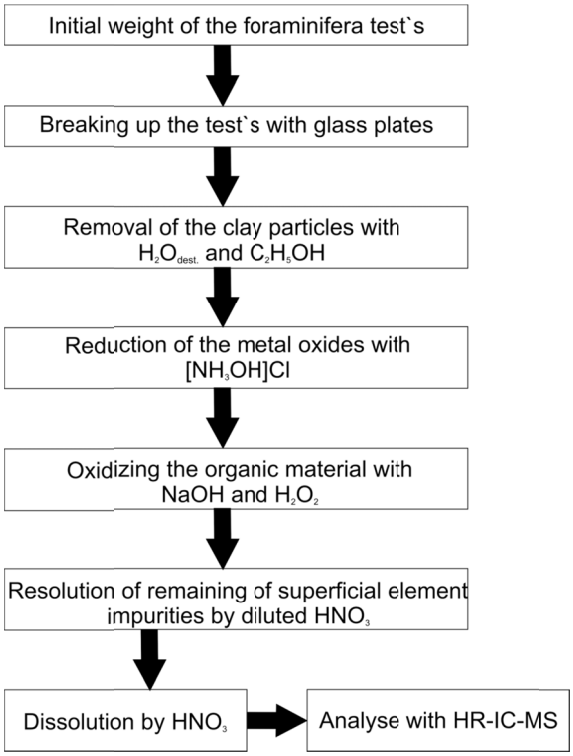

Fig.29 Flow chart of the modified purification process for foraminifera test (Meudt, 2004).

Second step: reducing solution step

This step includes the elimination of all metal oxides that form during diagenesis. They cover or adsorb onto the surface of living foraminifera tests. First, a one molar solution of the reducing agent hydroxyl ammonium chloride ($[NH_3OH]Cl$) in a 5% ammonia solution was generated. For this purpose, 10 ml of concentrated ammonia solution H_2O_{bidest} was filled up to 50 ml, dissolved in 3.6 g of hydroxyl ammonium chloride, and transferred under the hood in a 50 ml Teflon bottle. The reagent should be generated immediately before usage, because otherwise a gradual autoxidation decomposes the reducing agent (Jander et al. 2006; Holleman and Wiberg, 1995). The hydroxyl ammonium chloride and ammonia solution must be at least in p.a. quality.

500 µl of the reagent were pipetted into each sample. Resulting air bubbles were removed by tapping against the frame and the vessels were closed. Vessels were placed in an ultrasonic bath and heated at 60° C for 4-5 minutes. Reoccurring air bubbles were detached by tapping against the frame. After a one-minute break, the reagent was pipetted until only a residual layer was left at the base of the vessel. The tubes were filled again with H_2O_{bidest}. (1000 µl). Afterwards, the water was suctioned again. The last procedure was repeated three times and the samples were stored in an oven at 40° C overnight.

Oxidising solution step

This step was performed for the removal of all organic matter. In a small beaker, 100 µl H_2O_2 is added to 30 ml of 0.1N NaOH solution. Both reagents have p.a. quality. 250 µl of the reagent was added to each sample, air bubbles were removed by tapping against the frame. After that, the vessels were closed. The tubes were inserted into floating racks for 4-5 minutes at 60° C in a heated ultrasonic bath. Teflon tubes were filled with 500 µl H_2O_{bidest} and after the one-minute break, the reagent was pipetted until only a residual layer was left at the base of the vessel. Then, the tubes were rinsed three times with double-distilled H_2O (1000 µl) and the samples were stored in an oven at 40° C overnight.

Mild acid leaching

This step involves the partial dissolution of any remaining oxidic coatings from the surface of the foraminifera tests. 25 µl of 0.25% HNO_3 in sub-boil or ultrapure quality was added to each sample. After 2 minutes, the samples were filled up with 1ml H_2O_{bidest} and then pipetted off. Each sample was washed three times with double-distilled H_2O. After washing, the shell fragments were stored in a refrigerator.

Dissolution of the samples

To dissolve the remaining fragments, 100 µl of 1% HNO_3 (sub-boiled or in ultrapure quality) were added and subsequently exposed to an ultrasonic bath for 15 minutes. If any fragments were visible, additional 100 µl of 1% HNO_3 were added again and the procedure was repeated. Subsequently, the solution was transferred into a Teflon tube with a conical base. Then the addition of 1% HNO_3 in a reaction vessel followed. About 10 µl of insoluble residues remained in the reaction vessel, which could be discarded because they were usually intercalated silicate or coatings on the surface of foraminifera shells. These silicate materials could block the fine capillary tubes in the mass spectrometer. Now, the solution contained dissolved foraminifera that were ready for analyses by means of the mass spectrometry.

4. Results

4.1. Stratigraphy and Lithology

Splits of samples taken from the Rotem-Mishor quarry were used for the inorganic geochemical analyses. Samples were taken every 10 - 20 cm over a range of 50 m. A high-resolution sample set, composed of a total of N=266 samples, was used to determine the trace elements and C_{org} composition, while another set of N=45 samples, taken with a lower resolution (every 80 - 100 cm), was used to determine the main element and mineralogical composition. Sampling covered the uppermost part of the Phosphorite Member (PM) of the Mishash formation (5.8 m), the entire Oil Shale Member (OSM) (42 m), and the base of the Marl Member (MM) (~3 m) of the Ghareb formation. A detailed description on the lithology and biostratigraphy is given in (Ashckenazi-Polivoda et al., 2011).

Table 1 Overview of different investigates carried out within this work

Analyses	High resolution sample set (n=220)	Low resolution sample set (n=45)
Minor elements (ED-XRF)	x	
Major elements(WD-XRF)		x
Determination of C_{org}	x	
Determination of S_{total}		x
Determination of Fe_{HR}[9]		x
Mineralogical composition (XRD)		x
Trace elements in foraminifera		x
Sulphur isotopy		x

[9] Highly reactive iron

4.2. Mineralogical and geochemical composition

4.2.1. Mineralogical composition

Samples from the Ghareb fm. are termed as organic-rich carbonates, namely oil shales, being fine-grained rocks of grey colour. These rocks consist mostly of calcite (up to 55 wt. %), dispersed organic matter of up to 18 wt. % (OM), and quartz, with further minor or accessory amounts of clay minerals, apatite, gypsum, dolomite, goethite, and traces of pyrite. Of particular consideration are biogenic fragments, which typically contain noticeable parts of foraminifera. Details of the mineralogical composition are given in table 2.

Table 2 Average mineralogical composition of the oil shale (Mishor Rotem) calculated from wet chemical analyses*

Main minerals	Minor minerals
calcite max. 55 wt. %	dolomite
quartz, opal	gypsum*
organic matter – max. 18 wt. %	muscovite (?)
kaolinite/smectite/illite	microcline
	apatite* (~7 wt. %)
	goethite* (~3 wt. %)
	very low pyrite* (~1 wt. %) (by XRD not detectable)

After treatment with 3.5% peroxide and 10% hydrochloric acid, to remove organic matter content and carbonate, results from the diffractometry analysis reveal a pattern, which signify constituents of quartz, clay minerals and amorphous components of opal and iron-hydroxides, see fig. 30 and fig. 32. This is in accordance with Spiro and Rozenson, (1982, 1980) and Spiro, (1977), who report calcareous, locally bituminous shales with an assemblage of authigenic silicate minerals including microcline, heulandite, quartz, opal –CT, anatas, iron-hydroxides along with detrital quartz, kaolinite, smectite and illite, from the Ghareb fm., Campanian – Maastrichtian (Horon, Efe` syncline, Nebi Musa).

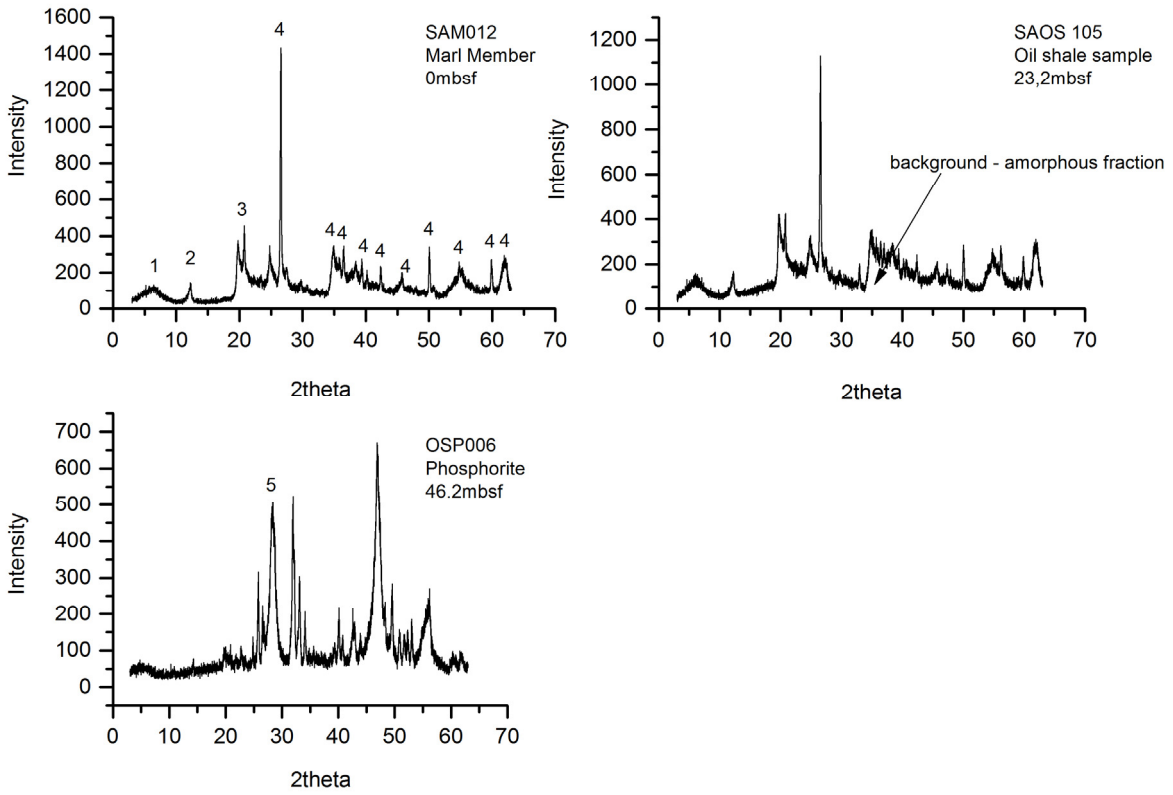

Fig.30 Graphs display examples of mineralogical analysis by XRD. Samples were pretreated with HCl and H_2O_2 to extract carbonate and organic matter. Number refers to identified major peaks for:(1) montmorillonite (2) kaolinite (3) feldpare – muscovite (4) quartz (5) apatite

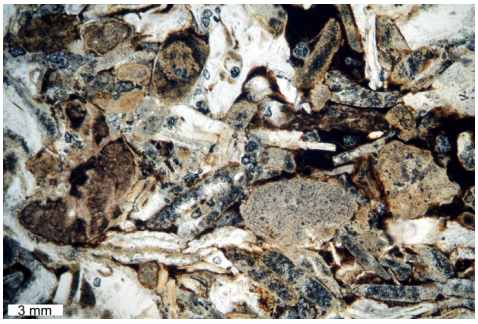

Fig.31 illustrates a mix of bones and amorphous apatite-like phases (rounded particles) (OSP013, 49.8m Phosphorite Unit) 1pol.

Phosphorites are grey-green coloured, conglomeratic rocks and consist mainly of apatite and micritic calcite. The apatite constituents include fragments of bones and teeth as well as amorphous, optically isotropic, phosphatic phases (fig. 31).

Based on the bulk sediment analysis (fig. 32), all three units are clearly distinguishable by their organic matter content (<2 wt. % in marl), their apatite content (max. ~60 wt. % in phosphorite), and the non-detection of clay mineral compositions in the PM. The mineralogical composition according to the XRD-results is similar to the Jordanian oil shales and Egyptian oil shales from the Red Sea, (Abed and Arouri , 2006) and (El-Sabagh et al. 2000).

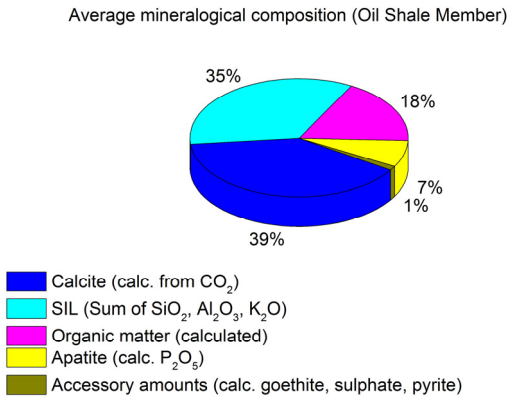

Fig.32 Bulk rock composition of the organic rich carbonates based on the semi- quantitative analysis (oil shale)

The relative abundance of the three most important groups of clay minerals was evaluated semi-quantitatively with PowderX by integrating the surface area of the peaks as delivered by the software for kaolinite, illite and smectite, at 7.16 Å, 10.0 Å and 17.0 Å, (fig. 33, table 3). For a detailed discussion, see (section. 5.1).

Table 3 comparison of XRD results from selected samples in OSM (note OSP 18 = 43.8 mbsf, SAOS 167 = 35.5 mbsf) analysis was done by the Israeli

Clay mineral	OSP 18	SAOS 167
Kaolinite	15%	12%
Smectite (high:low 67:33)	50%	44%
Illite	5%	8%
Mixed layer ISS (RO (70:24:6)	27%	35%
Chlorite	3%	1%

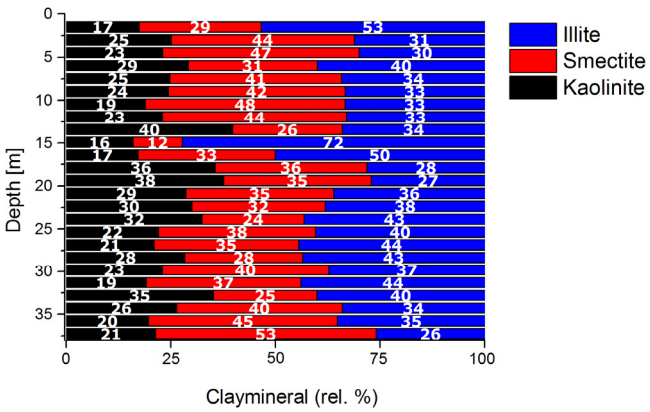

Fig.33 Downward fluctuation of the relative clay mineral content in the MM and OSM.

4.2.2. Major elements

The following lines describe the chemical pattern that occurred from the top of the PM (Mishash formation) to the OSM - MM (Ghareb formation). All depths are given in metres below surface (mbsf). Bulk element analyses show that SiO_2, CaO, Al_2O_3, P_2O_5, Fe_2O_3, SO_3, and organic carbon (C_{org}), are major constituents in all members, whereas MnO, MgO, TiO_2, Na_2O, and K_2O, are additional elements. All major elements are described and expressed as oxides.

Phosphorite Member (PM) 49.9 to 45 mbsf

Calcium content shows variations ranging from 27.9 - 48.7 wt. %, being the concomitantly highest fraction of all elements. Silicon, Mn, Ti, and K, are below the detection limit. Sodium and the Fe_2O_3, Al_2O_3 concentrations are very close to the detection limit, with an average concentration of 0.1 to 0.2 wt. %, respectively. The MgO content ranges from 0.2 - 0.5 wt. %, while P_2O_5 ranges from 10.2 to 15.4 wt. %. Regarding all analysed elements, a noticeable change in concentrations occurs at the transition horizon to the condensed layer (44.4 - 45 mbsf) and OSM.

Oil Shale Member (OSM) 44.2 - 2.8 mbsf

In this unit, calcium is the major constituent and ranges from 23.6 to 49 wt. %. Siliconoxide ranges from 4.9 - 19.4 wt. % and shows, together with Fe_2O_3, a concomitantly increasing trend, from the base to the top, regarding the concentrations. A reverse trend is observable for sulphur. Titanium concentrations range in the same magnitude (0.1 - 0.4 wt. %), compared to those of the PM, while Al_2O_3 ranges between 1 - 9 wt. %. MgO values are comparable to the PM and the MM and are close to the detection limit, ranging from 0.5 to 0.9 wt. %. Potassium and sodium concentrations are similar throughout the OSM. The K_2O and Na_2O concentrations range from 0 to 0.4 wt. %. P_2O_5 shows a drastically decreasing trend in the OSM. The content drops from 4.0 at the base to 0.8 wt. % at the top. Manganese concentrations are below the detection limit.

Marl Member (MM)

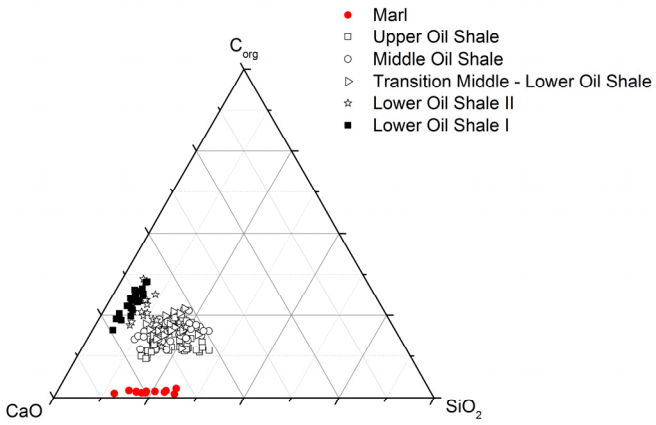

Fig.34 Ternary diagram displays a comparison of the different main constituents of bulk sediment between Oil Shale - and MM, which is CaO = carbonate, SiO_2 = quartz, C_{org} = organic carbon

In the MM, the average value of CaO is at 41 wt. %, which is higher than in the OSM. Siliconoxide concentrations are comparable to the OSM, values range from 10.8. - 13.3 wt. %. The Al_2O_3 values show slightly lower values than in comparison to the OSM. Within the MM, the average concentration is 5.4 wt. %, whereas the average Fe_2O_3 concentration varies from 1.8 to 2.2 wt. %. Phosphorus content is very similar to the OSM, the average concentration is 1.9 wt. %. The average concentration of MgO is 0.6 wt. %. Titanium oxide concentration (0.2 wt. %) is close to the detection limit. Sodium shows a concentration of 0.1 wt. % and Mn and K are not detectable. A ternary diagram (fig. 34) displays a clear separation between OSM and MM by their main components that are CaO, SiO_2 and C_{org} content. The classification of the complete profile in different subunits, which based on the different chemical and mineralogical bulk sediment composition, shows table 4 (page 91).

4.2.3. Minor elements

In the PM, some trace metals like Cu, Ni, Zn, and Cr show their lowest values. Exceptionally and in close relation to P, V, Mo, U, Cd have their highest concentrations at the top of the member. At 45 m a clear condensed layer evidently occurs. Within this zone, all elements drop in value. This transition zone separates the PM from the overlying OSM.

Within the OSM, a general decreasing trend in the concentrations of micronutrients, such as Ni, Cu, Zn, Cr, is observed. Such a pattern displays an up-section trend that correlates well with the content of organic carbon. Oxyanion building elements with low mobility under reducing conditions, such as Mo, V, U, and

As, display their highest concentrations in the basal part of the OSM. A sudden decrease of their concentrations at 35 mbsf marks a change in the deposition regime. Moreover, elements like Rb, Ga, and Ce, which are in conjunction to the detrital component, mirror the same increasing up-section trend that is known from the main elements. Finally, rare earth elements (La, Y), which are typical for conditions that favour the deposition of Ca-phosphate (phosphorite/ apatite), are in close relation to the constant (low) values of P throughout the remaining profile. These entire elements show a sudden decrease at around 25 mbsf. Throughout the transition from the OSM to the overlying MM, there are no significant deviations in terms of trace element concentrations observable. This notably features the covariance with the foraminiferal assemblages, indicating that at least a part of the chemical signals, observable in the sediments, are not only due to diagenetic remobilisation processes, but rather reflect changes in the depositional environment, which is mandatory for a successful utilisation of geochemical proxies. The application of such indicators, and the evaluation/interpretation of the geochemical data set by multivariate statistical methods, is shown in the following section. The variation in concentration of main elements and selected trace elements, along the section, are shown in fig. 35- 37. A summary of trace and main element data is given in Table 5.

Table 4 Classification of the organic rich carbonates (oil shale) in distinct subunits

Unit	mbsf	Abbreviation	Sub-division
Upper	3.2 – 21.2	UOS	Upper Oil Shale
Middle	21.4- 29	MOS	Middle Oil Shale
Middle	29.2 – 33.4	TMS	Transition Middle – Lower Oil Shale
Base	33.6 – 38	LOS II	Lower Oil Shale II
Base	38.2 – 44.2	LOS I	Lower Oil Shale I

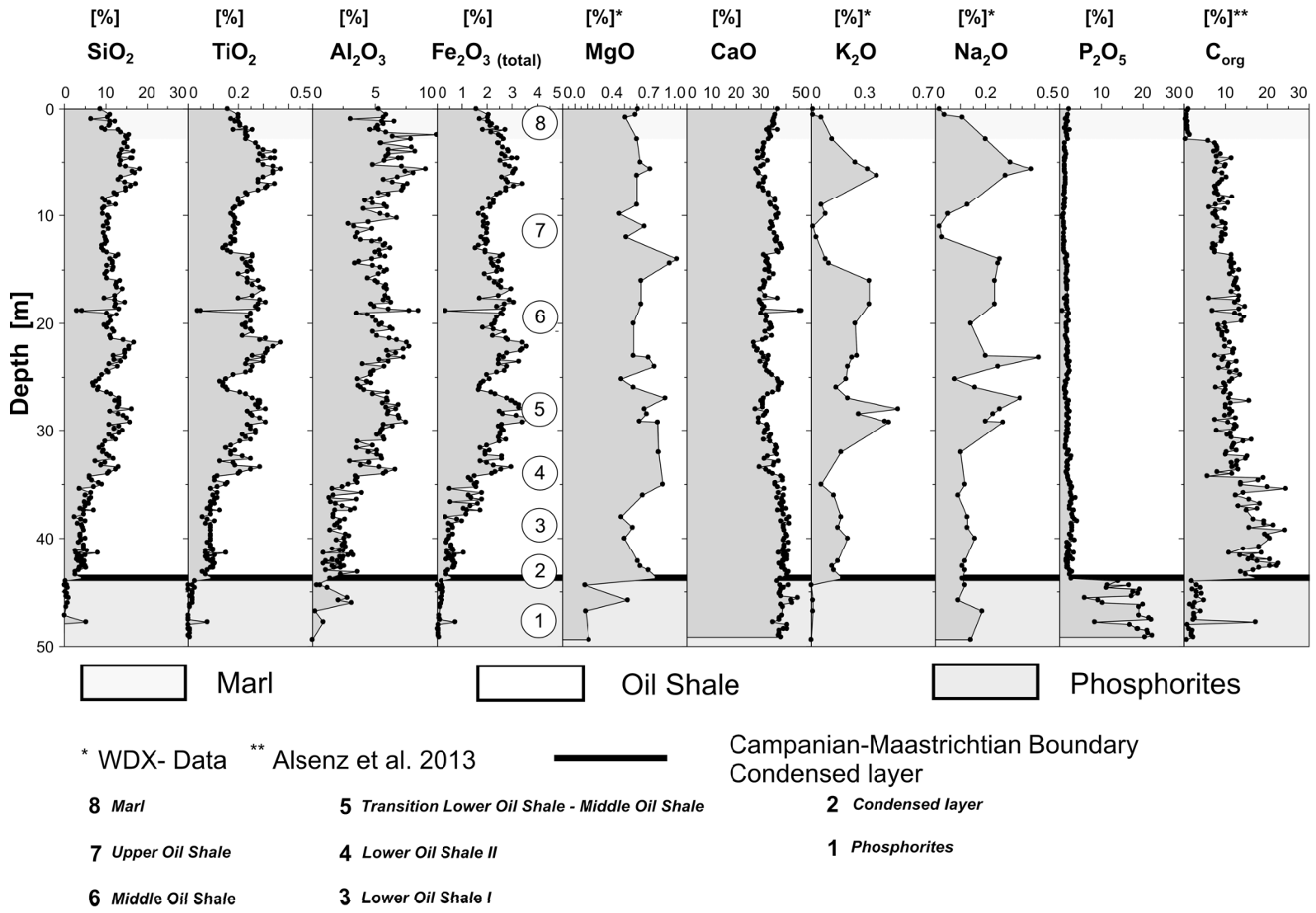

Fig.35 Distribution of major elements throughout the profile (Mishor Rotem – high resolution record)

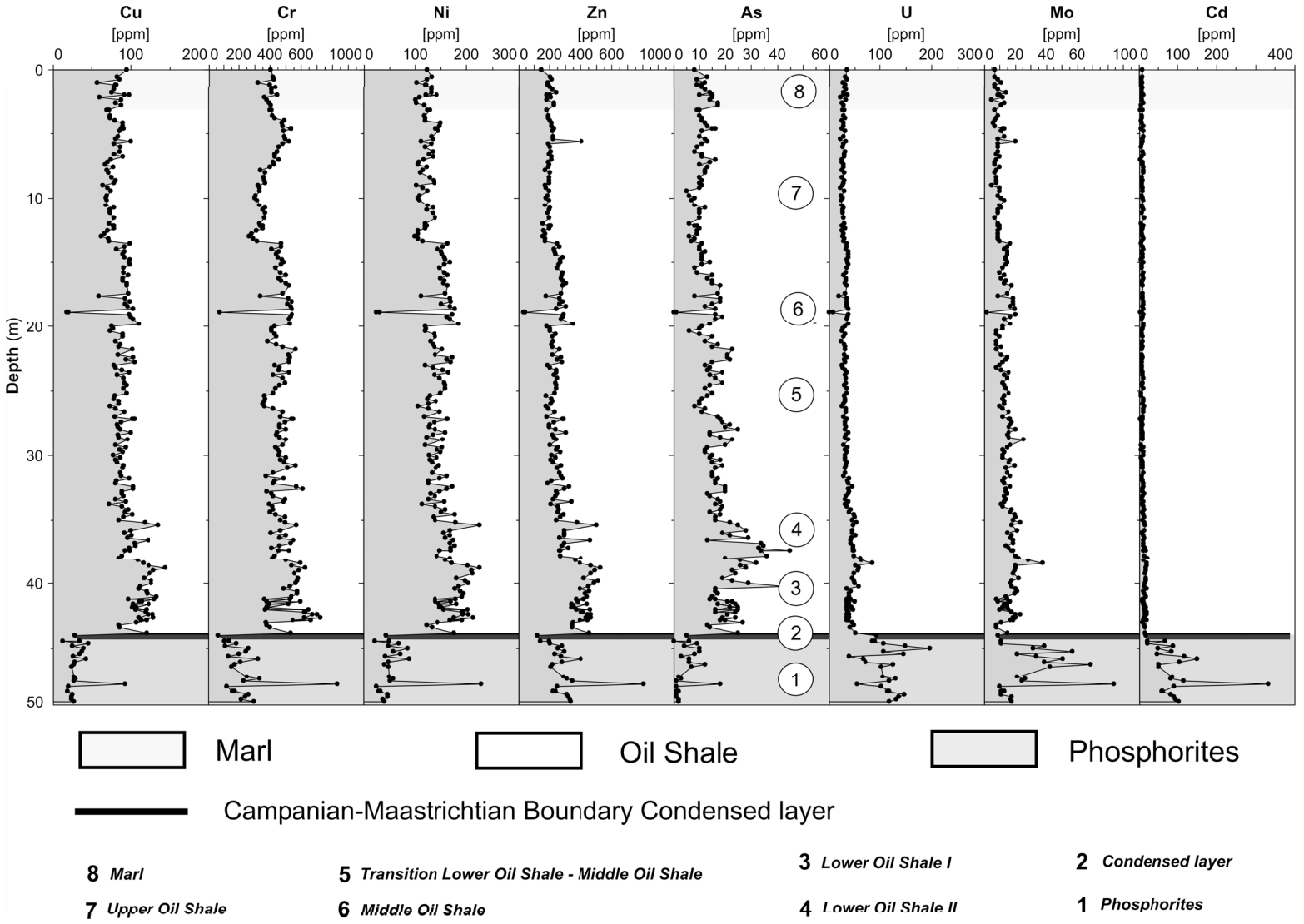

Fig.36 Minor element composition in three analysed units. Elements were grouped on basis the factoranalysis, results are shown in section 5.1. Numbers refers to the different subdivision of the profile.

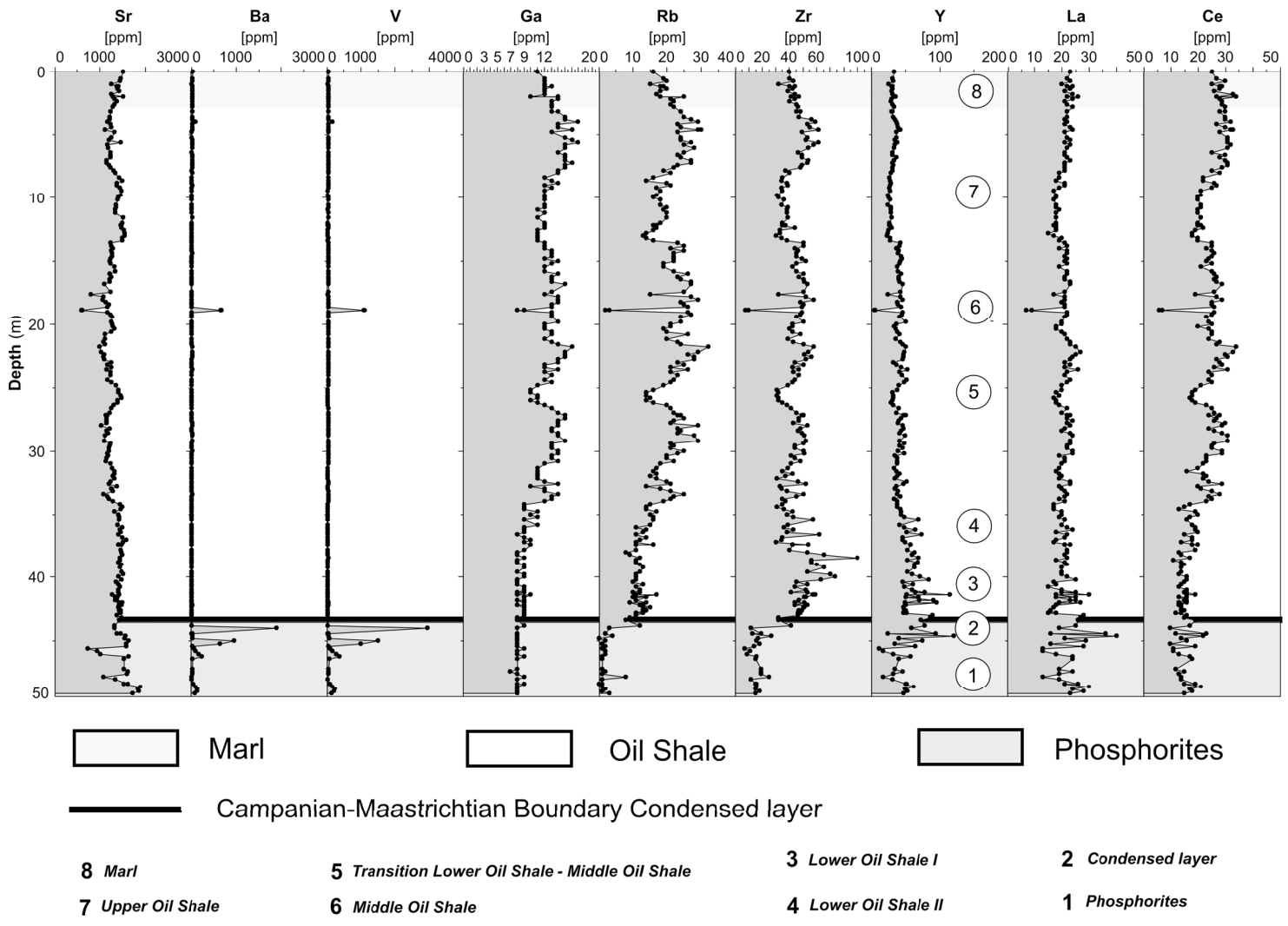

Fig.37 Minor element composition in three analysed units. Elements were grouped on basis the factoranalysis

Stratigraphic Unit	Phosphorite					Oil Shale					Marl				
[1] *Main Element [%]*	***n***	***Average***	***Max***	***Min***	***Stdev***	***n***	***Average***	***Max***	***Min***	***Stdev***	***n***	***Average***	***Max***	***Min***	***Stdev***
SiO_2	4	0.7	1.5	0.2	0.6	33	11.6	19.4	4.9	4.3	3	12.5	13.3	10.8	1.1
TiO_2	4	[6]bdl	[6]bdl	[6]bdl	[6]bdl	33	0.2	0.4	0.1	0.1	3	0.2	0.2	0.2	0.0
Al_2O_3	4	0.2	0.5	0.0	0.2	33	4.7	9.0	1.0	2.3	3	5.4	5.9	4.6	0.6
$Fe_2O_{3\,(t)}$	4	0.2	0.3	0.1	0.1	33	2.0	3.7	0.5	0.9	3	2.1	2.2	1.8	0.2
MnO	4	[6]bdl	[6]bdl	[6]bdl	[6]bdl	33	[6]bdl	[6]bdl	[6]bdl	[6]bdl	3	[6]bdl	[6]bdl	[6]bdl	[6]bdl
MgO	4	0.3	0.5	0.2	0.1	33	0.7	0.9	0.5	0.1	3	0.6	0.6	0.5	0.0
CaO	4	35.6	48.7	27.9	7.9	33	33.7	43.0	23.6	4.5	3	40.8	42.2	40.0	1.0
K_2O	4	[6]bdl	[6]bdl	[6]bdl	[6]bdl	33	0.2	0.5	0.0	0.1	3	[6]bdl	[6]bdl	[6]bdl	[6]bdl
Na_2O	4	0.1	0.2	0.1	0.0	33	0.2	0.4	0.0	0.1	3	0.1	0.1	0.0	0.0
P_2O_5	4	12.3	15.4	10.2	2.1	33	1.9	4.0	0.8	0.9	3	1.9	2.1	1.8	0.1
C_{org}	4	3.1	5.0	0.7	1.6	31	9.8	22.2	0.6	4.2	3	0.8	1.0	0.7	0.1
C_{carb}	3	6.0	7.7	3.3	1.9	23	4.8	6.9	3.3	1.0	3	7.0	7.6	6.6	0.4
[2] **SO_3**	4	2.5	4.3	1.6	1.1	32	6.4	14.1	0.4	2.1	3	1.1	2.5	0.3	1.0
[3] **OM**	4	5.5	8.9	1.2	2.9	31	17.5	39.7	1.0	7.5	3	1.5	1.8	1.3	0.3
LOI (950°C)	4	48.1	59.5	35.4	8.6	34	40.5	49.0	33.1	4.4	3	34.1	35.7	32.2	1.4
[4] **S_{total}**	4	1.0	1.7	0.6	0.4	32	2.6	5.6	0.1	0.9	4	0.4	1.0	0.1	0.4
[5] *Trace Element [ppm]*	***n***	***Average***	***Max***	***Min***	***Stdev***	***n***	***Average***	***Max***	***Min***	***Stdev***	***n***	***Average***	***Max***	***Min***	***Stdev***	***Detection limit (ppm)***
Cu	24	31	93	13	15	197	92	145	18	18	14	81	98	57	12	5
Cr	24	224	832	65	147	197	456	726	72	93	14	402	444	322	33	26
Ni	24	57	229	22	40	197	147	226	25	29	14	121	142	101	13	12
Sr	24	1477	1896	739	287	197	1295	1576	599	153	14	1378	1510	1245	85	1
Ba	24	213	1888	20	418	197	37	674	20	65	14	37	46	30	4	3
V	24	151	807	30	148	197	78	128	14	23	14	65	83	49	9	50
Mo	24	29	84	9	20	197	14	38	2	5	14	9	14	5	3	2
Zn	24	286	809	123	129	197	271	530	35	92	14	200	245	146	23	3
Cd	24	87	334	17	62	197	10	22	3	3	14	8	12	7	2	1
As	24	5	18	0	4	197	16	45	0	7	14	12	17	8	3	2
U	24	111	196	40	34	197	35	85	0	9	14	31	36	23	4	3
Ga	24	8	9	7	0	197	12	17	8	2	14	12	14	10	1	3
Rb	24	2	8	1	2	197	19	32	2	6	14	19	25	15	3	1
Y	24	48	121	12	25	197	44	116	5	15	14	32	36	26	3	0
Zr	24	16	27	7	4	197	45	90	8	10	14	42	47	32	4	2
La	24	23	40	13	7	197	21	30	7	3	14	23	26	20	2	4
Ce	24	15	23	10	4	197	22	34	6	6	14	28	34	25	3	4
Th	24	4	7	4	0	197	5	6	4	1	14	5	6	4	1	3
Pb	24	0	4	4	1	179	4	14	0	3	14	5	8	3	1	2
Nb	24	[6]bdl	[6]bdl	[6]bdl	[6]bdl	197	3	9	0	2	14	3	5	2	1	1
Ag	24	2	3	1	0	197	1	2	1	0	14	1	2	1	0	1
Sn	24	1	2	0	0	197	2	3	1	0	14	2	3	1	0	0

[1]WDXRF Standards: AGV-1 BHVO SDO **Material: melt tablets**

[2]$SO_3 = S_{csa}$ [wt%] x 2.5

[3]OM = C_{org} [wt%] x (100/75) x 1.34 (Tyson, 2001,Littke, 1993)

[4]CSA

[5]EDXRF Standards: AGV-1P GXR-2 GXR-3 GXR-4 GXR-5 GXR-6 SCO-1 SDO-1P SL1 SOIL V SOIL-VII **Material: powder samples**

[6]bdl: below the detection limit

H_2O content (85°C): 1-3 (wt%)

Table 5 Comparison between the main and minor content in the analysed profile

Interpretation of major and minor elements data and depth ranking:

Despite some pitfalls, (see also van der Weijden, (2002) and references therein), it is common to set the enrichment of a given element in contrast to the average crustal threshold. Regarding this, the enrichment factor of selected major and trace elements is defined as:

Equation 10

$$\text{Enrichment factor} = \frac{\text{Element/Aluminium}_{\text{sample}}}{\text{Element/Aluminium}_{\text{crust}}} \qquad \text{Eq.10}$$

In this work the North American Shale Composit (NASC) was used for the main elements (Gromet et al. 1984). Unfortunately, the author did not determine each trace element of the shale composition that is analysed here. Therefore, the average crustal values are taken from (Wedepohl, 1969-1972). An enrichment factor more than one (black doted line) signifies an enrichment above the crustal threshold, as defined by (McLennan, 1993; Gromet et al., 1984; Wedepohl, 1969-1972). On basis of the average threshold, the fig. 38 displays the calculated enrichment factors that are shown for the three investigated units (green line – MM, red line – OSM, black line – PM).

The major elements (Fe, Mn) show a depletion in all three units or a small enrichment in relation to the "crustal average". Unlike Ti, that shows enrichment by a factor of 10. Moreover, the EF`s of PM vary in two orders. However, in contrast to the EF`s of the OM, that vary only for one order of magnitude. This may signify a change, either in delivery source or regarding the transport mode (section 6) of sediments to the deposition area. Relative to the crustal average, redox-sensitive elements (As, Mo, U) are enriched chiefly in the PM up to 100 folds (U, Mo). In contrast, in the OM, As shows only a moderate enrichment (up to 10 fold) or sometimes even a depletion. „Nutrient type" microelements, like Zn, Cu, Ni, are enriched up to 100 times in the OS, whereas they are only moderately enriched in the MM (by a factor up to 10) (fig. 38, next page). Chromium follows the same trend as Zn, Cu, Ni.

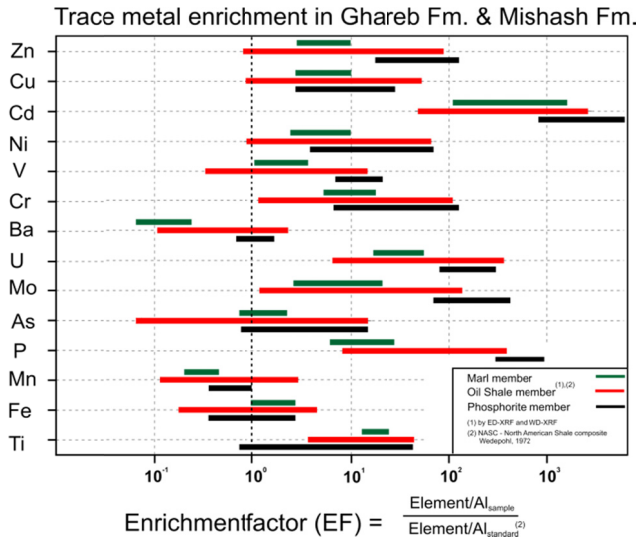

Fig.38 Comparison about the different calculated enrichment factors (EF) for the analysed elements throughout the profile. Dashed line marks the average crustal enrichment.

Two exceptions are noteworthy: the strong depletion of Ba in all units, and the extremly high enrichment of Cd that may be coupled to the enrichment of P. Due to their possibly biogenic origin, these elements show a high enrichment relative to the "crustal average", the enrichment factor can vary up to a factor of more than 100.

In summation, these findings indicate that the EF`s relativ to the "crustal average" show for all elements in the OSM and PM comparable pattern. Contrasting the MM an enrichment in a lower magnitude occurs.

Fig. 39 next page, shows a comparison between the aluminum normalised and non-normalised bulk trace element values throughout the profile. Most obvious fact is, that below 33 mbsf (LOS I, II), an intensively change of their enrichment is observed. Numbers in bold type represent the mean original bulk element concentrations (non-normalised). A comparison between these values (aluminium normalised vs. non-normalised) suggest apparently an enrichment of trace element in the LOS. The reason for this occurrence can be first, that their enrichment is caused due to the constantly extraordinary low aluminium content and secondly a change in the depositional regime.

It seems that the dilution effect cannot be the reason, due to the extraordinary low terrigenic input of Al_2O_3, responsible for the highest enrichment in chalcophile trace elements (CTE) in the LOS unit. The highest enrichment of CTE and their strong association with the organic carbon and sulphur might explain only the high primary productivity at the water surface and the carbon burial efficiency.

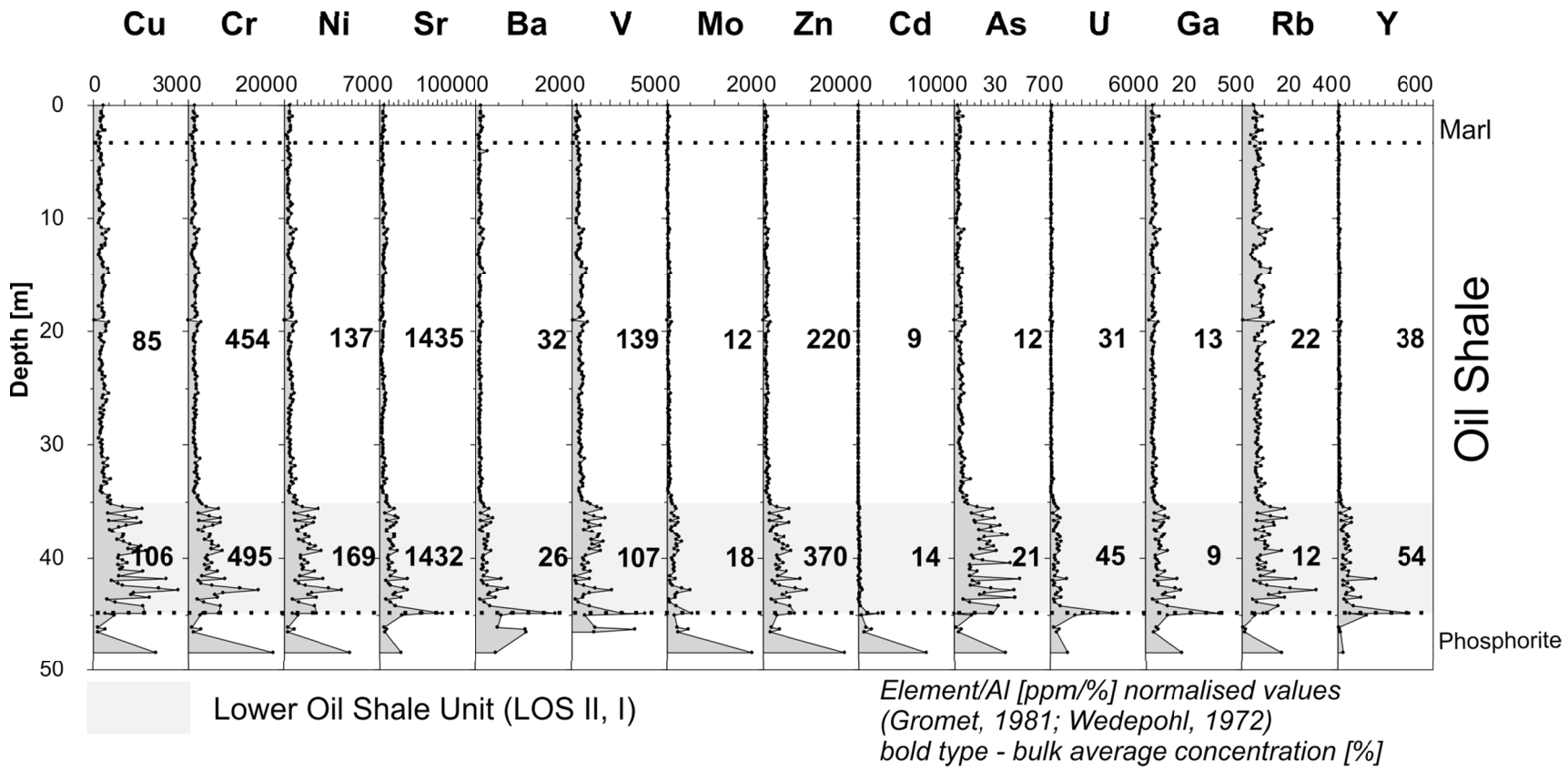

Fig.39 show the comparison between the average bulk concentrations in Upper Oil Shale unit and Lower Oil Shale unit (LOS). Numbers in bold type represent the mean original bulk element concentrations (non-normalised). A comparison between these values (aluminium normalised vs. non-normalised) suggest apparently an enrichment of trace element in the LOS. Concluding remarks might be that the preferred enrichment in the LOS is not caused due to dilution by terrigenic input.

4.3. Iron – Sulphur – Carbon systematics (Fe-S-C)

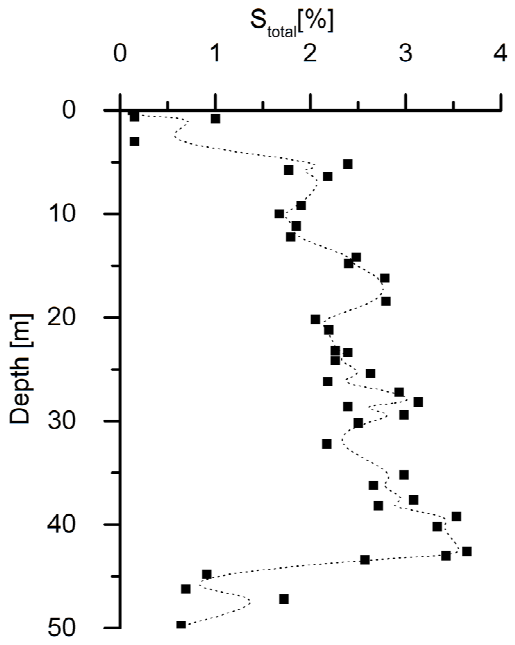

Fig.40 Total sulphur content in the profile (low-resolution data set, N=46). Highest values occur in lower parts of the oil shale unit, generally between 25-45 m depth.

Total sulphur content along the whole sections

A total of 46 samples were selected (low-resolution data set, fig. 40) to determine the total sulphur content. The highest values up to 3.3 wt. % (sd ±0.54) are observed for the LOS II. Throughout the OSM, a continuously decreasing trend is noticeable. A sudden drop in the total sulphur content marks the transition to the overlying marls. All three sections can be clearly distinguished by their different sulphur content.

Total organic carbon (C_{org})

The project partner at the University of Frankfurt carried out analyses to determine the organic carbon concentrations. Fig. 41 shows the corresponding results. On the first look, it seems as if the graph follows the same trend as for total sulphur. For the PM, an average organic carbon concentration of ~2.5 wt. % is observed. At a depth of 48.2 mbsf, a distinct value occurs. Here, the organic carbon shows a comparatively high value of 17.2 wt. %. It follows a sudden rise of the

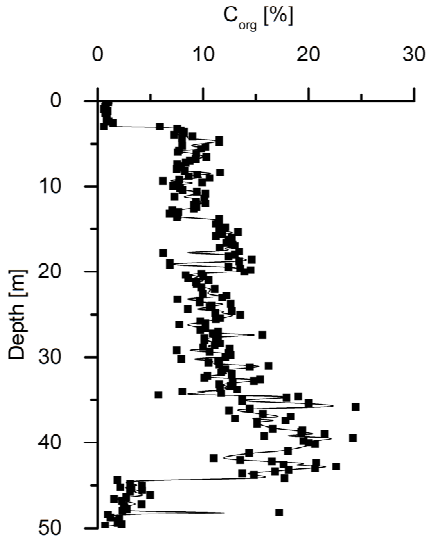

Fig.41 illustrate the organic carbon content in three analysed units. Note the dramatic change at 45mbsf the transition PM – OSM, and 3mbsf OSM - MM

organic carbon content at the transition from the PM to the OSM. Above the LOS, the organic carbon has highest concentrations of ~20 wt. %. At around 33 mbsf, the graph shows a sudden drop, the values decrease to the half. For the next 15 m of the profile the graph shows subtle changes in organic carbon. At 20 mbsf, a sharp increase in the C_{org} is observed. The values rise about 5 wt. %. At the depth of 13 mbsf, the values drop once more up to 6 wt. %. The next 10 m up-section, the values alternate between 6 and 12 wt. %. The transition from the OSM to the MM is marked by a sharp drop, their values decrease from 6 to 0.6 wt. %.

Degree of pyritization (DOP)

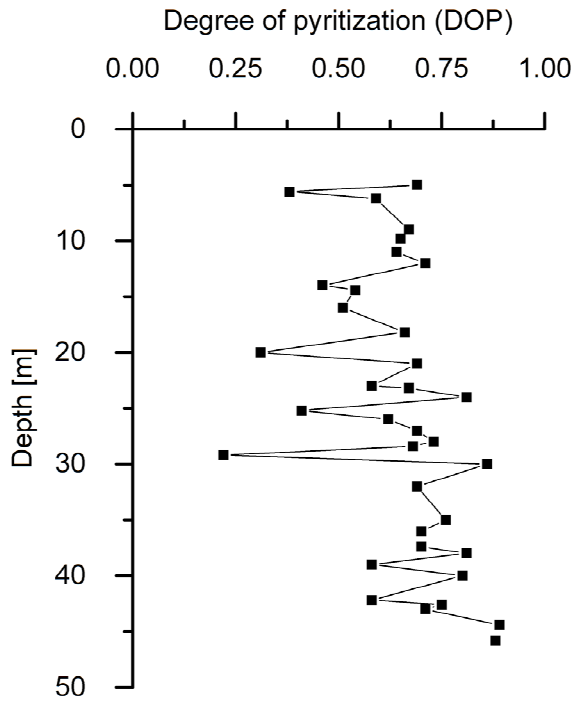

Fig.42 indicates the DOP (degree of pyritisation), for definition see text below

The iron content that is actually present as pyrite is shown in fig. 42. The values ranges between 0.27 - 0.83 and increases very weakly with depth.

4.4. Calcium-normalized – element content of foraminifera test`s

The determination of the trace element composition of benthic (*Gavelinella*) and planktic (*Heterohelix*) foraminifera tests aims at gaining insight on differences in the composition of surface and bottom water. This takes place to detect temporal compositional trends because of changes in the upwelling system as well as in the oceanic circulation of the southern Tethys during the Late Cretaceous. It is assumed that the enrichment of trace elements in foraminifera shells is a direct consequence of the process of biomineralisation (Weiner and Addadi, 2011, Erez, 2003). The vertical distribution of the Ca-normalised concentration of some potentially relevant elements in planktic and benthic foraminifera is shown in fig. 45, pages 105, 106. Unfortunately, for most of these elements, no regularities, which could have happened due to vertical concentration gradients between surface and bottom water or due to the existence of time dependent changes in ambient water chemistry, are observed. Several outliers, and the evidently capricious vertical distribution of the elements in both data sets, make the straightforward interpretation of these data sets, in terms of primary seawater signature, difficult and arguable. It is assumed that in both populations, typically marine micronutrients, such as Fe, Mn, Co, Ni, Cu, Zn, Cd, and Mo tend to correlate with each other and form distinct element associations. However, these associations do not reflect primary seawater signatures, but are rather due to the prolonged contact of the tests with pore and ambient waters, enriched in these elements during diagenesis. In other words, the enrichment of trace elements in benthic and planktic foraminifera tests should mirror the chemical composition of pore water and the water column. Therefore, for example, the benthic foraminifera from the lowest part of the OSM are deposited in the most oxygen deficient environment of the whole sequence. Relatively high contents of Cr and U, but low of Fe and Mn are measured. On the contrary, anoxic to euxinic bottom waters should rather have been depleted in Cr and U, and enriched in Fe and Mn. To evaluate possible interchemical relationships, a principal component analysis (PCA) was applied.

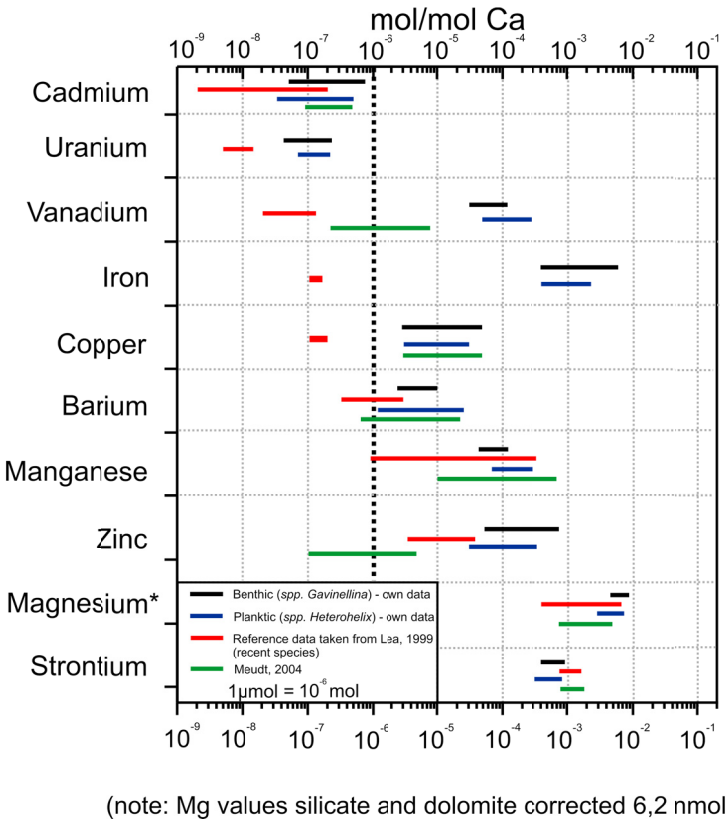

(note: Mg values silicate and dolomite corrected 6,2 nmol)

Fig.43 Trace element (TE) abundances in foraminifera shells (benthic and planktic) compared to reference values (red and green bars), taken from (Meudt, 2004; Lea, 1999). Dashed line marks the concentration of 1µmol/mol of TE in foraminiferal test`s.

The graph in fig. 43 shows the direct comparison between the analysed values and reference data from (Meudt, 2004) and (Lea, 1999). For most elements, there are no significant differences between analysed benthic and planktic trace element abundances in comparison to the reference values. However, the high levels of Fe and V are critical. Yet, due to their prolonged contact with the surrounding pore water, benthic foraminifera should show slightly higher values than their planktic counterpart does. Except for 3 elements (Cd, Mg, Sr), there are notable differences between the analysed values of this work and the reference values from (Lea, 1999). Sources for the exceptionally high values of magnesium can be clay minerals and dolomite precipitation, with respect to sulphate-reducing conditions by bacteria due to degradation of organic sediment (van Lith et al., 2003). On the basis of the own investigations, the observations are similar to Cléroux et al. (2008), showing very high Mg/Ca ratios. Most outstanding source for extraordinarily high Mg/Ca ratio in calcite are clay minerals that can contain up to 10 wt. % Mg (Jasmund, 1993). Depending on the weight of foraminifera shells (~15 µg), and according to (Barker et al. 2003), planktic foraminifera have an average Mg/Ca ratio of up to 3 mmol/mol. The authors calculate an increase of 10 wt. % in the measured ratio, equal to a rising of the Mg-content of one magnitude. Furthermore, an increasing content of magnesium of 1 wt. % raises the uncertainty in the measured Mg/Ca ratio.

Another possibility for a high enrichment of magnesium in foraminifera test`s arise either from incorporation by chemical exchange during the early diagenesis or the incorporation as micro particles during crystallization both as the mineral dolomite (Cléroux et al., 2008). The difficulty is to remove the dolomite contamination and by now there is not known a method to remove dolomite efficiently from the surface test`s. Otherwise, Cléroux et al. (2008) were able to show that 1 wt. % of dolomite and smectite in biogenic calcite rises the Mg/Ca by 5.6 mmol and 0.7 mmol respectively. Both Cléroux et al. (2008) and Barker et al. (2003) and other authors excluded such contaminated samples from the data set. Another possibilities for high magnesium values may be remaining organic detritus which is deposited in the inner chamber or at the surface on the shells (Martin and Lea, 2002; Rathburn and Deckker, 1997; Rosenthal et al., 1997). In such case and to prevent a higher contamination of the foraminiferal shells Martin and Lea, (2002) emphasize to rinse it with distilled water and methanol. Otherwise, the authors could not support the observation that higher organic matter contaminants enhance significantly the Mg/Ca ratio in benthic foraminifera.

Another option for the extraordinarily high enrichment of Mg involves the precipitation of dolomite minerals $Ca(MnMgFe^{2+})(CO_3)_2$ in form of magnesium-, manganese-, iron-rich carbonate by bacteria (González-Muñoz et al., 2008; van Lith et al., 2003; Vasconcelos et al., 1995). Many foraminifera show Mn-rich carbonate overgrowth or Fe and Mn rich (Fe/Mn oxyhdroxides) coatings. For example Glock et al. (2012) report that such coating is preferred on the unpurified inner surface shells of the shallow infaunal species *Uvigerina peregrine spp.* and *Bolivina spissa spp.* in the Peruvian upwelling site.

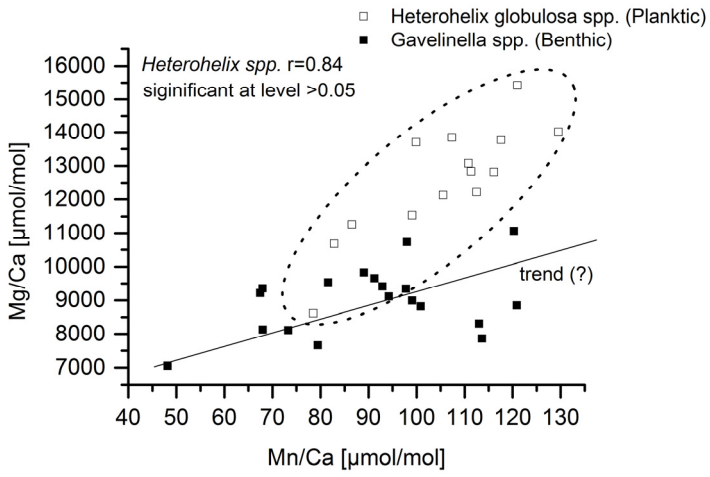

Fig.44 Correlation between Mg and Mn in foraminiferal test (note the non – statistically significant trend in benthic species), units in [µmol/mol]/ [µmol/mol]

In fact, as shown in fig. 44, there is a statistically significant correlation only between manganese and

magnesium in planktic, and only a slight trend in benthic, species with no statistically significant correlation between manganese and magnesium. This result is supported by the factor analysis shown in Factor 1 of benthic foraminifera, with a correlation between Pb, Cu, Ba, Cd, and Mn, which is typical for Mn-Mg rich carbonates. Results are supported by observations by Pena et al. (2005), who detected manganese-rich carbonates (kutnahorite-like) in the inner shells of unpurified foraminifera from the Panama basin. These shells show Mn/Ca ratios of up to 400 mmol/mol and a Mg/Ca-ratio of up to 50 mmol/mol, respectively. Furthermore, Pena et al. (2005) stressed that the cleaning residuals contain kutnahorite-like minerals. These enhance the Mg values up to 7-36%, which subsequently leads to an overestimation of the palaeotemperature up to 6° C. Own results, compared with those of Pena et al. (2005), indicate a low Mn- but a higher Mg content of up to 15 mmol/mol, for both the benthic and planktic shells, in the cleansed tests. On basis of SEM-EDX analyses, Pena et al. (2005) determined a magnesium content in analysed shells of about 11 wt. %. XRD analyses obtained by this study reveal that both planktic and benthic foraminifera contain dolomite. Therefore, we cannot rule out further dolomite phases (Fe- or Ca-rich) or Mn-Fe oxyhydroxides that contribute to a higher magnesium content. Vanadium is often scavenged at the surface of iron/manganese-oxyhydroxides. Therefore, high values for both are likely, but the extraordinarily high values were unexpected.

The reductive part comprises the dissolution of all metal oxides by hydroxyl-ammonium chloride, according to this chemical equation (Eq.11)

Equation 11

$$2Fe^{3+} + 2H_3NOH^{+} \rightarrow N_2 + 2Fe^{2+} + 4H^{+} + 2H_2O \qquad \text{Eq. 11}$$

It is reasonable that this dissolution/oxidation part is not fully completed. A reason for the incomplete dissolution may be the usage of different acids. Meudt, (2004) emphasises the necessity to remove the oxyhydroxide coatings from the surface tests, by using hydroxyl-ammonium chloride. Unlike Boyle, (1981), who obtained the best cleaning results by removing oxyhydroxides with sodium dithionate/citrate cleaning methods. Unfortunately, Meudt, (2004) did not analyse the iron and aluminium content, which is important to evaluate a possible enrichment in iron/manganese rich coatings. A complete guidance and a critical evaluation of the removal of Fe/Mn-coatings and high

magnesium contaminants is given in (Pena et al. 2005, Rosenthal et al. 2004, Barker et al. 2003). Figures 45, 46 on next pages, display a summary of the results of trace element content in analysed foraminifera.

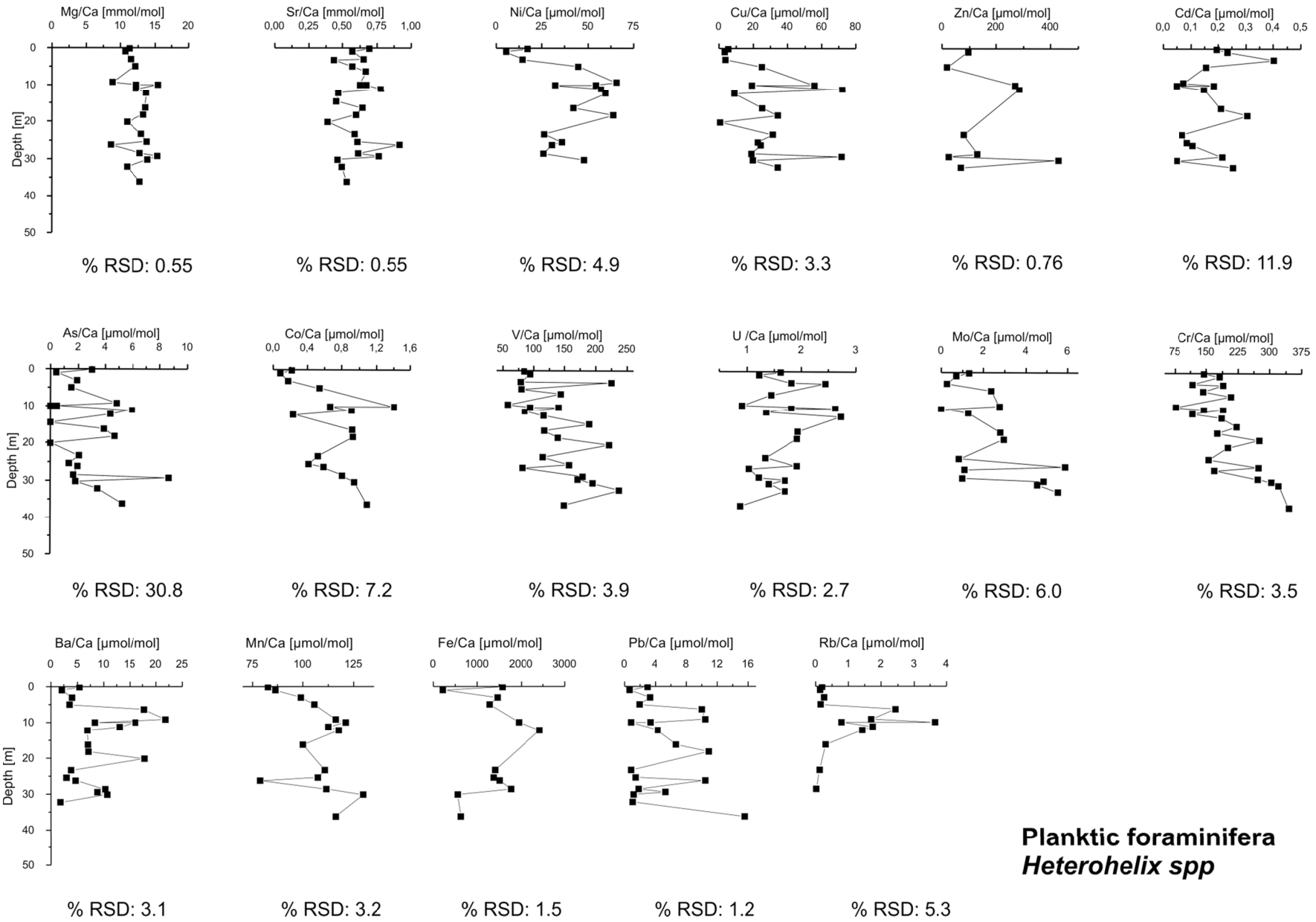

Fig.45 Contribution of trace element incorporated in planktic foraminifera along the section

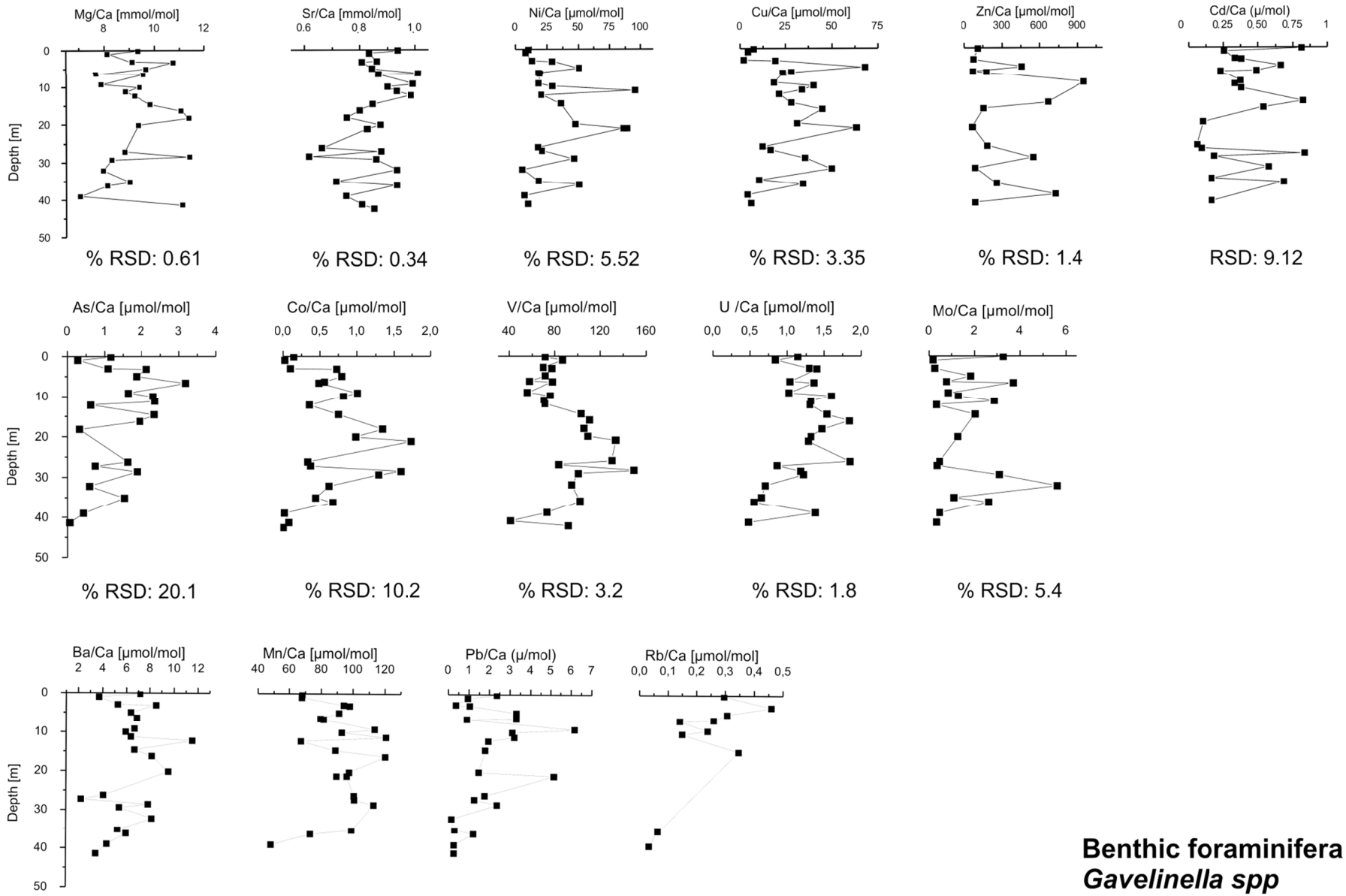

Fig.46 Contribution of trace elements incorporated in benthic foraminifera along the section

4.5. Sulphur isotopy

Absolute content

S_{total}, $S_{sulphate}$, S_{pyrite} $S_{organic\ sulphate}$, and $S_{organic\ sulphur}$

From the base to the top of the OSM, a continuously decreasing sulphur trend is observable (fig. 49, page 112). The *total sulphur* within the whole profile ranges upt to values of 3.6 wt. %. Obviously, there is a rapidly increasing trend up to 5-fold, from the underlying PM (0.7 wt. %) to the LOS (3.6 wt. %), detectable. The highest total sulphur values are observed in the LOS I, II, with up to 3.6 wt. %. The turnaround is marked at 38.2mbsf (LOS II). This depth marks the transition from the LOS II-horizon to the overlying transition horizon between the Middle- and the Lower Oil Shale layer. Very striking features are the exceptionally high total sulphur values of up to 2.5 wt. % in 20, 16, 14 mbsf (Upper Oil Shale). Around this depth, a similar trend to the sulphate content is detectable.

The *sulphate* content in the entire profile (N=45) reaches values of up to 2.7 wt. %, with an average content of 0.6 wt. %. Lowest sulphate values are observable in the LOS I, whereas in this part of the profile the highest organic sulphur values are also detectable. In depths, belonging to the OSM at 16.2 and 14.2 mbsf, two extraordinary spikes of 2.3 and 2.3 wt. %, respectively are evident. In the MM at 1 mbsf, another extraordinary spike of 2.7 wt. % is obvious.

The *sulphide sulphur* (chromium-reducible sulphur, CRS) at the base of the OSM is close to zero wt. %. The transition to the Lower Oil Shale Unit II shows an increasing trend up to 0.5 wt. %. During the transitional horizon the sulphur content of the pyrite stabilises at around 0.8 wt. %. The middle and upper part of the OSM display the alternating pyrite sulphur values. There is no pyrite detectable in the MM. The organic sulphur ranges between 1 and 2 wt. % in the Lower Oil Shale Unit (LOS). With some upward fluctuation trends, the *organic sulphur* displays a decreasing tendency. Both show the highest values in the LOS I, II, whereas in the remaining part of the profile alternating values are observable.

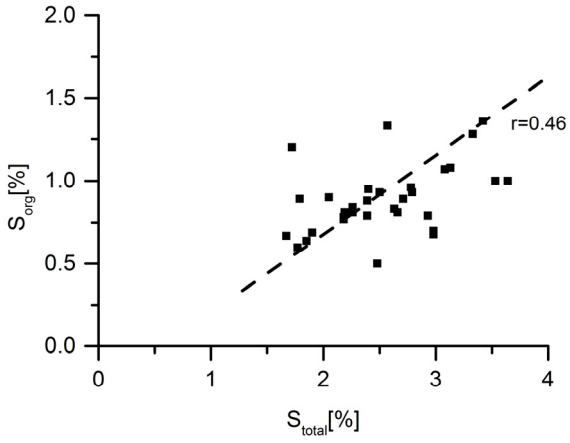

Fig.47 display the correlation between organic sulphur and total sulphur in the whole OSM, both are in units [wt. %]

Within the OSM, both organic and total sulphur display a significant correlation (r=0.46, p>0.05). This is supported by the observation that an overwhelming part of the total sulphur is bonded to the organic matter to form organic sulphur, fig. 47.

As shown in fig. 49, page 110, in the middle and lower part of the section the sulphate and sulphide sulphur display a weakly opposite trend. Sulphide and sulphate sulphur might increase moderately, whereas the organic bonded sulphur displays a decreasing trend.

Relative sulphur content in the different fractions

In oil shales, most of the sulphur (up to 94 rel. %) is bonded to the organic fraction. A gradually decreasing trend toward to the top of the OSM (40-50 rel. %) is observed (fig. 49, page 110). With values up to 45 - 67 rel. % for sulphur in the central and uppermost part of the OSM, the pyrite-S (CRS) is represented by a second, very common form of sulphur in the OSM. However, the concentration of pyrite is low in its basal, most organic rich part (<10 %). In the MM and PM, almost all of the sulphur occurs as sulphate, but in the oil shales the relative amount of sulphate-sulphur fluctuates strongly in a range mostly between 15 - 35 rel. % (except for some peak values of up to 65 rel. %). The AVS fraction is too low to allow the extraction of amounts sufficient for isotope measurements.

Complete data set listed in the appendix, table 25.

Sulphur isotopy

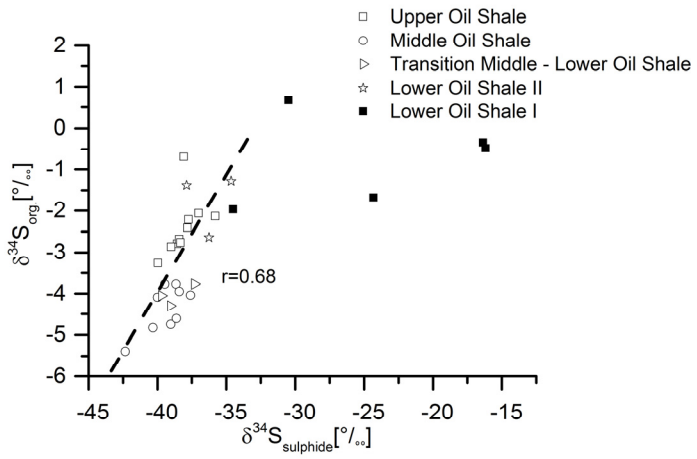

Fig.48 Observed correlation between $\delta^{34}S$ [‰] of sulphides and $\delta^{34}S$ [‰] of organic sulphur in the OSM, note the non – correlation in the LOS I.

The $\delta^{34}S$ values of the organic reduced sulphur (ORS) vary throughout the profile, in a relatively close range between -6‰ and +1 ‰, and are always considerably higher than the more scattered values recorded for pyrite-S (fig. 50, page 111). Sulphur in pyrite is typically strongly depleted in $\delta^{34}S$ (-43‰ to -34‰), but correlates rather well with the values of the ORS (r = 0.68; N=25;p>0 05), fig. 48, except for the samples from the lowest, most organic-rich part of the OSM (LOS I). In the PM, the $\delta^{34}S$-values increase suddenly by almost 20‰, attaining values as high as -16‰ (fig. 49, page 111).

$\delta^{34}S_{sulphate}$ (ASS)

As shown in fig. 50, page 111, $\delta^{34}S_{sulphate}$ starts with heavy values and shows a rapidly decreasing trend to lighter isotopes. During the transition, from the Phosphorite Unit to the Lower Oil Shale, a moderate decreasing trend is occurring. At about 38 mbsf, a sharp cut from 3‰ to – 15‰ indicates a very strong depletion. In the next 10m upwards an increasing trend to heavier values, with a short drop at 32m, is observable. From 32 mbsf to 25 mbsf, some fluctuations between -3‰ and -14‰ are observable. The most striking drop is at 25 mbsf, with the lightest values (-20 ‰) of $\delta^{34}S_{sulphate}$ in the profile. The next 10 mbsf show small turnovers in the values. At about 15 mbsf and 5 mbsf, light values occur; between these two stages an alternate trend with a slightly increasing tendency is observable.

$\delta^{34}S_{pyrite}$

The results show a distinct pattern for the whole profile (fig 50, page 111). From the bottom towards the top of the section, some changes in the isotopic sulphur composition of $\delta^{34}S_{pyrite}$ are observable. A clear cut occurs between the transitions from the Upper Phosphorite Unit to the Lower Oil Shale. The $\delta^{34}S_{pyrite}$ rises fast from the base of the PM to the transition horizon of the OSM, from -23‰ to -18‰. Up-section from 43.8 to 37 mbsf, a slow decreasing trend for $\delta^{34}S_{pyrite}$ is observable. From this point onwards a turnover with smaller ups and downs defines the remaining part of the oil shale section.

Organic sulphur ($\delta^{34}S_{intramolecular}$)

The value from the isotopic composition of the $\delta^{34}S_{intramolecular}$ begins with the heaviest results ~15‰ of the whole section (fig. 50). Subsequently, a strikingly sharp drop occurs at the transition to the Lower Oil Shale, where the values drop to very light results (-15‰). In the following OSM some turnovers occur. Increasing trends to heavier values complete the transition to the MM.

Organic sulphur ($\delta^{34}S_{intermolecular}$)

Organic sulphur isotopes show the highest fractionation rate, together with sulphate isotopes (fig. 50). It starts in the PM with very light values (-4‰, -3‰ and -5‰ respectively). In the transition zone, the values rise very fast, up to 2‰. With some fluctuations and a decreasing long-term trend, the values decrease to light values -6‰, similar to the values from the PM. At 25 mbsf, the opposite behaviour occurs, and values rise up to 2‰. The upper part of the OSM shows repeating turnovers, finally resulting in heavy values with an average of $\delta^{34}S$ 0.25‰ in the MM, comparable to the PM values.

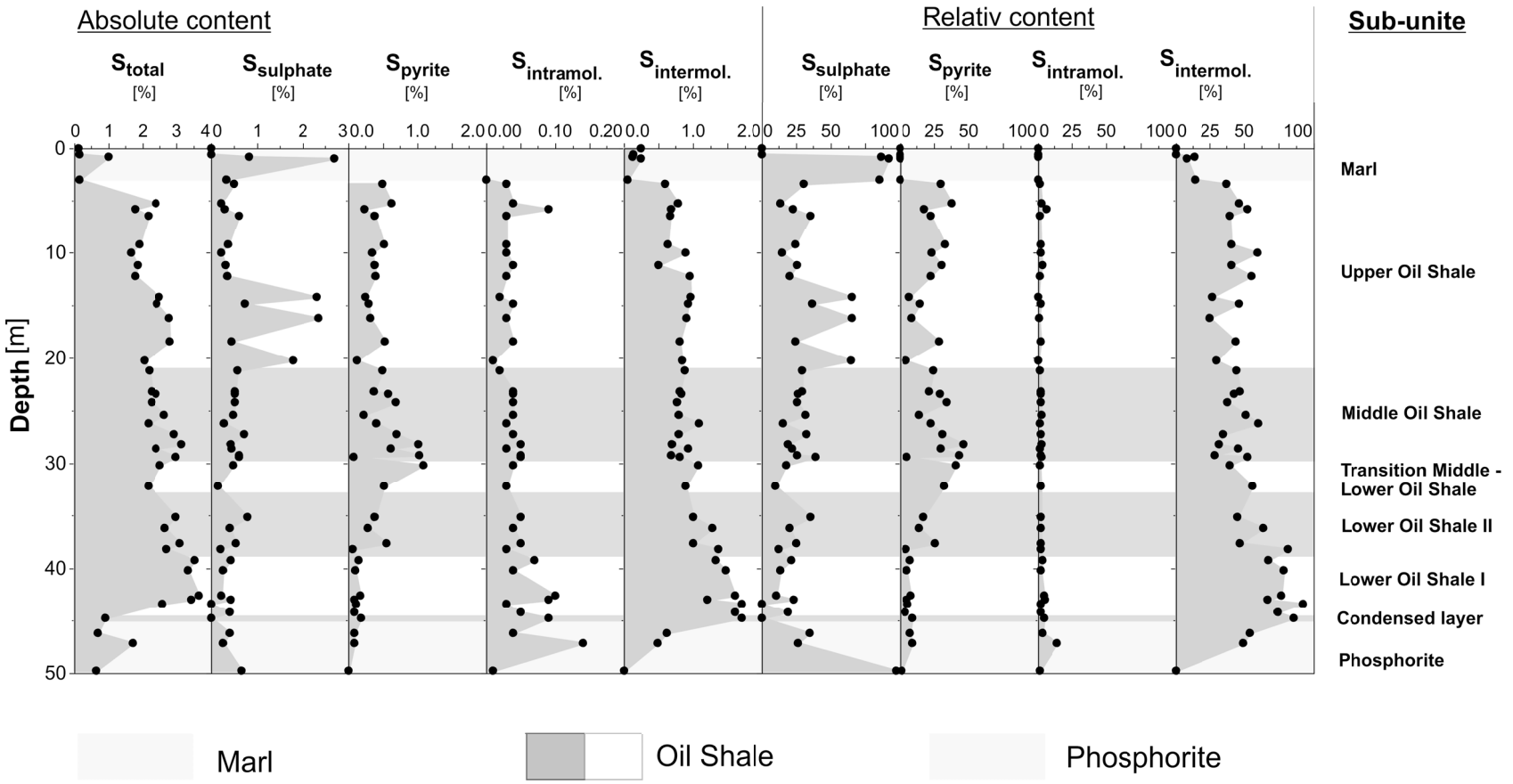

Fig.49 Absolute and relative content of different sulphur species along the section

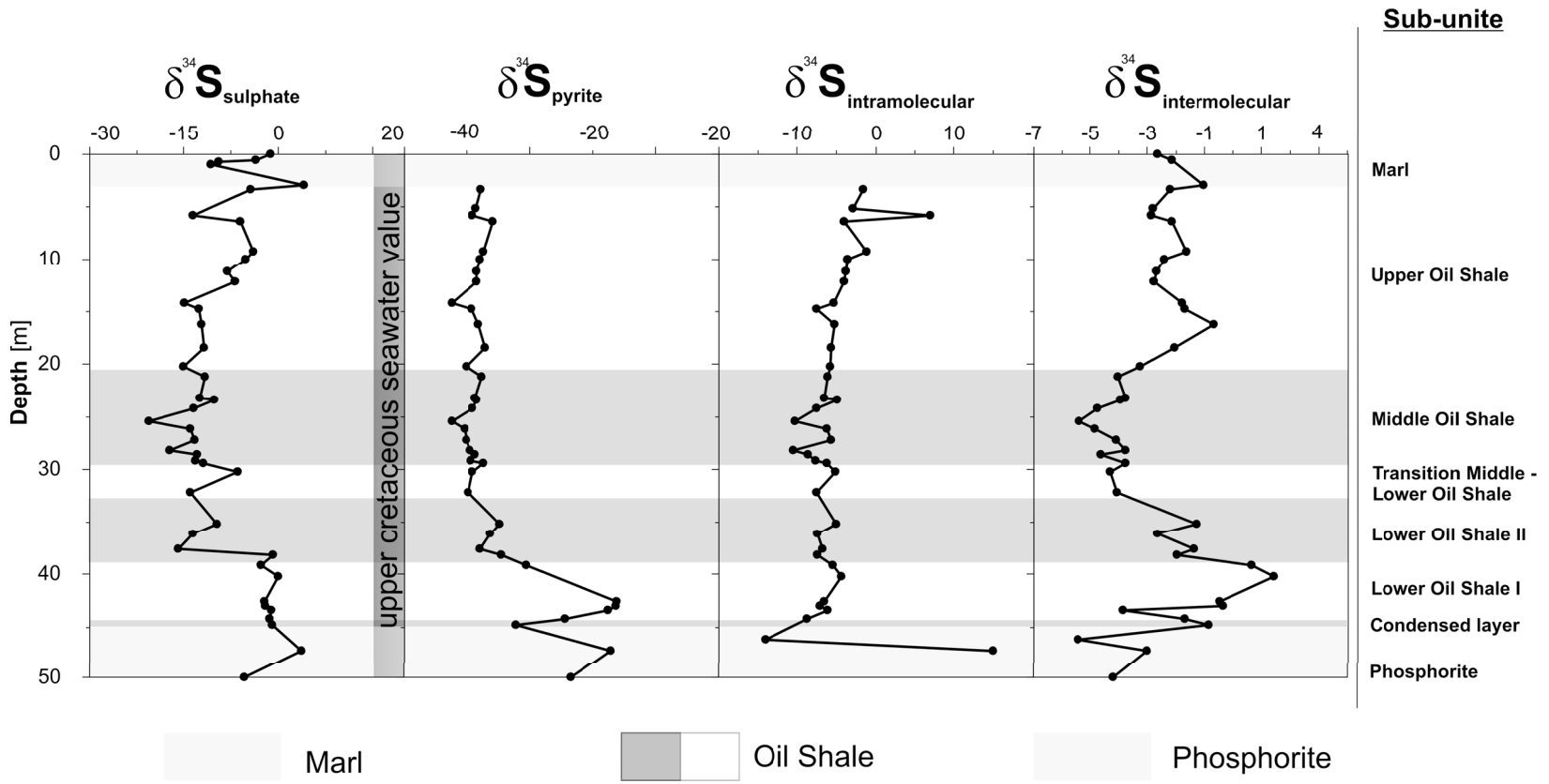

Fig.50 Distribution of sulphur isotopy in different S-bearing fractions along the section

5. A comprehensive interpretation of the available data with multivariate statistical methods

5.1. Factor analysis of bulk sediment

The results of geochemical analyses, obtained by energy dispersive X-ray fluorescence, have been interpreted by means of multivariate statistical methods. To assess inter-element relationships, a factor analysis was done. This method groups related variables, and thus geochemically coherent groups, into a limited number of factors that account for a substantial proportion of the variance of the data. Details from this method are given in (Suhr, 2009; Costello and Osborne, 2007). STATISTICA 6.0 was used for a principal factor analysis (PCA). After extraction of principal components, factor axes were rotated by normalised Varimax method to facilitate the interpretation loadings. Consequently, it is possible to draw conclusions from this, based on depositional factors and additional factors, determining the diagenesis in the sediments.

Results of the bulk sediments (OSM)

Many authors, (i.e. Sageman and Lyons, 2003; Werne et al. 2002; Dean and Arthur, 1998, Arthur and Sageman, 1994, Dean and Arthur, 1987), subdivide the terrigenic input into sedimentary deposits in three main components: (1) biogenic component that includes the amount of organic matter, carbonate content, and opal, (2) a detrital component that includes volcanogenic, fluvial and aeolian sources. A third, authigenic component are redox sensitive elements that occur in different valence states. Based on these categories, it is possible to group results from the factor analysis in two related factors. The factor analysis from the bulk rock analysis in Mishor Rotem explains 84% of the total variance.

Factor 1 accounts for 44% of the total variance. The first factor mirrors the degree of bottom water oxygenation (Cu, S, Ni, Zn, Cr, $C_{org,}$), while this also includes elements which stand for conditions that promote phosphorite deposition ($P_2O_{5,}$ U, As, Mo, Y). Trace elements (~20%) can be associated

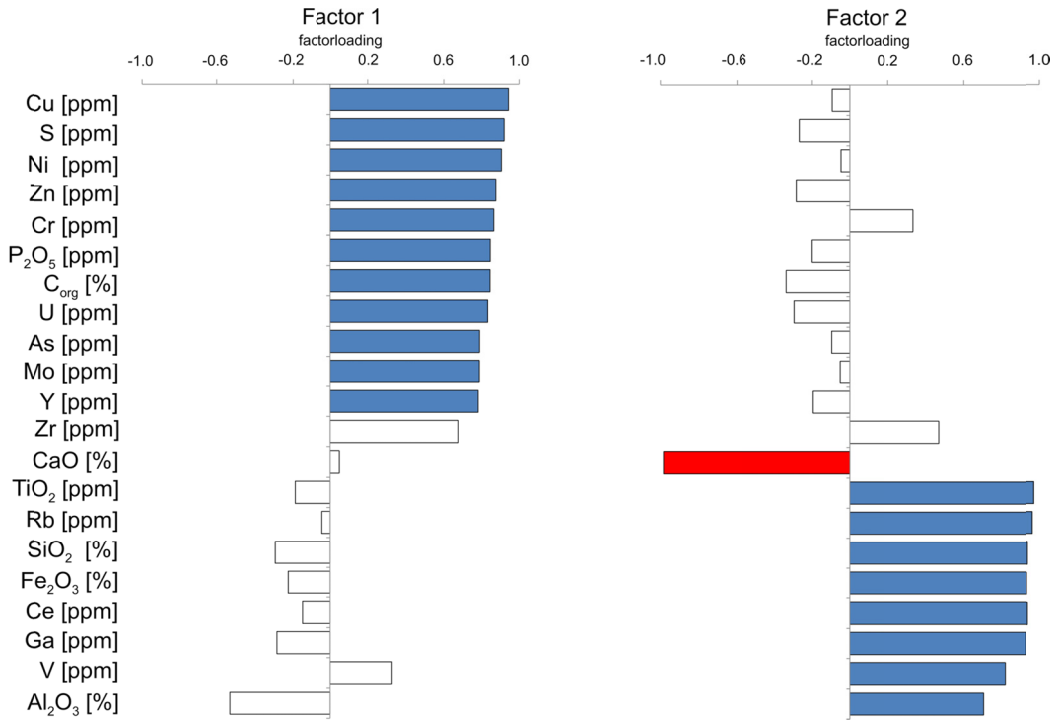

Fig.51 Bar plot of extracted factors and factor loading (blue labelled bar signifies positive, red labelled bars display a negative factor loading).

with organic matter and sulphur; see also Abanda and Hannigan, (2007, 2006) and references therein. As already indicated in previous section 3.1.1., up to 90% of sulphur is bond to the organic matter.

Factor 2 summarises 40% of the total variance, that is characterised by elements with high positive factor loadings for TiO_2, Rb, SiO_2, $Fe_2O_{3(t)}$, Ce, Ga, V, and Al_2O_3. Only CaO comprises a negative algebraic sign with an oppositely high loading.

We can therefore interpret, on basis of these results (fig. 51), **Factor 1** as degree of bottom – water oxygenation, and **Factor 2** as the input of siliciclastic bioclastic (carbonate) material. Significant factor magnitude is labelled in blue for positive and in red for negative factor loadings. A negative sign of factor loadings indicates an inverse relationship. Factor loadings are numerical values between +1 and -1, representing how each factor is associated with the individual variables.

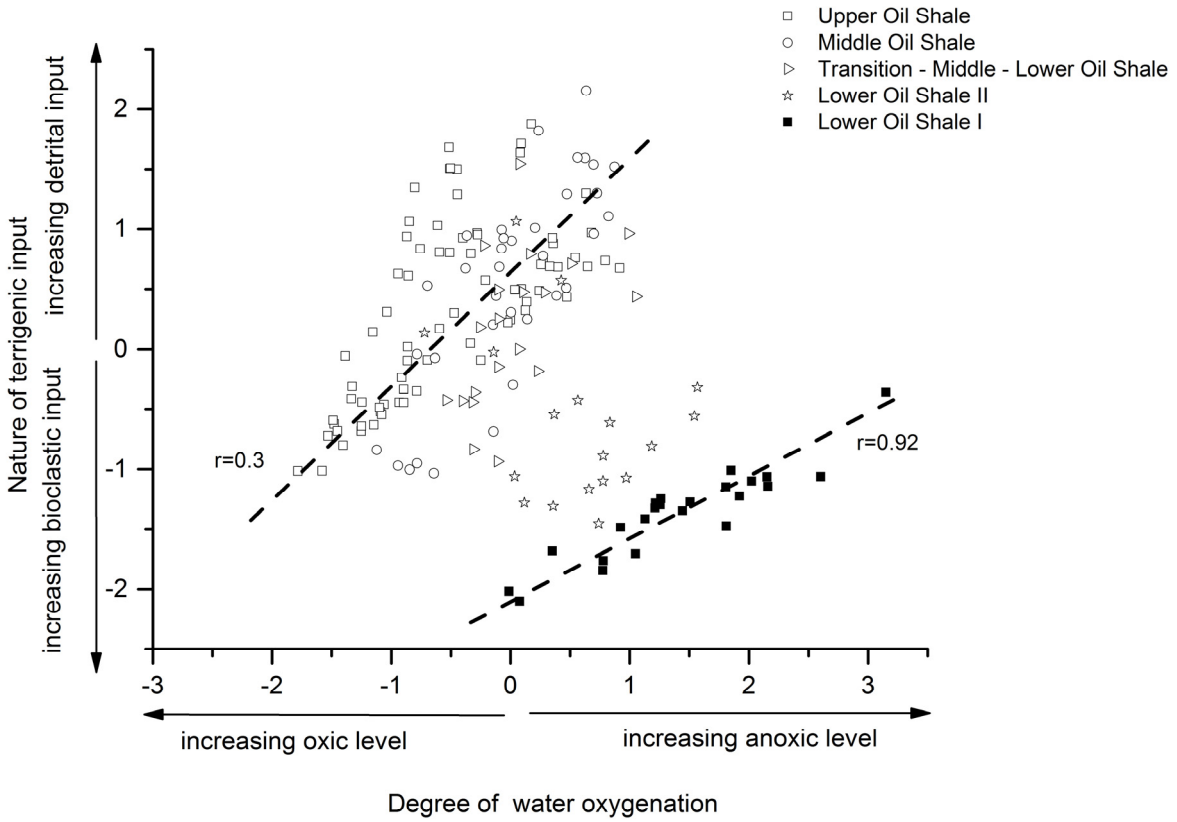

*Fig.52 Cross plot showing the relationship between the calculated factor scores of **factor 1** (bioclastic vs. terrigeneous detrital input) and **factor 2** (degree of bottom water oxygenation) in different parts of the OSM.*

As shown in fig. 52, the result from the factor analysis is represented in calculated factor scores. Samples are represented by points (factor scores) in the oil shale unit, which match a distinct sedimentary and environmental unit. The calculated factor scores allow assessing the relative contribution of these two factors in each of the samples and thus permit to trace more subtle variations in depositional conditions during the formation of the oil shales.

Previously, as noted in section 4.3, based on geochemical results, the section is divided into different units and sub-units. As a result, the bi-variate plot displays four sedimentary environments. The y-axis represents the nature of sedimentary input. Increasing factor scores on this axis are related to a higher input of detrital material. The opposite direction shows the influence of a stronger bioclastic input and weak detrital sedimentation, whereas the x-axis shows the degree of water oxygenation. Higher factor

scores on this axis display an increasing trend to anoxic conditions. The lower part of the scatter plot displays a high bioclastic input in a more pronounced anoxic environment.

Between the nature of sedimentary input and the degree of water oxygenation, a good statistical correlation ($r=0.3$, $n=112$, $p>0.05$) is observable for the middle and the upper part of the profile (fig. 52). The lower part (LOS I) shows an excellent correlation between the nature of sediment input and the degree of water oxygenation ($r=0.92$, $n=22$, $p>0.\ 05$), whereas the LOS II might be interpreted as a transition horizon between these subunits.

With these statistical results, this plot can be interpreted in the following way: A clear trend is observable from the base to the top of the profile. On the one hand, samples from the lower part of the profile (base of LOS I) fall in the field with a more intensive bioclastic input or carbonate sedimentation and a low oxic level. On the other hand, samples from the top of the oil shale unit show a high bioclastic input with a high oxic level. Most of the samples above the LOS II plot in a field with an oxic environment and increasing detrital input. In the lower part of the oil shales, the relative amount of detrital components tends to increase. Following a relatively short carbonate dominated episode, the clastic to carbonate ratio stays relatively constant for the next ca. 10 mbsf. At ca. 36 - 35 mbsf, a sudden drop in the relative amount of detrital input marks the beginning of a new episode with increasing amounts of detrital components, a trend that continues up to the top of the oil shales.

Scores of F2 describe a very flat gradient at the base of the oil shales, indicating a rapid increase in anoxia. Afterwards, the degree of anoxia tends to decrease gradually up to ca. 5 mbsf. The sudden drop in detrital input at 35 mbsf correlates with a similar shift towards even less anoxic conditions. At the same time, a turning point towards the development of a slightly less oxygenated depositional environment in an up-section direction is visible.

Bioclastic input

However, factor 2 comprises the factor loadings with an opposite algebraic sign for CaO and elements that contribute to clay – and silicate minerals. The main contributor to the bioclastic input is carbonate. Fig. 53 shows a very strong statistical correlation (r=0.98) of C_{carb} and CaO_{corr} This implies that gypsum/anhydrite and apatite are minor constituents in the OSM; otherwise, the main part of Ca is biogeneously bonded. Biogeneous ooze is either calcareous or siliceous (Li and Schoonmaker, 2004). Calcite tests of foraminifera are made up of $CaCO_3$ (low-Mg-calcite) or aragonite (Mason and Moore, 2001). Fig. 53 also shows a significantly high correlation between Ca/Al and Sr/Al (r=0.99). A good explanation for the extraordinarily high correlation coefficient, is given by the the fact that low-Mg calcite, formed by foraminifera, can contain up to 1100 ppm Sr (Turekian, 1968). Similar values have been obtained from own analyses, with benthic and planktic foraminifera containing up to 1300 ppm Sr. As earlier described in section 2, a high calcareous sedimentation (> 50 wt%) is mostly localised at the outer shelf, where the terrigeneous input is low (Brüchert et al., 2000). Whereas, silica (diatoms) and phosphor-rich sedimentation occurs, due to high terrigenic input and the resulting higher nutrient level in the inner shelf area. This leads to the preferred deposition of cherts and phosphate-rich rocks in the inner shelf area.

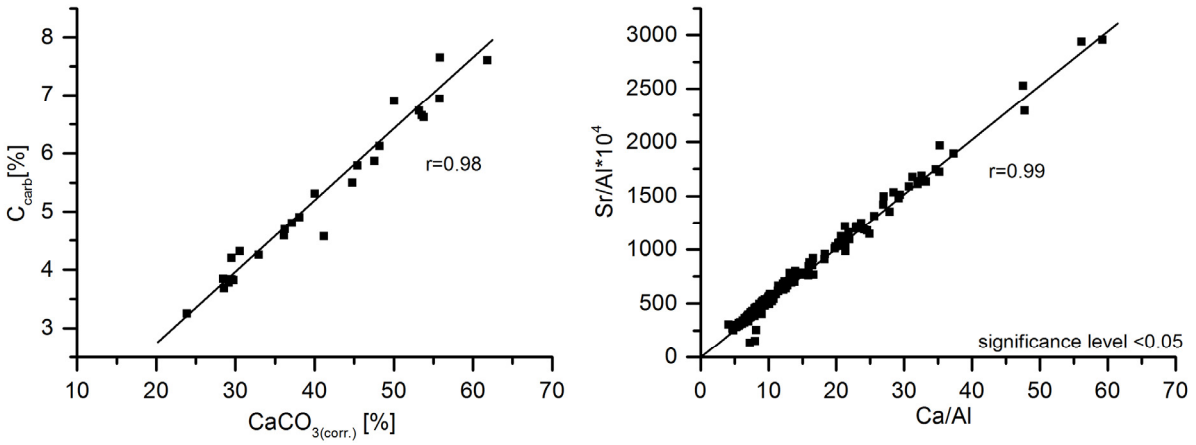

Fig.53 Left side: Correlation between inorganic carbon and corrected calcite, Sr vs. Ca respectively in the OSM (CaO corrected by the inorganic constituents $CaO = CaO_{sulphate}$-$CaO_{silicate}$-$CaO_{apatite}$). Right side: Graph displays the excellent correlation between Ca/Al and Sr/Al.

Calcium shows no correlation with P in the OSM. Assuming that all Mg was primarily bonded to the calcite, and pristine dolomite was absent (dolomite is mostly a result of late diagenesis[10]), the content of $MgCO_3$ in calcite was calculated. Calculations reveal that the lowest $MgCO_3$ (~below 1 Mol%) occurs in the PM, while the $MgCO_3$ content in the OM and the MM lies at about 2 Mol% in form of low Mg - calcite. Furthermore, with increasing diagenetic alteration due to equilibration with meteoric water, first a depletion in Sr^{2+}, Na^{+} and Mg^{2+} occurs Brand and Veizer, (1980), but calcite was later transformed to dolomite as indicated also by XRD analyses.

Terrigenic input and possible sources

Based on the results from factor analyses, factor 2 matches the interplay between bioclastic (e.g., carbonate sedimentation) and terrigenic input. (Sageman and Lyons, 2003) summarised the different possibilities to detect such variations. These include changes in element ratios, such as detrital clay minerals to the heavy minerals zircon $ZrSiO_4$ (Zr) and ilmenite ($FeTiO_3$) and/or rutile TiO_2 (Ti), changes in element ratios of detrital clays in relation to the (background) aluminium content, and ultimately, detrital input such as altered volcanic ash (K/Mg+Fe) in relation to the hemipelagic fluxes (illite). However, we can exclude terrigenic volcanic activity in time of deposition (Almogi-Labin et al., 2012). Throughout the following lines, it will be concentrate on changes in elemental ratios, in relation to aluminium and heavy mineral grains, within the OSM. Therefore, it should be possible to draw some conclusions from geochemical cross-plots concerning the source area.

As shown in fig. 54, page 119, in the Upper Oil Shale unit yields a high degree of correlation ($r= 0.85$, $p>0.05$) between Fe and Al. Ti also correlates well with Fe ($r=0.96$, $p>0.05$). This suggests that a part of the Fe and Ti are of detrital origin, possibly in the form of ilmenite. Trace elements like Ga, Rb, Ba, Ce, also show very good correlation with Al, possibly associated to form clay minerals. In spite of the slope of the regression line, fig. 54 also displays that all cross correlation reveal a sharp cut between the LOS and the overlying units. This may designate a change either in the supply of terrigeneous/detrital material or in

[10] Under certain conditions, as seen in section 4.1, an early diagenetic dolomite precipitation from supersaturated (hypersaline) (micro) environment would be possible

the source. It becomes apparent that all cross-plots show the same pattern; starting with a lack of correlation between Al/Fe and distinct heavy elements in the LOS I. This lacking correlation changes upwards in the profile. A tentative conclusion at this point is that firstly, during the transition from the LOS to the Upper Oil Shale a dramatic change in the terrigenic input to the palaeoenvironment took place, and secondly, in the Upper Oil Shale, no changes in the terrigenic input are observable. Concerning the remaining profile, this would imply a very stable environment over a long time slice. What is the reason for the dramatic change at the transition from the LOS to the UOS?

In general, most provenance analyses were done for clastic sediments or sandstones, where a significantly higher siliceous content occurs. During the Late Cretaceous, the area around the stable shelf acted as a stable uplift, and simultaneously, a subsidence along the northward continental margin (Levante Basin) caused a preferential northward transport of the sediment. (Ward, 1979, McKee, 1963). Supporting this, Tantawy et al. (2001), Soudry and Gregor, (1997), and El Beialy, Salah Y. (1995) recognised marine micro plankton, as well as pollen and *Nypa* palm mangroves, in a fossil fructification *Jodes spp.*, indicating a tropical wet climate with humid summers during the Maastrichtian in Israel and Egypt. A fluvial or episodic transport of delivered sediments by rivers under such conditions is conceivable. The Nubian sandstones are collectively termed as sandstone from Permian to Cretaceous age. They are described as a fine-grained coastal fluvial-plain and delta-plain sediments, which were deposited in ponds, lagoons, or marginal continental environments (El-Azabi and Farouk, 2011; Youssef, 2003; Shazly and Krs, 1973; McKee, 1963). The “Nubia sandstone formation” for example, from the Central Eastern desert in Egypt, can act as possible source area for terrigeneous input (Ward, 1979). However, other likely source area locations are in several outcrops in the Jordan (Am Abed and Amireh, 1983), North and South Jordan (Nasir and Sadeddin, 1989), or Saudi Arabian platform (Basaham and El-Sayed, 1998). So, Nasir and Sadeddin, (1989) described the mineralogical composition of the Early Cretaceous “Kunurb-Sandstone” in Jordan as follows: zircon, rutile, and tourmaline are frequent, less abundant epidote, garnet, and staurolite.

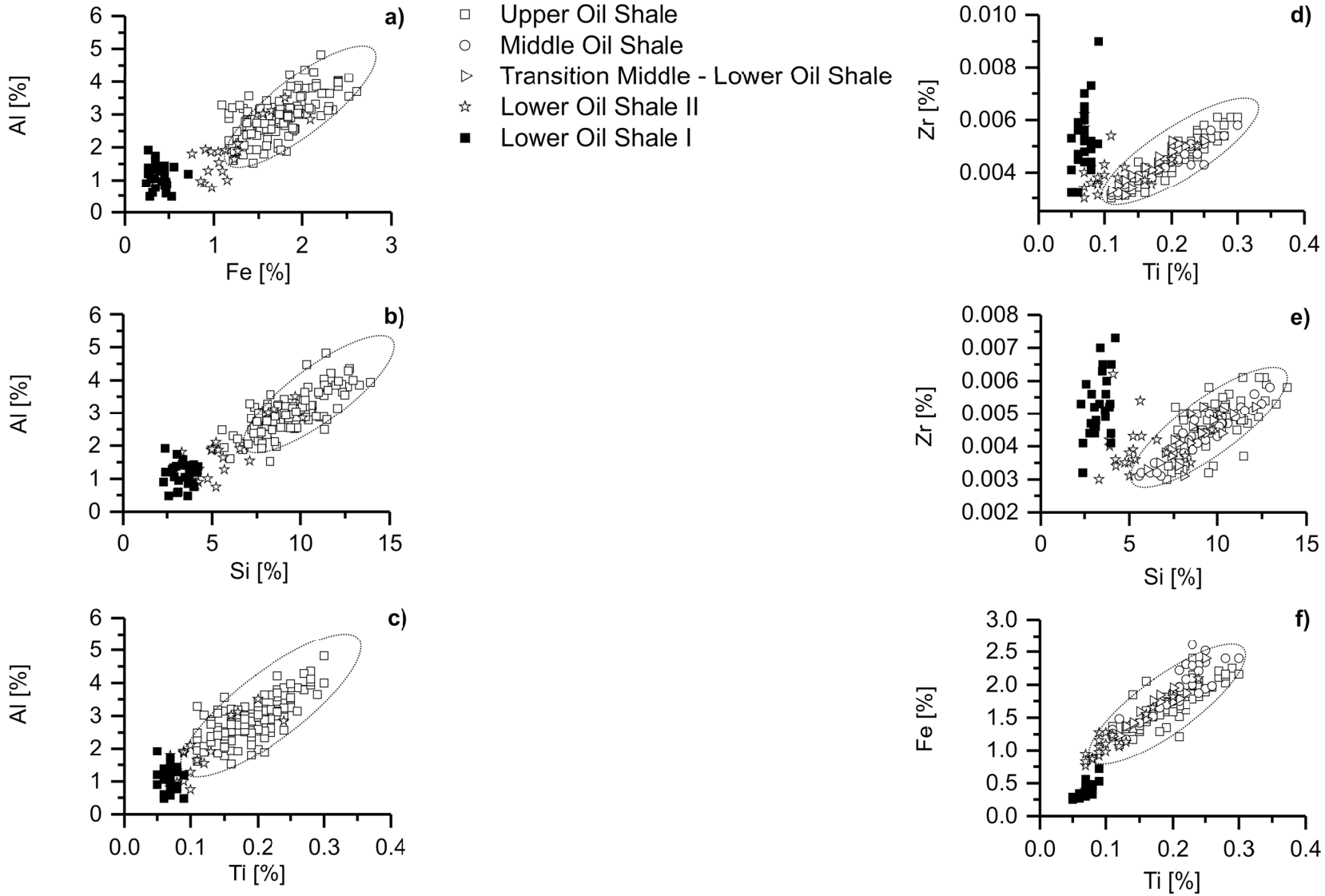

*Fig.54 All bi-variate plot show the same pattern Fe vs. Al **a)**, Si vs. Al **b)**,Ti vs. Al **c)**, Ti vs. Zr **d)**, Si vs. Zr **e)**,Ti vs. Fe **f)** :The base of the oil shale is marked bya sharp cut in the relationship between distinct heavy minerals from the overlying units (dashed line). Slopes of regression lines in units %/%.*

Another well described example for a provenance analysis was provided by Baioumy et al. (2003), who analysed the heavy mineral content in the Upper Cretaceous Duwi Shale in Egypt. The occurrence of zircon, epidote, tourmaline, rutile, and garnet, were accorded to a felsic or mafic source. Furthermore, Baioumy et al. (2003) used theoretical considerations, and results of field work of (Zhang et al. 1998), to show that the petrography of the analysed heavy minerals may indicate a shift from reworked sediment (Nubian Sandstone) to a mafic source. Recently, by an actual study, Baioumy and Ismael, (2010) supported this observation with new results on marine sediments from the Red Sea (Duwi fm.) in the Upper Cretaceous time. To locate the source area, where the sediment came from, we want to take a quick look at the way the sediment was transported and underwent a possible transformation from the source rock.

Al/Ti ratios in shales retain their source rock values (Hayashi et al. 1997). Based on this approach, the Al_2O_3/TiO_2 ratio change in different source rocks of mafic sources appear to range from 3-8, in intermediate igneous rocks from 8-21, and in felsic rocks from 21-70. These ratios can be used to recognise their provenance field (Hayashi et al., 1997). For the Egyptian oil shales, Temraz, (2005); and Amajor, (1987) have used this approach to discriminate between their granitic and basaltic origin.

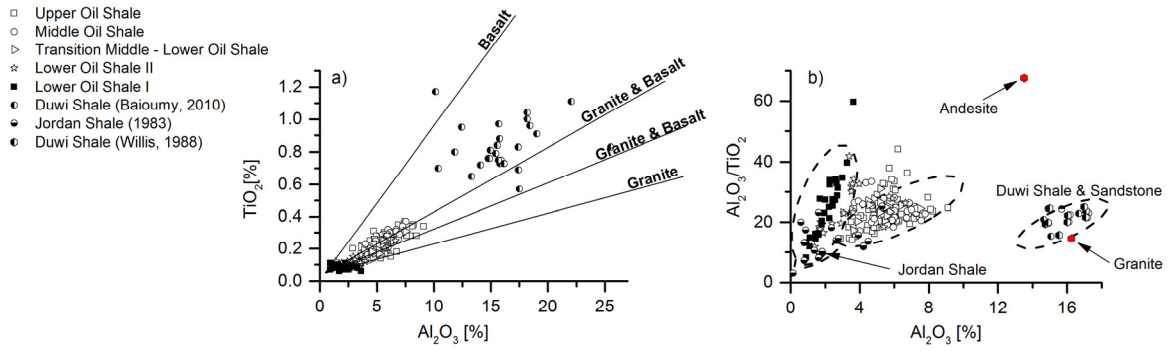

*Fig.55 Right side: Graph **(a)** illustrates the different Al_2O_3/TiO_2 relationships and shows that the provenance material varies from granitic to mixed granitic rocks (Temraz, 2005;Amajor, 1987). Left side: Plot **(b)** shows a clear discrimination between comparable oil shale deposits from the Ghareb fm. (Israel) and Jordan shale to the Duwi shale & sandstone.*

Based on the previous conclusions, it should be possible to distinguish between different contributions to the oil shale from distinct sources. Reference values from the Duwi (Baioumy and Ismael, 2010, Willis et al. 1988) and Jordan shale (Am Abed and Amireh, 1983) are also shown. On the left side, in fig. 55, a clear discrimination between Lower Oil Shale and the Upper Oil Shale unit (~20) is shown, based on the Al_2O_3/TiO_2 (~35) relationship. Based on the above mentioned premise, fig. 55, left side, suggests that the Jordan oil shale and shales from the Ghareb fm. might derive from the same source, in contrast to the Duwi Shale (red doted) values, plotted in the vicinity of a granitic source. Moreover, the change in the Al_2O_3/TiO_2-ratio between the Lower Oil Shale unit und the Upper Oil Shales, signifies a drastic change either in the source or in the delivery mode.

Another possibility arises by applying a ternary diagram (fig. 56) that yields information on the maturity of the sediments. The geochemical background discovered by this application, is that a preferred enrichment of zirconium takes place in the coarse fraction, whereas TiO_2 is mostly enriched in the fine-grained fraction, together with Al_2O_3.

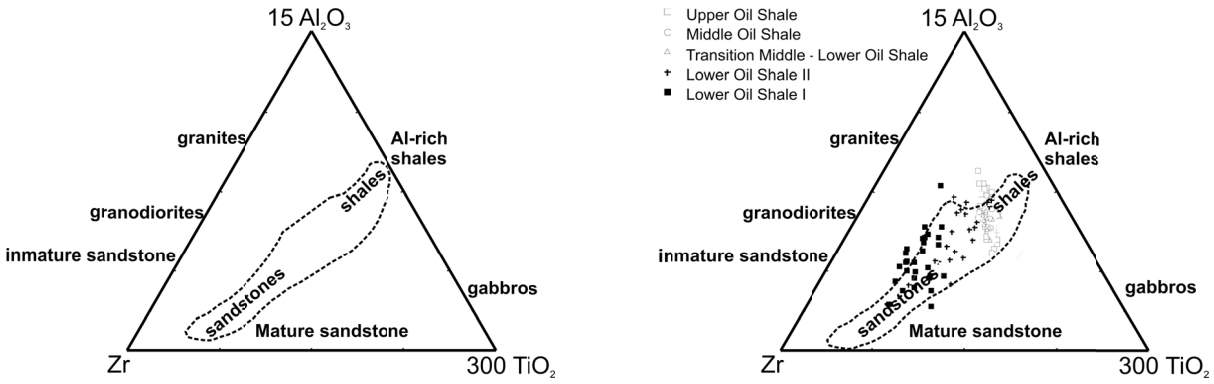

Fig.56 Left side: As previously mentioned, plots based on the premise that Al, Ti, Zr are immobile during chemical weathering. Typical minerals are rutile, zircon, and ilmenite. The content of these minerals varies in response to the degree of weathering (leaching process). However, their relative proportions underlie no modification during the transport into the deposition area (Garcia et al. 1994). Right side: A gradual change towards the top of the profile, from mature (heavy mineral) to more inmature (clay-rich) material, took place. Gradual transition horizon starts around 33 mbsf.

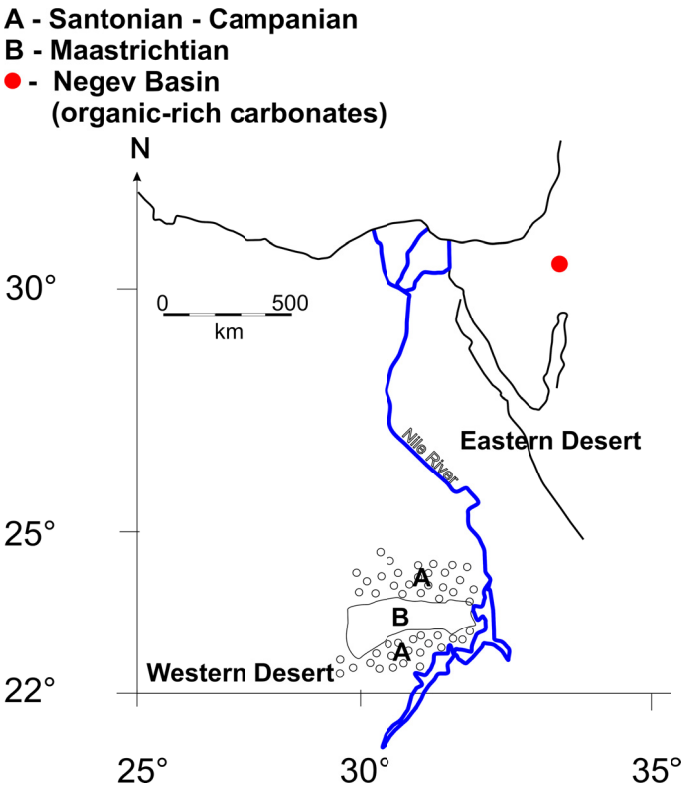

Fig.57 Map displays the possible source area for mineral transport in this time interval, redrawn after Mateer et al. (1992)

By interpreting these observations, it is apparent that Al_20_3 tends to increase with increasing TiO_2/Zr, and vice versa. Nevertheless, it is assumed that the relative proportion of these elements does not change until reaching the place for sedimentation. Thus, the ternary diagram helps to interpret the sorting process, regarding the path travelled by the deposited sediment. Thus, this ternary diagram is applied as a tool for the chemical identification of shales and sandstones (Garcia et al. 1994, and references therein).

As shown in fig. 56 (previous page), and regarding the above mentioned considerations, a tentative conclusion might be that the base of the OSM is affected by mature sediments, which suggest a short transport route to the place of deposition. In contrast to the overlying members, which are affected by immature detrital, which implies a longer distance to the deposition site.

With this information, it might be possible to differentiate between distinct source areas that contributed to the deposition area. Fig. 57 shows that the mature sandstone (Duwi Sandstone/Nubian Sandstone/ Duwi Shale) may act as a source for the transported sediments, which are deposited within the Lower Oil Shale. Unlike the Middle and Upper Oil Shale, the Duwi Shale (Quseire Shale) might act as a main contributor. According to this suggesting, the following conclusions can be drawn:

(1) The age of the Dahkla formation ranges about 71 - 63 Ma (CF8a-Plc[11]). Moreover, the contact between Duwi and Dahkla fm. marks the boundary between the Campanian-Maastrichtian and crosses the CF8a/b boundary (Tantawy et al., 2001).

(2) During the Palaeozoic time, the Nubian Shield and Arabian Shield were part of an uplift system. The eroded Palaeozoic material was transported in north-north-west direction, towards the Levante Basin, which acted as a subsidence basin.

(3) Both formations, Nubia Sandstone (Pre-Campanian) and Quseire Shale – (Pre-Campanian) as part of the Duwi fm., display differences in the mineralogical composition (Issawi et al., 1969). The first one can be described as a fine - grained quartz - arenite, which was deposited within fluviatile channels, Tantawy et al. (2001), whereas the shales of the Duwi fm (Quseire Shale) were deposited within a deltaic system (Soliman et al., 1986). The mineral content is represented by concentrations of rutile, zircon, and clay minerals (kaolinite, smectite, illite) (Baioumy et al., 2003). Both formations might have been as possible source areas for the delivered sediments, during the deposition of the organic rich carbonates.

(4) The results obtained by applying a ternary diagram ($Zr - Ti - Al_2O_3$) might indicate a change in transport mode and delivery source. Additionally, a tentative conclusion might be that in periods of deposition, the composition of the delivered sediment has gradually changed. A material, with a clastic component that yields a higher level of maturity, dominates the base (short transport paths). However, a gradual change towards the top of the profile, to more immature, clay-rich material, took place. Therefore, it can be concluded that the transport routes became gradually longer and the material came from increasingly farthest surrounding landmasses.

Degree of oxygenation (factor 2)

The second factor (F2) clusters elements, which typically accumulate in organic rich sediments, deposited under poorly aerated, oxygen depleted bottom waters. In addition to total organic carbon (C_{org}) and

[11] Maastrichtian is subdivided into eight biozones, labelled (CFl-CF8), Palaeocene foraminiferal subdivision (Plc)

sulphur, this factor includes chalcophile trace elements (Ni, Cu, Zn,), and oxyanion building elements with low mobility under reducing conditions (Mo, U). Moreover the combined "occurrence" of P, As, and Y, within this factor, might be interpreted in terms of a phosphatic component.

Minor elements that are closely related to the occurrence of phytoplankton, are of special interest. Compared to seawater concentrations, marine organisms are enriched in Ni, Zn, and V, by a factor greater than 1000 (Wedepohl, 1969-1972). Thus, for example, zinc and nickel show nutrient-like vertical distributions; they are depleted in surface waters as a result of uptake by the biota and increase in concentration with depth, as a result of the remineralisation of sinking organic matter (Morel, 2003). These elements are sensitive to restricted water circulation and therefore an indicator for oxygen-free conditions (Brumsack, 2006; Tribovillard et al., 2006; Rimmer, 2004; Riboulleau et al.; 2003; Mongenot and Tribovillard, 1996). Upwelling systems receive a large input of metals by the ascent of metal-enriched subsurface waters (Borchers et al., 2005). Results from factor analyses show a statistical distribution, which might be typical for anoxic sediments that are deposited in upwelling areas under restricted (stagnate?) water circulation. This will be shown in the next section.

Molybdenum

Tribovillard et al. (2004) stressed, in a comparative study of Mesozoic geological formations which contain high *sulphurised organic matter*, that Mo is systematically more enriched than other sulphide forming trace elements. This observation is not fully supported from the present study. A comparison of enrichment with different metals in the oil shale unit reveals that Mo ranges in the same magnitude as other trace metals (as calculated in the factor analysis). Moreover, a correlation between enrichment of Mo and the S_{org}/C_{org} relationship is observed. Such a correlation is not unusual, because the organic sulphur plays a critical role in fixing the Mo to sulphurised organic matter (Helz et al., 1996). However, Tribovillard et al. (2004) used the ratio to state the fact that a higher sulphurisation of the organic matter leads to a higher ratio of S_{org}/C_{org} (fig. 58). Furthermore, Tribovillard et al. (2004) emphasise the role of sulphurised organic matter, by trapping Mo, which preferentially occurs in an iron-limited system. Iron

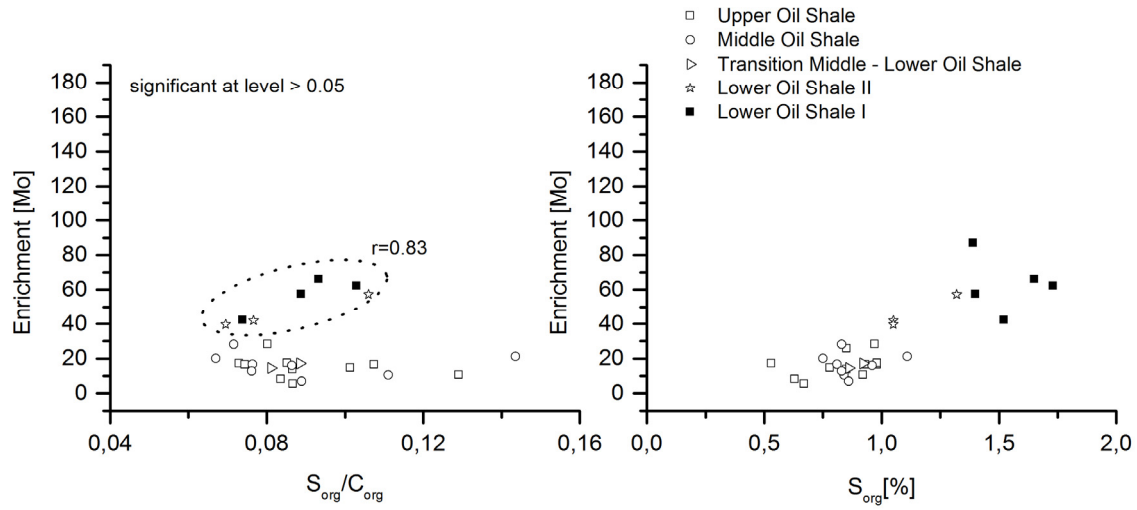

Fig.58 Right side: data in this fig. illustrate the fixation of molybdenum by organic sulphur compounds. The left side shows that a correlation exists between the intensity of sulphurisation and trapping of Mo in the sulphurised organic matter, which supports the assumption made by Zheng et al. (2000) and Helz et al. (1996). Enrichment of Mo is defined as: $\frac{Mo/Al_{sample}}{Mo/Al_{reference}}$

plays a critical role in such a system, by scavenging Mo and forming Mo-Fe-S clusters. An excess in particle-reactive iron, derived by riverine or aeolian input, promotes the formation of appreciable amounts of pyrite.

However, results imply that the iron content is too low to fix the H_2S, which results from bacterial sulphate reduction in the pyrite formation process. The reduced sulphur serves as a link between organic molecules and thiomolybdates (Tribovillard et al., 2004). The released H_2S or polysulphides may react with functionalised organic molecules, to form organic sulphur (Werne et al., 2000; Sinninghe Damsté and Leeuw, 1990; Francois, 1987). The process of sulphurisation occurs either on a intramolecular level by forming thiophene and thiophane, or by forming polysulphide bridges that result in the creation of a macromolecular framework (Schouten et al., 1995). Own results suggest exactly such a system, triggered by an unusually low terrigenic input (< 2.0 cm/ka), which leads to the deposition of iron poor sediments, preferably in the LOS. Fig. 59, on the next page, shows this scenario. A marine carbonate dominated system, affected by a low terrigenic input and high biogenic carbonate production caused by calcareous organism (foraminifera, coccolithophoriden).

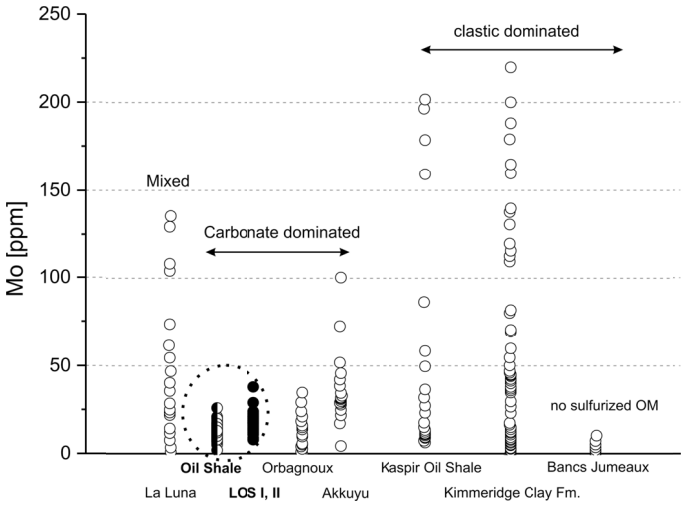

Fig.59 Graph is redrawn after Tribovillard et al. (2004) and illustrates the concentration of Mo in sediments from different environments, reference data taken from (Riboulleau et al., 2003; Mongenot et al., 1999).

Under such conditions, the high metabolic degradation of organic matter and the subsequent exhaustion of available electron acceptors, create an environment with a free circulation of H_2S in the bottom water or the water column, which promotes the fixation of Mo by reacting with the sulphurised organic matter to form thiomolybdate complexes.

However, the question is why are the values in Mo so low (0 – 40 ppm), in comparison to euxinic silled basins? In this regard, a further issue to be considered is the geometry of the oceanic basins. To be precise, the effect of water inflow and outflow on the oceanic residence time[12] of elements and, especially in this case, its influence on the enrichment of Mo (Algeo and Lyons, 2006).

As mentioned before, the strong correlation between Mo and organic matter in black shales and organic rich sediments could be explained by the uptake of sedimentary Mo by sulphurised organic matter. This notion is confirmed by other studies, (Algeo and Maynard, 2004; Helz et al., 1996; Brumsack, 1989). Nevertheless, there is no information on settings, in which low sedimentation rates and stagnate water bodies with restricted water mass exchange hamper with the residence time of trace elements (e.g. Mo) in such basins.

[12] the rate of a given element that is added or removed from a reservoir, Bruland (1980)

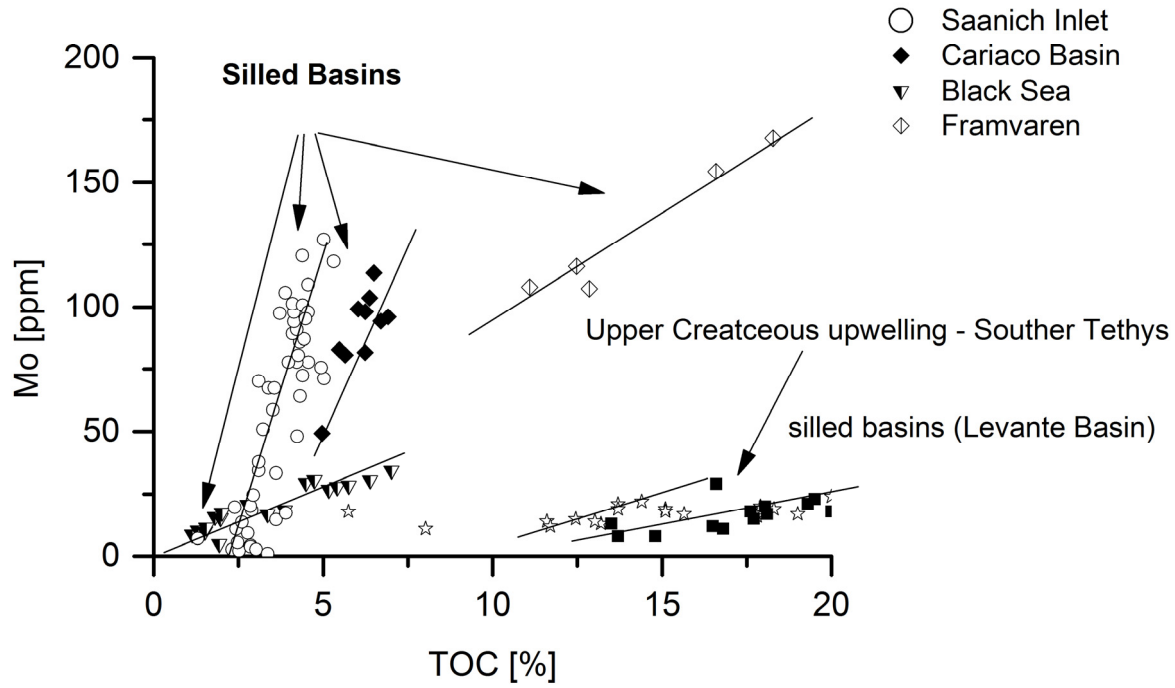

Fig.60 Diagramm shows slopes of rsMo/C_{org} ratios from different silled basins and own results (LOS). Regression lines yield the slopes for Saanich Inlet (45± 5), Cariaco basin (25±5), Framvaren Fjord (9±2), Black Sea (4.5±1), LOS II (0.5±0.2), LOS I (1.1±0.4). Note the low Mo content in ancient upwelling sites. Comparative data originally from Algeo and Lyons, (2006)

The degree of water mass restriction can be estimated, by applying a cross plot between the sedimentary Mo and TOC (rsMo/TOC). Thus, the obtained regression slope (rs) yields information about the water mass balance (e.g. in- and outflow). In modern marine sediments, the concentration of Mo is ~105nM, which corresponds to an rsMo/Mo of ~45. Moreover, the value ~45 reflects conditions that are more open water mass exchange. A decreasing trend in rsMo/TOC is interpreted in terms of a more restriction – less renewal time (τ_{DW}). Fig. 60 display a comparison between the "big four" silled – ancient - basins in their different values in rsMo and TOC. For example, Saanich Inlet shows a slope in rsMo/C_{org} is around 45, which signify less restricted water mass circulation and a high frequency in the renewal of deep water. This is in strong opposite to the Black Sea, which show a rsMo/C_{org} ~4.5 and a deep-water renewal time about 600-±125 years (Algeo et al., 2011; Algeo and Lyons, 2006).

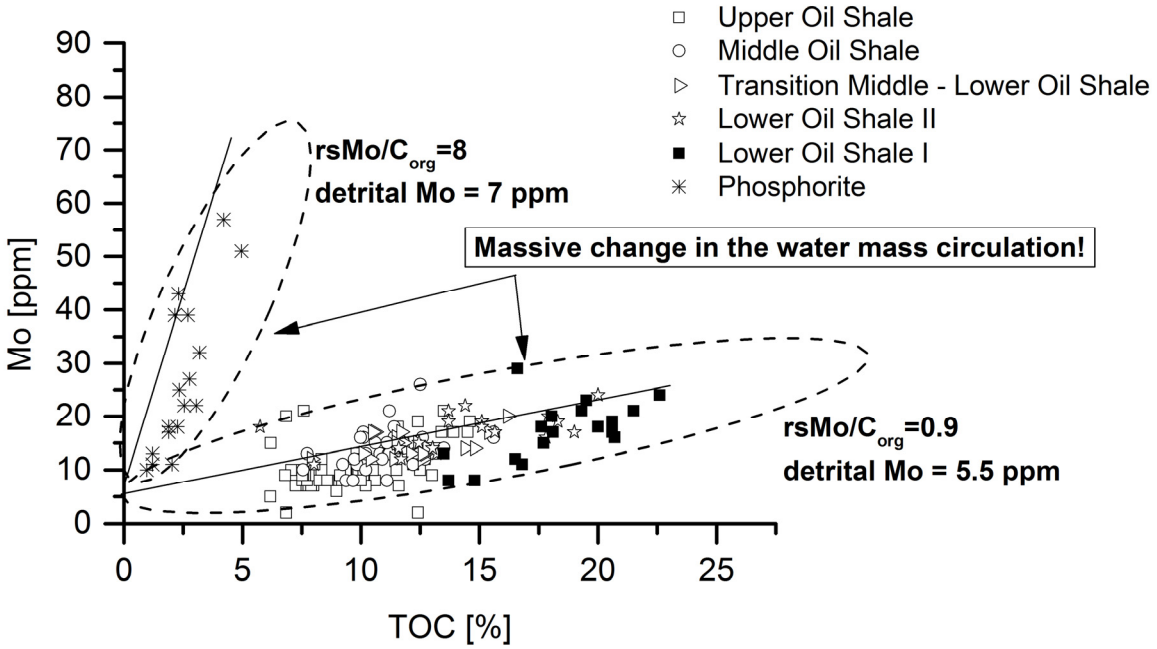

Fig.61 shows the distinct slopes in the regression line of rsMo/TOC from the PM and OSM differences might arise due to changes in the water circulation caused by sea level changes

Based on the above mentioned considerations, the study area lies within a series of silled basins (Krenkel, 1924). Regions surrounding the Levante Basin act as a subsidence area (instable shelf), whereas the uplift regions of the Arabo-Nubian shelf is depicted, at best, as a stable shelf area (Shahar, 1994). Moreover, there is a succession of numerous silled basins (pers. Communication Ari Meiljison) off the Negev Basin. Towards the inner shelf area, the water mass circulation should become more or less restricted, which results in an increasing water mass stratification within these "near shore basins".

In the present study, a equal correlation was observed as proposed by Algeo and Rowe, (2011) and Algeo and Lyons, (2006), but own results differ in terms of a distinct regression slope in rsMo/C_{org} from modern silled basins. Regression slopes between the different stages of oil shale deposition show quite similar patterns.

Own outcomes suggest quite similar results (fig. 61). From the underlying PM to the OS the rsMo/C_{org} decreases very fast from ~8 to ~1. Exactly, the PM define a regression slope 8, the intercept on the Mo axis 7ppm, whereas the overlying OSM is defined by a regression slope of 0.9 intercept on the Mo axis

5.5ppm of molybdenum contribution to the sediment (McArthur, et al., 2008). For the overlying MM, no correlation between the Mo/C_{org} is observed. According to McArthur, et al. (2008) and Algeo and Lyons, (2006), a very fast decreasing water mass circulation for the PM transition can be assumed – comparable to the Framvaren Fjord, Norway took place. This might be explained by the peak in the sea-level low stand during the Campanian-Maastrichtian transition (Haq, 2014; Barrera and Savin, 1999). In this respect the Oil Shale Meuber, shows a rather puzzling picture. The slope of the regression line ($rsMo/C_{org}$) is exceptionally low in this unit and could be interpreted in terms of a immense reduction in bottom water circulation, which might be much lower than in the modern Black Sea ($rsMo/C_{org}$ =4.5). Recently, Algeo et al. (2011) and Algeo and Lyons, (2006) note that slopes in regression line in modern upwelling differ significantly from those of silled basins, because these are topographically open areas with a fast deep water renewal time (τ_{DW}). The Namibian Shelf, shows a rsMo/TOC of 6±3, the Arabian Sea - Continental shelf area display a value of ~2 - 3, Mexican Shelf of ~3 - 4, Peru Shelf of 10 - 15.

It should be pointed out that Rowe Rowe et al. (2008) and McArthur, et al. (2008) successfully demonstrate the application of this proxy in the Palaeozoic Barnett-Fm. (Barnett-Shale). Based on the application of the $rsMo/C_{org}$ ratio, both authors' estimates the deep-water renewal time (τ_{DW}). Their study of sediments in the Mississippi Barnett-Fm. yielded an rsMo/TOC of ~2 (Algeo and Rowe, 2011; Rowe et al. 2008). However, the Lower Toarcian Black Shales (Cleveland Basin)

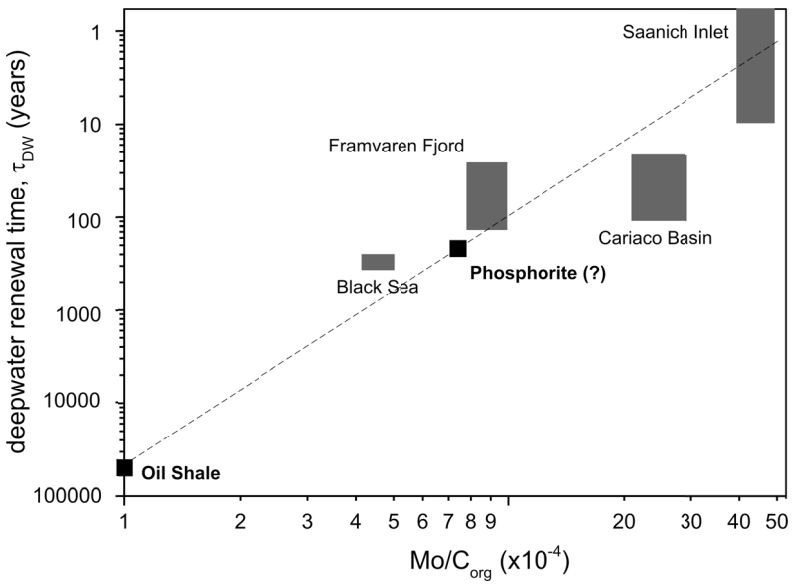

Fig.62 Deepwater renewal time (τ_{dw}) [Mo/C_{org}], for recent examples versus reference values; graphic is modified from (Algeo et al., 2011)

are an extreme example for low rsMo/TOC ~0.5 (McArthur et al. 2008). This result suggests an extreme water mass restriction.

As shown in fig. 62, own results probably indicate a dramatic change in water mass circulation by passing the transition from the PM (rsMo/TOC ~8) to the OSM (rsMo/TOC ~1). The reason for such a dramatic change might be a change in the sea level, from low sea level at the late Campanian – early Maastrichtian to a fast rising sea level, as proposed by (Haq, 2014; Miller et al., 2005).

A non-correlation between Mo and organic carbon, which was observed in the overlying MM, is carefully expressed – a very fast return to fully open oxic marine conditions in deep-water circulation below the sills. In summation, based on the proposed relationship and own estimations, a massive reduction in the deep-water circulation to more open marine conditions, regarding a deep-water renewal time, took place during the transition from Campanian to Maastrichtian time.

Chromium

Chromium plots in factor 1 (chalcophile component), which implies a strong affinity to sulphur and organic carbon.

The average seawater content of chromium is 0.002 ppm at 3.5‰ salinity (Turekian, 1968), and ~90 ppm in shales (Wedepohl, 1969-1972). This is in strong contrast to the oil shales of the Ghareb fm., where the content in chromium ranges between 250 – 700 ppm. Chromium is mostly supplied by the detrital fraction as hexavalent Cr and, under anoxic condition, stabilises as trivalent Cr (Tribovillard et al., 2008, 2006; Kotaś and Stasicka, 2000; Cranston, 1983). In an anoxic environment, the Cr(VI) is easily reduced to Cr(III) by forming aqua hydroxyl-cations $Cr(OH)_3$, $(Fe,Cr)(OH)_3$), and can adsorb onto the surface of Fe/Mn- oxyhydroxides. A further possibility is given by the complexation by humic acids (Algeo and Maynard, 2004; Kotaś and Stasicka, 2000; Breit and Wanty, 1991). Chromium is not known to form sulphides or to be taken up by Fe-sulphides. Cranston (1983) claimed that Cr is mainly incorporated up to 6.6 ppm into the hard parts of siliceous organisms (valves – in diatoms).

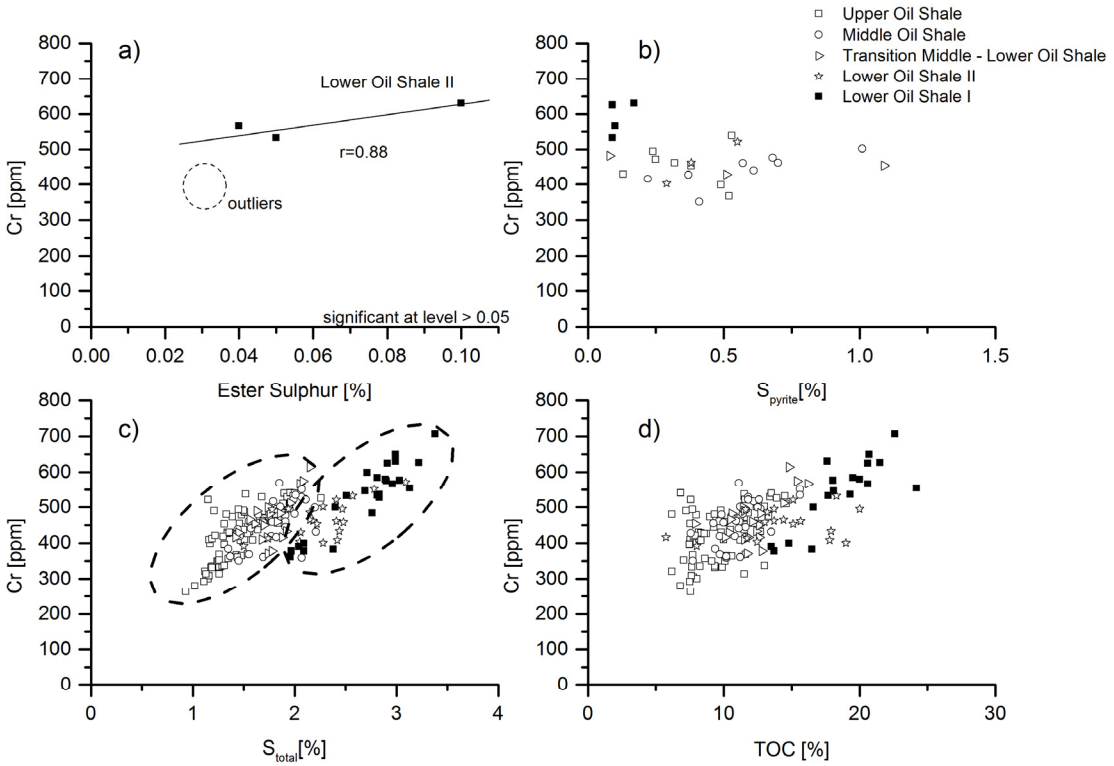

*Fig.63 Cross correlation plots of **a)** ester sulphur ($S_{intramolecular}$), **b)** pyrite sulphur (S_{pyrite}), **c)** total sulphur (S_{total}), and **d)** total organic carbon (TOC) vs. Cr respectively*

Tribovillard et al. (2008) could show that Cr in the Orca Basin has either an authigenic or organic origin. Borchers et al. (2005) report an average content of 83 ppm in the diatom ooze in the Namibian upwelling. Indeed, Borchers et al. (2005) supports the observation by Cranston, (1983), and observed a correlation to the TOC (r=0.63), which may indicate a connection to the productivity. In oil shales from the Ghareb formation, results of this study reveal also a good correlation to the C_{org} content (r=0,67, n=197), which may support an affinity to productivity and the observation by (Borchers et al. 2005). In anoxic environments, an environment in which a reduction of Cr(VI) to Cr(III) takes place, is created by the presence of sulphate-reducing bacteria (SRB) (Arias and Tebo, 2003; Fendorf et al. 2000; Smillie et al., 1981). In such surroundings, the $Cr(OH)_3$ diffuses from the overlying water column downward, along a redox gradient, onto the sediment/water interface, where it is complexed by humic acids or adsorbed on

the surface of clay minerals (mostly illite). The observed correlation to $S_{intramolecular}$, ester bonded sulphur[13], and total sulphur, supports this view (see also fig. 63).

Considering the high Cr concentration of up to 700 ppm (table 7), an attempt was made to understand the cause for these high values. Unfortunately, own outcomes do not present clear picture. Results in the correlation matrix show additional correlation of Cr to Ni and Cu (r= 0.74; r= 0.76; N= 197). An additional explanation would be that the extraordinarily high values of chromium, and the significant correlation to nickel and copper, suggests a mafic or ultramafic source. Another, more allusive, correlation between chromium and zircon is observed (r=0.71, N=197).

The high Cr contribution is possibly due to the Cretaceous ophiolite belt in the eastern Mediterranean Sea and Middle East. This could include the ophiolite-chromite deposits in Jurassic serpentinites on Karpathos and Rhodes (ultramafic that intruded in dolerite dykes) and Cretaceous ophiolites from southern Turkey (Taurides), Cyprus, and Crete. The element composition and trace element signature is typical for island arc basalts (Koepke et al., 2002; Guiraud and Bosworth, 1997).

Table 6 Comparison of Cr, Cu, Ni concentration (ppm) from Rößler & Lange (1972) and own results

Trace element	*$Schists_{RL}$*[14]	*Lower Oil shale* *Min- Max*	*$Carbonate_{RL}$*[15]	*$Ultrabasic_{RL}$*[16] *Min-Max*	*Marl* *Min-Max*	*Oil shale* *Min-Max*	*Phosphorite* *Min-Max*
Cr	90	362-706	11	1600-2000	322-444	72-726	65-832
Cu	45	72-145	4	10-20	57-98	18-145	13-93
Ni	68	113-226	20	2000	101-142	25-225	22-229

[13] sulphur from the cell-interior wall of sulphate reducing bacteria
[14] Rösler and Lange (1972)
[15] Rösler and Lange (1972)
[16] Rösler and Lange (1972)

Copper, Nickel, Zinc

In aquatic systems, the heavy metal concentrations are generally low (Falasco et al., 2009). In view of this, it is common to differentiate between trace metals that are "essential" for growth and photosynthesis. Cu, Ni, Zn, and Fe are commonly associated with phytoplankton, mostly green algae, which are able to adsorb these metals (Morel, 2003). It is often reported that a deficit in Fe limits the growth of algae. Then again, "non-essential" elements (Hg, Cd, Pb) can also be adsorbed by algae (Falasco et al. 2009). Especially black shales show a high concentration of essential elements. In the photic zone, these metals are removed from the surrounding water by plankton growth and consumed from organic debris. Upon death, they pass the water column (incorporated in fecal pellets) and settle on the seabed (Calvert and Pedersen, 1993). For this reason, Ni and Zn show a similar gradient to silicates[17] (Piper, 1994).

One of the trace elements, which are commonly associated with organic rich sediments, is copper. It is well known that Cu plays a role as micronutrient, together with Ni and Zn.

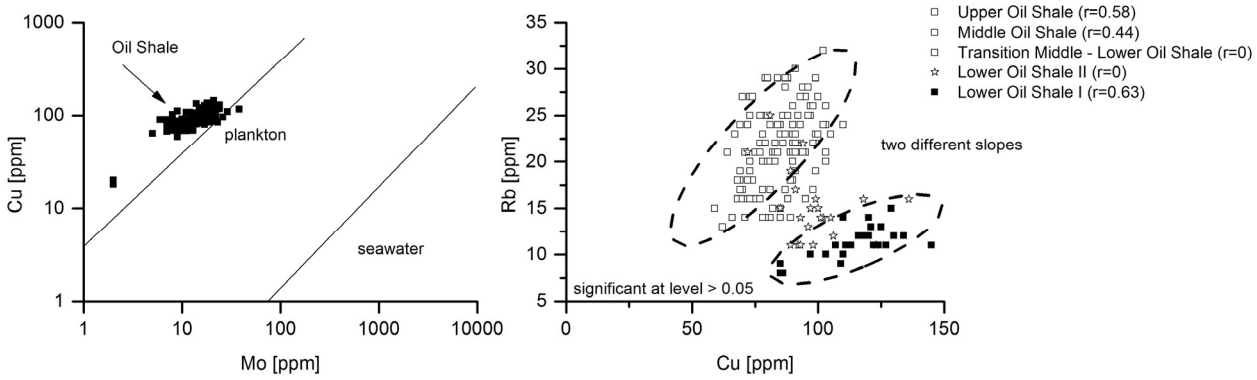

Fig.64 Left side: Relations between Mo [ppm] and Cu [ppm], reference values are taken from, (Piper, 1994). Right side illustrates the significant correlation between Cu [ppm] and Rb[ppm]and their different slopes in correlation in distinct units of OSM.

[17] silicates regarded as diatoms that contribute more than 80% to the phytoplankton community

The average shale concentration is 45 ppm (Wedepohl, 1969-1972). Copper occurs in two valence states (Cu (II), (I)), as Cu^{2+} can replace Fe^{2+} and Mg^{2+} in mineral structures and it mainly occurs in sulphide minerals (Okrusch, 2005). In oxic marine environments, Cu is mainly bonded to organometallic ligands (Algeo and Maynard, 2004, Calvert and Pedersen, 1993).

In anoxic marine environments, Cu^{2+} is reduced to Cu^{1+} and can be incorporated in sulphide phases, mainly pyrite and chalcopyrite ($CuFeS_2$) – mostly in environments that are highly affected by bacterial sulphate reduction (Huerta-Diaz and Morse, 1990). Pedersen et al. (1986) state that in pelagic sediments Cu is coupled to a low sedimentation rate, and can possibly be diagenetically fixed by clay minerals, e.g., smectite. Then again, copper can be scavenged on the surface of Mn/Fe-oxyhydroxides and released by reductive dissolution, or by decaying organic matter, to the surrounding pore water (Tribovillard et al., 2006).

This scenario is supported for the present study, suggesting a strong relationship between Cr, Ni, and Zn. Each of these elements is in strong correlation with C_{org}. Concomitantly, a high correlation coefficient to sulphur and organic sulphur (r=0.88, r=0.73) supports the presumed strong link to organically bonded sulphur[18].

As illustrated in fig. 64, copper shows a different correlation to Rb, which is interpreted in terms of a strong association to clay minerals and organic matter. In summation, copper is released by decaying organic matter, and fixed into the clay minerals under a low sedimentation rate, due to adsorption and incorporation (Pedersen et al., 1986). In anoxic (weak sulphidic) environments, clay minerals do indeed form a framework together with the sulphurised organic matter and the diagenetically fixed copper.

Nickel

There are at least three possible sources for an enrichment of Ni (and V) in the marine sediments. Inorganic (detrital) sources of Ni can be in ultrabasic, mafic rocks, in the weathering residue of which it

[18] Note, a non-correlation to pyrite-bonded sulphur

can be mobilised by humic acids, and can therefore be a strong contributor to the elevated concentration in seawater (Algeo and Maynard, 2004; Calvert and Pedersen, 1993). Because their uptake and incorporation, marine organisms living in the anaerobic bottom water are sources for that (Lewan and Maynard, 1982; Meinecke, 1973). Another possibility for this metal enrichment can arise by downward diffusion from the interstitial water, by metallation of tetrapyroles (Piper and Perkins, 2004; Nameroff et al. 2002; Lewan and Maynard, 1982). Upon sulphate reducing conditions, Ni can be incorporated in pyrite and pentlandite $(FeNi)_9S_8$. The average Ni concentration in seawater is ~0.005 ppm (Henderson and Henderson, 2009), whereas a concentration in coastal sediments is ~ 39 ppm (Turekian, 1968). As mentioned above, nickel shows a nutrient-like distribution, and in sulphidic areas, a higher concentration than expected in an oxidising environment. In samples from the oil shale section, the average Ni content is 147±29 ppm (N=197). Highest values are found in the LOS section with ~ 226ppm, unlike in the Upper Oil Shale, which indicates a decreasing trend in Ni values. In factor analysis, Ni[19] is plotted together with C_{org} and sulphur and shows a strong positive correlation with Cr (r= 0.76, N=197).

A correlation of Ni with V is observed in the LOS I (r=0.94, N=23), but not in the LOS II, only to correlate once again in the Upper Oil Shale Unit (r=0.62, N=114). A weak negative correlation (r=-0.48, N=123) with Al_2O_3 might suggest that Ni is not bonded to the clay fraction and instead forms a preferred association with the sulphurised organic matter

The Ni-V proportionality is determined by the environmental conditions in which their source rocks were deposited (Lewan, 1984). Diffusion from the overlying water column, by forming metallo-organic complexe and their incorporation in organic rich sediments leads to an enrichment of V and Ni in the sediment. Normally, reservoir alteration (migration, maturation) could change this proportionality. Nevertheless it has repeatedly been shown that these proportionality remains unchanged (Lewan, 1984; Lewan and Maynard, 1982). Based on the high stability of this proportionality under different environmental conditions, make the application of this proportionality ideal for the use as a proxy. For the

[19] detailed discussion in section chromium, that might indicate a same source area

research area, no maturation or migration has been shown. For the deposition area, this is repeatedly shown and confirmed by the analysis of biomarker and rock-eval pyrolysis as kerogen typ I, II[20] (Lewan and Henry, 2001; Bein et al., 1990; Rullkötter et al., 1984; Spiro et al., 1983; Amit and Bein, 1982; Dinur et al., 1980).

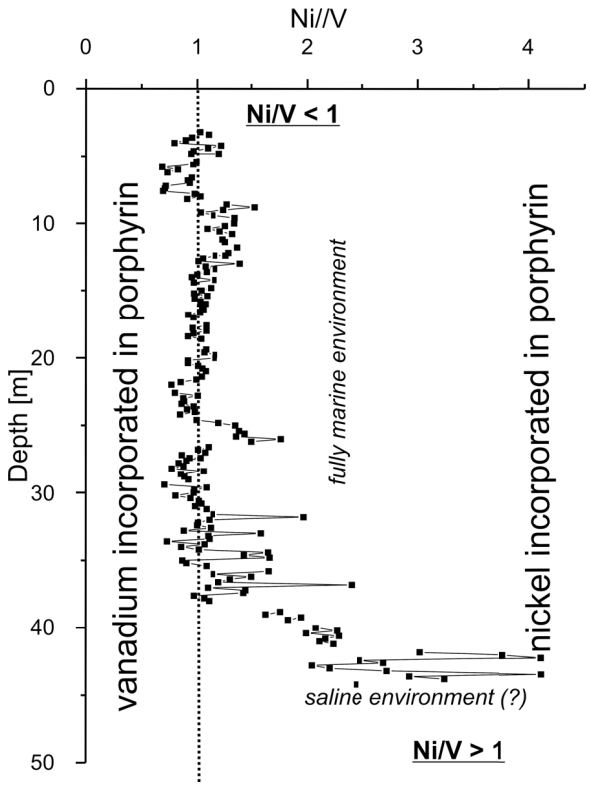

Fig.65 Variation of Ni/V ratios along the studied profile as an empirical tool for identifying environmental conditions and the source of organic matter.

Barwise, (1990) explained a Ni/V ratio < 0.5 by a preferred incorporation of V into the porphyrin, instead of Ni (fig. 65). A higher Ni/V ratio than one is explained by the low input and preservation of porphyrin into an environment that changes from a marine carbonatic (non-siliciclastics) to a marine siliciclastic and/or lacustrine/non-marine environment. Based on the work of Barwise, (1990), and Lewan, (1984), results obtained by this study suggest a value of > 2 for the LOS II, which, in return, suggests a low preservation of porphyrin and incorporation of Ni instead of V into the organic matter.

Slightly oscillating values ~ 1, profile-upwards, might indicate input of marine algae (porphyrin), unlike in the LOS. This horizon is marked unambiguously by Ni/V values > 2 and a trend to a higher Ni/V ratio, as well as a higher sulphur content. Based on this premise, a tentative conclusion might be that the source of organic matter has changed significantly. A preferred higher Ni/V ratio, at the base of the oil shale, can be interpreted in terms of a more saline bottom water. This is in strong contrast to the overlying OSM. A sharp contrast between these units might indicate the beginning of a new episode in primary

[20] Kerogen Typ, I, II is defined by inmature organic matter of marine origin

production at the surface. Furthermore, it would support a gradual shift from a restricted water circulation to more open marine conditions during the deposition of the MM.

Uranium

According to the statistical analysis, U plots with high factor loadings on factor 1. There are at least four important ways, in that a U accumulation in marine settings occurs.

The loss of U from the sediment is explained by oxididation of the reduced U. Bioturbation injects oxygen into deeper sediment layers, mixing with the oxygen pore water cause that the previously reduced U is oxidized and transported towards the overlying oxic sediment layers (Morford et al., 2009; Zheng et al., 2002). The other possibility involves transport of authigenic U as particulate- non lithogenic uranium (PNU) along with the particulate organic matter accumulation in sediments (Zheng et al., 2002). Such a process could explain the strong correlation with the (sulphurized) organic matter and sedimentation rate. A slow sedimentation allows more time for diffusion of uranyl-ions into the overlying sediment where they are fixed onto the organic matter. Other authors have shown that the kinetics of the fixation of U onto the surface of the organic framework is very slow, but it can be catalysed by the activity of sulphate reducing bacteria that is in relation to the sedimentation rate (Sundby et al., 2004). Generally, the bacterial activity in the sediment can be expressed as a function of the sedimentation rate, because a higher rate of sedimentation contributes to more degradable organic material for sulphate reducing bacteria. Figure 66 (next page), shows a sequence of graphs with possible scenarios in which uranium may be deposited and fixed.

The first plot ***(1)*** illustrates, that a low sedimentation rate might enhance the downward diffusion of dissolved uranium along an oxygen gradient into turbidic sediments from the Madeira abyssal plain (Crusius and Thomson, 2000). Obviously, own results do not support this observation. The plot illustrates that U values are not affected by sedimentation rates, which is in accordance with Böning et al. (2005), who questioned the above-mentioned considerations for sediments of the Chilean upwelling margin.

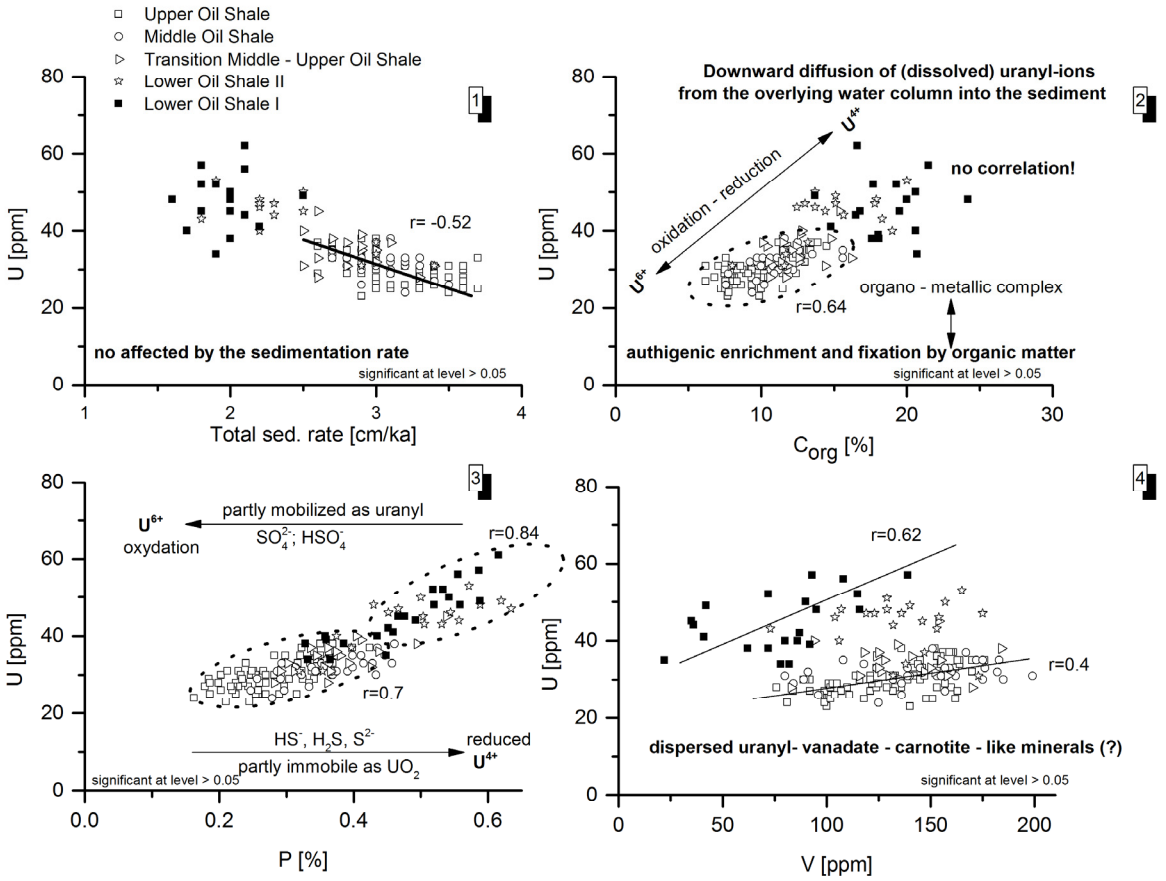

*Fig.66 Scatter plots of Sed. Rate (cm/ka) vs. U [ppm] **1)**, and C_{org} [wt. %] with U [ppm] **2)**, P[wt. %] vs, U [ppm] **3)**, and V [ppm] vs. U [ppm] **4)** detailed description see text below*

Plot ***(2)*** shows the relationship between organic matter and U. Many authors have shown that uranium is fixed by organic matter, as well as where the highest OM flux occurs (Böning et al., 2009; Morford et al., 2009; Klinkhammer and Palmer, 1991; Kniewald and Branica, 1988). Result from this study implies a lack of the proposed correlation between C_{org} and U in the LOS, unlike in the overlying oil shale sequences. Here, the correlation (r=0.63) may confirm the observation that under anoxic circumstances, a part of the dissolved uranium can neither be reduced by inorganic (Fe^{2+}, V^{3+}), nor by metal reducing bacteria (Lovley, 1995). This may lead to the formation of organo-metallic ligands that have been adsorbed onto the surface of organic matter (McManus et al., 2005). In an anoxic/acidic environment, U^{4+} remains mobile and is not fixed onto the surface of the organic matter.

In times of a short-term oxygen supply, the U^{4+} immediately, can be oxidised to U^{6+} and is fixed by organo-metallic complexes. This might explain the better correlation in the upper part of the oil shales. The oxidation of OM is accompanied by a reduction of U^{6+} to U^{4+}, by bacteria see also eq. 12, (Barnes and Cochran, 1993).

Equation 12

$$CH_2O + 2UO_2(CO_3^{2-})_3^{4-} + H_2O + H^+ \rightarrow 2UO_2 + 6HCO_3^- + CO_2 \quad Eq.12$$

Plot ***(3)*** shows the different environments in which an incorporation or adsorption of U on apatite takes place. Sulphate reducing bacteria (SRB) create an environment in which HS^-, a reducing agent for U^{6+}, is produced (Langmuir, 1978). As shown above, in an anoxic environment U^{4+} is immobile and is adsorbed on apatite, under the same conditions in which H_2S, HS^-, S^{2-} are stable and occur in pore water (Dybek, 1973). In contrast, under oxic conditions, in the presence of SO_4^{2-}, HSO_4^- respectively, most uranium is mobile, in the form of U^{6+} (uranyl carbonate). The behaviour of uranium in different Eh/pH conditions is described according to the following equation (eq. 13). The reduction of U^{6+} to U^{4+} takes place due to the activity of SRB (Klinkhammer and Palmer, 1991; Anderson et al., 1989; Langmuir, 1978):

Equation 13

$$4UO_2(CO_3)_3^{4-} + HS^- + 15H^+ \rightarrow 4UO_2 + SO_4^{2-} + 12CO_2 + 8H_2O \quad \text{Eq. 13}$$

Marine apatite contains up to 0.1% U, and bone beds even contain up to 0.5% uranium. More than 90% of all bonded uranium occurs as U^{4+} (Dybek, 1973).

In plot ***(4)***, a significant correlation between vanadium and uranium can be seen in the LOS (r=0.62, N=24) and the UOS (r=0.4, N=133). This high correlation between V and U in the LOS, is interpreted to be due to the formation of uranyl-vanadate (carnotite - like) minerals. The possible occurrence of such minerals, and the differences in the slope of their regression lines, might indicate slightly oscillating oxygenation at times of their deposition. The carnotite-like minerals are at least soluble in pH ranges of 5 – 8.5 (Langmuir, 1978).

As shown in the bar plot from the factor analysis, vanadium is a constituent of the factor 1 and shows a preferred correlation to the total iron (r=0.77, N=133) in the Upper OSM. This may imply that the correlation to iron could be due to a preferred adsorption onto iron-hydroxides.

In the Lower Oil shale, the high uranium values may be a result of the incorporation of U^{4+} in hydroxyl-apatite – the most common form of apatite in marine sediment. Moreover, it is assumed that apatite can incorporate significant amounts of pore water U, in which uranium is present as U^{4+} or U^{6+}. Because of their similar ionic sizes, U^{4+} can easily substitute for Ca^{2+} in the apatite structure. Another possibility arises from the fact that U^{6+} can be fixed (adsorbed) outside of the structure as uranyl carbonate because of its much larger ionic radius (Pana and Fleet, 2002; Rakovan, 2002).

In summation, the different amounts of uranium in the bulk sediment might be interprete in the following way: The incorporation of U^{4+} takes place under anoxic/sulphidic conditions below the sediment/water interface. In such an environment, uranium only occurs as U^{4+}, which is stable in a pH range from 3 – 4 (Langmuir, 1978). In contrast to the base of the oil shale, along the profile upward oscillating oxygenation allows the fixation of uranyl-ions as U^{6+}, onto the surface of the deposited organic matter, or onto the surface of apatite. The fixation of uranyl-ions signifies a fluctuating sedimentation regime with (short-term) injections of oxygen into the pore water. In terms of differences in redox potential, both sections (Lower Oil Shale Unit vs. Upper Oil Shale Unit) may differ significantly. Thus, it is possible to use the uranium content as proxy for the oxygenation state in the bulk sediment.

Correlation between P_2O_5 and As

It has been reported that a large member of mono (Na^{+})-, di (Sr^{2+}, Pb^{2+}, Ba^{2+}, Mn^{2+})-, tri (REE^{3+})-, tetra (Th^{4+}, U^{4+})-, hexa (U^{6+})-valent cations substitute for Ca in apatite minerals (Pana and Fleet, 2002). The same holds true for the substitution of anions $(CO_3)^{2-}$, $(SO_4)^{2-}$, $(AsO_4)^{3-}$ for the tetrahedral $(PO_4)^{3-}$. Factor 2, with high loadings for P_2O_5 and rare earth elements (La, Y – Xenotime-group), stays for conditions which favour the deposition of Ca-phosphate (Phosphorite /apatite). Additionally, the element arsenic is one of the contributors to this factor, which implies the substitution of the anion $(AsO_4)^{3-}$ for $(PO_4)^{3-}$. Arsenate is found in rivers and lakes, transported to the open sea, where it is bonded or adsorbed on Fe/Mn-oxyhydroxides, sulphates and carbonates (Ruokolainen et al., 2000). Therefore, it can be a source for biological uptake by phytoplankton. Phytoplankton can take As up in the upper water column and transport it down to the sediment by biogenic debris (fecal pellets), but not to the intermediate water where it is regenerated like phosphor (Cutter and Cutter, 1995; Andreae, 1978). Arsenic is thermodynamically stable as As^{5+} in oxic environments, whereas, under anoxic conditions, it occurs as As^{3+}. The specification of As depends on the strength of the primary production, the activity of bacteria and (de)composition of organic matter (Sohrin et al., 1997). There are at least two explanations for the

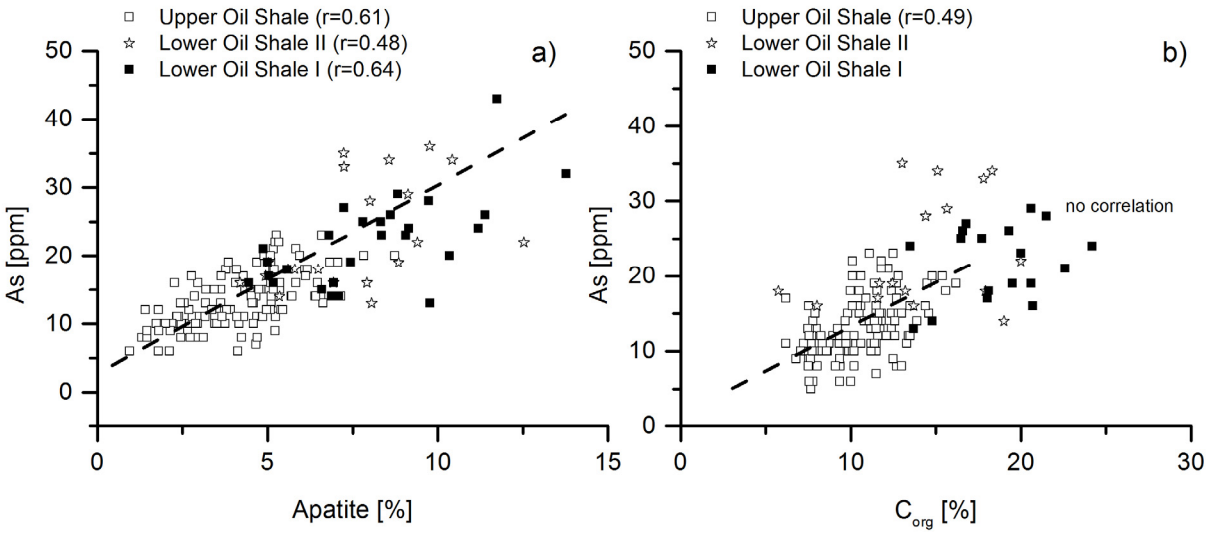

*Fig.67 Left side: Cross correlation between apatite [wt. %] vs. As [ppm] **a)** and right side: C_{org} [wt. %] with As [ppm] within the OSM **b)**, detailed explanation see text. Formula for calculation of apatite content was taken from American Mineralogist database.*

observed correlation of arsenic and apatite. The diagenetic formation of arsenates ideally leads to the precipitation of johnbaumite [$(Ca_5(AsO_4)_3(OH)]$ or svabite [$Ca_5(AsO_4)_3F$]. Johnbaumite is stable in a range of circumneutral conditions (Yokoyama et al., 2012). However, the observed lack of correlation, with CaO, does not support their existence. An increasing plausibility of the diadoch substitution of AsO_4 for the tetrahedral $(PO_4)^{3-}$ comes from an observed correlation between arsenic and apatite (fig. 67). The correlation coefficient decreases upwards in the profile, whereas a weak, but statistically significant correlation, concurrently between arsenic and the organic carbon, is observed. This might be due to the decreasing apatite content in the UOS. Another possible explanation might be due to the preferred adsorption of arsenic onto the organic matter. It might be possible that a release of trace elements by oxidative weathering of organic matter and subsequent dissolution/re-precipitation process leads to a secondary enrichment of arsenic in the sediment. Moreover, originally a precipitation of pyrite together with arsenic as arsenopyrite is conceivable, which might be supported by its precipitation in an suboxic/euxinic environment (Huerta-Diaz and Morse, 1992, 1990). In any case of pyrite oxidation under such conditions, the weathering solution was transported into the pore water and a subsequent precipitation of arsenic as AsO_4 and a formation of apatite (svabite $Ca_5(AsO_4)_3F$) took place.

5.2. Interpretation of the trace element data in planktic and benthic foraminifera

A further objective of this thesis is to refine the relationship between the occurrence of benthic and planktic foraminifera, and the concentration of trace elements in the bulk sediments. To achieve this goal, an additional principal component analysis (PCA) has been conducted by comparing the results from the bulk geochemistry and the clustered abundance of the benthic and planktic foraminiferal assemblages, which were obtained by our Israeli co-partners (Ashckenazi-Polivoda et al., 2011).

Based on their relative abundance, Ashckenazi-Polivoda et al. (2011) clustered the different planktic and benthic taxa of foraminifera in respect of the productivity in the surface water. The cross-plot in fig. 68 compares the results of the geochemical analyses between their biostratigraphical counterparts, as defined by (Ashckenazi-Polivoda et al., 2011).

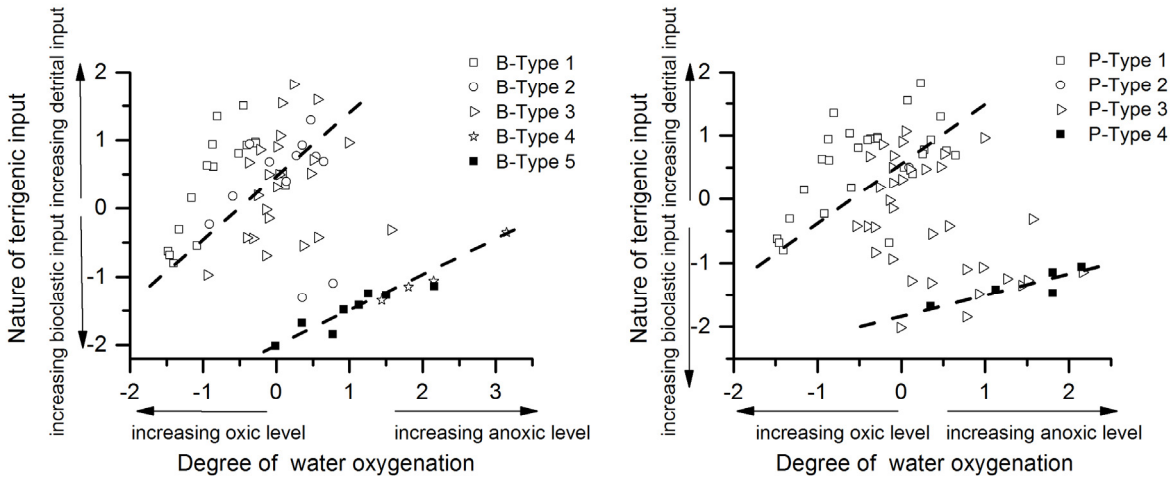

*Fig.68 Cross correlation of calculated factor scores between degree of oxygenation and nature of terrigenic input for benthic foraminifera **(left)** and planktic foraminifera **(right)**. Both plots display same pattern as is previously shown in fig. 52, which might support a fundamental aggreement between micropalaentology and inorganic geochemistry.*

Integration of chemostratigraphic and biostratigraphical results

The chemostratigraphical and biostratigraphical results were combined, to gather more detailed information on the distribution of the planktic assemblages P-Types 1 and 4 (*Globigerinelloides spp., Heterohelix spp., Hedbergella spp.*), and the benthic assemblage B-Types 1 and 4 (*Gyroidinoides Elhasaella spp., Triserial buliminids, Gavelinellids spp.*), which parallel the variations in the degree of bottom water oxygenation and detrital input.

Planktic (P1-P4) and benthic foraminifera (B1-B4) are clustered according to their abundances in different parts of the OSM. Main contributor to the planktic foraminiferal (P4 - P3) assemblages are *Globigerinelloides spp.*, a shallow planktic foraminifera species, which lives preferentially in the euphotic zone (10 - 50 m) and favours extremely eutrophic water masses. Whereas the other contributor, *Heterohelix spp.*, is mainly defined by mesotrophic water mass conditions (Ashckenazi-Polivoda, 2011). *Hedbergella spp. (Globigerina cretacea)* increase in richness and contribute to the foraminiferal assemblages (P2 - P1). When the surface water becomes less oxygenated, deep dwelling species disappear. Only surface dwelling species (*Globigerinelloides spp, Hedbergella spp, Heterohelix spp.)* survive such conditions and their abundances actually increase (Ifrim et al., 2011; Leary et al., 1989). Generally, in shelf slope areas, these assemblages contribute more than 50% to the total planktic community. Fluctuations in their richness are often interpreted due to the expansion of the OMZ in the upper water column. Owing their tolerance to low oxygen levels, they are able to survive in such conditions (Ghourchaei et al., 2014; Abramovich et al., 2010; Keller and Pardo, 2004; Leckie, 1987).

Planktic foraminifera *Heterohelix* display notably high abundances in a variety of marine environments and an ability to adjust to a wide range of water column conditions (Ashckenazi-Polivoda et al., 2011). P-Type 4 (dominance of Globigerinelloides) samples plot in a field with a low oxygen level. The factor score of P-Type 3 falls in a wide range of -1.5 to 2.8 on the x-axis and -2 to 2 on the y-axis. It seems that P-Type 3 (*Heterohelix*) is highly adapted to a wide range of environmental features, thus tolerating fast fluctuating conditions of oxygen in the water column. Samples of P-Type 2 match in factor score from on

the y- axis from -1 to 0, wheras scores on the x-axis plot from -0.5 to 0.8. Theses factor scores mark a transition cluster to more oxygenated conditions with higher detrital contribution.

The benthic communities B5 to B4 are mostly dominate by triserial buliminids, whereas assemblages from B3 to B1 are controlled by *Gyroidinoides spp*. (Ashckenazi-Polivoda et al. 2011). Triseral buliminids are often regarded as infaunal species, which are indicate a very low oxygenated seabed, simultaneous to a higher organic matter flux (Friedrich, 2009). Whereas *Gyroidinoides spp*. are typical in abyssal depths and also regarded as shallow infaunal taxa that thrive under meso-trophic conditions with very little or no tolerance for oxygen-poor environments (Ghourchaei et al., 2014; Ashckenazi-Polivoda, 2011; Erbacher et al. 1998; Widmark, 1997).

B-Type 4 (triserial buliminids and *Gavelinella spp*.) is limited to the base of the OSM. This field is characterised by strong anoxia and a higher bioclastic input. B-Type 3 tolerates larger content of oxygen. Moreover, B-Type 3 (*Gyroidinoides spp)* gather in a smaller range and "switch" between low anoxic and low oxic levels. Factor scores from sedimentary input indicate a small transition range from bioclastic to detrital input. B-Type 2 (*Gyroidinoides spp)* behave similar to P-Type 2 and cluster in a narrow range that indicates more aerated conditions in the pore water and water column, respectively.

Factor scores from P-Type 1 and B-Type 1 indicate a cluster pattern in a wide range of increasing detrital input and increasing oxic level.

In summation, P-Type 1 and 2 (high *Heterohelix*) assemblages coincide with a gradual decrease in biogenic carbonate production and a relatively weak anoxic response to the increase in terrigeneous input. In contrast, assemblages P-Type 4 (dominance of *Globigerinelloides*) and B-Type 4 (triserial buliminids and *Gavelinella spp.*) are limited to the base of the oil shale and are characterised by strong anoxia and high carbonate production, as reflected by scores of factors 1 and 2.

Final remarks

Based on inorganic geochemical analysis (minor and main elements) and multivariate statistical methods, the above mentioned notions support the biostratigraphic results obtained by (Ashckenazi-Polivoda et al., 2011).

Consequently, a high calcareous sedimentation indicates that foraminifera are the main contributors to the calcareous sedimentation during the time of interest. A cross-plot between these two related factors yields more detailed information about the palaeoenvironment. Moreover, the bi-variate plot reveals a continuous weakening in the biogenic calcareous contribution to the whole terrigenic input. A remarkable trend from strong anoxic to more oxic conditions is observable, which implies a change in the sedimentation regime, but also, in the combined interplay between the oceanographic features, biogenic contribution, and terrigenic input, respectively.

The integration of biostratigraphical data with the chemostratigraphic counterparts reveals almost identical results. The combined interpretation offers information that is more precise in the evolution of the Upper Cretaceous organic rich shales in the Negev. The occurrence of P4 and B4 assemblages is interpreted in terms of highly anoxic conditions at the bottom and an expansion of the OMZ within the water column. Chemostratigraphic data reveals a similar scenario; a flat gradient in the regression slope is interpreted in terms of a rapid onset of anoxic conditions and an expansion of the OMZ. The top of the profile is stronger affected by increasing terrigenic input and more aerated conditions. At about 33 mbsf depth, fluctuating conditions between these two extremes are marked. The changing pattern in the richness of the taxa could be interpreted as the result of a shift from eutrophic to mesotrophic conditions and changes in the organic matter influx.

Patterns occurring in the bulk inorganic sediment chemistry and organic carbon coincide with gradual up-profile directed changes in benthic and planktic foraminiferal communities. This is in accordance with the results of the Israeli project partners', implying a gradual shift from base to the top of the OSM, from

eutrophic to mesotrophic and strong anoxic to dysoxic conditions (Schneider-Mor et al., 2012; Ashckenazi-Polivoda et al., 2011). This coincides with my own results, implying a gradual shift from calcareous, bioclastic sedimentation in a strong anoxic environment towards to the top of the profile, i.e., a change to more aerated conditions, and simultaneously, to an increasing detrital input.

Connection between element composition of foraminifera tests and biostratigraphic data

In course of the thesis, an attempt was made to interpret the element composition of the analysed foraminifera tests. Before being evaluated foraminifera tests, some facts will be present about the environment in which they live.

Gavinellina spp.

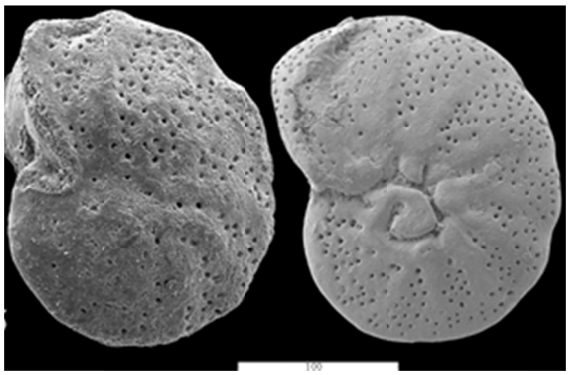

Fig.69 SEM picture from Gavinellina spp. of (Ashckenazi-Polivoda, 2011) length of the bar 10µm

The habitat of (benthic) *Gavinellina spp*. is less well known (Ashckenazi-Polivoda, 2011). Some authors state that *Gavinellina spp.* represents an infaunal[21] species, which is regarded to live in a neritic-middle bathyal environment, tolerant to low levels of oxygen and surviving on substrates with high food supply (Ashckenazi-Polivoda, 2011; Erbacher et al., 1998; Widmark, 1997). Moreover, Erbacher et al. (1998) note that *Gavinellina spp*. is very common in black shale deposits.

[21] infaunal species that live within the sediment and therefore exposed to elevated pore water concentrations

Heterohelix globulosa spp

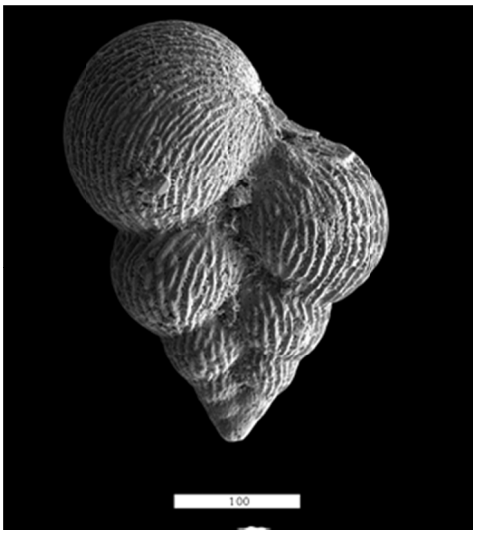

Fig.70 SEM picture from Heterohelix spp. (Ashckenazi-Polivoda, 2011), length of the bar 100µm

Palaeontological studies on the Upper Cretaceous, eastern Pacific margin, Sliter, (1972), point to inner slope to shelf areas as the habitat of planktic *Heterohelix globulosa*. D'Hondt and Zachos (1998) and (Leckie, 1987) regard *Heterohelix globulosa* as a variable species, which is highly adapted to near surface/intermediate depths, e.g., open marine shallow water (Keller and Abramovich, 2009). Moreover, Eicher and Worstell, (1970) could show that *Heterohelix globulosa* is one of the species that are highly adapted to marine transgression/regression cycles, appearing and disappearing depending on the sea level curve. *Heterohelix globulosa*, as infaunal species, dominate areas with a high food supply, being highly adapted to nutrient-rich surface water, tolerant to oxygen-depleted conditions with a preference for cooler life habitats (Darvishzad and Abdolalipour, 2009; Keller and Abramovich, 2009; van der Zwaan et al. 1999).

The occurrence of benthic species in low-oxygen environments could be interpreted in terms of their fast adaption, radiation, and colonisation in niches and new environmental conditions. Recently, many authors note that benthic (infaunal) species tolerate anoxia and are able to survive under sulphidic conditions (Langlet et al., 2013; Friedrich, 2009; van der Zwaan et al., 1999). They can tolerate a dissolved hydrogen sulphide concentration of up to 12 - 100 µM and live in symbiosis with bacterial assemblages (*Thioploca spp.)* (Høgslund et al. ,2008). Based on experimental setups in marine settings, it has been report that benthic species are able to survive in highly anoxic environments for a period of one year (Langlet et al., 2013; Metzger et al., 2013; Moodley et al., 1998).

As shown in fig. 71, page 151, a multivariate analysis was performed, in order to evaluate the palaeo-environment in which these foraminifera lived, based on interelemental relationships in foraminifera shells. Before processing, outliers were excluded from the dataset. For the sake of an unambiguous interpretation and a better statistical significance, only factor loadings that show higher values (> 0.7) were used. Regarding the benthic foraminifera eigenvalues account for 82% for the total variance. Thereby, 3 factors have been selected.

(1) **Factor 1** accounts for 40% of the total variance and includes the elements Pb, Cu, Cd, Ba, Mn

(2) **Factor 2** accounts for 22% of the total variance and includes the elements Co, Ni

(3) **Factor 3** accounts for 19% of the total variance and includes the elements Mg and Sr.

The same criterion holds true for the statistical evaluation of **planktic foraminifera**. Here, based on the statistical analysis, eigenvalues account for 81% for the total variance. According to the above mentioned findings, the selected factors were interpreted as follows:

(1) Factor 1 accounts for 42% of the total variance and includes the elements Co, Ni, V, Cr

(2) Factor 2 accounts for 39% of the total variance and includes the elements Cu, Rb, Ba, Pb

The interpretation of the results obtained for the numerous outliers is difficult. However, it is possible to draw some conclusions. By comparing the results of the factor analysis for benthic vs. planktic foraminifera, it is seems conspicuous that both planktic and benthic foraminifera have a similar element contribution.

- Planktic foraminifera Cu, Rb, Ba, Pb – contribute 39% to the total variance
- Benthic foraminifera Pb, Cu, Cd, Ba, Mn – contribute 40% to the total variance

Results of the planktic factor analysis show that Mn and Cd are unrepresented in the data sets. Unlike the benthic data set, in which Rb shows no contribution to the total variance. Viewed together, both show a striking similarity to one another in terms of comparable element contribution.

Due to their incorporation in phytoplankton and subsequent release, the elements (Cu, Cd, Ba, Zn) track the seawater inventory. Then again, elements like Cd and Zn can be fixed to sulphide minerals (CdS, ZnS) in an anoxic-dysoxic environment.

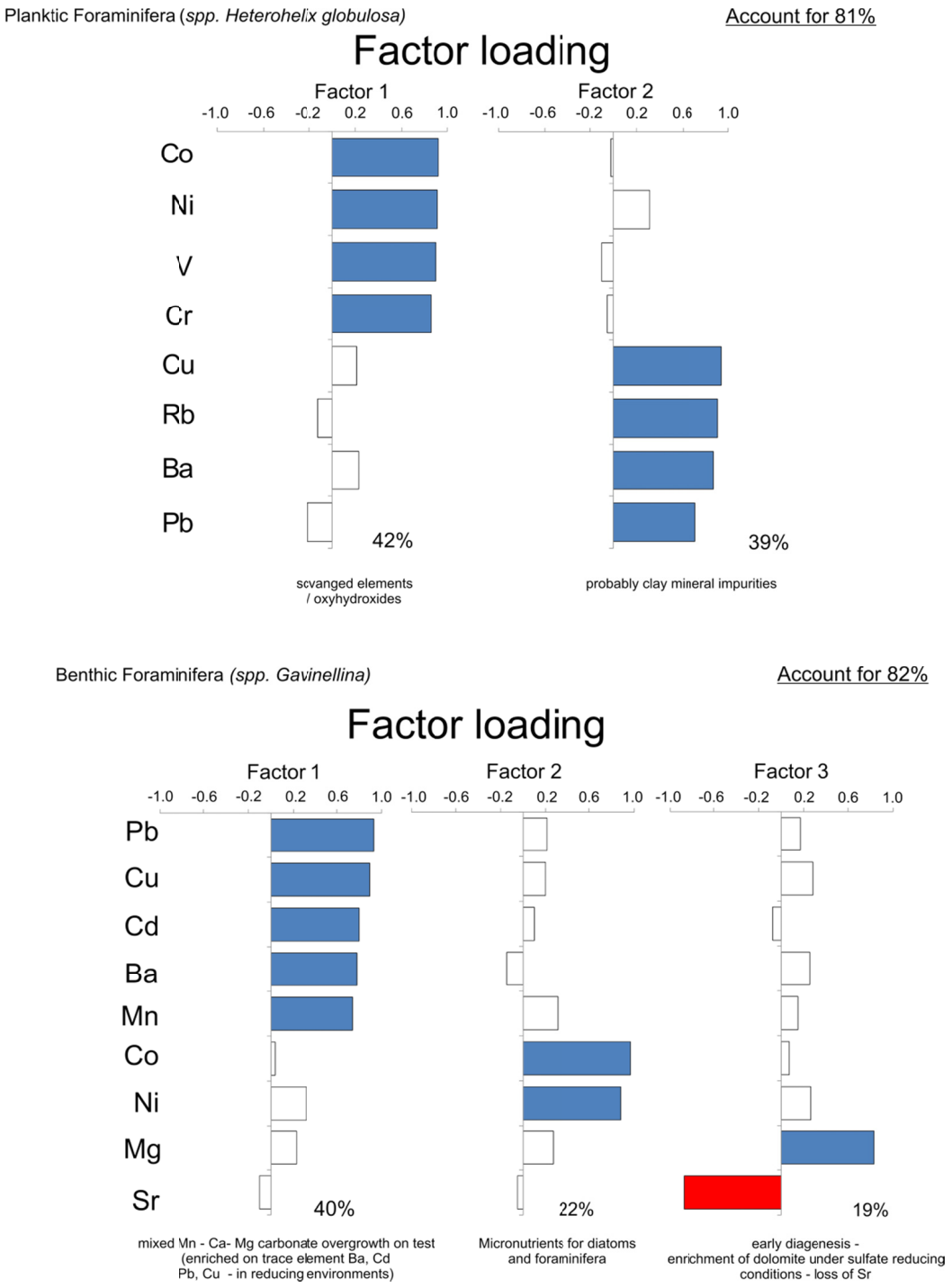

Fig.71 Bar plot of the factor analysis show factor loadings calculated for analysed trace element content in benthic (N=31) and planktic foraminifera (N=25). Blue label signifies positive factor loadings whereas red labels negative factor loadings.

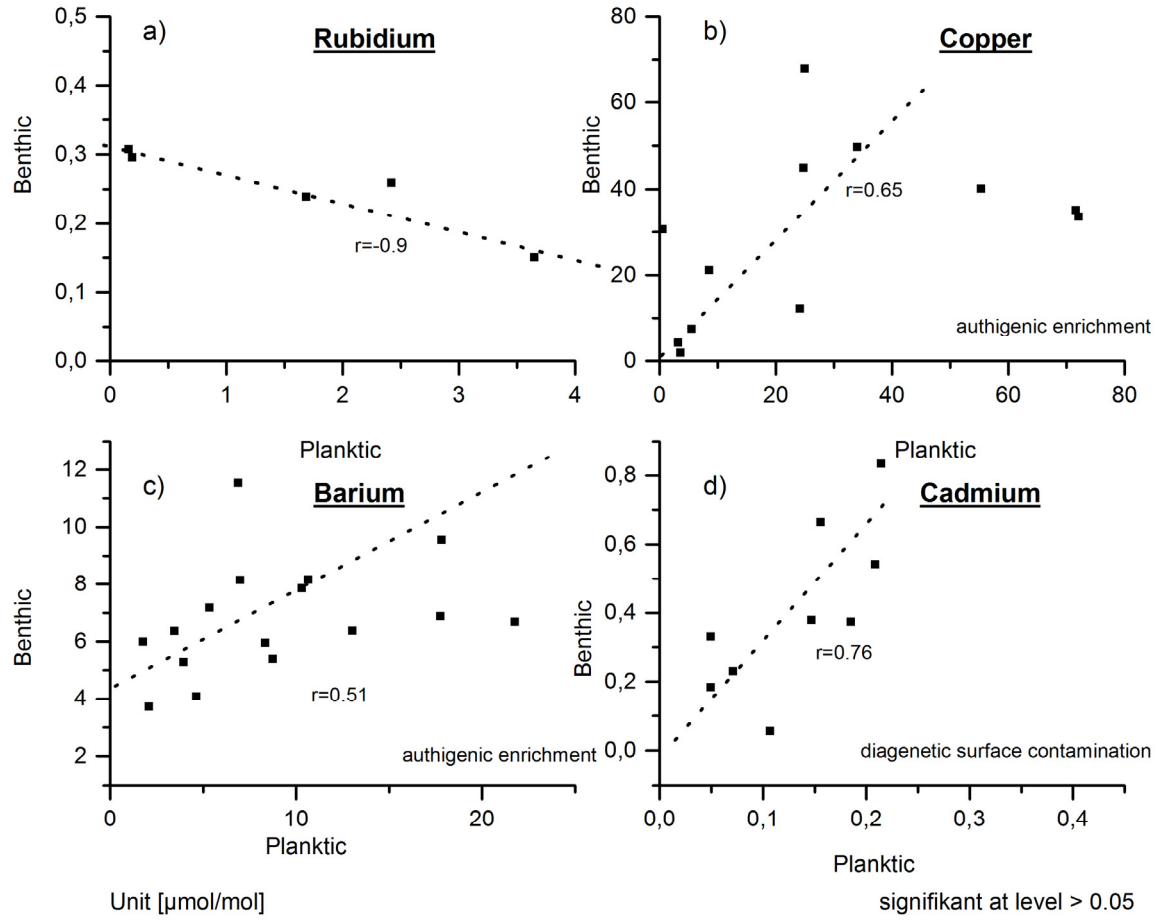

Fig.72 Sequence of plot show correlation of trace elements in planktic and benthic foraminifera to ***a)*** *Rb,* ***b)*** *Cu,* ***c)*** *Ba,* ***d)*** *Cd. All concentrations are expressed in units of [µmol/mol].*

Results suggest that elements, which plot in factor 1 (benthic dataset) and factor 2 (planktic dataset), correlate well with each other (fig. 72), suggesting that both populations were exposed to the same conditions. In comparison to the reference data set taken from Lea, (1999), own results show elevated concentrations of Fe, V, Zn, and Cu. Recently, it was discovered that Mn-carbonates/hydroxides display a strong affinity for the incorporation of other trace metals (V, Co, Ni, Zn, Ba, and Cd). Moreover, it is difficult to eliminate manganese overgrowth in foraminifera tests (Rosenthal et al. 1997; Hastings and Emerson, 1996; Hastings et al., 1996; Boyle, 1981). Organic matter and iron hydroxides are the most prominent source of trace elements by scavenging. Living infaunal species of benthic foraminifera

Gavinellina spp. should mirror the pore water concentration. It is commonly assumed that planktic and benthic foraminifera control their trace element inventory through different mechanisms (Boyle, 1981).

However, selective dissolution is an important factor that may significantly alter the fossil communities (Speijer and Schmitz, 1998; Martin et al., 1995). If we imagine that planktic species, sinking down to the sediment/water interface, where they covered by the sediment, underwent a selective dissolution, it is safe to assume that the dissolution of foraminifera depends on the size of the tests, as smaller specimen are dissolved more rapidly than bigger ones. This finally leads to accumulation of an assemblage, composed of larger sized planktic forms mixed with benthic forms, which typically have thicker walls and are therefore better preserved (Nguyen et al., 2009). The thicker shell of the benthic foraminifera prevents their buoyancy in the water column, being better protected against abrasive wave action (Erez, 2003). Additionally, benthic and planktic species differ in their calcification rate. Planktic species show a calcification rate which is higher by a magnitude, when compared to their benthic counterparts (Erez, 2003).

Further support for this hypothesis arises from a non-cross correlation between the specimens' richness, P/B[22] ratios, and their trace element content. Seawater serves as a main source of ions and is therefore incorporated via vacuoles in the calcified tests (Bentov et al., 2009). A widespread adoption states that benthic foraminifera show a higher trace element concentration than planktic foraminifera in the upper water column and the pore water itself. This is due to the pore water, which may reflect closed system conditions, in which the trace element threshold should be higher than in the overlying water column (e.g. open system) (Burdige, 2006).

To point out on-going biogeochemical processes that lead to the enrichment of trace metals in foraminiferal tests, some master variable defines the pore water chemistry, which includes the concentration of NH_4^-, PO_4^{3-}, organic matter input, and Fe^{2+}, Mn^{2+}-concentrations. This occurs in interaction with additional sedimentological parameters, which define the pore water chemistry and

[22] The ratio of planktic to benthic foraminifera (=planktic/(planktic + benthic foraminifera)).

therefore the chemical constituents (**Pb, Cu, Cd, Ba, Mn, Rb)** in foraminiferal tests, e.g., bioturbation, benthic macro fauna, bottom currents and more.

Therefore, it can be concluded that the trace element composition of both planktic and benthic foraminifera might not represent palaeoenvironmental conditions. Moreover, in course of the thesis it is proposed that both signs may represent a mix between two signals, which primarily come from the pore water concentration (benthic assemblages) and the conditions in the overlying water column, by tracking the sea water inventory (planktic assemblages). Regarding fig. 72, it should be noted that in terms of depth ranking, the P/B ratio is in close relation to both geochemical and biogeochemical bulk sediments of benthic foraminifera; neither increasing nor decreasing trends are visible. After their burial in the sediment, both species are exposed to the same (pore water) conditions and undergo a similar dissolution process. In this regard, the conclusion is might support that the palaeoenvironmental conditions are not represented here.

6. Discussion

6.1. Modification of primary environmental signals due to diagenesis or alteration

The pristine geochemical signal can be overprinted due to late diagenesis. In those specific circumstances leads this to misleading interpretations. However, by combining a multivariate statistical analysis with a multi-proxy approach, it should be possible to eliminate or attenuate the effect of late diagenetic overprint (Meudt, 2004). The high correlation coefficient between barium and strontium is attributable to the fact that barium may substitute for K in K-feldspar (celsian) and K-mica, because of similar ionic radii.

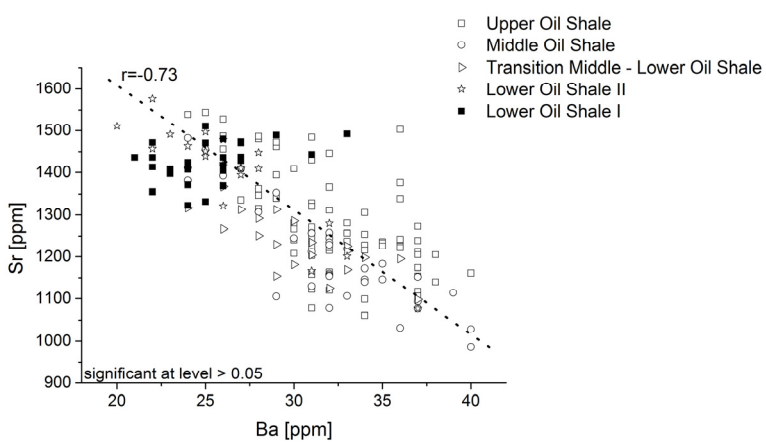

Fig.73 Negative statistical correlation between strontium and barium contents [ppm] through the oil shale profile.

The negative cross correlation, shown in fig. 73, may be due to differences in the solubility of both barite and celestine. The negative correlation seems implausible at first sight, because of the well-known isomorphic substitution of Ba by Sr in barite. However, under normal marine conditions, celestine is more soluble than barite. During progressive diagenesis, which is linked to the transition lime mud/chalk, a strong dissolution and precipitation of Sr^{2+}, which is freely circulating in the pore water, can occur. Such a process leads to an increased Sr content in pore water, whereby biogenic calcite contains 3-5 times more Sr than abiotically precipitated inorganic calcite (Hesse, 1986; Turekian, 1968).

However, the weathering process involves the loss of K and other cations including Rb and Sr, and the oxidation of Fe, leading to the formation of illite, which was detected by my own XRD analysis. Such a process is well described and confirmed, by the work of (Spiro and Rozenson, 1982; 1980), in sediments from the Ghareb fm. Moreover, the same authors report, based on Mossbauer spectrometry and SEM

analysis, an authigenic formation of iron hydroxides and microcline. Weathering of feldspar resulting in the release of potassium and silicic acid, subsequently leads to the authigenic precipitation of microcline and chert. A similar process is described in eq. 14, that demonstrate an example for the formation of authigenic clay minerals and quartz (Anderson, 2009**;** Spiro and Rozenson, 1982; 1980). This is in accordance with observations resulted from this study, obtained through XRD-analysis. These results suggest the occurrence of kaolinite, (authigenic) quartz and K- feldspare.

Equation 14

$$KAlSi_3O_8(s) + \frac{3}{2}H_2O(l) \leftrightarrow \frac{1}{2}Al_2Si_2O_5(OH_4)(s) + 2SiO_2 + KOH \qquad \text{Eq. 14}$$

K-feldspare kaolinite quartz

The same process, as described above, could also have led to unfeasible results, caused by the oxidation of pyrite. This can be shown by applying ternary diagrams (see below), which display the content of highly reactive iron (Fe_{HR}) as determined by di-thionate extraction in relation to pyrite bonded sulphur and organic carbon. In recent years it has become obvious that this ternary diagram has been used to differentiate between environments that are linked to an iron-limited and iron-non-limited system (Hetzel et al., 2009; Böning et al., 2005; Lückge et al., 1999; Littke, 1993). The grey–shaded areas, in the diagrams shown in fig. 74, represent a system in which the sulphur is in excess and signifies an iron-limited system. Under such conditions, iron is fixed in silicate and clay minerals; therefore, it is not available for pyrite formation. This kind of iron-bond (Fe*) can be calculated by the following equation 15 (Lückge et al. 1999):

Equation 15

$$Fe^* = Fe - (0.25 \times Al) \qquad \text{Eq.15}$$

Samples that plot below this pyrite line signify an iron-limited system. In contrast the diagram on the right side, those show all extractable di-thionate iron (Fe_D), that imply the real bulk iron and di-sulphide sulphur values, latter one based on wet chemical extraction scheme by (Mayer and Krouse, 2004).

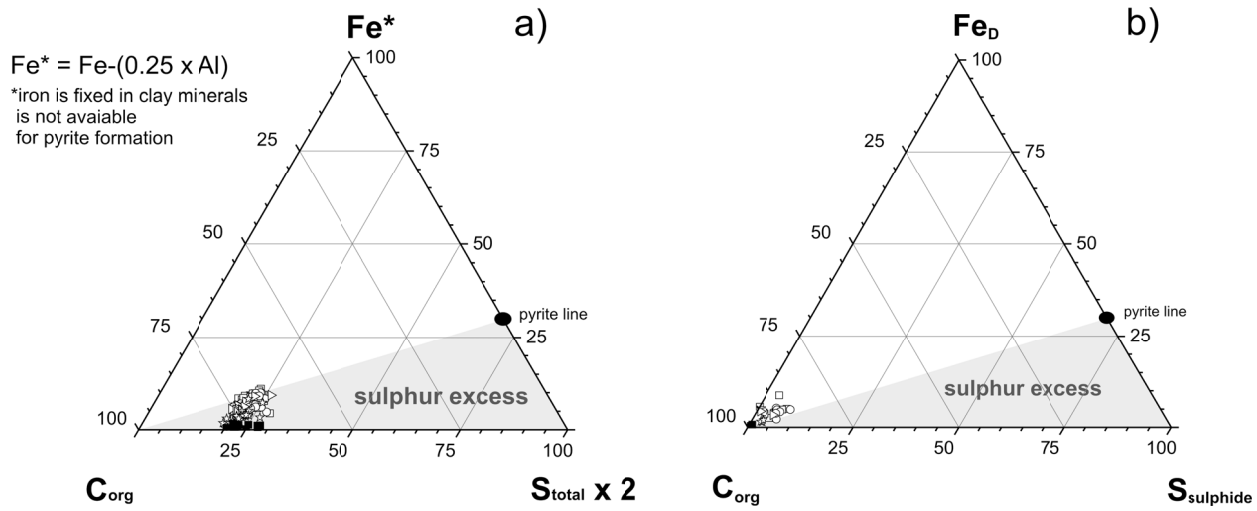

Fig.74 Ternary diagrams that can be use to indicate possible iron limitations, specify a iron-limited system ***a)*** *However, obtained results by di- thionate extraction method (F_D di- thionate iron), support a a non- iron-limited system* ***b)*** *Gray shaded area indicate iron – limitation.*

From this ternary diagram, two conclusions are possible: firstly, F_D value was changed by oxidative weathering to Fe(OOH), (Spiro and Rozenson, 1980), and secondly, $S_{sulphide}$ was highly affected by oxidative sulphate formation. In order to understand this, multiple tests were conducted to see how this relation could be affected.

Fe_{py}/Fe_{HR} (pyrite oxidation)

An example for oxidative weathering is shown in equation 16 that includes an oxidation of the pyrites according to (Bierens Haan, 1991).

Equation 16

$$FeS_2 + 3.5O_2 + H_2O \rightarrow Fe^{2+} + 2SO_4^{2-} + 2H^+ \qquad \text{Eq. 16}$$

This comprises a transformation of pyrite sulphur to sulphate sulphur and subsequently to iron oxides. Optical and XRD analyses as well as the detection of sulphate sulphur by wet chemical analysis (ASS-sulphur) confirm this assumption. This consequently leads to a change in the Fe_{py}/Fe_{HR} relationship. Oxidative weathering alters the relationship between pyrite-bonded iron and highly reactive iron.

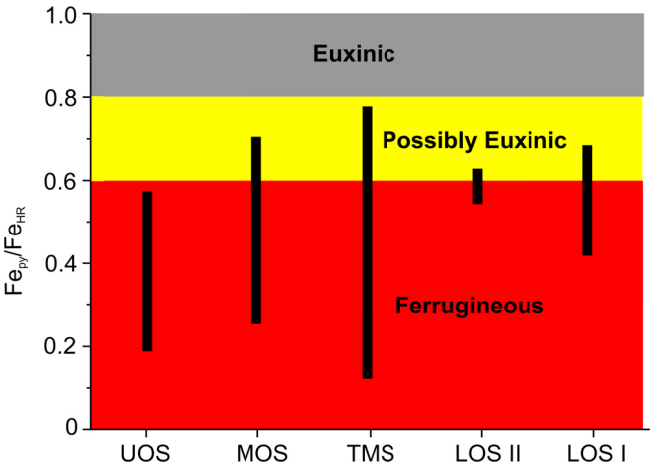

Fig.75 Plot show variations in the ratio of pyrite bound iron (Fe_{py}) and highly reactive iron (Fe_{HR}) - obtained by di-thionate extraction. X - axis display the complete OSM from the LOS I (Base) to the UOS (top). Boundaries might be interpreted with caution, modified after Raiswell and Canfield, (2012).

Subsequently, this results in a change in the relationship between pyrite-bonded (Fe_{py}) and highly reactive iron (Fe_{HR}). Results support the notion above and might suggest from alongside the profile a shift to a higher content of highly reactive iron (fig. 75). In such a case, the application of the Fe_{py}/Fe_{HR} leads to a misrepresentation of the values. As previously shown, the own results implying that the sedimentation of the LOS took place in a high reducing environment. Again, fig. 75 samples do not support this unambiogiusly. Sample from the LOS plot in a field, which indicating moderate anoxic, weak oxic conditions. This is paradoxicial, and corroborates assumptions and interpretation that has to be done about the careful use of the Fe_{py}/Fe_{HR} relationship as a proxy for separating between anoxic and euxinic conditions (Raiswell and Canfield, 2012).

At this point, it is useful to introduce other possibilities to quantify the reactive iron content in sediments that are capable to react with total reduced sulphur. One of them is recommend by Raiswell and Canfield, (2012) by use the ratio of highly reactive iron to total iron that is plotted against the degree of pyritization.

Raiswell and Canfield, (1998) point out that the ratio between Fe_{HR} and Fe_T in oxygen deficient sediments (deposited from stratified or anoxic/ euxinic water columns), plots within an area defined by two lines with slopes between 0.04 and 0.4. In fig. 76, samples marked with blue and green dots, plot in a

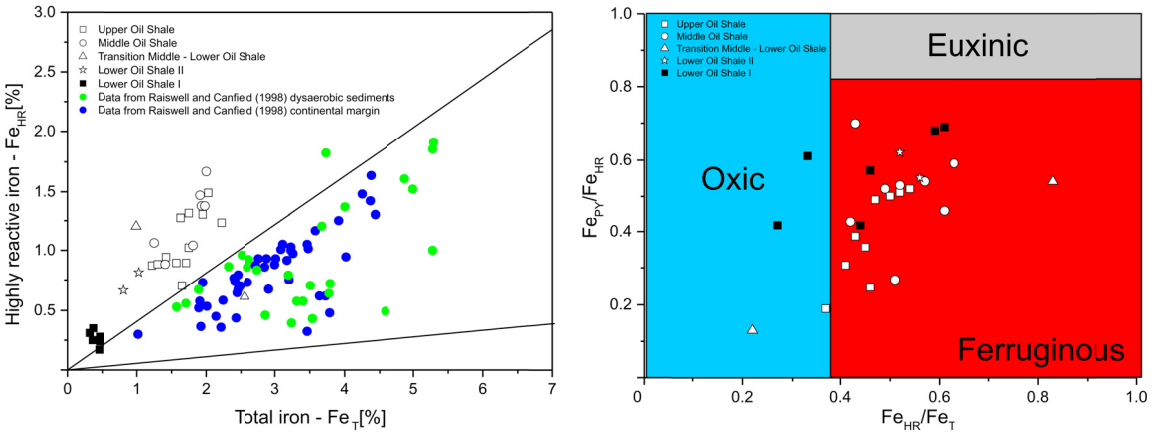

Fig.76 ***Left side****: Variation of highly reactive iron Fe_{HR} in relation to the total iron Fe_T for continental margin and dysaerobic sediments (data from Raiswell and Canfield, 1998).* ***Right side:*** *Cross plot of the ratios of pyrite bound Fe to highly reactive Fe against highly reactive iron and total iron. Coloured boundaries based on empirical results and might be interpreted with caution (see text below). Both plots are in reference to the present study (white coloured and black dots).*

range that originally has been deposited in anoxic/dysoxic environments. From the fig.76 it becames also evident that samples from the studied oil shales do not plot into this area, and consequently may not correspond to the conditions as predicted by (Raiswell and Canfield, 1998) and others.

In summation of all results, this mismatch might support the assumption that an additional enrichment of highly reactive iron (Fe_{HR}) (possibly from oxidation) shall be taken into account.

Distinguishing between anoxic –euxinic conditions, C/S ratio

As shown in section 2.4, an attempt was made to understand in which environment the sedimentation took place. In order to differ between anoxic and euxinic conditions, the C/S ratio was originally introduced by (Leventhal, 1983). In fact, by comparing the outcomes of the present study with data from recent upwelling sediments, obviously a puzzling picture is shown (see also section 2.4). Our results (OSM C/S 56.54) show atypical high C/S ratios which are in accordance to high C/S ratios in recent sediments, that come from Fe-limitation (Lyons and Berner, 1992; Morse and Emeis, 1990; Berner and Raiswell, 1984). Sulphate limitation and low C/S values are atypical for marine environments and are more characteristic for fresh-water environments. Consequently as seen in fig. 77, S/C values in the oil shales of around 0.12 would suggest a deposition in a non-marine environment.

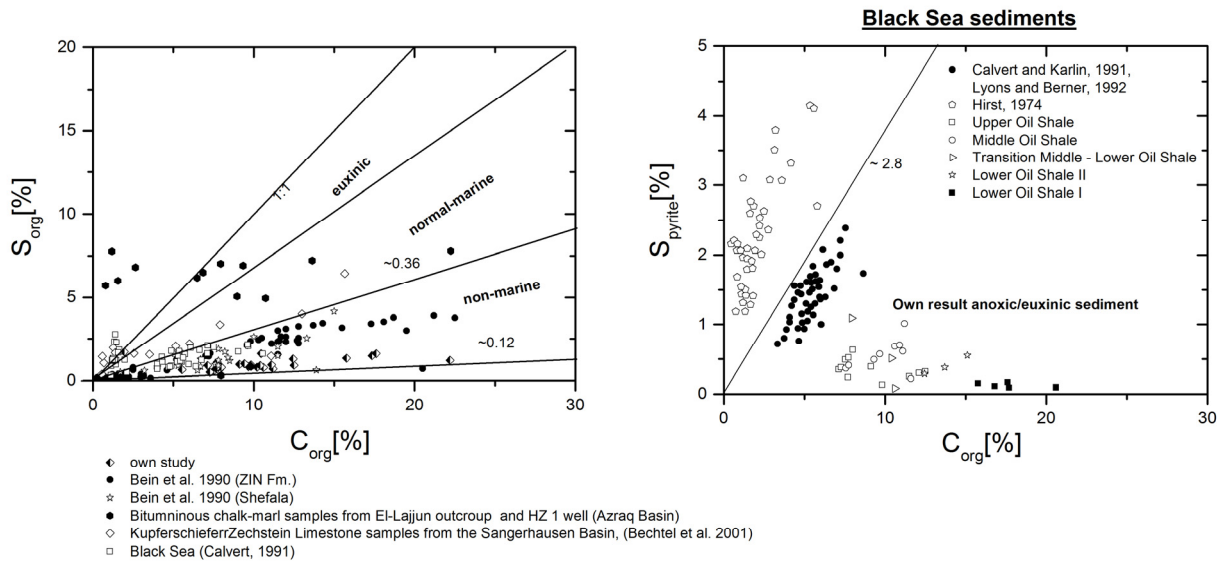

Fig.77 ***Left side****: Samples from Mishor Rotem oil shales define a regression line in a C_{org}/S_{org} cross plot with a very flat slope (0.16). Flat inclination indicates a pattern typical for sediments in freshwater conditions. The* ***right side*** *indicates that results from the present study, do not plot in a typical range of Black Sea sediments, which are deposited in a strong anoxic/euxinic environment.*

Previously, Minster et al. (1992), Bein et al. (1990), and Dinur et al. (1980), also found comparable S/C ratios of = 0.09 in the Shefala Basin (Ghareb Fm.), and an S/C ~0.13 – 0.15 in Mishor Rotem (Minster et al., 1992). However, sulphate limitation could possibly also occur in stratified water columns or within the sediment (close system conditions), not necessarily reflecting fresh water environments. An additional feature which might affect the C/S relationship is reported by Pratt, (1984), and (Westrich and Berner, 1984). The authors show that bioturbation also has an influence on the C/S ratio in sediments. There is a limitation in the supply of sulphate by diffusion in micro-bioturbated or fine-laminated sediments, rendering the injection of fresh oxygen unlikely. This results in a limitation of sulphate reduction by bacteria, leaving smaller amounts of H_2S in the surrounding pore water and limiting the degradation of organic carbon. Furthermore, slower sedimentation rates allow more time for organic matter to be degraded at the sediment surface, prior to the onset of sulphate reduction, leaving smaller amounts of organic carbon for sulphate reduction (Canfield, 1994).

In summation, most of the S in the studied section is commonly associated with OM, pyrite, and gypsum. Otherwise, the XRD- and wet chemical analyses indicate negligible amounts of pyrite ~ 1 wt. %. This is in accordance with the findings of Amrani et al. (2005), who found no measurable amounts of pyrite in the Ghareb Fm. of the northern Negev. In contrast to Bein et al. (1990), sulphate sulphur is determined by ASS extraction. However, the author reported only negligible amounts of gypsum because most of it had been removed by percolating aqueous solution.

This puzzling picture should be interpreted with care. Emeis and Morse, (1993) offer a different point of view by comparing the C/S ratios in sediments from different upwelling sites (Peru, Namibian, Oman C/S ~ 0.25), which deviate significantly from the regression slope of ±2.8 that is thought to be common in normal marine sediment. All three sites show a specific limitation, regarding iron-limitation, the quality of degradable organic matter, and the amount of sulphate in the pore water. Consequently, all three restrictions affect and lead to the significant deviation in C/S ratio. Emeis and Morse, (1990) conclusively state that this method is inadequate to differentiate between oxic and anoxic environments, as well as marine and lacustrine environements, respectively.

This is supported by Rickard, (2012), who has shown that in an euxinic system the amount of pyrite-bonded sulphur is not in line with the amount of organic carbon. In such a system the availability of reactive iron plays a critical role, and therefore high C_{org}/S_{pyrite} ratios are atypical for euxinic sediments (Lyons and Berner, 1992).

If we take into account that own values display a late diagenetic overprint, by which most of S_{pyrite} is lost due to oxidation, through a penetrating, oxidising solution, which leads to the formation of sulphate sulphur. In consequence, obtained S_{pyrite} and C/S ratio don`t match the real scenario.

Clay mineralogy

Based on the results obtained by XRD analysis, in course of the thesis the sedimentological processes will be evaluate that enable us to document under which conditions the deposition of clay minerals took place. An alteration of deposited sediment during periods of interest is a scenario that might be possible for a authigenic and detrital formation of illite, as proposed by (Spiro and Rozenson, 1982; 1980), for sediments in the Ghareb fm. Recent investigations confirm this notion and indicate that the dominant clay mineral in the Syrian arc deformation belt is smectitic IS (interstratified illite/smectite rich, in smectite layers) (Shoval, 2004a, 2004b).

Our investigation supports these results, which include the detection of the relative abundance of the three most important groups of clay minerals: (detrital) kaolinite, (partly detrital) smectite (Nathan, 1969), and (authigenic) illite (Spiro and Rozenson, 1982) respectively, as the three major constituents. It is thought that these clays, especially illite-smectite (main clay component) as part of the detrital contribution to the whole sedimentary record, were transported by upwelling currents across the continental shelf towards the deposition side (Inthorn et al., 2006; Shoval, 2004a, 2004b).

Therefore, it is assumed that the observed fluctuations in the herein considered clay mineral ratios must have a different explanation. Although in void of hand-tight evidence it seems rather speculative, that the observed fluctuations in clay mineralogy might be due to changes in the direction and the weighting of different detritic transport mechanisms (e.g., aeolian and fluviatile, possibly shelf currents) and authigenic formation. The weathered sandstone reflects the continental source of the Arabo-Nubian Shield, whereby the detrital kaolinite is transported (Goldberg, 1978). The occurrence of kaolinite represents a continental weathering product formed during a warm and humid period at the southern Tethys margin during the early Palaeozoic era (Bolle and Adatte, 2001).

Moreover, it is worth noting that no terrestrial magmatic activity occurred in Israel between the Santonian and late Oligocene time (Almogi-Labin et al., 2012; Garfunkel, 1989). Thus, the conclusion can be drawn

that the occurrence of smectite cannot be the a result of the weathering of terrestrial basaltic rocks (Shoval, 2004b). Thereby argillised submarine volcanic rocks act as the main sources of illite-smectite interlayers (Sandler and Harlavan, 2006). Consequently, these clay minerals have rather been transported by upwelled water across the continental slope to the inner shelf area (Inthorn et al., 2006).

$\delta^{18}O$, $\delta^{13}C$ – planktic and benthic foraminifera

Modern marine $\delta^{13}C$ values of total dissolved carbon (DIC) are close to zero ‰, thus reflecting the dissolved CO_2 in seawater that is commonly used for photosynthesis, while the $\delta^{13}C$ values in planktic and benthic foraminifera range from +2 to +3‰ (Maslin and Swann, 2006). The formation of shells and the incorporation of dissolved inorganic carbon is in isotopic equilibrium within surrounding water (Schiebel and Hemleben, 2005). This explains the use of the $^{18}O/^{16}O$ and $^{13}C/^{12}C$ ratios as palaeoceanographic proxy for seawater temperature, salinity and primary productivity (Katz et al. 2010, Emiliani, 1955). Vital effect is another important factor that contributes to the isotopic composition of living foraminifera and their

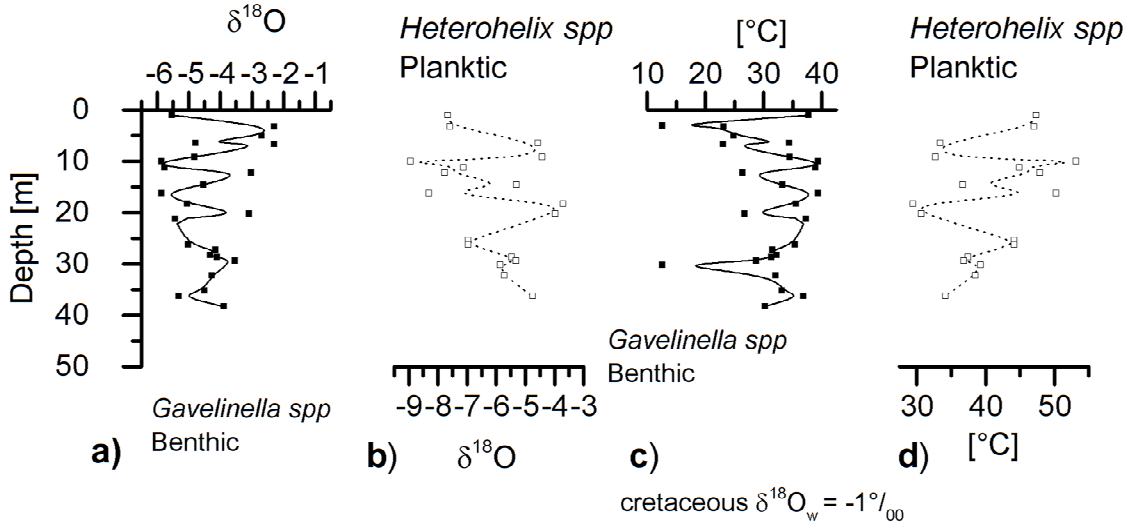

*Fig.78 Graph shows the influence of meteoric water on isotopic composition of $\delta^{18}O$ in both benthic **(a)** and planktic **(b)** foraminifera. Both species display significant lighter values than expected for Upper Cretaceous seawater. Palaeo seawater temperature was calculated according to Erez and Luz, (1983) for benthic **(c)** and planktic **(d)** species. A Upper Cretaceous seawater value ($\delta^{18}O_w$) of -1‰ was taken into account for calculation (Friedrich et al., 2012).*

calcification rate (Maslin and Swann, 2006; Schiebel and Hemleben, 2005). The foraminiferal assemblage preservation can also be used to reveal additional insights into late diagenesis. Additionally, the analysis of $\delta^{18}O$ and $\delta^{13}C$ in planktic and benthic foraminifera supports outcomes present above that a part of the profile might have been affected by late diagenesis. As is shown exemplary in fig. 78, the analysis of the ^{18}O from *Gavelinella spp*. (benthic) and *Heterohelix spp*. (planktic) foraminifera, by our Israeli co-partner, reveals light values in $\delta^{18}O$ up to ~ -7‰. The results also show a decreasing trend towards the base of the profile. Figure 78 (c, d) shows the calculated palaeo- seawater temperature for the Upper Cretaceous. If these values are used as a proxy for the past, seawater temperatures yield unusually and unrealistically high temperatures (10 – 20 fold higher), which is reported from this time, (Friedrich et al. 2012) and references therein.

An efficient tool for the assessment of diagenetic effects and alteration in sedimentary rocks and enclosed fossil material is the use of cross plots between $\delta^{18}O$ and $\delta^{13}C$. It is assumed that, a relatively uniform supply of meteoric cements, leads to a shift in the absolute contents in primary trends of $\delta^{18}O$ (Griffiths et al., 2013; Stüben et al., 2003, 2002). A penetration of oxygen or the percolation of meteoric water cause

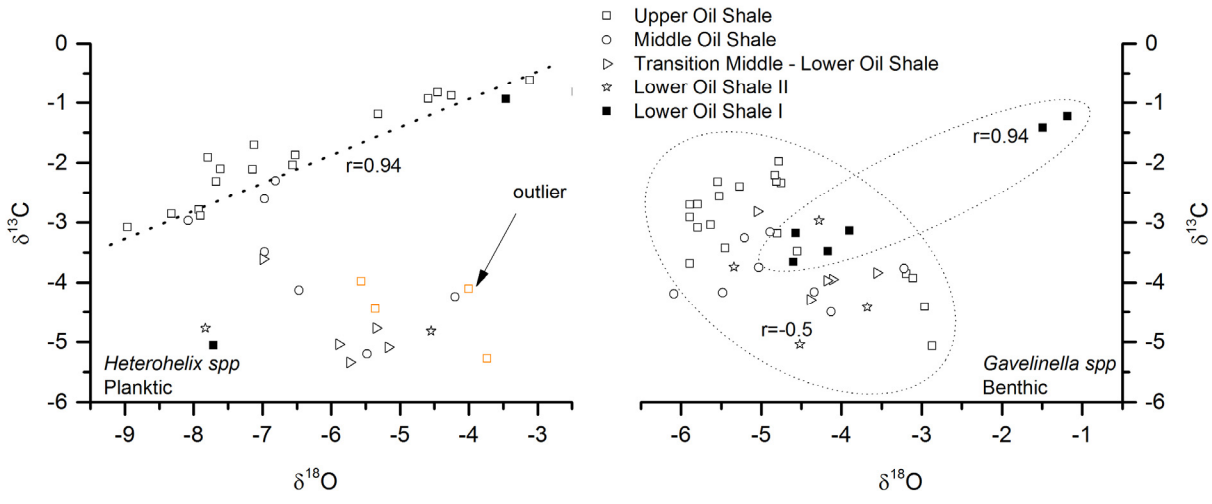

Fig.79 Cross plot between ^{18}O and ^{13}C supports an infiltration of the profile by percolating meteoric water. ***Left side:*** *Planktic foraminifera show a stronger coefficient r=0.94, p>0.05 and a slope of 0.44 in the regression line.* ***Right Side****: Whereas benthic foraminifera show two signs; Firstly, In the UOS a negative correlation r=-0.5, and secondly a positive trend in the LOS I r=0.94; p>0.05.*

an oxidation and might significantly alter the composition for example of $\delta^{18}O$ (input of fresh/ meteoric water) and the amount and composition of organic matter by the loss of organic carbon.

Recently, studies on the effects of meteoric alteration of the element contents of foraminifera have been receiving more and more attention. It seems obvious that the meteoric water could change the element contents of foraminifera similar to the $\delta^{18}O$ through mixed signals. Fig. 79 shows the relationship between $\delta^{18}O/\delta^{13}C$ values from benthic and planktic foraminiferal species (*Heterohelix spp*., *Gavelinella spp*.) as a cross plot. The plot also indicates that benthic $\delta^{18}O$ values range in a smaller array ~-3‰, unlike planktic foraminifera, which plot in a larger range ~6‰. Their isotopic counterparts in $\delta^{13}C$ range from -6 to -1‰ (benthic), while plantic foraminifera values in plot from -5.5 - -0.5‰. These values may indicate different influence by differential diagenesis on different foraminifera species and may also suggest a higher degree/sensitivity in alteration or infillings of chambers in foraminifera, because of the large deviation from reference values. The negative correlation between $\delta^{18}O/\delta^{13}C$ values of benthic foraminifera might suggest a higher resistance against diagenetic overprint. From these observations, it might be concluded that there are three possible scenarios for explaining trends in a $\delta^{18}O/\delta^{13}C$ cross plot.

(1) From an experimental setup, Spero et al. (1997) conclude a covariance between $\delta^{18}O$ and $\delta^{13}C$ that shows a regression slope between 0.29 – 0.33, which would fit to values (0.44) obtained within this study from planktic foraminifera, fig. 79. Furthermore, the author states that such a covariance might be a consequence of subtle changes in the alkalinity of seawater (CO_3^{2-}). This might be true for the planktic foraminifera, whereas benthic species show a negative correlation, which would imply no sensitivity to changes in alkalinity.

(2) Such covariance might also be explained by a mixing of different water masses or changes in the precipitation/evaporation cycle, as a consequence of a mixing in the isotopic composition of the end-members ($\delta^{18}O/\delta^{13}C$, planktic and benthic species).

(3) The $\delta^{13}C$ mainly controlled by the solid-phase because of the generally low levels of organic carbon in the pore water during early diagenesis. Consequently, the meteoric alteration changed the isotopic

composition of carbonate only slightly toward smaller values (Faure and Mensing, 2005). In contrast, the $\delta^{18}O$ is stronger controlled by the fluid phase, shifting its value towards lower (negative) values (Marshall, 1992; Banner and Hanson, 1990). At the DSDP Site 525, a meteoric alteration of foraminifera tests caused a negative shift of ~ 3‰ in the $\delta^{18}O$ values, while at El Kef les Pins, Tunisia, where the sedimentary rocks were affected by the precipitation of carbonate cements, a similar effect could be observed (Stüben et al. 2003).

The primary character of the positive correlation, between the distribution pattern of the $\delta^{18}O$ and $\delta^{13}C$ in the benthic and planktic shells, has a substantially uniform lowering effect on the $\delta^{18}O$ over 2/3 of the section. Such a relatively constant supply of meteoric water leads to the filling of pore space and the precipitation of cement onto the surface of benthic and planktonic foraminifera tests. While this causes an alteration of the absolute $\delta^{18}O$ values, the relative trends are still more or less intact and might be able to be used for palaeoenvironmental interpretations.

6.2. Preservation of organic matter

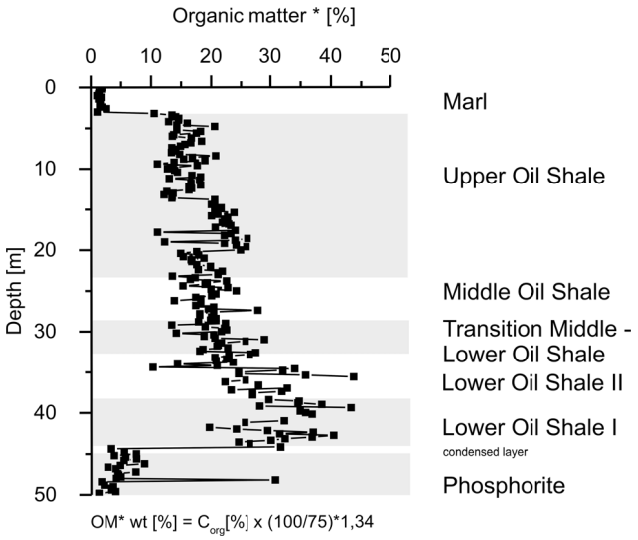

Fig.80 Calculated organic matter (OM) content along the profile*

In fig. 80 is shown the calculated organic matter content* according to (Tyson, 2001; Littke, 1993). This plot also suggests a dramatic drop in organic matter content around 35 mbsf. What could be the reason for such a drastic trend? In general, it is accepted that there is a positive relationship between sedimentation rate and organic carbon content (Tyson, 2001; Stein, 1990; Bralower and Thierstein, 1987).

Moreover, in coastal upwelling zones, a high sedimentation rate is often observed, which is controlled by high productivity (Wilkerson and Dugdale, 2008; Mohtadi et al. 2005; Summerhayes et al., 1992; Diester-Haass and Schrader, 1979). Interaction between productivity and flux of organic matter leads to an increased preservation of organic matter in sediments (Littke, 1993; Stein, 1990). This relationship is only true in oxic environments, as first noted by (Tyson, 1987). In marine sediments with low sedimentation rates and anoxic conditions, an inverse relationship is detectable (Stein, 1986). Such conditions are well documented in the Mediterranean Sea, Black Sea, and Cariaco Basin. Canfield (1994) argues that if the anaerobic processes of organic carbon decomposition would dominate in such environments, it would be less efficient than decomposition with 0_2 present and in consequence lead to a higher enrichment of organic carbon. Low sedimentation rate and high organic carbon content do not exclude one another.

There are three possible explanations for the comparatively high organic matter content in the LOS unit (16-45 %, n=45), as opposed to the transition horizon to the overlying oil shale horizon (17-30 %, n=145) (fig. 80):

(1) Mayer (1994) noted that the surface area of mineral grains controls the preservation of organic matter. In cores from the American Shelf, he found evidence that organic matter is adsorbed onto the surface of clay minerals. This promotes the better preservation of organic matter. In support of this thesis, Kennedy et al., (2002) observed that in Cretaceous Black Shale, from the Western Interior Seaway, 85% of the organic carbon is strongly associated with clay minerals.

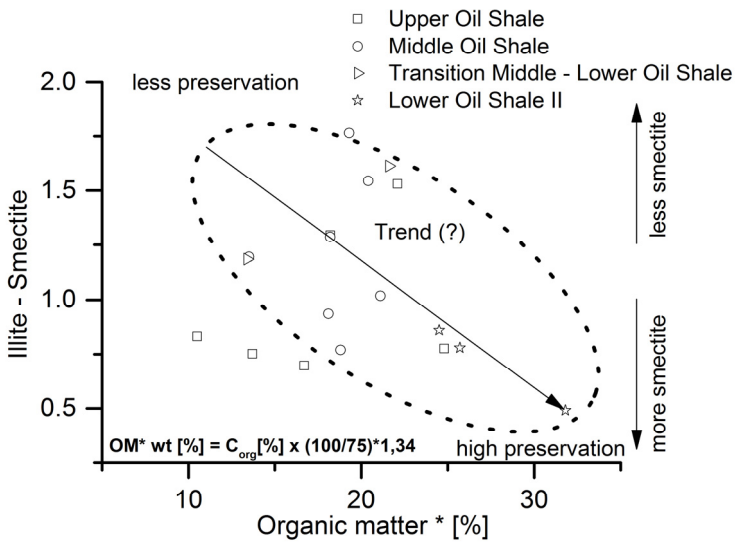

Fig.81 Graph showing the calculated illite-smectite ratio determined by a semi-quantitative X- ray analysis vs. the calculated OM content.

(2) surface (detrital smectite or smectitic mixed layer illite-smectite I-S), promoting the preservation of the organic matter. The enhanced preservation may be due to a larger surface area of smectite ($800m^2/g^{-1}$), compared to illite ($30m^2/g^{-1}$). The highest values of organic matter in Lower Oil Shale, in comparison to the upper part of the profile, may confirm the notion of Kennedy et al. (2002), and Mayer, (1994). Own results from the semi-quantitative clay mineral analysis reveal that the calculated illite-smectite relationship shows a decreasing trend towards the base of the section. This might indicate that the highest C_{org}- content shows a trend to a lower illite-smectite relationship than the upper part of the profile, fig. 81 (previous page). That would imply a contribution of smectite clay minerals to the major terrigenic input. In fact, this might also indicate that clay minerals are contributors to the preservation of organic matter. Nevertheless, regarding the low terrigenic input, it may be implausible that clay minerals contribute significantly to the preservation of organic matter.

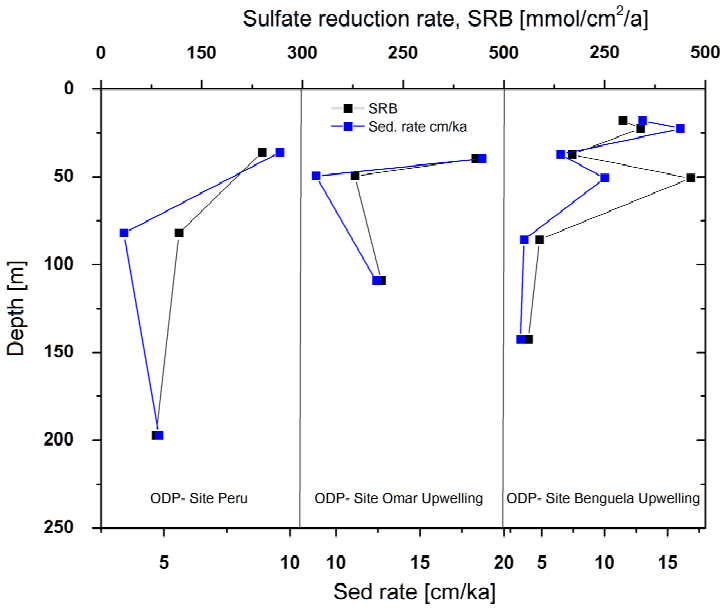

Fig.82 Dependency of SRB as a function of sediment depth and sedimentation rate in three different marine settings ODP sites from Peru, Omar upwelling, and Benguela upwelling, respectively. Reference data are taken from (Emeis and Morse, 1993)

(3) Sulphurization of organic matter In the present case, it is more likely that sulphurisation (natural vulcanisation) acts as the critical factor for a higher preservation of organic matter. This results in sulphurised organic matter that can contain up to 90 % sulphur (Bein et al., 1990). The process behind it involves the incorporation of sulphur into organic matter through "cross-linking" to form kerogen (Kok et al., 2000c; Eglinton et al., 1994; Schouten et al., 1990; Orr and Sinninghe Damsté, 1990).

During early diagenesis, the process of sulphurisation is explained by a complete rearrangement of organic matter, through the insertion of reduced sulphur species into organic matter, which leads to a protection of functionalised lipids against further degradation (Wakeham et al., 1995; Kohnen et al. 1990). Similar observations are reported from the Tarfaya Basin (SW Morocco) in iron limited Cenomanian/Turonian black shales. Iron limitation, in combination with an excess of sulphide and refractory organic matter, leads to the sulphurisation of kerogen in stages of early diagenesis, caused by changes in sedimentation rate and sea level fluctuations (Kolonic et al. 2002). The exact process that leads to the sulphurisation and therefore the protection of sulphurised organic matter are out of the scope of this thesis. The author of the thesis recommend reading more detailed explanations of this process by other authors (Werne et al., 2008; 2004; Kok et al., 2000; van Kaam-Peters et al., 1998).

As shown in fig. 82, the sedimentation rate can be interpreted as changes in the delivery mode and source of terrigenic input. Consequently, the low sedimentary input (below 2 cm/ka) in the Lower Oil Shale unit, where the highest organic matter content is observable, can be interpreted in terms of the occurrence of refractory organic matter that survives under such anoxic conditions (Tyson, 2001). It is commonly assumed that the organic matter sulphurisation is dependent (1) on the availability of reactive iron, (2) creation of an anoxic/sulphidic (?) environment, (3) a sulphate reservoir, which allows sulphate-reducing bacteria to consume sulphate for microbial activity and (4) organic matter that acts as a substrate (energy source) for bacteria (Canfield, 1994, Jørgensen, 1982).

Together with slow sedimentation rates, this permits high rates of organic carbon mineralisation in the sediment, because a low sedimentation rate allows a free circulation of sulphate in the sediment/pore water reservoir – open system, causing high rates of sulphate reduction (Brüchert et al., 2000). Prominent examples from this phenomenon come from recent investigations in the Cariaco Basin (Werne et al. 2003), the Namibia slope (Pichevin et al. 2004), the Peruvian margin (Eglinton et al. 1994, Emeis and Morse, 1993), and ancient sediments (Tribovillard et al. 2004). If there is no significant terrestrial input and therefore no significant reactive iron input, a sulphurisation of organic matter will occur. Originally it

is assumed that the pyritisation is kinetically favourable over the sulphurisation, as observable in the Kimmeridge Clay Formation (KCF), (van Kaam-Peters et al. 1998), Cenomanian-Turonian high organic rich sediment in the Tarfaya Basin, Morocco (Kolonic et al. 2002), and the Black Sea (Raiswell and Canfield, 2012; van Kaam-Peters et al. 1998). Once all of the highly reactive iron is exhausted, the sulphurisation takes place. A concomitant reduction of iron hydroxides and the release of polysulphides, which act as a precursor to the formation of organic sulphur, the sulphurisation of organic matter can take place. Similar observations have been documented in Holocene sediments from the Mud lake, Florida (Filley et al. 2002), in estuarine sediments from the St. Andrew Bay, Florida (Brüchert and Pratt, 1996), and in lake sediments (Urban et al., 1999).

6.3. Sulphate isotopes as a tool for reconstruction of the late diagenetic processes

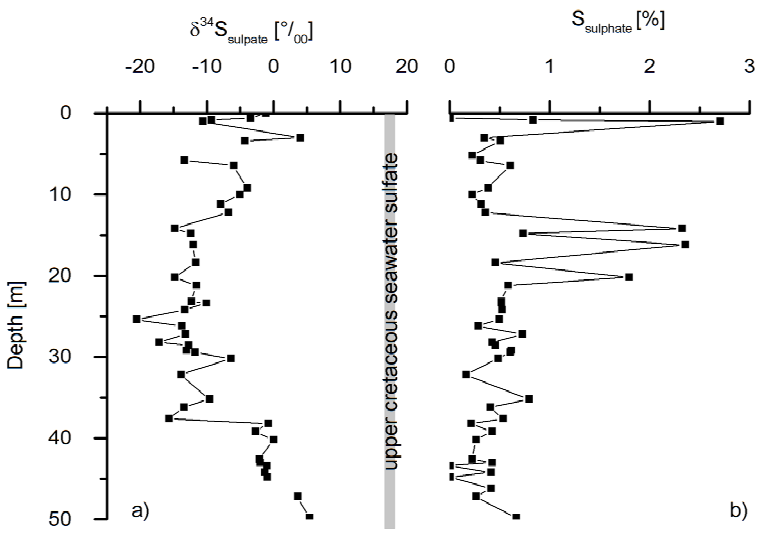

Fig.83 Comparison between the value of $\delta^{34}S_{sulphate}$ as a result of the study and the Upper Cretaceous $\delta^{34}S_{sulphate}$ (grey shaded bar) ***a)*** *and the absolute content of sulphate sulphur* ***b),*** *along the profile*

The proposed $\delta^{34}S$ value of seawater sulphate in in the earth`s history has been changed for several times. In the Upper Cretaceous time the $\delta^{34}S$ for marin sulphate lies around +19‰ (Sweeney and Kaplan, 1980), and +17‰ (Strauss, 1999), see also fig. 83. Own results suggest a much different value. This means that the values of the $\delta^{34}S_{sulphate}$ do not show the original isotopic composition of seawater sulphate at this time. One of the main reasons could be the mixing of two signals. The isotopic composition represents a value which comes firstly, from original seawater isotopes (Upper Cretaceous time) and secondly from the oxidised pyrite.

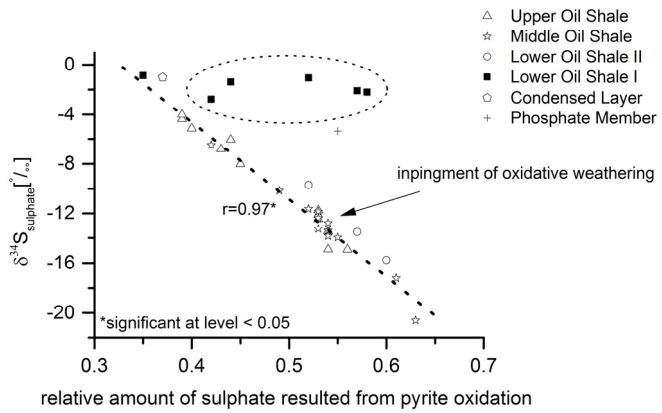

Fig.84 Plot indicates a strong correlation between the isotopic composition of $\delta^{34}S_{sulphate}$ and the part of sulphate, which resulted from pyrite oxidation. Note the non – correlation for the LOS I and PM.

The results suggest a late-/post diagenetic influence on the measured sulphate isotopic values due to the oxidative weathering of pyrites. As a rule, the oxidation of pyrite shows no fractionation. Because during both bacterial sulphate reduction and thermal sulphate reduction residual sulphate is always enriched in ^{34}S, these values are hard to be interpreted in terms of isotope fractionation during sulphate reduction. Rather, a late-stage re-oxidation of reduced sulphur species during the exhumation history of the sequence should be considered. The measured sulphate-$\delta^{34}S$ values represent a mixture between the isotopic composition of pristine marine sulphate and oxidized pyrite. It is possible to calculate for each sample the relative proportion of these two fractions, because the pyrite oxidation is not accompanied by a notable isotope fractionation. In eq. 17, $\delta^{34}S_{SW-SO_4}$ represents the isotopic composition of the Upper Cretaceous seawater, the term A_{SW-SO_4} is the amount of measured sulphate. While the terms $\delta^{34}S_{py.(ox.)}$, and $\delta^{34}S_{measured-SO_4}$, representing their measured values of isotopes.

Equation 17

$$\delta^{34}S_{SW\text{-}SO_4} * A_{SW\text{-}SO_4} + \delta^{34}S_{py.(ox.)} * A_{py.(ox.)} = \delta^{34}S_{measured\text{-}SO_4} \quad \text{Eq. 17}$$

In a cross-plot (fig. 84) between the obtained chromium-reducible sulphur - pyrite- bonded - $\delta^{34}S$ (CRS) values and the calculated fraction of oxidised CRS. The samples clearly define a mixing line, with end members corresponding to the assumed isotope composition of marine sulphate (17‰) and that of average CRS (-31‰), respectively. Exceptions are the samples from the PM, and the lowest part of the OSM, which plot outside of this mixing line, in accordance with their distinctly different isotopic composition. The portion of sulphate resulted from pyrite oxidation varies between ca. 35‰ and 65‰, with a weak

trend to lower values in the upper 20 mbsf of the OSM and a higher portion of oxidised CRS between 20 mbsf and 35 mbsf.

6.4. Reconstruction of the depositional conditions

Sedimentation rate

In fig. 85, the calculation of the sedimentation rate is shown, which is based on a theoretical and practical approach by (Davis et al. 1999; Berner, 1980). Grain densities are taken from Schön, (2004). The prevalent clay mineral in oil shale samples is smectite (2.53g/cm^3). Rock density of $CaCO_3$ and organic matter is 2.71g/cm^3 and 1.0 g/cm^3, respectively. The calculated bulk accumulation rate (mg/cm^2/ka) has been converted to sedimentation rate (cm/ka). Calculated whole rock density (0.9g/cm^3 – 2.4g/cm^3) is quite comparable to similar organic-rich sediments of up to 2.25g/cm^3 (Minster, 2009; Caplan and Bustin, 1996). Estimations about thickness and time duration of the OSM are from (Ashckenazi-Polivoda et al., 2011). For the calculation of sediment density, a high estimate for sediment porosity (10%) is used. Calculation was only done for the OSM, simply because solely for this part of the profile an estimation of duration exists. The rough estimate shows a moderate increasing trend up-section from 1.4 cm/ka to 3.81 cm/ka (mean 2.85 cm/ka), with a standard deviation of ± 0.5 cm/ka (shaded area). Lowest sedimentation rate

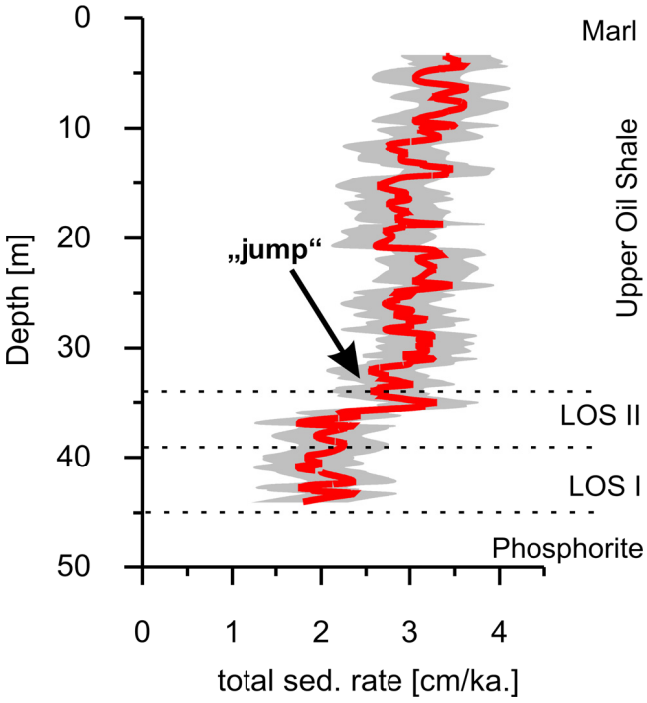

Fig.85 shows a rough estimation of the sedimentation rate along the profile by using algorithm from (Davis et al. 1999). Gray shaded area represents the calculated standard deviation

is observed at the basal part in the OSM. From the base (44.2 mbsf - 34 mbsf), an almost constant increasing trend is observable. A drastic rise by about 1.3 cm/ka is observed around 34 mbsf. This "jump" marks the transition from the Lower Oil Shale to the overlying parts of the OSM.

Discussion

It seems that below the base of the OSM, the terrigenic input starts at ~1 cm/ ka. Due to this extraordinarily low sedimentation rate, a condensed interval was formed. Such intervals are commonly interpreted in terms of a decrease in accumulation rate, as well as a mixture of fossil assemblages (Gómez and Fernández-López, 1994). The exact meaning of a low sedimentation rate is not univocally defined (Baraboshkin, 2009). Referring to the Mesozoic black shale deposition, for example Einsele, (2000) noted that their deposition in continental basins took place under a transgression cycle, with sedimentation rates varying between 0.5 – 10 cm/ ka. This would mean that the accumulation of organic matter within the oil shales of the Ghareb fm. is a consequence of the sedimentation in a condensed section! Another reason for the low sedimentation rate is that marine transgression and regression cycles, from the Senonian to the Eocene time, took place along a shoreline that was 600-1000 km to the south of the present day shoreline (Garfunkel, 1989; Garfunkel, 1988). This notion is confirmed by (Almogi-Labin et al., 2012). The authors emphasise that the Upper Tethyan upwelling belt covers a palaeo slope with a range of about 250 km. Such a huge shelf area, which is much wider than recent continental slopes (section 2.2.), would explain the low terrigenous input and the extraordinarily low sedimentation rate in the basin (Shoval, 2004b). Moreover, it cannot be excluded that parts of the terrigenic sediment inputs, which contribute to the deposition in the basins, are recycled sediments from the continental margin (Inthorn et al. 2006).

Terrigenic (clastic) vs. carbonatic (biogenic) sedimentation

The biogenic sediment (carbonate skeletal and opaline silica) can be of autochthone origin because of bioproductivity in the surface water. Therefore, a high surface productivity (preferred foraminiferal assemblages) leads to biogenic carbonate sedimentation. Unlike terrigenic (clastic) sedimentation, the

carbonate sedimentation pattern shows a more or less constant deposition (fig. 86), which may suggest that the bioproductivity was not changing. At the same time, the organic matter content shows a decreasing trend. The sedimentation rate of clastic sediments is mainly controlled by two factors:

(1) distance of the source area and (2) characteristics of the source area. The distances to the deposition area are decisive for the specifics of the terrigenic (clay vs. heavy mineral) input. The large distance from the source area may be one reason for the extraordinarily low terrigenic input (Einsele, 2000). From the fig.s 86a-c, some conclusions can be drawn.

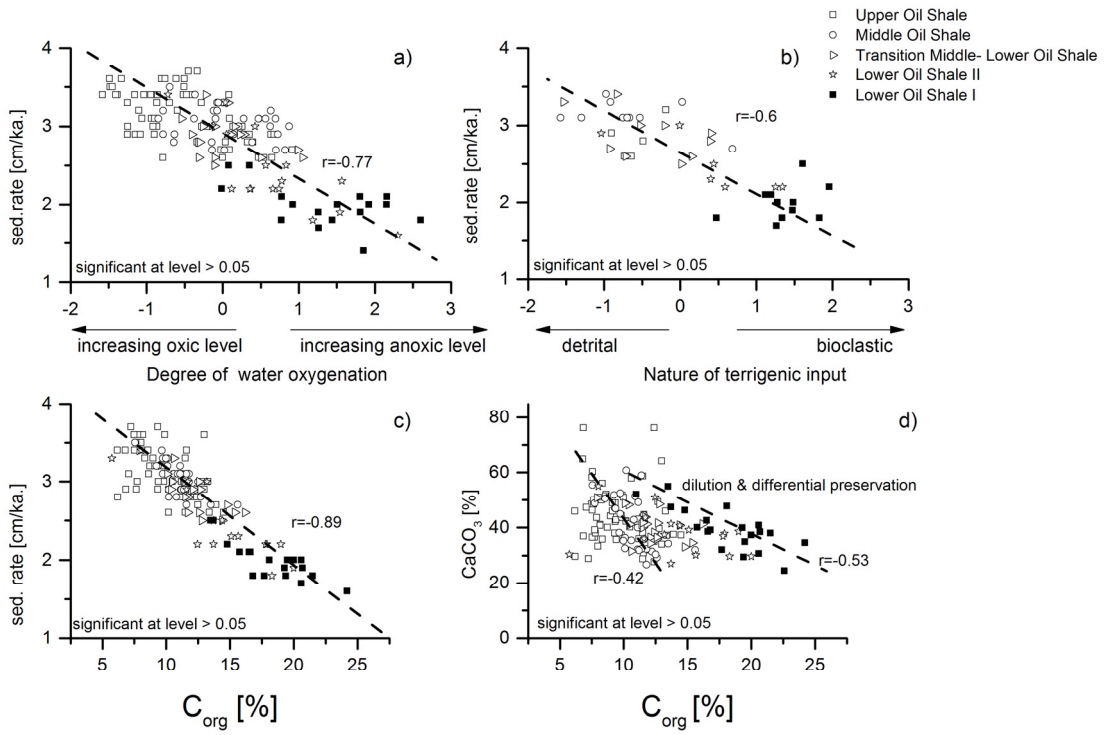

*Fig.86 Different correlations between degree of water oxygenation and sedimentation rate **a)**, the nature of terrigenic input vs. sedimentation.rate **b)**, C_{org} vs. sedimentation .rate **c)** and C_{org} vs. carbonate content **d)***

In fact, as shown in fig. 87 page 176, the carbonate sedimentation contributes about 50% of the total sedimentation rate in basal sequences of the OSM. In contrast, the terrigenic input contributes only 25% of the total sedimentation rate. The observed negative correlation (r=-0.6, N=220, fig. 86b) of the biogenic (carbonate) sedimentation is only caused due to changes in the composition and the amount of terrigenic

input. This is known as dilution effect, the dominant control in the accumulation of organic matter in an anoxic environment (Tyson, 1991; Stein, 1990), (fig. 86a,c). Normally, a positive correlation between the C_{org} sedimentation and sedimentation rate is observed in oxic environments. It seems like an inverse or lack of correlation in association with low sedimentation rates is very common in anoxic environments, which, inter alia, has been reported from sediments in the Black Sea, slowly subsiding platforms, and condensed sections (Einsele, 2000; Tyson, 1991; Stein, 1986; Bralower and Thierstein, 1984). Due to the extraordinarily low terrigenic input at the base of the OSM, the organic matter content is more affected by a low dilution effect, simultaneously increasing sulphurisation of the organic matter (Kolonic et al., 2002). However, with decreasing depth the dilution effect increases, and vice versa. This outcome is further corroborated by calculated enrichment factors, which is shown in the previous section. Moreover, the environmental conditions change to more oxic with a high dilution effect in an up-section direction (fig. 86a).

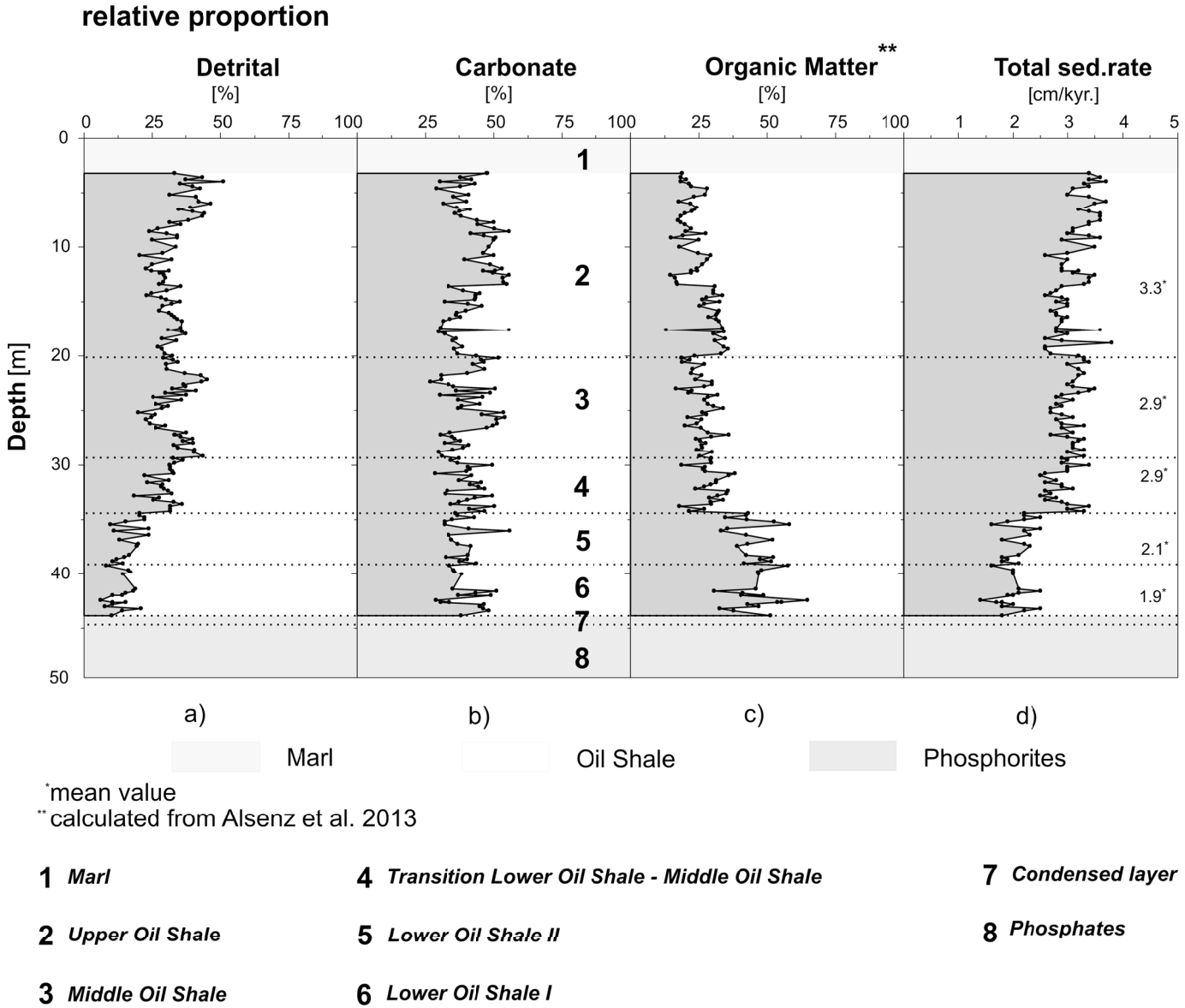

Fig.87 shows the relative contribution to the whole sedimentary record in the oil shale section) ***a)*** *calc. detrital input* ***b)*** *carbonate sedimentation* ***c)*** *organic matter, and* ***d)*** *total sedimentation rate(numbers indicate the calculated mean total sed. Rate)*

Primary bioproductivity

($\delta^{13}C_{carbonate}$,$\delta^{13}C_{org}$)

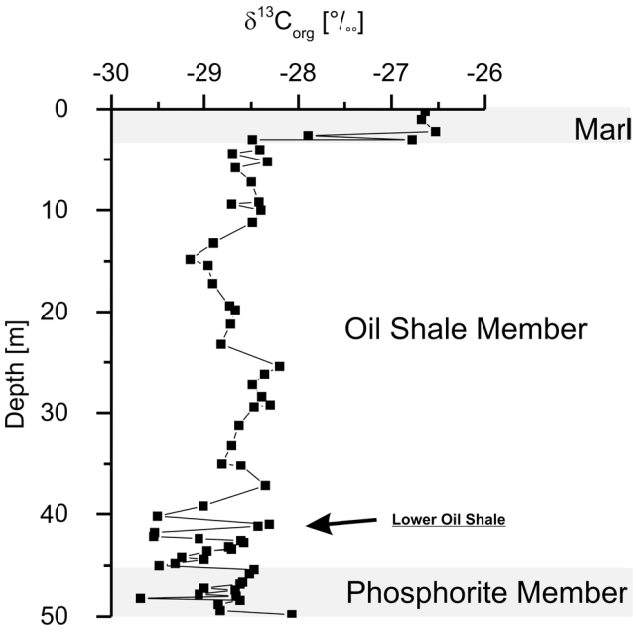

Fig.88 $\delta^{13}C_{org}$ values along the profile

Own values of $\delta^{13}C_{org}$ indicating in fig. 88 four trends along the profile:

(1) a drop in $\delta^{13}C_{org}$ values at the PM to the OSM, (2) strong alternating light values at the base of the oil shale, followed by a sharp increase around 40 mbsf, (3) during the remaining oil shale section an almost constant trend is occurring, (4) around 5 mbsf, a sharp increasing trend to heavier values is indicated. Such trends can be interpreted in following ways: variation of palaeoproductivity (primary productivity); decomposition of organic matter, and change in the taxonomic composition of organic matter (phytoplankton).

Similar values are reported from the Black Sea by (Lein and Ivanov, 1991) (-26 to -25‰), unlike to (Strizhov et al. 1989) who report significant lighter values that ranges from -32‰ to -27‰. From the Kimmeridge Clay Formation (KCF), (van Kaam-Peters et al. 1998) show $\delta^{13}C_{org}$- values that range from -27‰ to -21‰. Such light$^{13}C_{org}$- values as indicated from the KCF are explained by the deposition in a basin under alternating euxinic conditions, with water mass restriction (Miller, 1988, Oschmann, 1988). Indeed, our values confirm the widely held view, that all marine organic matter was isotopically light (-29 to -25‰) in the Cretaceous time as proposed by (Tyson, 1991; Dean et al. 1986).

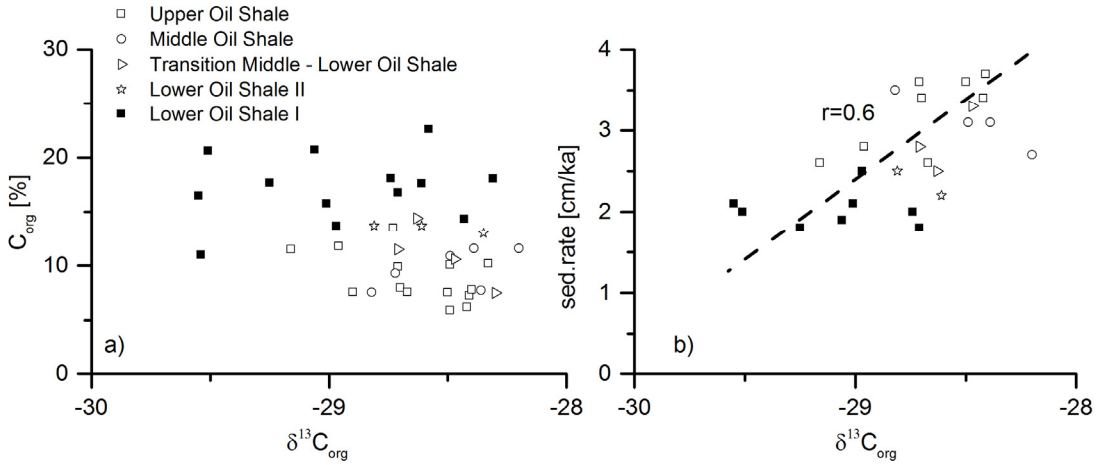

Fig.89 Left side shows the non-correlation between C_{org} and $\delta^{13}C_{org}$ ***a)****, right side represents the statistically significant correlation between sedimentation rate and $\delta^{13}C_{org}$* ***b)***

Moreover, own isotopically light $\delta^{13}C_{org}$ values could support the scenario, that is outlined by (van Kaam-Peters et al. 1998), which is known from the Kimmeridge Clay Formation. This issue will be further discussed in section 6.3.

A shift of 2-3‰ in $\delta^{13}C_{org}$ values can also be explained by a relatively fast accumulation in the Campanian - Maastrichtian time, under restricted anoxic - sulphidic conditions (Hertelendi and Vetö, 1991, Hayes et al. 1989, Dean and Arthur, 1987). However, as shown in fig. 89a, the interpretation of C_{org} as a proxy for primary productivity should mirror a positive correlation between the enhanced primary productivity and organic matter accumulation (C_{org}). This is not fully supported by own data. Based on the the interpretation of Tyson, (1991) and references therein, a non-correlation between these two factors is significant in overlying oil shales. According to Tyson, (1991), it is thought that such lack or non-correlation between C_{org} and $\delta^{13}C_{org}$ could be explained by (1) variation in the terrestrial - marine organic matter ratio, and (2) by differences in the redox conditions. As mentioned previously, the exact circumstances, achieved by the application of the U/ P_2O_5 as proxy for oxygenation state, precisely match the evolving Upper Oil Shale horizon.

Iron-Sulphur-Carbon Systematics (Fe-S-C)

As mentioned in section 4.2., knowledge about the amount of iron that is able to form pyrite is important for encrypting the sedimentary conditions at the time of sedimentation. One of the most studied examples of anoxic or euxinic sedimentary environments is the Black Sea. This area is well suited for distinguishing between the different stages of oxygen-deficit in the sediment. Calvert and Karlin (1991) presented DOP values in sediments from the Black Sea (Unit I) and concluded that pyrite was formed within the water column under Fe-limited conditions. In fact, as shown below in fig. 90, the sediment can be clearly distinguished by their DOP values.

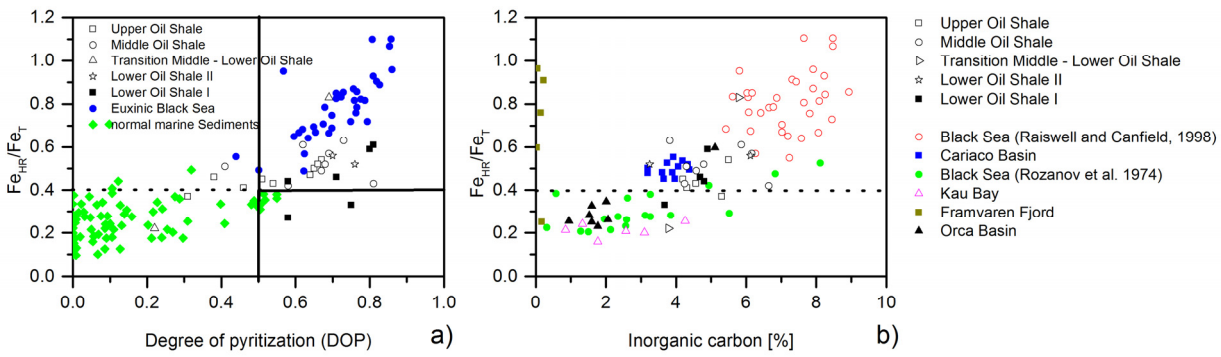

Fig.90 ***a)*** *Plot displaying the ratio of highly reactive iron to the amount of total iron, plotted against the degree of pyritization (DOP)* ***b)****: Diagramm shows the ratio of highly reactive iron to the amount of total iron (Fe_{HR}/Fe_T) in relation to the inorganic carbon, for a detailed explanation see text below. Graphs are modified after Raiswell and Canfield, (2012) and Shen et al. (2002).*

As we can see in fig. 90, on right side a scatter plot of Fe_{HR}/Fe_T versus inorganic carbon reveals a high inorganic content associated with a large contribution of biogenous compounds to the sediment (Raiswell and Canfield, 2012, 1998, 1996). In sediments from the Black Sea, the author determined the ratio of Fe_{HR}/Fe_T >0.4, suggesting an enrichment of highly reactive iron, which is associated with the carbonate coming from coccolithophorida (*Emiliana huxleyi spp*), as one of the major carbonate contributors to the sediment. Based on the high correlation coefficient between Fe_{HR} and carbonate, it has been inferred that

highly reactive iron was scavenged on the surface of these shells and subsequently transported down to the bottom (Raiswell and Canfield, 1998). As mentioned previously, in section 2.2., upwelling areas are mainly determined by the accumulation of different types of biogenic organisms - coccolithophorida, planktic foraminifera and diatoms (Schiebel et al. 2004; Giraudeau et al. 2000), depending on the supply of nutrients. Therefore, the same mechanism, as mentioned by Raiswell and Canfield, (1998), may be responsible for a likely correlation between Fe_{HR}/Fe_T and inorganic carbon, which stands for a possible link between the occurrence of biogenic carbonate and highly reactive iron.

Unfortunately, own results do not fully support these observations. These arise mainly from an observed non–correlation between Fe_{HR} and the carbonate content. This is largely due to changes in the Fe_{HR} content during diagenesis, which alters the Fe_{HR}/Fe_T. Subsequently, this leads to an increase in the reactive iron content and concomitantly to a lowering in Fe_T- content. Furthermore, own results within this study indicate that Fe_{HR}/Fe_T values of samples from the Ghareb fm. plotted versus the inorganic carbon (and DOP) fall in the Black Sea field (fig. 90). Therefore, the supply of highly reactive iron might have taken place under similar condition as in Black Sea or the Cariaco Basin.

Fig. 91 shows a comparison between the degree of pyritisation in different locations, including the Peru margin, Namibian margin, Black Sea, and Cariaco basin, which are all exposed to highly anoxic conditions, including the results obtained by this study. Own data can be divided into two parts, on the one hand, coming from samples that are highly affected by oxidative alteration (Upper Oil Shale horizon), and on the other hand - LOS II with only slight alteration effects. Based on Black Sea data, (Lyons and Severmann, (2006), Anderson and Raiswell, (2004), Lyons and Severmann, (2006) and Raiswell et al. (1988) have introduced a DOP threshold of ~ 0.8 to define euxinic conditions. This value is based on di-thionate soluble iron ($F_{HR} = Fe_D + Fe_{py}$) and allows the distinction between euxinic/anoxic and normal marine (oxic) conditions.

Surprisingly, own results are comparable with results from modern analogues. As previously mentioned, obtained outcomes by this study suggest a strong late diagenetic overprint, which has led to a misleading Fe_{py}/Fe_{HR} relationship. Therefore, the DOP should not match a true deposition scenario.

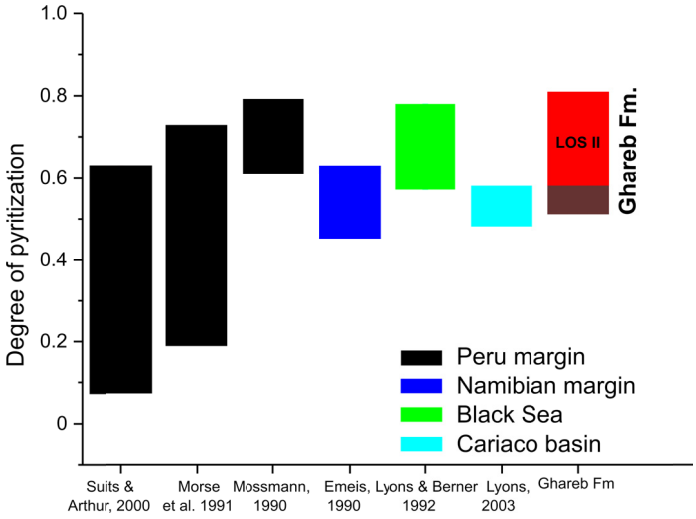

Fig.91 DOP values obtained from different authors in distinct highly reducing marine environments in comparison to results of this study (red and brown coloured bar. The X-axis displays different references that are taken from the literature.

For the Peruvian upwelling margin, Mossmann et al. (1990) noted that the supply of reactive iron is too low for a complete pyritisation (Fig. 91). These results are partly in agreement with Suits and Arthur, (2000), who reported in sediments from the Peruivian margin also a high pyrite content and a DOP of 0.12 to 0.6, and concluded that a high availability of reactive iron is responsible for the DOP values. Regarding the DOP values in recent basins, Canfield et al. (1996) reported values from the Black Sea that range from 0.2 – 0.78 (fig. 91). The highest values are preferably in the centre of the basin, where the maximum in euxinic conditions occurs. However, this value is explained by the rapid sulphurisation of the Fe^{2+} in the upper water column, and concomitantly due to its scavenging by settling biogenic fabrics. The sulphide diffuses into the ambient water where the pyrite is formed. This is in agreement with similar observations in the Cariaco basin (Lyons et al., 2003a).

Summing up these notions, own values indicate predominantly euxinic conditions in the Lower Oil Shale unit II in spite of being affected by diagenesis, and DOP values of 0.58 to 0.89 indicate an iron limited system, in agreement with the observation of Raiswell and Canfield, (2012), and (Canfield et al. 1996). The extraordinarily low terrigenic input of total iron (Fe_t ~ 0.5 % wt.) in the Lower Oil Shale, leads to the exhaustion of the entire reactive iron pool and subsequently to the sulphurisation of organic carbon by the

remaining H_2S, and to the formation of sulphur-rich kerogen. However, such a high DOP would imply that pyrite is formed in both the water column and the sediment pore water (Berner, 1984), which is not reasonable for the Ghareb Formation as indicated by the occurrence of benthic foraminifera.

Sulphur Isotopes

$\delta^{34}S_{pyrite\ (CRS)}$

The timing of pyrite formation and subsequent sulphurisation of organic matter depends on the availability of reactive iron species (e.g. oxyhydroxides and iron oxides) and the existence of organic matter (Berner and Raiswell, 1984; Leventhal, 1987). Pyrite can form in the water column (syngenetic pyrite) or in the sediment (diagenetic pyrite). Syngenetically formed pyrite is isotopically lighter in comparison with diagenetic pyrite, because of the large reservoir of dissolved sulphate in the water column (e.g., open system) (Calvert et al. 1996).

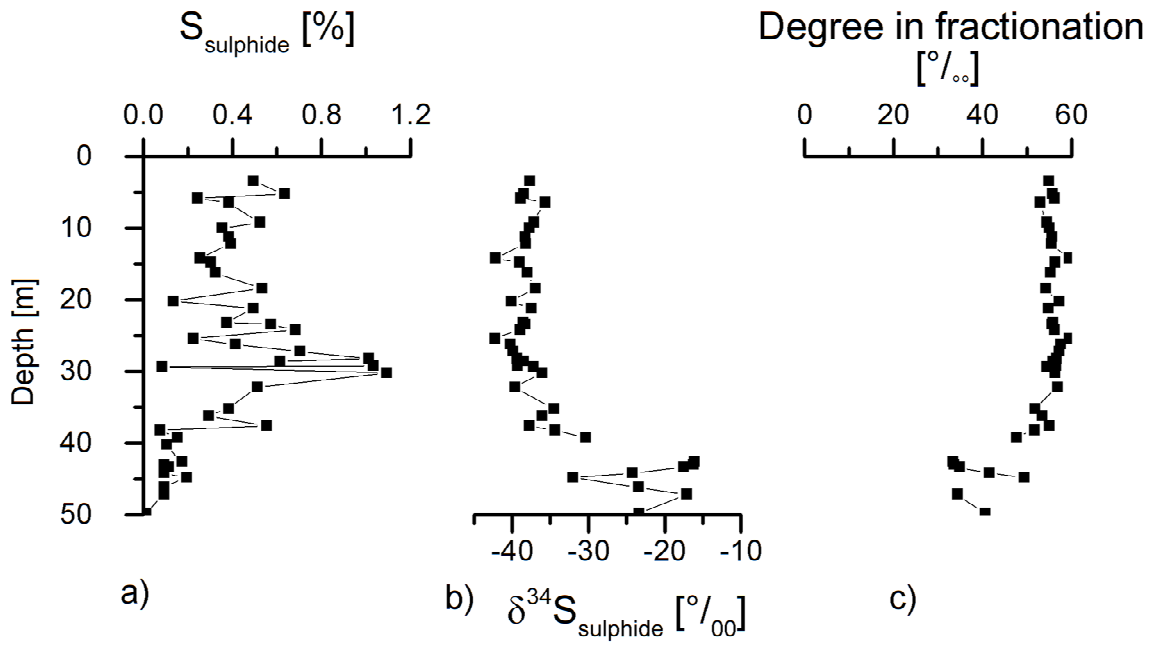

*Fig.92 display the sulphide content (wt. %) **a)**, isotopic composition of $\delta^{34}S_{sulphide}$ **b)**, and the degree of fractionation $\Delta\delta^{34}S\ S_{sulphate} - S_{sulphide}$ **c)**, alongside the profile. Note the columns **b)** and **c)** are expressed in unit [‰].*

A mass balance of diagenetically and syngenetically formed pyrite in the Cariaco Basin (Werne et al. 2003) could show that the majority of the pyrite is formed in the water column. Normally, the isotopic composition of syngenetic pyrite is -32‰ (Fry et al. 1991; Werne et al., 2003). In course of this study, results for $\delta^{34}S_{pyrite}$, shown in fig. 92, display a trend to progressive enrichment in lighter values (30‰ to -42‰) in the up-section direction. For example, at the base of the Phosphate Member a value of -24.33‰ (depth 49.4 mbsf) can be measured, implying an isotopic composition of about +17‰ for seawater sulphate in the Upper Cretaceous time (Sweeney and Kaplan, 1980; Strauss, 1999). For the near bottom water at the continental shelf, this corresponds to an apparent isotopic fractionation of about 41‰. This might indicate a more open system and formation of pyrites, which are preferably formed in the water columns (syngenetic pyrite).

This high fractionation factor indicates high sulphate reducing conditions and open systems resulting in an strong enrichment of light isotopic values (-24.33‰). This condition changed in the sediments at the depth 46.8m. At this depth is a trend visible to heavier values for $\delta^{34}S_{pyrite}$ (-17.21‰), consequently lower fractionation rates of about 36‰. Lower degree of fractionation and a trend to heavier values; indicate possibly a semi-closed system. Higher deposition rates can also induce a (semi) closed system (Wijsman et al., 2001). Finally, this is supported by slightly higher sedimentation rate (sample OSP006, OSP013), this covers the sediment and restrict a circulation of sulphate in the near bottom sediment. Through decreasing depth (up-section) with small turnovers in the degree of fractionation legitimate an assumption about continuous sulphate supply and indicating small fluctuations in the bottom water aeration.

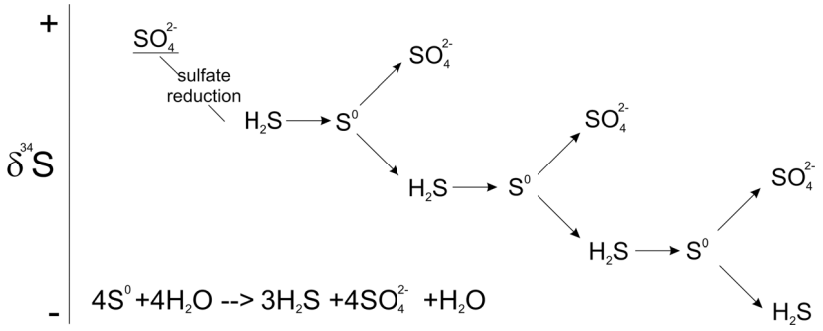

Fig.93 Representative scheme of the development of the S isotopic fractionation of dissolved sulphate and sulphide in terms of repeated disproportionation cycle, modified after Canfield and Thamdrup, (1994).

However, the observed differences in the isotopic composition of pyrite in OSM, relative to the isotope composition of Upper-Cretaceous seawater sulphate of about +17‰ Strauss, (1999), is huge (up to 60‰) and can be explained by a repeated partial re-oxidation of the produced H_2S, followed by disproportionation of the resulted sulphur compounds with intermediate oxidation state such as elemental sulphur, thiosulphate, and sulphite (see fig. 93) (Böttcher and Thamdrup, 2001; Habicht and Canfield, 1997; Canfield and Thamdrup, 1994). However, such a mechanism implies the diffusion of the produced H_2S into the oxic part of the sediment or into the oxic/dysoxic water column, where the disproportionation of oxidised sulphur compounds occurs. Moreover, both field and laboratory observations indicate that euhedral pyrite may precipitate directly from pore waters oversaturated with respect to pyrite (but not with respect to Fe-monosulphides; (Taylor and Macquaker, 2011) and references therein). Framboidal pyrite (as frequently observed in the OSM), does not form directly, but via a metastable precursory Fe-sulphide phase (‘amorphous’ FeS, mackinawite and greigite) of iron-dominated pore-waters, where sulphide production rates are locally high enough to reach supersaturation, with respect to FeS (Taylor and Macquaker, 2011; Rickard and Luther, 2007; Schoonen and Barnes, 1991; Morse et al. 1987).

The transformation of FeS to pyrite is controlled by the availability of an oxidant to produce sulphur species with intermediate oxidation states (Neumann et al. 2005; Schoonen and Barnes, 1991b). In anoxic sediments, beneath oxic or dysoxic bottom waters, such conditions occur close to the sediment/water interface, where not only the downwards diffusion of sulphate, but also that of oxidants required for pyrite growth, are facilitated by bioturbation or resuspension. The moderate fluctuation of the $\delta^{34}S$ values along the section is interpreted to reflect slight changes in the reactivity of organic matter. Which, by controlling the kinetics of sulphate reduction, indirectly has an influence on the degree of isotopic fractionation. Alternatively, slight oscillations in redox or in sedimentation rate may also be considered as potential factors in the production of variations in the isotopic composition of sulphur, by controlling the diffusion of sulphate and/or oxidants.

In summation, the sulphur isotope data suggests that the deposition of the OSM was triggered by the massive accumulation of organic matter, which led to the development of a thin layer of euxinic bottom water during the deposition of the LOS. However, micropalaeontological analysis carried out by the Israeli partner does not fully support this. Within this time slice, their results indicate a fast radiation and adoption of benthic foraminiferal assemblages; whicht might support newer observations in that benthic foraminifera are able to survive highly anoxic conditions (Bernhard et al., 2012). Moreover, the depositional system evolved progressively toward more and more aerated conditions, with dominantly dysoxic bottom waters, culminating in the installation of normal marine conditions at the boundary to the MM of the Ghareb fm. Due to the abundant input of organic matter and the continuous diffusion of sulphate from the seawater pool, the formation of pyrite in the LOS was limited virtually only by the amount of reactive iron, but in the higher levels of the studied section also by the availability of an oxidant to produce sulphur species with intermediate oxidation states. Excess H_2S, the amount of which was controlled by the sulphate diffused from above into the interstitial space of the sediment, was consumed for the sulphurisation of organic matter. At later stages, probably concomitantly with exhumation, ca. 1/3 to 2/3 of the pyrite was oxidised to sulphate.

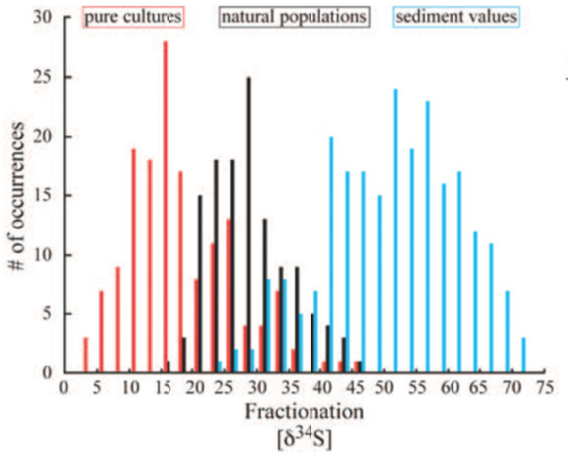

Fig.94 Range of isotope fractionations in pure cultures of sulphate reducers (red) natural populations (black) and marine sediments from (Johnston, 2010), originally in (Canfield, 2001a, Habicht and Canfield, 1997)

Another way to explain this high fractionation factors and light isotopic composition is the effect through microbial disproportion of S^0, $S_2O_3^{2-}$, and SO_3^{2-}.

As shown in fig. 94, there is a discrepancy between the degree of fractionation observed in natural, cultured and marine sediment populations. Some sediments, for example Cabo Frio, South-eastern Brazil (Diaz et al. 2012), Cariaco Basin (Lyons et al. 2003a;

Werne et al. 2003; Fry et al. 1991), Japan Sea ODP-Site 127-795 (Masuzawa et al. 1992), show a higher degree in fractionation than in cultured population. Most of them can be explained by the "classical way" in accordance with (Jørgensen, 1990) and references therein. Another possible explanation shows fig. 94, which display a higher degree in fractionation in sedimentary environments. Significant degrees of fractionation in $\delta^{34}S$, of up to 70‰, were observed in modern and in ancient sediment from the lake Lago di Cadagno in the Swiss Alps (Canfield et al. 2010), in hypersulphidic interstitial water (Wortmann et al. 2001), in hypersulphidic pore water in the Cariaco Basin, (Werne et al. 2003) and in the Cascadia Basin, ODP Leg 168 (Rudnicki et al. 2001), respectively. To draw conclusions about the degree in fractionation (Sim et al., 2011), isolated sulphate-reducing d-proteobacterium [*Desulfovibrio sp*., (DMSS-1)] from marine coastal sediments from Cape Cod, Massachusetts, and show that a pure actively growing culture of *Desulfovibrio sp*. can deplete $\delta^{34}S$ by up to 66‰ during sulphate reduction alone, and in the absence of any extracellular oxidative sulphur cycle. The isolated bacterium, DMSS-1, reduces sulphate to sulphide using various organic compounds or hydrogen as electron donors, ferments glucose, and by disproportionation of thiosulphates (Sim et al. 2011). Is it possible that the deposition of organic-rich carbonate took place in a hypersulphidic environment? In course of this study, results are in strong contrast to results from experiments with cultured bacteria, which show a smaller degree in fractionation between produced sulphides and the residual sulphate!

$\delta^{34}S_{organic\ sulphur}$ (intramolecular - sulphur)

As mentioned in the chapter "material and methods", there are different types of organic sulphur in the studied sediments. The isotopic composition of this organically bonded sulphur (intramolecular-sulphur) is shown in fig. 95. According to Werne et al. (2008) and references therein, there are two pathways by which OS can be formed. These include the active uptake of sulphate into the cell and its subsequent reduction. This sulphur termed as "biogenic" sulphur represents only ~10 - 25% of the sedimentary organic sulphur (Werne et al., 2003).

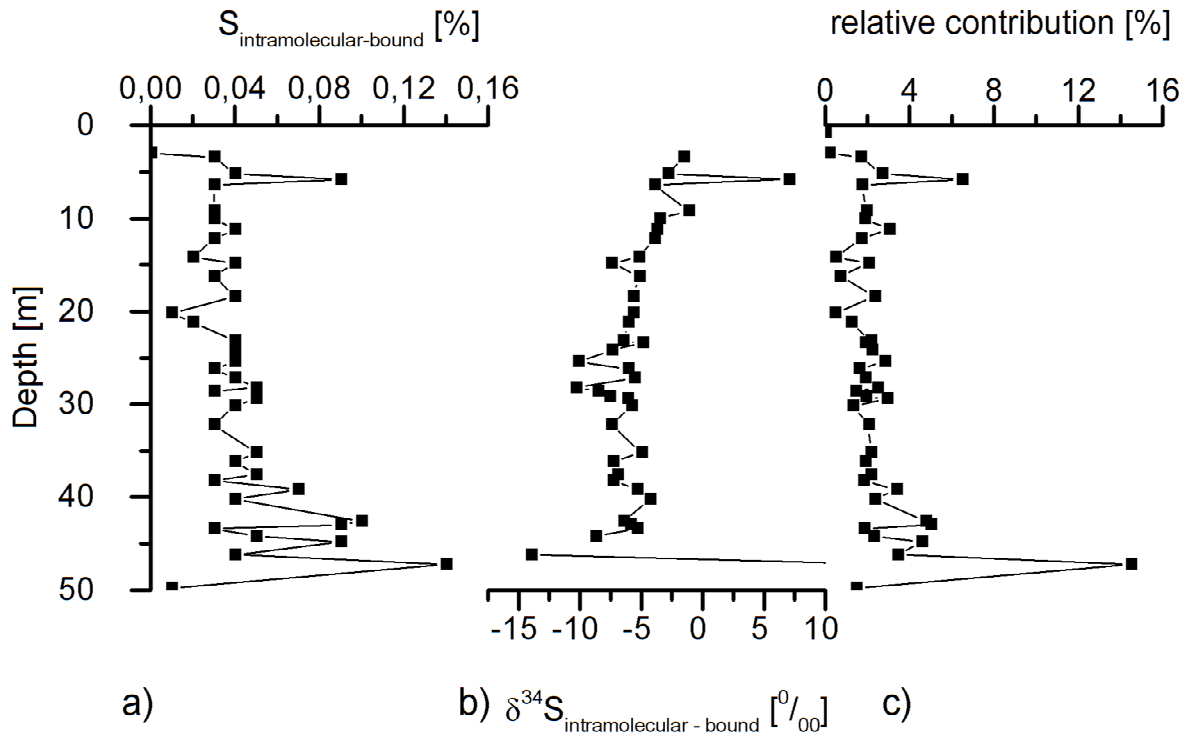

Fig.95 This graph shows absolute content of $S_{intramolecular}$ in [%] ***a)****, the isotopic of $\delta^{34}S_{intramolecular}$ values in [‰]* ***b)*** *and the poor contribution of intramoleculary bonded sulphur to the bulk sediment in [rel. %]* ***c)****, that are briefly explained below.*

The low concentration in intramolecular (ester)-bonded sulphur is mostly explained by its lability in stages of late diagenesis, compared to other forms of organic matter (Werne et al., 2003). The other possibility requires the incorporation of reduced forms of sulphur from the pore water into the organic matter by bacterial activity, either directly or via intermediates, and its subsequent incorporation into the organic matter. In this section, the focus is set on the ester-bonded sulphur, which is commonly incorporated in bacteriohopanoids and is linked to polysulphides as intramolecular S (de Leeuw and Sinninghe Damsté, 1990). These kinds of organic sulphur observed in the Thode-fraction, is found by the sequential-extraction scheme according to (Mayer and Krouse, 2004). Secondly, it is found that this intramolecular sulphur contributes only 1-14.5 % to the total sulphur (mean 2.4%, N=44), throughout the profile, with two exceptions (OSP001, depth 47.2 mbsf and SAOS 018, depth 5.8 mbsf), there are no significant deviation from the mean. The extraordinary low contribution to the complete sulphurized organic matter might support the assumption of Werne et al. (2003), and Wakeham et al. (1995) that is explained by the

very labile character of this sulphur compound during late diagenesis. To identify which fraction we obtained from the wet chemical sulphur extraction, it is helpful to draw a cross-plot between distinct organically bond sulphur and TOC. This pattern may typical for sulphur that is bond neither to lipids (e.g. proteins) nor to the kerogen. It has been suggested by Francois, (1987) on basis of results from Cuhel et al. (1981) that an organic sulphur /TOC relationship from 0.007 to 0.012 (as is shown in shaded area in fig. 96), is typical for marine bacterial strains of *Pseudomonas halodurans* and *Alteromonas luteoviolaceus*. Indeed, a comparison yields almost a slightly lower S_{org}/TOC relationship (median = 0.00385 ±0.0019; N=31).

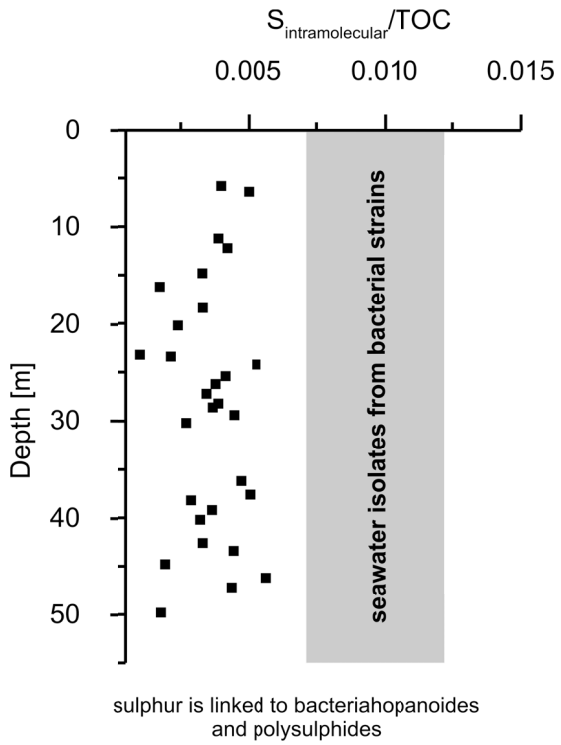

Fig.96 Comparison between the S_{org}/TOC ratio from a literature survey and own results.

This could be explained by two effects. Firstly, the sulphur is predominantly present in labile forms (i.e., proteins) and is highly sensitive to late diagenetic processes that lead to its (partial) removal (Anderson and Pratt, 1995, Wakeham et al. 1995). Secondly, with respect to its source, newer results indicate that polysulphides are the most likely form for organic matter incorporation (Werne et al., 2008). Cuhel et al. (1981), who could show that in bacterial strains most of the organic sulphur is derived from sulphate and thiosulphates. This may explain the differences between my results and those from (Cuhel et al., 1981). On the other hand, Werne et al. (2008) note that the source of biogenic sulphur that contributes to the organic matter is a mixture of distinct sources of organic sulphur.

However, results might support that a part of the organically bonded sulphur, which is obtained by so-called Thode-fraction, is intramolecular S, which is linked to a bacterial source. What does this mean for

the isotopic composition? Researchers seem to agree that the kinetics of sulphurisation are quite slow within about several hundred or thousand years (Kok et al. 2000; Werne et al., 2000). The presence of unreacted lipids in surface sediments from the Cariaco Basin suggest a slower sulphurisation of organic matter than originally proposed (Werne et al., 2000). From the kinetics, it is assumed that the sulphur which is incorporated into organic matter was formerly derived from the surrounding pore-water sulphide and shows no fractionation! In other words, the sulphur within the organic matter is similar to the isotope composition of pyrite isotopes ($\delta^{34}S_{H_2S}$).

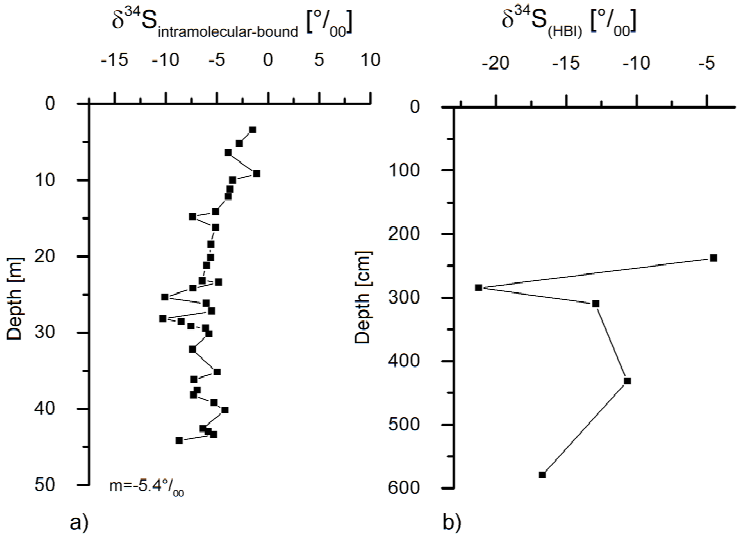

Fig.97 shows a comparison of $\delta^{34}S$ values with data from the Cariaco basin (Werne et al., 2008). Own data displays heavier values than that of the Cariaco Basin.

However, results obtained by this study do not fully support this observation. Unfortunately, isotope data from the organic sulphur isotopes (intramolecular bonded sulphur – Thode fraction) is still scarce. Only a few data sets are available, as shown in fig. 97, such as reference data from the Cariaco Basin (Werne et al., 2008). Results from this study plot in a smaller range than those from the Cariaco Basin (-15‰). Isotopically heavier values than previously reported by Werne et al. (2008), would signify that the degree of fractionation of SRB was not high. It is known that there are numerous factors which contribute to the extent of fractionation (sulphate reduction rate, sulphate concentration, organic matter oxidation pathway, and the species of sulphate reducing bacteria, sulphate reduction per cell, open vs. closed system) (Donahue et al., 2008; Brüchert, 2004; Canfield, 2001).

$\delta^{34}S_{organic\ sulphur}$ (intermolecular sulphur)

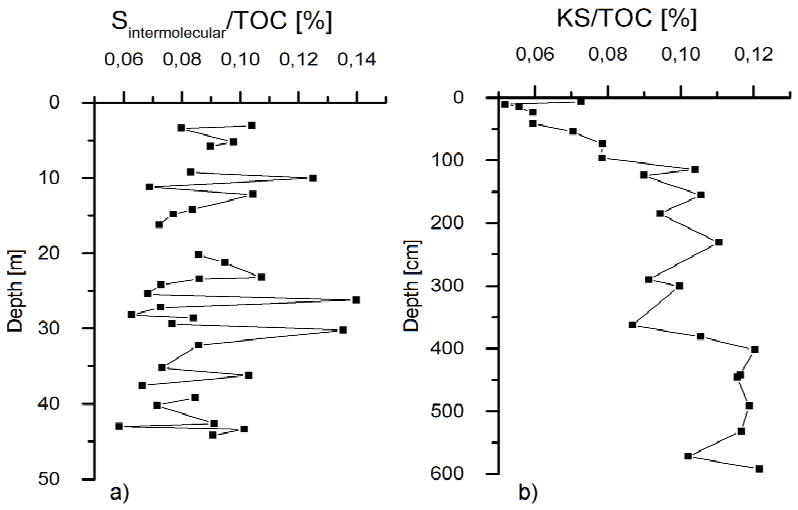

Fig.98 The relationship $S_{intermolecular}$/ TOC (own results) ***a)****, KS/TOC kerogen bonded sulphur (carbon bonded- KS) was compared with reference data from (Werne et al., 2003)* ***b)****.*

As is shown in fig. 98, the organic sulphur/ organic carbon ratio as determined by means of the wet chemical sulphur extraction method, corresponds well to the kerogen/ organic carbon ratio as previously reported by (Werne et al., 2003; Eglinton et al., 1994; Orr and Sinninghe Damsté, 1990). This supports, that the last fraction in the sequentially sulphur extraction scheme (organic sulphur by the Eschka- procedure), corresponds to the kerogen bond sulphur. There are some differences in the isotopic composition of the sulphurized organic matter pool. The bacterially bond organic sulphur show lighter values (m= -5.5‰ ± 0.5, N=36) than the kerogen bond sulphur do (m= -2.6‰ ± 0.25, N=42) (fig. 99 next page). Cross plot between these two organic sulphur compounds reveal a strong correlation, that suggest a coincident formation of both. The incorporation of reduced sulphur species into organic matter (OM) is generally assumed to have negligible $\delta^{34}S$ fractionation (Amrani and Aizenshtat, 2004). Experimental studies and field observations show that organic sulphur is enriched in $\delta^{34}S$ by up to 30‰ in relative to co-existing pyrite. In contrary to Amrani and Aizenshtat, (2004) own results display a huge difference (up to 45‰) between $\delta^{34}S_{pyrite}$ and OSM (-5 to +1‰).

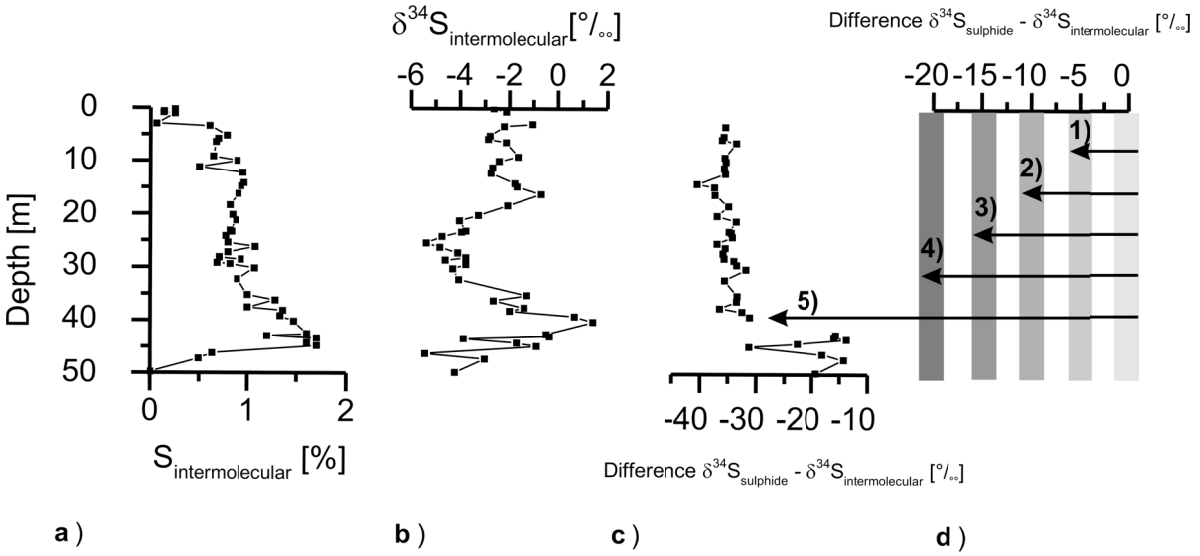

1) Amrani et al. 2005 (exp.) 2) Werne et al. 2003 (Cariaco Basin) 3) Anderson & Pratt, 1995

4) Amrani et al. 2005 (pyrolsyis exp.) 5) result from this study

*Fig.99 Results from wet chemical analysis and sulphur isotopes for organically bond sulphur. For comparison, figure display the absolute content of intermolecular bond sulphur **a)**, their isotopic composition **b)**, the calculated difference of the isotopic composition between the sulphide and intermolecular bond sulphur **c)**, as well as the calculated differences from the literature **d).** Numbers in bold (1-5) indicates the cited literature and own results.*

Results from C/N ratio and Pr/Ph relationship as well as $\delta^{15}N$ and $\delta^{13}C$ values suggest that marine algae are the main component that is preferably degraded (Schneider-Mor et al., 2012). The correlation of the organic reduced sulphur (ORS) and chrom – reducible sulphur – pyrite sulphur (CRS) $\delta^{34}S$-values is not further remarkable, because the H_2S involved in sulphurization of both organic matter (ORS) and reactive iron (CRS), was formed by the bacterially mediated reduction of sulphate of marine origin, which is an isotopically quite homogenous pool. A positive shift in the isotopic signature of the ORS, relative to CRS, was often observed in ancient or modern organic rich sediments Werne et al. (2003); but reported shifts are usually much lower than the differences of around 35‰ found in the OSM (fig. 99). The cause for the relatively heavy $\delta^{34}S$ values of the ORS is not straightforward, because the sulphurisation of organic matter is actually not accompanied by a substantial fractionation of the sulphur isotopes (Amrani and Aizenshtat, 2004; Raiswell et al., 1993).

In course of this study, this shift was interpreted to be primarily due to the difference in the time at which the sulphurisation of reactive iron and organic matter occurs. Because the pool of reactive iron is more susceptible for sulphurisation than the organic matter Raiswell and Canfield, (2012), authigenic Fe-sulphides will start to form in the sediment, practically simultaneously with the on-set of bacterial sulphate reduction. In contrast, relative to the formation of pyrite, the sulphurisation of organic matter started later, only after the pool of reactive iron in sediment was exhausted, possibly at a time when the interstitial volume, in which the bacterial sulphate reduction took place, became isolated from the water column above. This process is known from the installation of a chemocline, or a thin euxinic layer, leading to thermal water stratification, caused water mass restriction. Under such conditions, neither fresh supply of sulphate nor re-oxidation could occur, nor could the sulphate reduction evolve under closed system conditions. During the gradual enrichment of the residual sulphate in ^{34}S, isotopically relatively heavy H_2S was formed.

Magnesium content in foraminifera test`s as an indicator for palaeotemperature

In order to obtain some conclusion about the sea-surface temperature at time of deposition, an attempt was made to calculate the sea surface temperature (SST) and the bottom water temperature (BWT), by using the calcification temperature of planktic foraminifera and benthic foraminifera. Marine invertebrates, included in the foraminifera tests, are composed of either aragonite or calcite (Brand and Veizer, 1980). This includes the incorporation of Ca, Mg and Sr in their shells. According to Brand and Veizer, (1980), the content of magnesium is primarily a function of the CO_3-content and temperature in seawater. The inclusion of Mg in the calcite lattice, or rather its content in the foraminifera tests, is an exponential function of temperature, salinity and pH. Among these, temperature is by far the most important contributor (Lea, 1999; Mucci and Morse, 1983).

However, due to the low lattice compatibility, a part of Sr is lost during the diagenetic alteration and recrystallisation of calcite. Results from the foraminiferal factor analysis confirm this notion. As clearly shown in the bar plot from principal component analysis (PCA), results from the benthic foraminifera show a clear negative correlation between strontium and magnesium. In a Sr versus Mg cross plot (fig. 100), planktic and benthic species plot in distinct fields, with consequently higher values for *Heterohelix spp.* Although Sr contents were often found to correlate with Mg, (e.g. Carpenter and Lohmann, 1992), this association is considered to result from lattice distortions.

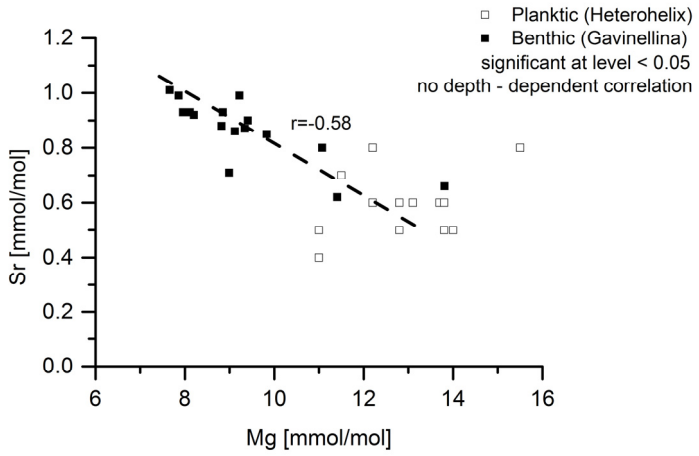

Fig.100 Cross plot of Mg vs Sr content [mmol/mol] in planktic and benthic foraminifera species.

Equation 18

$$\frac{Mg}{Ca}\left(\frac{mmol}{mol}\right) = Be^{AT} \quad \text{Eq. 18}$$

This in return, is caused by the substitution of Ca by Mg, which simultaneously allows the incorporation of increasing amounts of Sr (Mucci and Morse, 1983).

Nevertheless, due to the low lattice compatibility, primary in the planktic foraminifera due their as in comparison to the benthic foraminifera, thin shell body a part of Sr is lost during the diagenetic alteration and recrystallization of calcite.

In accordance with the thermodynamic considerations of Lea et al. (1999), Rosenthal et al. (1997), the Mg incorporation into biogenic calcite should be mainly controlled by the temperature. This prediction is consistent with experimental results from Mg incorporation into inorganic calcite; see also (Mucci, 1987, Mucci and Morse, 1983). Based on these theoretical and experimental works, an estimation about the calcification temperature in biogenic calcite is possible (see also fig. 101, and eq. 18). Many researchers used the magnesium content in both planktic and benthic foraminifera to draw conclusions about the sea-surface temperature (SST) (see for example (Bian and Martin, 2010; Creech et al. 2010; Hoogakker et al.

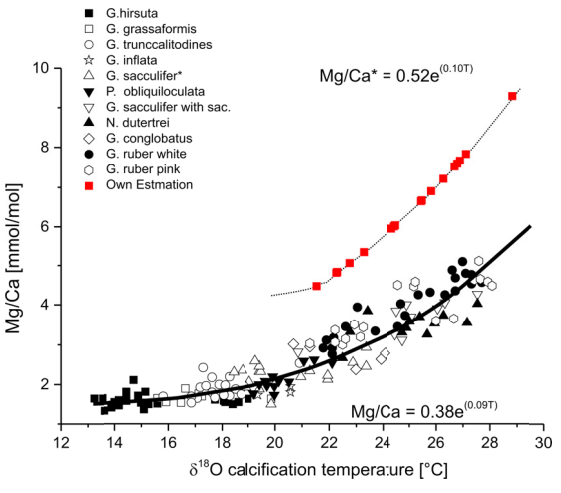

Fig.101 Foraminiferal temperature estimation based on Mg/Ca ratio in planktic foraminifera, modified graph is taken from (Anand et al. 2003)

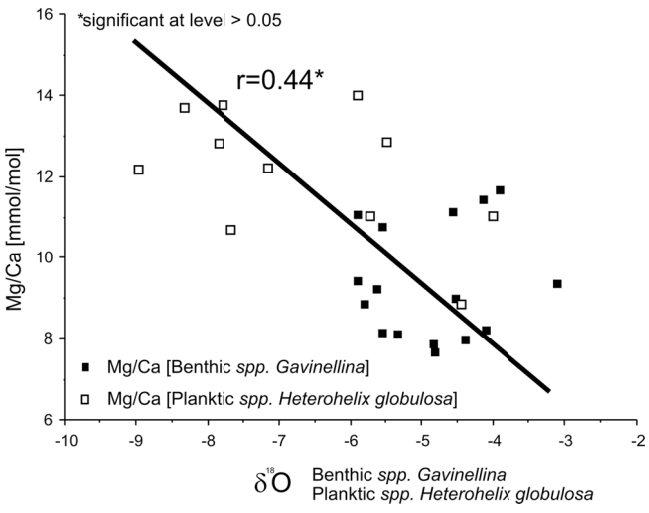

Fig.102 Significant correlation between oxygen isotopy in benthic & planktic foraminifera and Mg/Ca ratio

2009; Bryan and Marchitto, 2008; Cléroux et al. 2008; Kisakürek et al. 2008), and bottom-water temperature (BWT) (Allison et al. 2011; Fhlaithearta et al. 2010; Allison and Austin, 2008; Rosenthal et al. 2006; Billups and Schrag, 2002; Lear et al. 2002). In fig. 102 a cross plot show the correlation of $\delta^{18}O$ versus Mg/Ca content in both planktic and benthic species. On basis the statistically significant correlation between these two variables, this enables to use the Mg/Ca content as a proxy for the determination of the palaeo seawater temperature.

Nonetheless, as shown in fig. 101 and 103 by using the magnesium content it should be possible, to draw some conclusion about the palaeothermometry during this time slice. In eq. 18, the value of the pre-exponentially constants A and B depends on vital- and diagenetic effect. In this context, variation in surface and bottom seawater temperature along the section was calculated. By using the exponential relationship between the Mg/Ca ratio in *G. sacculifer* Anand et al. (2003) and *spp. Cibicoides* Lear et al. (2002), as established in culture experiments by Lea, (1999) and field research in the Saragasso sea – sediment traps (Anand et al. 2003), and core top analysis (Elderfield and Ganssen, 2000).

To calculate the magnesium calcification temperature the exponentially relationship was used between the temperature and $\delta^{18}O$ that is introduced by (Anand et al., 2003). As shown in eq. 18, the pre-exponential constant was used for *G. sacculifer*, where is B=0.52, A=0.10 (Elderfield and Ganssen, 2000). *G. sacculifer* calcified in an average surface temperature about 24-30°C. For the estimation of bottom-water temperature (BWT) the pre-exponential constant was used for benthic species *spp. Cibicoides* taken from (Lear et al., 2002). In this equation pre-exponential constants are B=0.867, A=0.109.

The surface seawater temperatures calculated from the planktic *Heterohelix spp.* ranges between 28° - 21.5°C, N=17 that are consistently higher than the values obtained from the Mg content of the benthic *Gavelinella spp*, and are in range from 24.0 and 18.3°C, respectively (fig.103). The calculated average surface water temperature during the deposition of the OSM is 25°C, which is more or less identical with the value assessed by TEX_{86} for the same section (Alsenz et al., 2013).

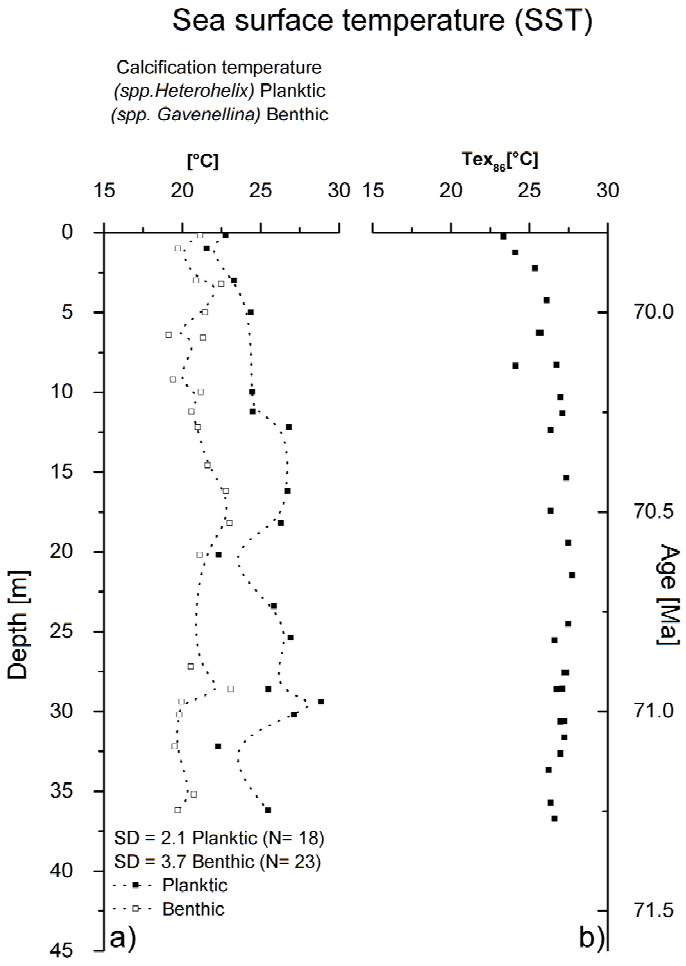

Fig.103 Own findings from SST and BWT reveal a temperature gradient of ~ 4.4°C ***a)****, in comparison to Alsenz et al. (2013)* ***b)*** *and the estimated Maastrichtian equatorial Pacific SST ~ 24° - 30°C by (Wilson and Opdyke, 1996).*

A similar correction for the benthic Mg/Ca- values yields an average bottom water temperature of 21°C, and a vertical temperature gradient between surface and bottom water of ~4°C. In the Late Cretaceous the palaeo-position of the Gondwana shoreline was between 8°-15°N (Totman Parrish and Curtis, 1982).

However, most probably, these values are overestimations due to traces of dolomite that were incorporated in tests either as micro particles during crystallization or by chemical exchange during early diagenesis. Nevertheless, although the presence of traces of dolomite was proved by XRD (fig. 104, next page) in both bulk rock and foraminifera, the assumption of an average amount of 0.7 wt. % dolomite is at best an approximation, only. Further, on the use of an equation established on basis of a planktic species for a benthic form is not rigorous, either. According to Cléroux et al. (2008) the contamination of pure calcite with 1 wt. % of dolomite, would increase the overall Mg/Ca ratio by 6 mmol/mol. After eliminating 5 outlier values and correcting the Mg/Ca ratios by assuming an average 0.7 wt. % of diagenetic dolomite. A similar correction for both benthic and planktic species yields an vertical temperature gradient between surface and bottom water of 4.4°C. Considering the setting of the depositional environment within the mixed layer, such a gradient is definitely realistic.

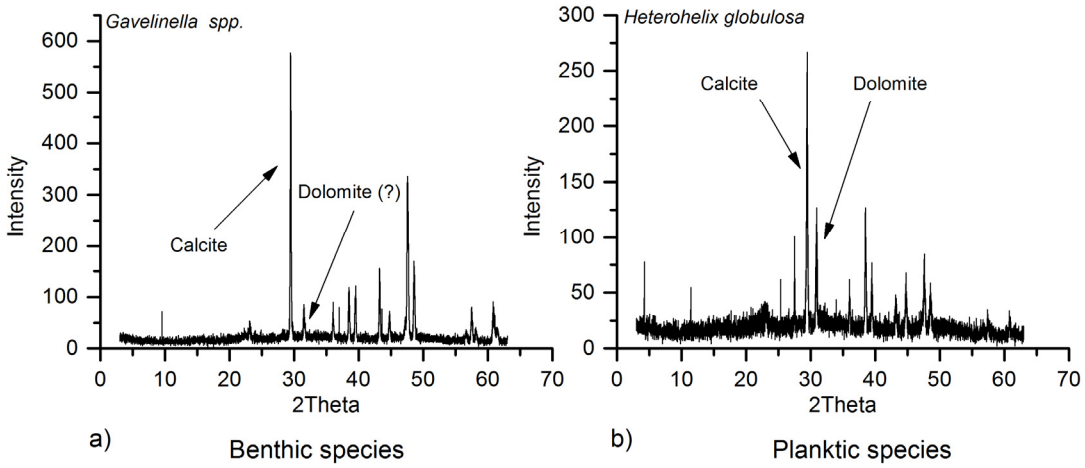

*Fig.104 XRD results from benthic **a)** and planktic **b)** species confirm the assumptions about the presence of dolomite contamination as a possible source of the erroneous determination of the palaeotemperature.*

However, even though the accuracy of these estimates is arguable, the temperature trend during the deposition of the OSM is similar to that established with TEX_{86}, and reflects real conditions with high probability. The water temperature was relatively low but increased during the deposition of the lower part of the OSM, to very gently decrease again afterwards, towards the top of the section.

Strontium calcium relationship as a proxy for sea-level changes

A promising proxy to identify sea-level changes is given by using the strontium concentration in marine sediments, as successfully demonstrated in Cretaceous, by (Stüben et al., 2003, 2002; Stoll and Schrag, 2001, Li et al., 2000; Stoll and Schrag, 1996). In comparison to modern times, vast shelf areas were flooded in the Cretaceous time. Carbonate sedimentation is a major sink for dissolved Sr in seawater (8 ppm). The concentration of Sr in calcite or aragonite depends on, and is changed with, the sea-level (Steuber and Veizer, 2002, Schlanger, 1988). In time of low sea level, exposed shelf areas have lost up to

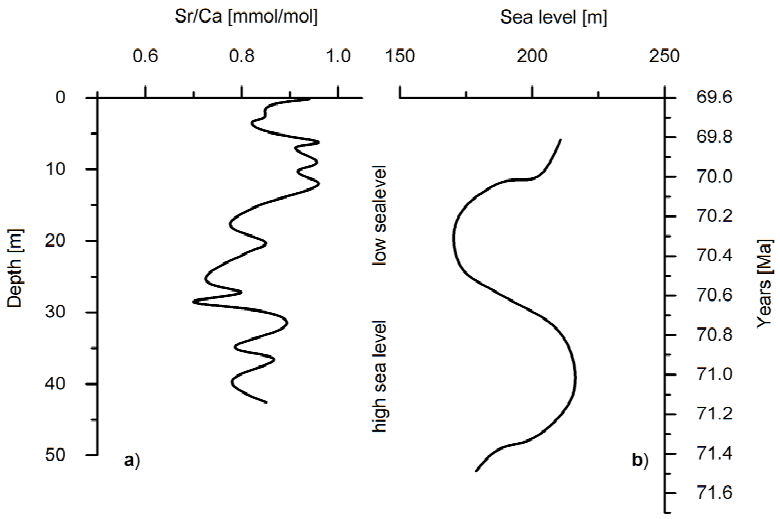

*Fig.105 is shown a similar trend in Sr/Ca ratio from benthic foraminifera (**Gavinellina spp**.) **a),** and changes in sea-level, which suggest the occurrence of two regression cycles in the research area **b)**. Reference data are taken from (Haq, 2014)*

90% of their Sr content in the sediment. When released into the ocean, this resulted in a higher Sr/Ca ratio (Stoll and Schrag, 1998, Steuber and Veizer, 2002).

As previously mentioned above, a serious problem may arise from the diagenetic alteration of biogenic bonded strontium, which leads to a preferred removal of Sr^{2+} from the foraminifera tests, and subsequently a release to the pore water (Brown and Elderfield, 1996). A shift in $\delta^{18}O$ to more depleted (negative) values, and decreasing strontium concentrations in foraminifera shells as well, indicates a higher diagenetic influence on the foraminifera test (fig. 105). However, a cross plot between $\delta^{18}O$ and Sr/Ca (*Gavinellina spp.*) reveals no significant correlation that might indicate a strong

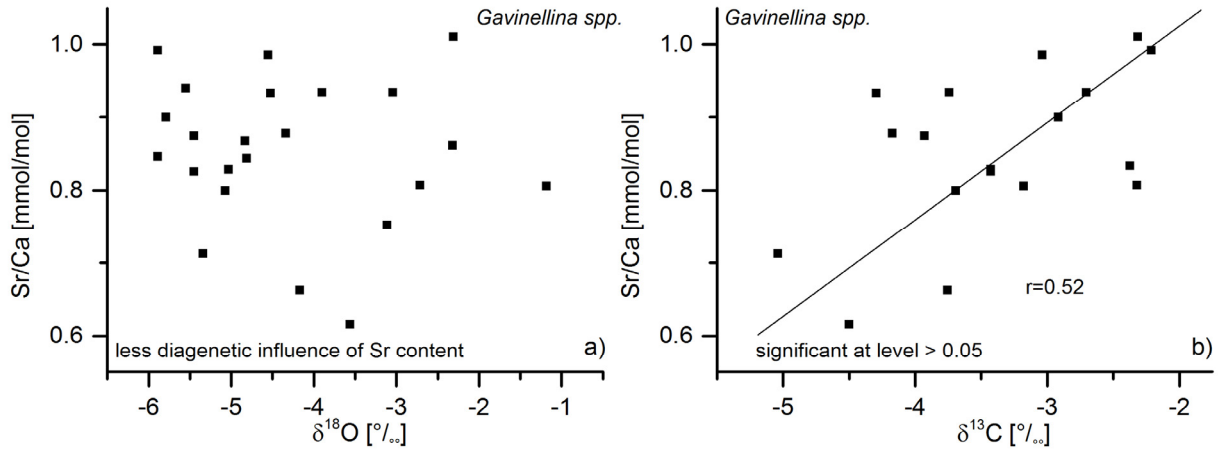

*Fig.106 A non-correlation between Sr/Ca and $\delta^{18}O$ **a)**, whereas a slight correlation to $\delta^{13}C$ **b)** is observable, all correlation are in units [mmol/mol] vs. [‰].Gavinellina spp. is referred to a benthic foraminifera species.*

diagenetic overprint by meteoric water (fig. 106**a)**, on the next page). Li et al. (2000) explains a correlation between $\delta^{13}C$ and the Sr/Ca ratio, with a decreasing trend in surface productivity and a falling sea-level (fig. 106, **b)**).

Li et al. (2000) report a higher Sr/Ca due to a greater release of Sr by diagenetic alteration, However, as is clearly shown in fig. 105, the results show a strong connectivity between Sr/Ca in benthic foraminifera (*Gavinellina spp.)* and sea level changes in the Oil Shale unit. A main conclusion from the cross plot above might be that transgression - regression cycles probably occur in the oil shale. This is also explained by a retreating sea level, which leads to exposure of the shelf area, concomitantly with a decreasing trend in surface productivity.

6.5. The evolution of the Upper Cretaceous Upwelling System: a conceptual geochemical model

Deposition of Phosphorites: Campanian/ Maastrichtian boundary

The Upper Cretaceous Phosphorite Belt was deposited throughout several millions of years in north and northeast Africa and the Near East. The time interval spans from the Santonian to the Early Eocene. The sedimentation of these rocks comprises an alternating deposition of siliceous-carbonate-phosphate bearing rocks (Si-C-P). These successions are mostly interpreted in terms of changes in the location and strength of the upwelled water. It was concluded that several transgression and regression events have resulted in near shore areas with a restricted water circulation - lagoons, with reworked sediments, partly with glauconite, porcellanites, phosphatic rocks (Soudry et al., 2012, 2006; Abed et al., 2007; Baioumy, 2007; Abed and Amireh, 1999). For the Negev area, two different phosphorite facies have been detected, which firstly comprise pristine phosphorites with low phosphor content that indicate a more reducing environment. Unlike pristine phosphorite, the reworked granular facies is enriched in P, and was deposited in conditions that are more oxic. The gradual shift from anoxic to oxic conditions was accompanied by an increase in F, total U, U(IV), REE, and Y in the apatite, and fractional removal of residual organic matter (OM), Cd and other sulphide-bonded trace metals (Zn, Cr, Ni, Cu, Mo, and V) from the phosphorite (Soudry et al. 2012).

Obtained results are partly in line with (Soudry et al., 2012, 2002) (fig. 107). In this section the focus is set only on the the abundance of Cd because of its important role as disclosing source of phosphor. There is a correlation observed between P_2O_5, (e.g. sedimentary apatite) Cd, and C_{org} in phosphorite, but only as long as the C_{org} content is low enough, which is in strong accordance with (Soudry et al., 2012, 2002, Baioumy and Tada, 2005, Nathan et al., 1997, 1996).

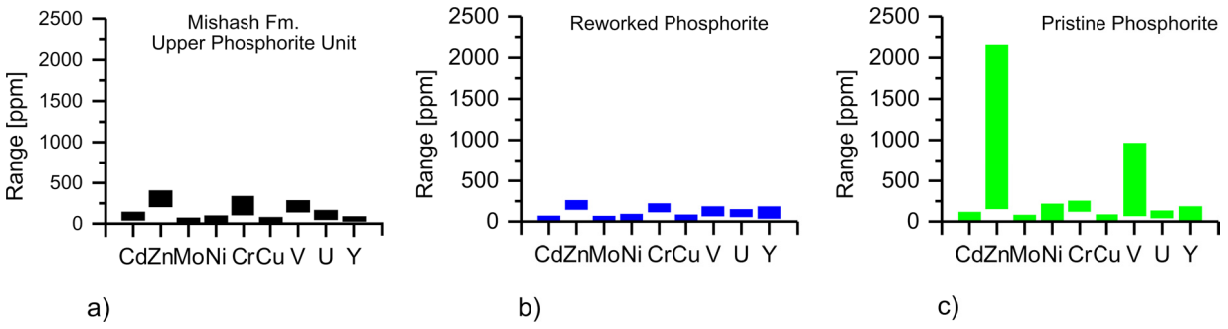

*Fig.107 Geochemical comparison between obtained results by this study **a)** and distinct phosphorite facies [reworked **b)** - pristine phosphorite facies **c)]** reference values obtained from Soudry et al. (2012).*

Soudry et al. (2012) observed distinct relationships in Cd/P_2O_5, U/P_2O_5, Y/P_2O_5, and V/Cr between pristine and reworked facies, and used them to distinguish between the two facies. The application of these relations is based on the fact that Cd, U, Y are incorporated in different ways into calcium-fluor-apatite (CFA). For example, Y and REE show much higher concentrations in pristine than in the reworked facies, but similar differences also in the abundance of trace elements, where higher concentrations in pristine facies than in the reworked facies occur (Soudry et al., 2012).

As shown in table 7 and fig. 107, own results do not exactly match any of the reported data sets. The Upper PM (upper 5 m) may not represent a classical scheme in terms of the phosphorite deposition, as outlined by (Soudry et al. 2012).

Table 7 Comparison between different geochemical proxies and own results, (reference values are taken from (Soudry et al. 2012)

Facies	**Cd/P_2O_5**	**U/P_2O_5**	**Y/P_2O_5**	**V/Cr**
Pristine*	5.0 (N=19)	4.0 (N=19)	1.2 (N=19)	2.7 (N=17)
Reworked*	0.2 (N=17)	4.3 (N=17)	4.6 (N=17)	0.8 (N=17)
Own study	5.7 (N=19)	6.3 (N=18)	2.5 (N=20)	1.1 (N=15)

Deposition of the condensed section (sea – level changes)

During the Campanian - Maastrichtian time very low sedimentation rates are recognised in the Negev (0.4 - 1.4 cm/ka) (Soudry et al. 2006). Similar results are reported from Ashckenazi-Polivoda et al. (2011) and Gvirtzman et al. (1989) (~2.4 cm/ka), and own results (~2.8 cm/ka), respectively. Such extraordinarily low rates in sedimentation are mostly explained by the concept of the deposition of a condensed section (Baraboshkin, 2009; Einsele, 2000). Commonly, Upper Cretaceous phosphate deposits contain condensed layers, which separate overlying or underlying phosphate deposits or cherts, limestone and organic rich carbonates. Repeated third-order, transgression-regression cycles may correspond to these deposits (Soudry et al. 2006; Haq et al., 1987; Lucas and Lucas-Prèvot, 1996). Fig. 108 may confirm the widespread adoption that changes in sea level affect the height of the OMZ along the coastal areas, which has recently become known.

During the transition from the Campanian – Maastrichtian time, short term sea level changes resulted in a sea level difference of about 50 m (e.g., (Haq, 2014; Browning et al., 2008; Haq and Schutter, 2008).

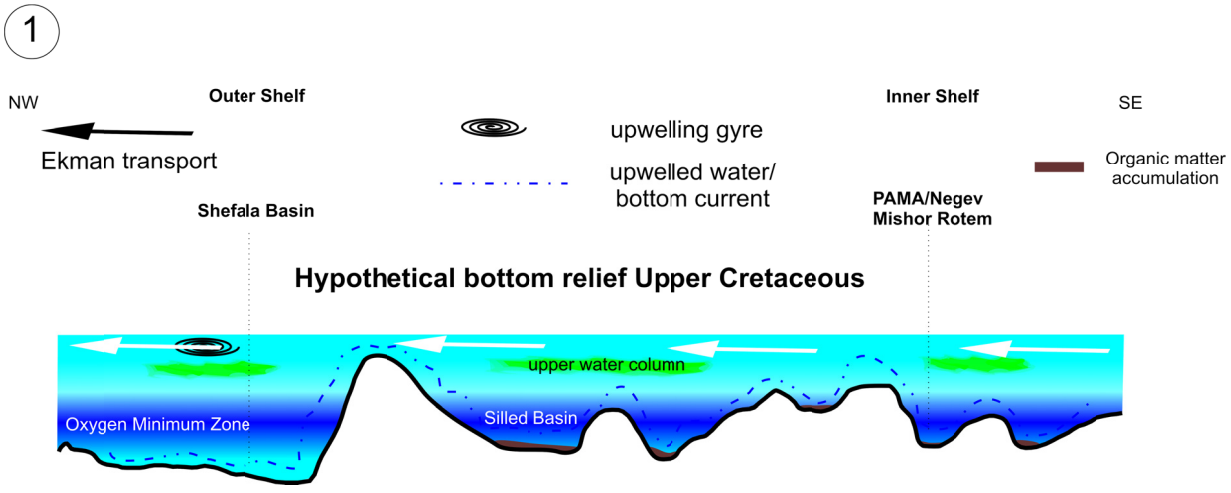

Fig.108 Hypothetical bottom topography on basis Eocene topography, (Fleischer and Gafsou, 2003), Geological Survey Israel

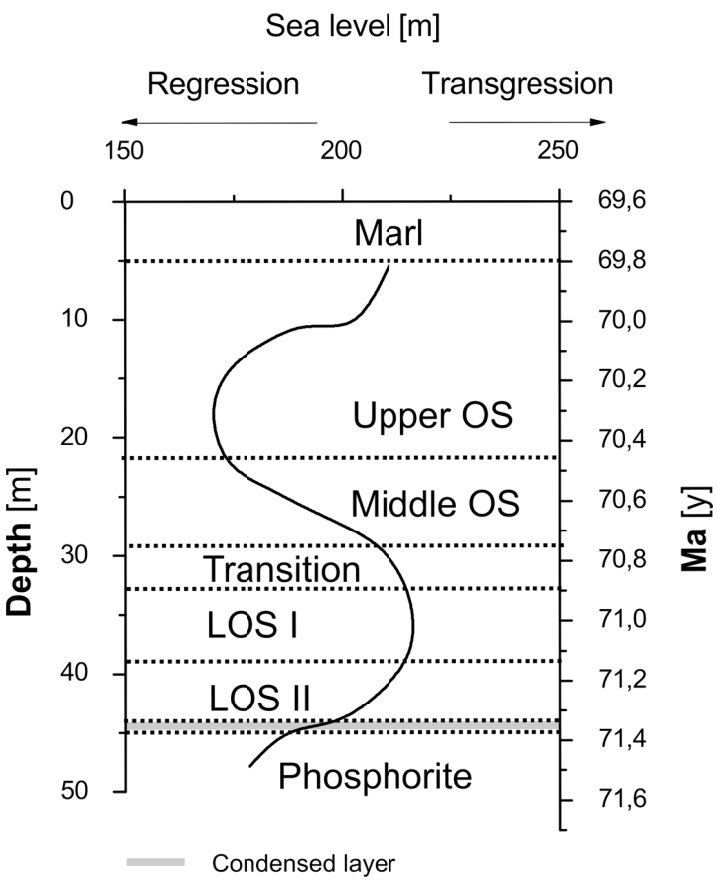

Fig.109 Short term sea level changes during the transition from Campanian to Maastrichtian time, modified after (Haq, 2014)

As shown in fig. 109, short term sea level fluctuations beyond the transition of the Campanian-Maastrichtian boundary occurred. The fast sea level rise triggered a cascade of processes that led to an enhanced mobilisation of benthic phosphorus from the sediment. A similar scenario, a short-lived anoxic event (Faraoni event), is described by Bodin et al. (2006) in Hauterivian sediments of the western Tethys.

Several authors proposed a combination of both sea level rise and enhanced nutrient input (Bodin et al., 2006; Soudry et al., 2006; Jarvis et al., 2002; Ingall and Jahnke, 1997; Föllmi, 1996).

These different models include a reworking of sediments and soils, from the flooded landmasses, intensified seawater evaporation due to the enhanced epicontinental seas that cover the shelf, and a positive feedback between benthic phosphorus regeneration and marine productivity. As a tentative conclusion, in course of the thesis, a model is proposed that might be able to explain the formation of the organic rich carbonates at the Campanian-Maastrichtian transition. This model based on sea level oscillations as a master variable, which ultimately control the interplay among three categories of factors: changes in the extent of the epicontinental area, climatic factors (notably wind velocity) and primary productivity. In the brief discussion below, the following should be taken into account (fig. 110, next page).

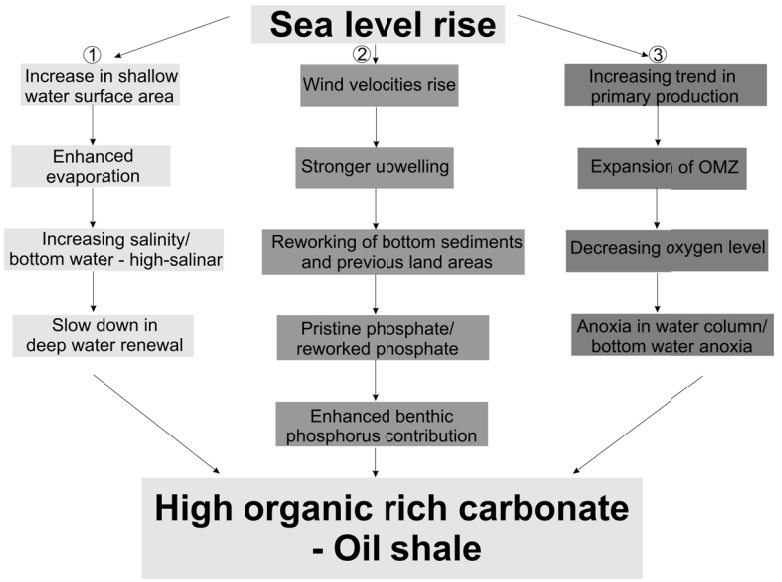

Fig.110 Model for development of organic rich carbonates after passing the Campanian-Maastrichtian bondary, see text for explanation

The regression cycle increases the areas of weathering and erosion, and hence the return of phosphorus to the oceans. Supported by the extraordinarily low sedimentation rate, phosphorite layers are formed in times of low (lack) sedimentation or even during times of erosion (Soudry et al., 2012; Füchtbauer and Müller, 1988).

1. **Increase in shallow water area**: Estimates by several authors reveal that a huge area was covered by shallow water during the Cretaceous time. Thereby occur, for example, the estimates about the extended Upper Cretaceous palaeoslope of 250 km in comparison to recent slopes 140 km off Namibia, 10 - 20 km off Peru (Almogi-Labin et al., 2012; Monteiro et al., 2005; Monteiro and Roychoudhury, 2005; Acha et al., 2004). Due to its larger sea surface area, a higher evaporation accelerates both the continental weathering and the rising transport of sediments to the coastal sites (Föllmi, 1996). Moreover, a higher rate in evaporation also favours the thermal stratification within water mass and a transport downwards from high salinity water to the bottom, as a last consequence; this is expressed by a high saline deep-water with a sluggish deep-water circulation.

2. **Wind velocities:** From mathematical simulations and meteorological observations, it is suggested that a greater contrast between continental landmass and the ocean surface produces a greater contrast in temperature. By using these considerations, because of the enhanced heat loss from the surface water, a greater wind stress along the shore and cooler sea surface temperatures occur.

Due to the greater contrast in the atmospheric pressure between landmass and open sea, a transgression cycle that transports more coastal water to the epicontinental areas might lead to increasing wind velocities, which result in a stronger upwelling regime. Ultimately, this transports more nutrients to the coastal sites (Garreaud and Falvey, 2009; Bodin et al., 2006; Barron et al., 2004; Berger and Wefer, 2002, Iruthayaraj and Morachan, 1978). Furthermore, this results in high-energy bottom currents, stronger wave activities, tidal currents, consequently a reworking of bottom sediments. In coastal sites, such a reworking of bottom sediments, together with microbial activity, leads to a mobilisation of phosphorus or P-rich bottom water currents from the pore water and a diffusion of dissolved phosphor in the overlying water column, to subsequently form authigenic apatite (Ruttenberg, 2004, Soudry, 1987).

3. **Increased primary production**: A release in the sedimentary phosphor, a stronger upwelling activity together with a shoaling of the OMZ, results in a high primary surface productivity, which implies oxygen depletion conditions both down to the bottom and in the water column, as well as enhanced carbon burial rates.

These are prerequisites for the sedimentation of high organic-rich sediments and the burial of organic carbon. Anoxia events may have occurred mostly in times of thermohaline stagnation and filled both the upper water column and the subsequent basins that are situated in closer proximity to the continental landmass (Southam et al., 1982). This scenario will be briefly discussed below.

The formation of anoxic/ euxinic conditions

On basis of the statistical results, wet chemical analysis, isotopical investigations, and XRF analysis as well, a conceptual geochemical model has been developed, that is shown in fig. 111, which explains the factors under which the deposition organic carbonates at the Campanian-Maastrichtian transition took place.

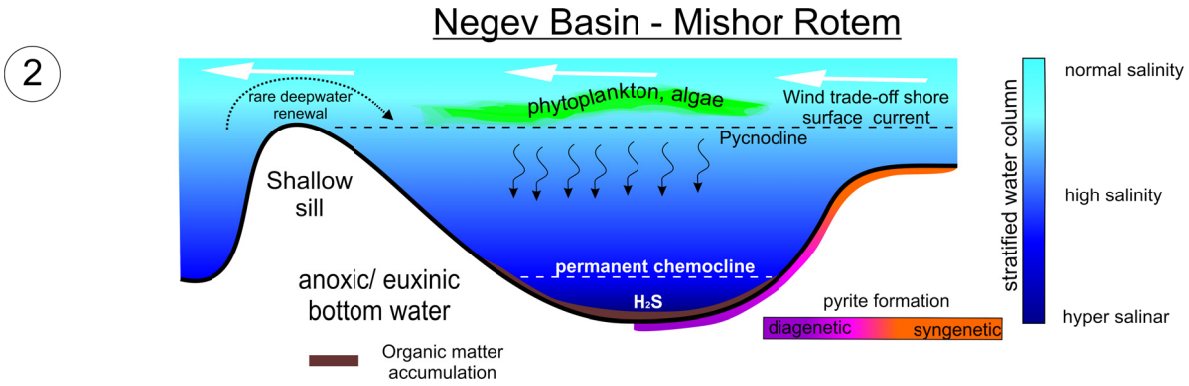

Fig.111 Hypothetical sediment deposition model according to the conclusions from the present study

A rapid sea-level rise at the transition from the condensed layer to the OSM is responsible for the installation of highly anoxic/ euxinic condition at the base of the OSM (LOS I, II). This is corroborated due to the formation of total reduced sulphur by microbial activity. Own sulphur isotopy results mirror this trend. Which includes, heavier values at the transition from the condensed section to the Lower Oil shale, such heavy isotopic values (~ 20‰ $^{34}S_{sulphide}$) is be mostly interpreted in terms of an sulphate –limiting – semi- closed system. Yet more, the geochemical data suggest that these organic rich sediments were deposited in an even more oxygen deficient environment than the overlaying beds, possibly even with free H_2S in the water or under the vicinity of a thin euxinic layer down to the bottom sediments. The rising sea level and an enhanced surface water productivity forces the shoaling of the OMZ and transport more oxygen depleted water close to the inner continental shelf areas. Because the extraordinary low oxygen level in the upper water column, in such an environment typically syngenetic pyrite forms within the water column, immediately beneath the redox boundary and sink to the sea floor before they can reach appreciable diameters (Wignall et al., 2005; Wilkin et al., 1996). However, such pyrite is isotopically even more depleted in ^{34}S than diagenetic pyrite formed within the sediment or at the sediment/ water interface (Lyons et al. 2003a; Werne et al., 2003; Wilkin and Arthur, 2001). Because of the low sedimentary input and proposed iron limited conditions here, it is unlikely the presence of appreciable amounts of syngenetic pyrite here. However, although the shallow water depth and the proximity of the redox boundary to the bottom, should impeded the formation of syngenetic pyrite. Another likely explanation might be due to the installation of highly anoxic condition in the upper water column.

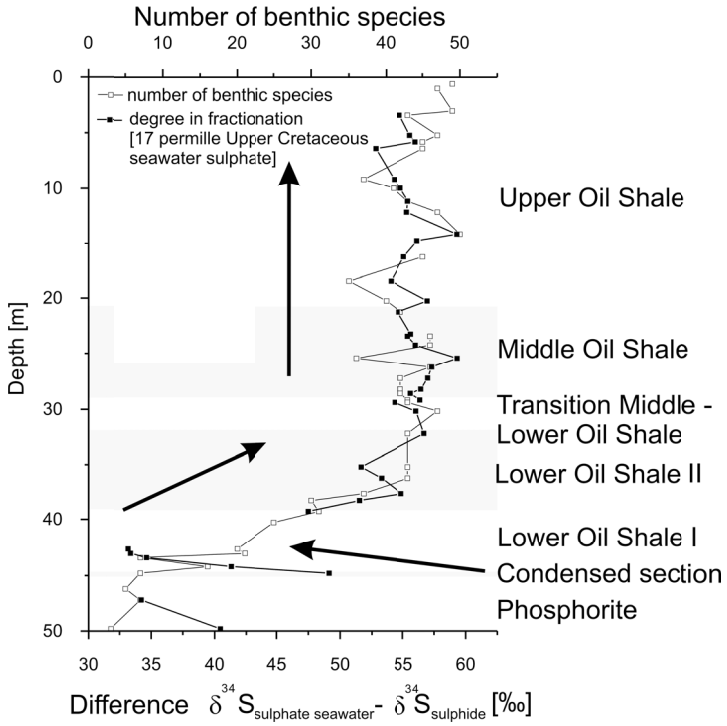

Fig.112 Degree of sulfur isotope fractionation and increasing number of benthic foraminifera indicate short-term injection of oxygen into the sediment, foraminiferal data from (Ashckenazi-Polivoda et al., 2011)

In times of a massive reduction in the water mass reduction circulation, which enhances the possibility of syngenetic super heavy pyrites as reported from the Framvaren Fjord by (Sælen et al., 1993). Such super-heavy pyrite show $\delta^{34}S$ values up to -22‰. Which is quite comparable to own values in the LOS (~ -18‰). In the Framvaren Fjord, several sills favour a sluggish water circulation. Sælen et al. (1993) could show, that the formation of the super-heavy (syngenetic) pyrite took place in a euxinic basin with a restriction in the deepwater renewal. In the opinion of the author of this thesis, these conditions are likely and similary to the deposition of the Lower Oil Shale unit.

The overlying Upper OSM represents a completely opposite system. This is due to the very negative sulphide sulphur isotopy (-30‰ - 60‰) and also due to its depleted values of about 40‰ - 60‰, in comparison to the isotopic composition of the sea water sulphate. Short-term oxygen injections into the bottom sediment, concomitantly a falling sea level, as well as a subsequent sulphur-disproportion by bacteria, as pointed out by Jørgensen, (1990), may explain the obtained values. Due to the decreasing trend in sea level, the OMZ retreats back out to the outer shelf area, which allows bioturbation by substrate organisms living at the seafloor. This return of the benthic life is supported by the research of our Israeli partner, who detected an increasing trend in the number of benthic foraminifera and concomitantly a shift from infaunal species to more epifaunal species profile upward based on their palaeontological results (fig. 112). This is explained by a transition from a more anoxic seafloor to more aerated conditions

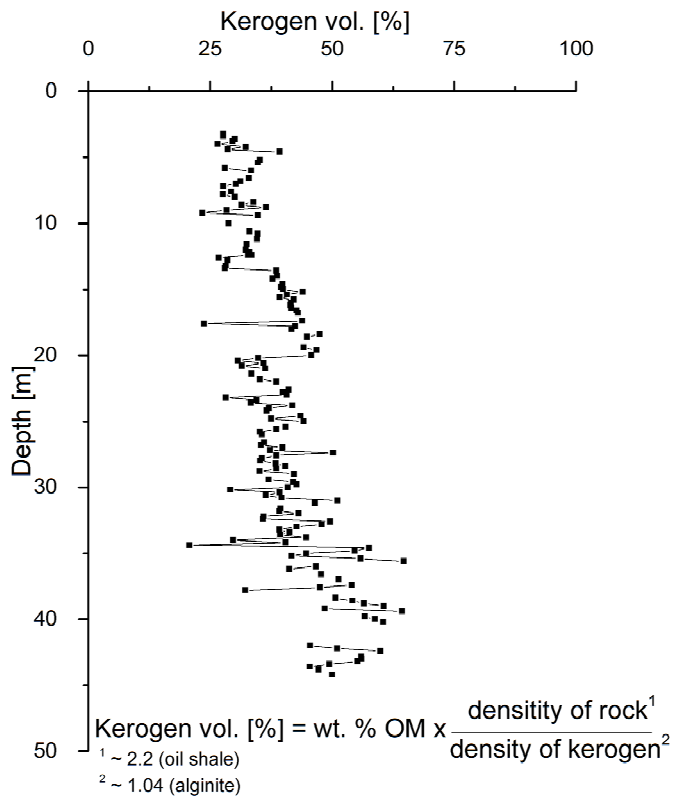

Fig.113 shows significant differences in the kerogen content between the LOS (45 - 33mbsf) and Upper Oil Shale unit.

at the top of the OSM (Ashckenazi-Polivoda, 2011). The distinct geochemical pattern between LOS and Upper Oil Shales can also be shown by their distinct trace element enrichment.

As is figured out in section 4.1.2., the different concentrations of trace elements in the OSM are also shown by their distinct enrichment factors. Unlike the overlying Middle- and Upper OSM, where the highest enrichment of trace elements is occurs at the base of the oil shale (LOS I, II).

Such distinct trends could be explained not only by their high organic matter enrichment. In such surroundings, trace elements (Cu, Ni, Zn, Cd) are clearly connected to the organic matter. The clear distinction between these sub-units might also be explained by an additional enrichment in the Lower Oil Shale. This is due to the high kerogen content, which is twice as high as in the Upper Oil Shale horizon (fig. 113). Higher kerogen (Lower Oil Shale) content, due to its larger surface, is more susceptible to scavenge trace elements. Under similar conditions, but even with a lower content of kerogen (Upper Oil Shale) that might induce a circulation of dissolved (most trace elements are not fixed into the sediment under reducing conditions) trace elements in the pore water.

In an iron-limited environment, natural sulphurisation is the most likely sink for total reduced sulphur and its incorporation into the organic matter. It is assumed that the cross-linked total reduced sulphur by

forming a intramolecular framework is widely distributed in marine sediments (Sinninghe Damsté et al., 1989; Stankiewicz et al., 1996; Kok et al., 2000b). Similar observations as proposed here occur in the Kimmeridge Clay (van Kaam-Peters et al. 1998), Orbagnoux Formation (Mongenot et al. 1999), Tarfaya Basin, Morocco (Kolonic et al. 2002), and Kashpir Oil Shales (Riboulleau et al., 2003). All these sediments were deposited in an iron-limited euxinic environment, in which the organic matter shows an early diagenetic sulphurisation. The presence of isorenieratane derivatives in the Tarfaya Basin is linked to changes in the sedimentation rate, which in turn affects the degree in sulphurisation (Kolonic et al., 2002). This exact process is proposed right here, in the present case! For the Upper Oil Shale horizon, a retreatment of the OMZ and simultaneously an increasing trend in the sedimentation rate prevents a higher sulphurisation of the organic matter, because of higher amounts of reactive iron for the formation of syngenetic pyrite.

Oscillating conditions, as preferable in the Upper Oil Shale horizon, might induce favourable conditions for a downward migration of dissolved species along a decreasing redox gradient in the sediment, where it is secondarily fixed onto the surface of organic matter. This might be the reason for the extraordinarily high enrichment of trace elements in the Lower Oil Shale unit, in comparison to the Upper Oil Shales. It seems that the enrichment of trace elements depends on preservation and sulphurisation of organic matter in pore water that is not affected by oxygen penetration. Under such conditions, the organic matter accumulation and trace element enrichment might not represent a signal for productivity but rather, a signal for enhanced preservation!

Open marine conditions (MarlMember)

Figure 114 (next page) shows a scenario which may explain the “rise and fall” of the Upper Cretaceous upwelling belt, which starts at the Coniacan, culminating at Campanian-Maastrichtian, and ends with the decline at the end of Maastrichtian time. The complex interplay between plate tectonic movement, climate change, and atmospheric and marine water circulation are the main factors regarding the repeated accumulation of organic rich (Si-C-P) rocks (Soudry et al., 2006).

These comprise new information from the early Maastrichtian cooling or glaciation event, which might play a key role in the rapidly falling sea level, followed by a rise, during the transition from the Campanian (phosphorite) to the Maastrichtian (oil shale) time (Haq, 2014, Friedrich et al., 2012; Voigt et al., 2012).

Several processes that affect sea level changes over different time scales, including, among others, factors like (1) glacio eustacy due to the melting of sea- or land ice; (2) tectono-eustacy due to subsidence and accompanied the regional uplift (Schäfer, 2010, Einsele, 2000, Cronin, 1999). In the time period of interest and a similar area, two regression cycles have been reported from El Kef, Tunisia. Within this area, a low sea level has been associated with high terrigenic input, high TOC and Sr/Ca ratio, unlike times with increasing sea level, which inhibit reverse conditions (Li et al., 2000). Such a general statement

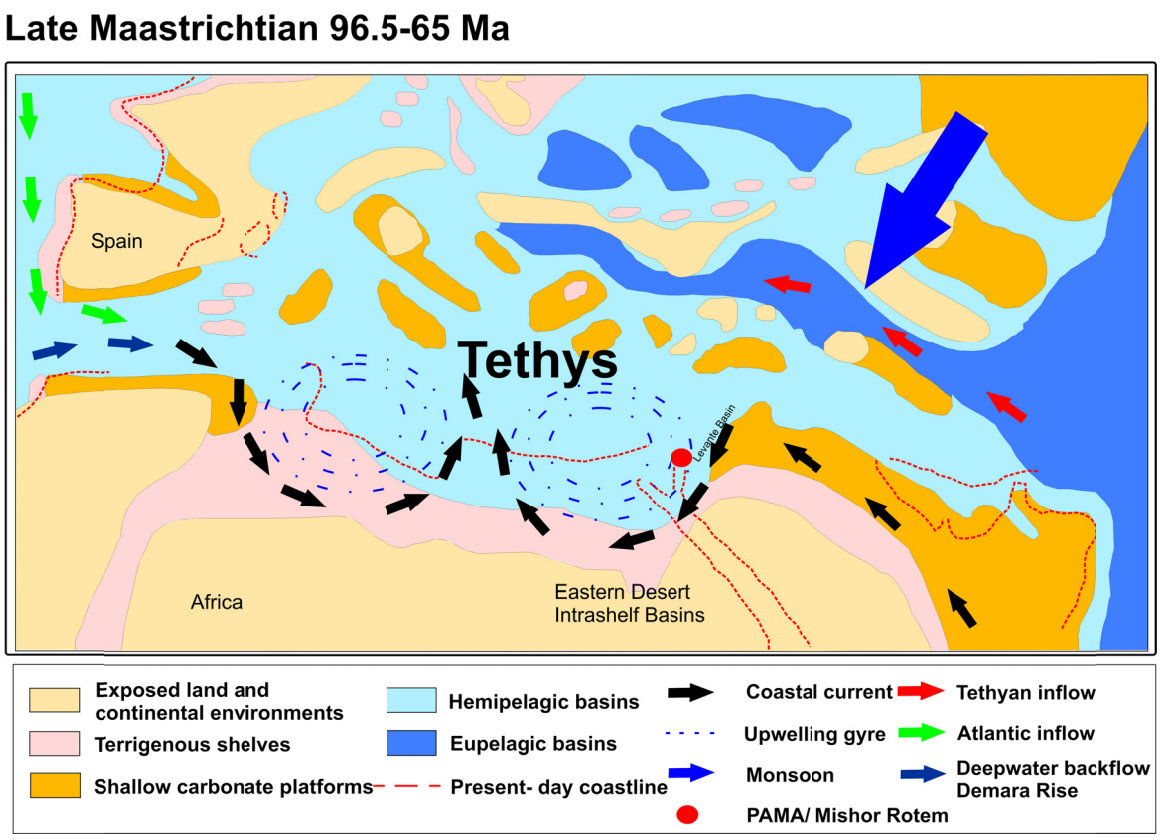

Fig.114 Estimated palaeo current flow at Upper Cretaceous time, data from palaeo currents is taken from (MacLeod et al. 2011; Soudry et al. 2006), and palaeo topography, reference data are taken from (Guiraud et al. 2005; Camoin et al. 1993).

is not fully supported by results in course of this study, which yield a puzzling picture that suggests a different pattern in Sr/Ca ratio and TOC concentration. The latter shows a decreasing trend during times of sea level changes. However, fluctuations in sedimentary input and Sr/Ca in benthic foraminifera are in general agreement with observations obtained by this study.

The transition from the OSM to the MM is accompanied by repeated transgression cycles, which suggest a return to “open-marine conditions”. However, the question may arise at that point, why this scenario does not lead to increasing TOC- and trace elemental content in the bulk sediment levels, in comparison to the base of the OSM. Moreover, a new model that includes a complete reorganisation of the surface- and deep-water currents, which have changed during the transition to the overlying MM, is needed.

The comparison with the California Borderland basin, as a recent analogue, reveals some similar features for the Upper Cretaceous Upwelling belt. The coastline of the Arabo-Nubian coast is also mainly composed of a series of silled basins. The sea level that increased once, at the transition from the OSM to the MM, has not led to the deposition of organic rich carbonates again. This is in full agreement with $^{13}C_{benthic+planktic}$ isotopy, which signifies a decreasing trend to lower surface productivity. It seems rather speculative to evaluate the reason for the constantly decreasing trend of the surface productivity. A shift and reorganisation of surface and deep water current is the most likely explanation (fig. 114).

The California Continent Borderland Basin - a recent analogue?

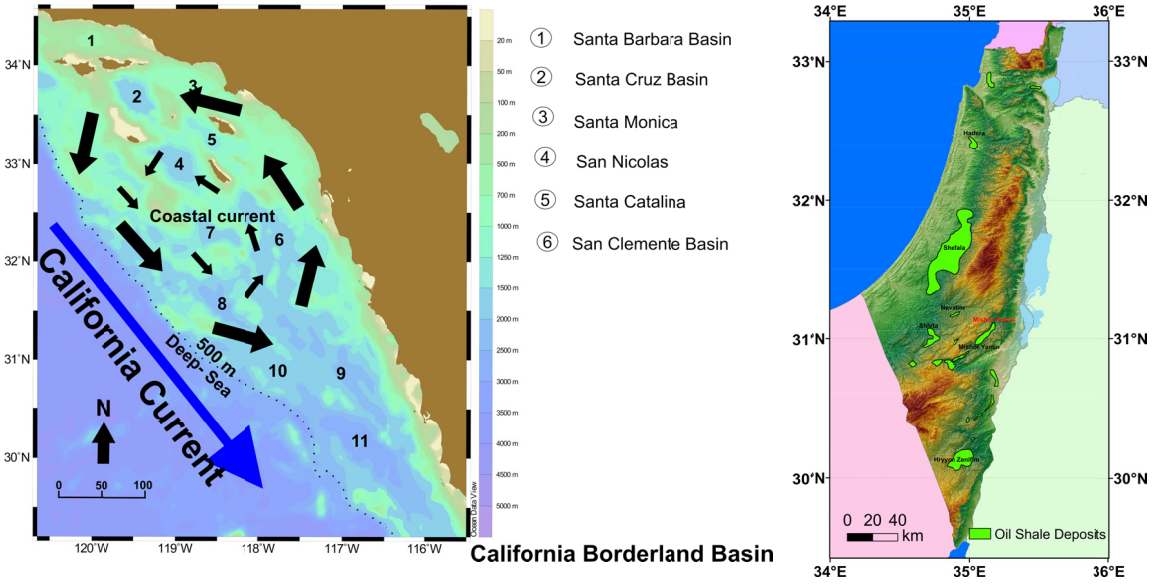

Fig.115 Left: The continental margin of southern California consists of silled basins that include islands, banks and ridges –similar in comparison to the Upper Cretaceous margin at the Levante Basin, which also comprise a series of silled basins (green coloured area) off the Arabo-Nubian continent (Right), modified after Minster, (2009), Pinet, (1992) and Atwater, (1970).

A recent analogue for a scenario that might be comparable to the Upper Cretaceous continental shelf is the Southern California Borderland basin (fig. 115, left). Therefore, the continental shelf is a very narrow area from up to <10 km wide, in the case of the Southern Continental Borderland. The bottom topography is best described as a series of silled (elongated) basins, as a direct consequence of plate tectonic movement. Sediments in the basins are largely controlled by turbidites, which contain only minor amounts of clastic sediments, ooze and clays (Pinet, 1992). This may be in complete opposition to the research area, which is described as a very wide shelf, with up to 250 km, off the coast (Almogi-Labin et al., 2012). In terms of the ancient analogue, it is still not well known from where the majority of the deposited sediments originate. Nevertheless, it is important to note that the bottom topography and oceanography include surface currents, and the deep-water current may have been similar. The surface currents off the Southern Californian Borderland coast can be best described as counter-clockwise rotating eddies (fig. 118, left). One of the principal characteristics of the stagnant, cool temperate, anoxic deep-water in the silled basins is that it contains higher salt concentrations and denser water. The oxygen content of this water shows a

trend decreasing with depth and inhibits seasonal variations of <0.1 ml O_2/l, (Blanchet et al. 2009). This deep-water flows over the sills and flushes neighbouring basins. More importantly, the coastal water is affected by wind-induced Ekman transport, which allows cold, dense water upwelling to the surface, to induce phytoplankton blooms (Pinet, 1992).

A similar scenario might be given for the Upper Cretaceous upwelling off the North African coast, which has led to the accumulation of phosphate and organic-rich carbonates. Their greatest differences arise from the larger relations in response to the coast. The former coast off the Arabo-Nubian and North African landmass had a length of more than 2000 km, which is much more than what the Southern Borderland coast comprises, with ~900 km.

7. Summary and Conclusions

An upwelling belt was formed during a period from the Senonian to Maastrichtian time. Within the Levante Basin, deposited organic rich carbonates, commonly termed as “oil shale”, were deposited as a part of the Upper Cretaceous Upwelling system. The formation and the oceanographic history of this upwelling are determined by the interactions of a set of common factors: sea water temperature, salinity and chemistry, primary production, biology, wind and water circulation systems, and air conditioning. Specific parameters can greatly modify the massive deposition of organic rich sediments in detail, such as the distance from the coast, sediment transport and submarine topography. The main goal of this thesis was to recognise the parameters that change the deposition history of these organic rich sediments. New insights in the deposition and late diagenetic history come from the application of well-constrained proxies, e.g. trace element enrichment, U/P_2O_5, Ni/V, $Mg/C_{benthic+planktic,}$ $Sr/Ca_{benthic}$ foraminifera, Mo/C_{org}, $\delta^{18}O$, $\delta^{34}S$, and Fe-S-C systematics. These results are briefly summarised below:

Trace elements were analysed by means of XRF analysis. The results were further processed by a principal component analysis (PCA) that shows two opposite factors. The first factor reveals the degree of bottom water oxygenation (C_{org}, S, Ni, Cu, Zn, Cr, P_2O_5, As, Mo), whereas the second factor reflects the interaction between bioclastic-carbonate (Ca) and terrigeneous input (Al, Si, Ti, V, Fe, Rb, Ga, Ce). By comparing these chemostratigraphic features with the foraminiferal distribution patterns by the Israeli working group, a strong interdependence between geochemical and the micropalaeontological environmental indicators can be found.

From results obtained by $\delta^{34}S_{pyrite}$, several conclusions are obvious: At the base of the OSM, high isotopic values (diagenetically formed pyrite ~-20‰) and a low degree in fractionation permit the conclusion that the organic rich sediment was deposited in a restricted, sulphate-limited system which underlies no bioturbation (closed conditions). Additionally, the formation of a chemocline was perhaps sufficient to prevent the partial re-oxidation and disproportionation of sulphur compounds.

In a sulphate- and iron-limited system, a process called natural vulcanisation started and led to the formation of sulphur- and organic-rich sediments. This occurred within a macromolecular framework that prevented microbial attacks and enhanced the preservation of organic biomarkers. Obviously, the combined interplay of these processes might have led to the preservation of the enormous high organic carbon content (~20 wt. %) in the Lower Oil Shale.

This is in strongest contrast to the overlying OSM. The sediment was deposited under conditions that allow bioturbation and short time injection of oxygen. Consequently, this conclusion is supported by the low isotopic values (syngenetically formed pyrite of -35‰ to -45‰) and a high degree in fractionation (~55‰). These sediments were deposited in a sulphate-unlimited system.

Both sections, Lower Oil Shale vs. Upper Oil Shale, show a striking difference with respect to the trace element concentrations and their former redox conditions. Own findings suggest a high trace element enrichment in the Lower Oil Shale unit. Concomitantly, a strong connection to the enrichment of the OM and a classical distribution of chalcophile elements took place. The application of the proxies U/C_{org}, U/P_2O_5, U/V for the bulk sediment might suggest a high-grade anoxia in the pore waters in a pH range from 3 - 4, or a thin euxinic layer must have passed at this time slice. Unlike the basal part of the oil shales, the upper part exhibits significantly lower organic carbon and trace element enrichments. The preferred occurrence of trace element concentrations in the basal part can be explained by an additional enrichment of trace elements due to partial re-oxidation of the organic matter. In such a scenario, downward migration of the released trace metals and a second fixation onto the surface of organic matter led to the extraordinary high enrichment of trace elements.

The sea surface temperature is an important feature to achieve conclusions about the palaeoclimate and the distribution of water masses during the time slice of interest. Such a possibility is given by the application of Mg palaeothermometry and oxygen isotopes. Cross plots of $\delta^{18}O$ and Mg/Ca show negative trends and hence, the application of the Mg/Ca in foraminifera is allowed (section 5.2). Nevertheless, own results suggest a late diagenetic overprint of $\delta^{18}O$ by meteoric water and a high Mg overgrowth, which might

originate from the installation of a saline bottom environment. In spite of these limitations, it was possible to estimate a trend in sea-surface temperature (SST) and bottom-water temperature (BWT). Results within this study reveal a SST of about ~25°C and a BWT of ~21°C. Such findings are in agreement to modern values and the Upper Cretaceous temperature gradient of ~4° C (Barrera and Savin, 1999). This gradient and the occurrence of middle bathyal and upper abyssal benthic foraminiferal species argue for a palaeowater depth of about 400 m, which is probably consistent with the palaeontological results by the Israeli working group.

The rsMo/TOC ratio supports this interpretation. The application of this proxy reveals an rsMo/TOC~ 8 in the PM, contrasting the rsMo/TOC ~1 for the Oil Shale unit. Such findings are further corroborated by micropalaeontological results that show a sharp decline in benthic and planktic foraminiferal assemblage compositions, which is interpreted in terms of a complete reorganisation of the water mass circulation (Ashckenazi-Polivoda et al., 2011, Eshet and Almogi-Labin, 1996).

Such findings might indicate an environment with restricted deep water circulation, a positive water balance and slightly saline waters. This would have been similar to the recent Southern California Borderland margin, the Black Sea, and Baltic Sea. Further support to this assumption comes from our German co-partner who found several sulphur containing compounds (thiolane(3-methyl-5-(3,7,11-trimethyldodecyl)-thiolane), which belong to the aromatic hydrocarbon fraction. These results may suggest a deposition of such hydrocarbons in sediments, which were deposited under hyper-saline and euxinic conditions (pers. com. Wilhelm Püttmann, 2010).

To reveal evidence about possible sea-level changes, the application of the Sr/Ca relationship in benthic foraminiferal species was used for its determination. The incorporation of Sr in calcitic organisms takes place under conditions in equilibrium to the surrounding seawater. Obtained results from Sr/Ca in the OSM may coincide with the Cretaceous sea-level curve by (Haq, 2014). Additional support for these results is given by the occurrence of keeled foraminiferal assemblage, which is commonly interpreted in terms of a change in the position of the OMZ in the upper water column.

One of the main tasks of this thesis was to provide new insights into the late diagenetic history of the sediments. Therefore, different proxies like sulphur isotopy, oxygen isotopy and Fe-S-C systematics were used. Light $\delta^{34}S_{sulphur}$ isotopes from 0‰ to -20‰ and light O^{18} values from benthic and planktic foraminifera display similar results, in form of a re-oxidation of the profile. Results acquired from the use of the Fe_{HR}/Fe_T relations support a late diagenetic overprint. Regarding typical marine C_{org}/S_{pyrite} ratios of about 2.8 ± 0.8 and compared to the own extraordinarily high ratios with C_{org}/S_{pyrite} values ~46, the notion about isotopic values is confirmed. Re-oxidation after exhumation led not only to a shift in the isotopic values towards lighter results, this process also led to an underestimation of pyrite-bonded sulphur. Regarding this result, (Rickard, 2012, Emeis and Morse, 1993) have noted, that for the application of this proxy, no distinction is possible between anoxic and euxinic conditions.

The weathering processes of feldspar and muscovite in sediments of the Ghareb fm. led to a loss of interlayer K along with other interlayer cations, including Rb and Sr and the introduction of a hydrated Mg - Fe interlayer. As a result, the formation of authigenic illite took place, which was detected by own XRD analysis.

8. References

Abanda, P.A., Hannigan, R.E., 2006. Effect of diagenesis on trace element partitioning in shales. Chemical Geology 230 (1–2), 42–59.

Abanda, P.A., Hannigan, R.E., 2007. Chapter 13 Mineral control of minor, trace and rare earth elements during black shale weathering at near-neutral pH, in: Dibyendu Sarkar, R.D.a.R.H. (Ed.), Developments in Environmental Sciences : Concepts and Applications in Environmental Geochemistry, vol. 5. Elsevier, pp. 273–301.

Abed, A.M., Amireh, B.S., 1999. Sedimentology, geochemistry, economic potential and palaeogeography of an Upper Cretaceous phosphorite belt in the southeastern desert of Jordan. Cretaceous Research 20 (2), 119–133.

Abed, A.M., Arouri. K. (Eds.), 2006. Characterization and genesis of Oil shales from Jordan, International Conference on Oils Shale.

Abed, A.M., Sadaqah, R., Al-Jazi, M., 2007. Sequence stratigraphy and evolution of Eshidiyya phosphorite platform, southern Jordan. Sedimentary Geology 198 (3), 209–219.

Abramovich, S., Keller, G., Stüben, D., Berner, Z., 2003. Characterization of late Campanian and Maastrichtian planktonic foraminiferal depth habitats and vital activities based on stable isotopes. Palaeogeography, Palaeoclimatology, Palaeoecology 202 (1-2), 1–29.

Abramovich, S., Yovel-Corem, S., Almogi-Labin, A., Benjamini, C., 2010. Global climate change and planktic foraminiferal response in the Maastrichtian. Paleoceanography 25 (2), 1–15.

Acha, E.M., Mianzan, H.W., Guerrero, R.A., Favero, M., Bava, J., 2004. Marine fronts at the continental shelves of austral South America: Physical and ecological processes. Journal of Marine Systems 44 (1–2), 83–105.

Algeo, T.J., Kuwahara, K., Sano, H., Bates, S., Lyons, T., Elswick, E., Hinnov, L., Ellwood, B., Moser, J., Maynard, J.B., 2011. Spatial variation in sediment fluxes, redox conditions, and productivity in the Permian–Triassic Panthalassic Ocean: Permian - Triassic ecosystems: collapse and rebuilding. Palaeogeography, Palaeoclimatology, Palaeoecology 308 (1–2), 65–83.

Algeo, T.J., Lyons, T.W., 2006. Mo–total organic carbon covariation in modern anoxic marine environments: Implications for analysis of paleoredox and paleohydrographic conditions. Paleoceanography 21 (1), PA1016.

Algeo, T.J., Maynard, J.B., 2004. Trace-element behavior and redox facies in core shales of Upper Pennsylvanian Kansas-type cyclothems: Geochemistry of Organic-Rich Shales: New Perspectives. Chemical Geology 206 (3-4), 289–318.

Algeo, T.J., Rowe, H., 2011. Paleoceanographic applications of trace-metal concentration data. Chemical Geology (324-325), 6–18.

Allison, N., Austin, H., Austin, W., Paterson, D.M., 2011. Effects of seawater pH and calcification rate on test Mg/Ca and Sr/Ca in cultured individuals of the benthic, calcitic foraminifera Elphidium williamsoni. Chem. Geol. 289 (1-2), 171–178.

Allison, N., Austin, W.E.N., 2008. Serial Mg/Ca and Sr/Ca chronologies across single benthic foraminifera tests. Chemical Geology 253 (1–2), 83–88.

Almogi-Labin, A., Ashckenazi-Polivoda, S., Edelman-Furstenberg, Y., Benjamini, C., 2012. Anoxia-Dysoxia at the Sediment-Water Interface of the Southern Tethys in the Late Cretaceous: Mishash Formation, Southern Israel, in: Altenbach, A.V., Bernhard, J.M., Seckbach, J. (Eds.), Anoxia, vol. 21. Springer Netherlands, pp. 553–572.

Almogi-Labin, A., Bein, A., 1993. Late Cretaceous upwelling system along the Southerm Tethys Margin (Israel):Interrelationsships between productivity,bottom water enviroments and organic matter production. Paleoceanography 8 (5), 671–690.

Alsenz, H., Regnery, J., Ashckenazi-Polivoda, S., Meilijson, A., Ron-Yankovich, L., Abramovich, S., Illner, P., Almogi-Labin, A., Feinstein, S., Berner, Z., Püttmann, W., 2013. Sea surface temperature record of a Late Cretaceous tropical Southern Tethys upwelling system. Palaeogeography, Palaeoclimatology, Palaeoecology 392 (0), 350–358.

Am Abed, Amireh, B.S., 1983. Petrography and geochemistry of some oil shales from North Jordan. Journal of Petroleum Geology 5 (3), 261–274.

Amajor, L.C., 1987. Major and trace element geochemistry of Albian and Turonian shales from the Southern Benue trough, Nigeria. Journal of African Earth Sciences (1983) 6 (5), 633–641.

Amiot, R., Lécuyer, C., Buffetaut, E., Fluteau, F., Legendre, S., Martineau, F., 2004. Latitudinal temperature gradient during the Cretaceous Upper Campanian–Middle Maastrichtian: $\delta^{18}O$ record of continental vertebrates. Earth and Planetary Science Letters 226 (1-2), 255–272.

Amit, O., Bein, A., 1982. Organic matter in Senonian phosphorites from Israel -- origin and diagenesis. Chemical Geology 37 (3-4), 277–287.

Amrani, A., Aizenshtat, Z., 2004. Mechanisms of sulfur introduction chemically controlled: ^{34}S imprint: Advances in Organic Geochemistry 2003. Proceedings of the 21st International Meeting on Organic Geochemistry. Organic Geochemistry 35 (11-12), 1319–1336.

Amrani, A., Lewan, M.D., Aizenshtat, Z., 2005. Stable sulfur isotope partitioning during simulated petroleum formation as determined by hydrous pyrolysis of Ghareb Limestone, Israel. Geochimica et Cosmochimica Acta 69 (22), 5317–5331.

Anand, P., Elderfield, H., Conte, M.H., 2003. Calibration of Mg/Ca thermometry in planktonic foraminifera from a sediment trap time series. Paleoceanography 18 (2), 1–15.

Anderson, G.M., 2009. Thermodynamics of natural systems, 2nd ed. Cambridge University Press, Cambridge, 641 pp.

Anderson, R.F., 1987. Redox behavior of Uranium in an anoxic marine basin. Uranium 3 (2-4), 145–164.

Anderson, R.F., Fleisher, M.Q., LeHuray, A.P., 1989. Concentration, oxidation state, and particulate flux of uranium in the Black Sea. Geochimica et Cosmochimica Acta 53 (9), 2215–2224.

Anderson, T.F., Pratt, L.M., 1995. Isotopic Evidence for the Origin of Organic Sulfur and Elemental Sulfur in Marine Sediments, in: , Geochemical Transformations of Sedimentary Sulfur, vol. 612. American Chemical Society, pp. 378-396.

Anderson, T.F., Raiswell, R., 2004. Sources and mechanisms for the enrichment of highly reactive iron in euxinic Black Sea sediments. American Journal of Science 304 (3), 203–233.

Andreae, M.O., 1978. Distribution and speciation of arsenic in natural waters and some marine algae. Deep Sea Research 25 (4), 391–402.

Arias, Y.M., Tebo, B.M., 2003. Cr(VI) Reduction by Sulfidogenic and Nonsulfidogenic Microbial Consortia. Applied and Evironmental Microbiology 69 (3), 1847–1853.

Arnaboldi, M., Meyers, P.A., 2006. Geochemical composition of ODP Site 210-1276 shales: Supplement to: Arnaboldi, Michela; Meyers, Philip A (2006): Data report: Multiproxy geochemical characterization of OAE-related black shales at Site 1276, Newfoundland Basin. In: Tucholke, BE; Sibuet, J-C; Klaus, A (eds.) Proceedings of the Ocean Drilling Program, Scientific Results, College Station, TX (Ocean Drilling Program), 210, 1-16

Arthur, M.A., Sageman, B.B., 1994. Marine Black Shales - Depositional Mechanism and Environments of Ancient Deposits. Annual Review of Earth and Planetary Sciences 22, 499–551.

Arthur, M.A., Schlanger, S.O., 1979. Cretaceous ' oceanic anoxic events' as causal factors in development of reef-reservoired giant oil fields. American Association of Petroleum Geologists, Bulletin 63 (6), 870–885.

Ashckenazi-Polivoda, S., 2011. The Late Cretaceous Southern Tethyan Upwelling System: A Case Study from the High Productivity Sequence, Negev, Israel. Dissertation, Beer Sheva, 185pp.

Ashckenazi-Polivoda, S., Abramovich, S., Almogi-Labin, A., Schneider-Mor, A., Feinstein, S., Püttmann, W., Berner, Z., 2011. Paleoenvironments of the latest Cretaceous oil shale sequence, Southern Tethys, Israel, as an integral part of the prevailing upwelling system. Palaeogeography, Palaeoclimatology, Palaeoecology 305 (1-4), 93–108.

Ashckenazi-Polivoda, S., Edelman-Furstenberg, Y., Almogi-Labin, A., Benjamini, C., 2010. Characterization of lowest oxygen environments within ancient upwelling environments: Benthic foraminifera assemblages. Palaeogeography, Palaeoclimatology, Palaeoecology 289 (1-4), 134–144.

Atwater, T., 1970. Implications of Plate Tectonics for the Cenozoic Tectonic Evolution of Western North America. Geological Society of America Bulletin 81 (12), 3513–3536.

Baioumy, H., 2010. Sulfur geochemistry of Jurassic high-sulfur coals from Egypt. Chemie der Erde 70 (1), 61–67.

Baioumy, H., Attia, A.E.-K., Boulis, S., Hassan, M., Helmy, M., 2003. Rock composition and origin of late Cretaceous shales in the Duwi Formation, Upper Egypt. Journal of Mineralogical and Petrological Science 98, 76–86.

Baioumy, H., Tada, R., 2005. Origin of Late Cretaceous phosphorites in Egypt. Cretaceous Research 26 (2), 261–275.

Baioumy, H.M., 2007. Iron-phosphorus relationship in the iron and phosphorite ores of Egypt. Chemie der Erde 67 (3), 229–239.

Baioumy, H.M., Ismael, I.S., 2010. Factors controlling the compositional variations among the marine and non-marine black shales from Egypt. International Journal of Coal Geology 83 (1), 35–45.

Bakun, A., 1990. Global Climate Change and Intensification of Coastal Ocean Upwelling. Science (247), 198–201.

Banner, J.L., Hanson, G.N., 1990. Calculation of simultaneous isotopic and trace element variations during water-rock interaction with applications to carbonate diagenesis. Geochimica et Cosmochimica Acta 54 (11), 3123–3137.
Baraboshkin, E.Y., 2009. Condensed sections: Terminology, types, and accumulation conditions. Moscow Univ. Geol. Bull. 64 (3), 153-160.
Barker, S., Cacho, I., Benway, H., Tachikawa, K., 2005. Planktonic foraminiferal Mg/Ca as a proxy for past oceanic temperatures: a methodological overview and data compilation for the Last Glacial Maximum: Multiproxy Approach for the Reconstruction of the Glacial Ocean surface. Quaternary Science Reviews 24 (7–9), 821–834.
Barker, S., Greaves, M., Elderfield, H., 2003. A study of cleaning procedures used for foraminiferal Mg/Ca paleothermometry. Geochemistry, Geophysics, Geosystems 9 (4), 1–20.
Barnes, C.E., Cochran, J.K., 1993. Uranium geochemistry in estuarine sediments: Controls on removal and release processes. Geochimica et Cosmochimica Acta 57 (3), 555–569.
Barrera, E., Savin, S.M., 1999. Evolution of late Campanian-Maastrichtian marine climates and oceans, in: , Geologogical Society of America Special Papers, pp. 245–282.
Barrie, A., Prosser, S.J., 1996. Automated analysis of light-element stable isotopes by isotope ratio mass spectrometry. Mass spectrometry of soils. New York, Marcel Dekker, 1–46.
Barron, J.A., Bukry, D., Bischoff, J.L., 2004. High resolution paleoceanography of the Guaymas Basin, Gulf of California, during the past 15000 years. Marine Micropaleontology 50 (3-4), 185–207.
Barwise, A.J.G., 1990. Role of nickel and vanadium in petroleum classification: Energy & Fuels. Energy & Fuels 4 (6), 647–652.
Basaham, A.S., El-Sayed, M.A., 1998. Distribution and Phase Association of Some Major and Trace Elements in the Arabian Gulf Sediments. Estuarine, Coastal and Shelf Science 46 (2), 185–194.
Beckmann, B., Flogel, S., Hofmann, P., Schulz, M., Wagner, T., 2005a. Orbital forcing of Cretaceous river discharge in tropical Africa and ocean response. Nature 437 (7056), 241–244.
Beckmann, B., Wagner, T., Hofmann, P., 2005b. Linking Coniacian–Santonian (OAE3) black-shale deposition to African climate variability: a reference section from the eastern tropical Atlantic at orbital time scales (ODP site 959, off Ivory Coast and Ghana). SEPM Special Publication 82 (3), 125–143.
Bein, A., Almogi-Labin, A., Sass, E., 1990. Sulfur sinks and organic carbon relationships in Cretaceous organic-rich carbonates; implications for evaluation of oxygen-poor depositional environments. American Journal of Science 290 (8), 882–911.
Bentov, S., Brownlee, C., Erez, J., 2009. The role of seawater endocytosis in the biomineralization process in calcareous foraminifera. Proceedings of the National Academy of Sciences 106 (51), 21500–21504.
Berger, W.H., Wefer, G., 2002. On the reconstruction of upwelling history: Namibia upwelling in context. Marine Geology 180 (1–4), 3–28.
Berner, R.A., 1970. Sedimentary pyrite formation. American Journal of Science 268 (1), 1–23.
Berner, R.A., 1980. Early diagenesis: a theoretical approach. Princeton University Press, New Jersey.
Berner, R.A., 1984. Sedimentary pyrite formation: An update. Geochimica et Cosmochimica Acta 48 (4), 605–615.
Berner, R.A., Raiswell, R., 1983. Burial of organic carbon and pyrite sulfur in sediments over phanerozoic time: a new theory. Geochimica et Cosmochimica Acta 47 (5), 855–862.
Berner, R.A., Raiswell, R., 1984. C/S method for distinguishing freshwater from marine sedimentary rocks. Geology 12 (6), 365–368.
Berner, Z.A., Puchelt, H., Nöltner, T., Kramar, U., 2013. Pyrite geochemistry in the Toarcian Posidonia Shale of south-west Germany: Evidence for contrasting trace-element patterns of diagenetic and syngenetic pyrites. Sedimentology 60 (2), 548–573.
Bernhard, J.M., Edgcomb, V.P., Casciotti, K.L., McIlvin, M.R., Beaudoin, D.J., 2012. Denitrification likely catalyzed by endobionts in an allogromiid foraminifer. ISME J 6 (5), 951–960.
Bian, N., Martin, P.A., 2010. Investigating the fidelity of Mg/Ca and other elemental data from reductively cleaned planktonic foraminifera. Paleoceanography 25 (2), PA2215.
Bierens Haan, S. de, 1991. A review of the rate of pyrite oxidation in aqueous systems at low temperature. Earth-Science Reviews 31 (1), 1–10.
Billups, K., Schrag, D.P., 2002. Paleotemperatures and ice volume of the past 27 Myr revisited with paired Mg/Ca and $^{18}O/^{16}O$ measurements on benthic foraminifera. Paleoceanography 17 (1), 3-1-3-11.
Birkeland, P.W., 1984. Soils and geomorphology. Oxford University Press New York.
Bjerrum, C.J., Bendtsen, J., Legarth, J.J.F., 2006. Modeling organic carbon burial during sea level rise with reference to the Cretaceous. Geochemistry, Geophysics, Geosystems 7 (5), Q05008.

Blanchet, C.L., Thouveny, N., Vidal, L., 2009. Formation and preservation of greigite (Fe3S4) in sediments from the Santa Barbara Basin: Implications for paleoenvironmental changes during the past 35 ka. Paleoceanography 24 (2), 1–15.

Bodin, S., Godet, A., Föllmi, K.B., Vermeulen, J., Arnaud, H., Strasser, A., Fiet, N., Adatte, T., 2006. The late Hauterivian Faraoni oceanic anoxic event in the western Tethys: Evidence from phosphorus burial rates: Causes and Consequence of Marine Organic Carbon Burial Through Time. Palaeogeography, Palaeoclimatology, Palaeoecology 235 (1-3), 245–264.

Bohlen, L., Dale, A.W., Sommer, S., Mosch, T., Hensen, C., Noffke, A., Scholz, F., Wallmann, K., 2011. Benthic nitrogen cycling traversing the Peruvian oxygen minimum zone. Geochimica et Cosmochimica Acta 75 (20), 6094–6111.

Bolle, M.-P., Adatte, T., 2001. Palaeocene-early Eocene climatic evolution in the Tethyan realm: clay mineral evidence. Clay Minerals 36 (2), 249–261.

Böning, P., Brumsack, H.-J., Schnetger, B., Grunwald, M., 2009. Trace element signatures of Chilean upwelling sediments at ~36°S. Marine Geology 259 (1–4), 112–121.

Böning, P., Cuypers, S., Grunwald, M., Schnetger, B., Brumsack, H.-J., 2005. Geochemical characteristics of Chilean upwelling sediments at ~36°S. Marine Geology 220 (1–4), 1–21.

Bontognali,, T.R.R., Vasconcelos, C., Warthmann, R., Bernasconi, S.M., Dupraz, C., Strohmenger, C.J., McKenzie, J.A., 2010. Dolomite formation within microbial mats in the coastal sabkha of Abu Dhabi (United Arab Emirates). Sedimentology 57 (3), 824–844.

Boonchayaanant, B., Nayak, D., Du, X., Criddle, C.S., 2009. Uranium reduction and resistance to reoxidation under iron-reducing and sulfate-reducing conditions. Water Research 43 (18), 4652–4664.

Borchers, S.L., Schnetger, B., Böning, P., Brumsack, H.J., 2005. Geochemical signatures of the Namibian diatom belt: Perennial upwelling and intermittent anoxia. Geochemistry, Geophysics, Geosystems 6 (6), 1–20.

Bornemann, A., Norris, R.D., Friedrich, O., Beckmann, B., Schouten, S., Damsté, J.S.S., Vogel, J., Hofmann, P., Wagner, T., 2008. Isotopic evidence for glaciation during the cretaceous supergreenhouse. Science 319 (5860), 189–192.

Böttcher, M.E., Lepland, A., 2000. Biogeochemistry of sulfur in a sediment core from the west-central Baltic Sea: Evidence from stable isotopes and pyrite textures. Journal of Marine Systems 25 (3-4), 299–312.

Böttcher, M.E., Schale, H., Schnetger, B., Wallmann, K., Brumsack, H.-J., 2000. Stable sulfur isotopes indicate net sulfate reduction in near-surface sediments of the deep Arabian Sea. Deep Sea Research Part II: Topical Studies in Oceanography 47 (14), 2769–2783.

Böttcher, M.E., Thamdrup, B., 2001. Anaerobic sulfide oxidation and stable isotope fractionation associated with bacterial sulfur disproportionation in the presence of MnO_2. Geochimica et Cosmochimica Acta 65 (10), 1573–1581.

Bottrell, S.H., Coulson, J.P., 2003. Preservation of environmental sulfur isotope records in maritime peats: a test of baseline pre-anthropogenic signal and diagenetic effects in a mid-Pleistocene peat. Chemical Geology 201 (3-4), 185–190.

Boyle, E.A., 1981. Cadmium, Zinc, Copper and Barium in foraminifera tests. Earth and Planetary Science Letters 53 (1), 11–35.

Boyle, E.A., Keigwin, L.D., 1985. Comparison of Atlantic and Pacific paleochemical records for the last 215,000 years: changes in deep ocean circulation and chemical inventories. Earth and Planetary Science Letters 76 (1–2), 135–150.

Boyle, E.A., Labeyrie, L., Duplessly, J.-C., 1995. Calcitic Foraminiferal Data Confirmed by Cadmium in Aragonitic Hoeglundina: Application to the Last Glacial Maximum in the Northern Indian Ocean. Paleoceanography 10 (5), 881–900.

Bralower, T.J., Thierstein, H.R., 1984. Low productivity and slow deep-water circulation in mid-Cretaceous oceans. Geology 12 (10), 614–618.

Bralower, T.J., Thierstein, H.R., 1987. Organic carbon and metal accumulation rates in Holocene and mid-Cretaceous sediments: palaeoceanographic significance. Geological Society, London, Special Publications 26 (1), 345–369.

Brand, U., Veizer, J., 1980. Chemical Diagenesis of a Multicomponent Carbonate System--1: Trace Elements. Journal of Sedimentary Petrology 50 (4), 1219–1236.

Branson, O., Redfern, Simon A. T., Tyliszczak, T., Sadekov, A., Langer, G., Kimoto, K., Elderfield, H., 2013. The coordination of Mg in foraminiferal calcite. Earth and Planetary Science Letters 383 (0), 134–141.

Breit, G.N., Wanty, R.B., 1991. Vanadium accumulation in carbonaceous rocks: A review of geochemical controls during deposition and diagenesis: Trace Metals in Petroleum Geochemistry. Chemical Geology 91 (2), 83–97.

Brock, J.C., McClain, C.R., 1992. Interannual variability in phytoplankton blooms observed in the northwestern Arabian Sea during the southwest monsoon. Journal of Geophysical Research: Oceans 97 (C1), 733–750.
Brown, S.J., Elderfield, H., 1996. Variations in Mg/Ca and Sr/Ca ratios of planktonic foraminifera caused by postdepositional dissolution: Evidence of shallow Mg-dependent dissolution. Paleoceanography 11 (5), 543–551.
Browning, J.V., Miller, K.G., Sugarman, P.J., Kominz, M.A., McLaughlin, P.P., Kulpecz, A.A., Feigenson, M.D., 2008. 100Myr record of sequences, sedimentary facies and sea level change from Ocean Drilling Program onshore coreholes, US Mid-Atlantic coastal plain. Basin Research 20 (2), 227–248.
Brüchert, V., 2004. Physiological and ecological aspects of sulfur isotope fractionation during bacterial sulfate reduction, in: Amend, J.P., Edwards, K.J., Lyons, T.W. (Eds.), Sulfur Biogeochemistry—Past and Present, pp. 1–16.
Brüchert, V., Jørgensen, B.B., Neumann, K., Riechmann, D., Schlösser, M., Schulz, H., 2003. Regulation of bacterial sulfate reduction and hydrogen sulfide fluxes in the central namibian coastal upwelling zone. Geochimica et Cosmochimica Acta 67 (23), 4505–4518.
Brüchert, V., Pérez, M.E., Lange, C.B., 2000. Coupled primary production, benthic foraminiferal assemblage, and sulfur diagenesis in organic-rich sediments of the Benguela upwelling system. Marine Geology 163 (1-4), 27–40.
Brüchert, V., Pratt, L.M., 1996. Contemporaneous early diagenetic formation of organic and inorganic sulfur in estuarine sediments from St. Andrew Bay, Florida, USA. Geochimica et Cosmochimica Acta 60 (13), 2325–2332.
Bruland, K.W., 1980. Oceanographic Distributions of Cadmium. Zinc, Nickel, and Copper in the North Pacific. Earth and Planetary Science Letters 47 (2), 176–198.
Bruland, K.W., Lohan, M., 2004. Controls of Trace Metals in Seawater, in: Holland, H.D., Turekian, K.K., Elderfield, H. (Eds.), Treatise on Geochemistry. Volume 6: The Oceans and Marine Geochemistry, vol. 6. Elsevier, Amsterdam, pp. 23–47.
Bruland, K.W., Rue, E.L., Smith, G.J., 2001. Iron and Macronutrients in California Coastal Upwelling Regimes: Implications for Diatom Blooms. Limnology and Oceanography 46 (7), 1661–1674.
Brumsack, H., 1989. Geochemistry of recent TOC-rich sediments from the Gulf of California and the Black Sea. Geologische Rundschau 78, 851–882.
Brumsack, H.-J., 2006. The trace metal content of recent organic carbon-rich sediments: Implications for Cretaceous black shale formation. Palaeogeography, Palaeoclimatology, Palaeoecology 232 (2-4), 344–361.
Bryan, S.P., Marchitto, T.M., 2008. Mg/Ca-temperature proxy in benthic foraminifera: New calibrations from the Florida Straits and a hypothesis regarding Mg/Li. Paleoceanography 23 (2), 2–17.
Bryan, S.P., Marchitto, T.M., 2010. Testing the utility of paleonutrient proxies Cd/Ca and Zn/Ca in benthic foraminifera from thermocline waters. Geochemistry, Geophysics, Geosystems 11.
Burdige, D.J., 2006. Geochemistry of marine sediments. Princeton University Press, Princeton, NJ, 609 pp.
Butler, I.B., Rickard, D., 2000. Framboidal pyrite formation via the oxidation of iron (II) monosulfide by hydrogen sulphide. Geochimica et Cosmochimica Acta 64 (15), 2665–2672.
Calvert, E.S., Karlin, R.E., 1991. Relationships between sulphur, organic carbon, and iron in the modern sediments of the Black Sea. Geochimica et Cosmochimica Acta 55 (9), 2483–2490.
Calvert, E.S., Pedersen, T.F., 1993. Geochemistry of Recent oxic and anoxic marine sediments: Implications for the geological record: Marine Sediments, Burial, Pore Water Chemistry, Microbiology and Diagenesis. Marine Geology 113 (1-2), 67–88.
Calvert, E.S., Pedersen, T.F., 2007. Elemental proxies for paleoclimatic and paleooceanographic variability in marine sediments: Interpretation and application, in: Claude Hillaire–Marcel and Anne De Vernal (Ed.), Developments in Marine Geology : Proxies in Late Cenozoic Paleoceanography, 1st ed. Elsevier, pp. 568–625.
Calvert, E.S., Thode, H.G., Yeung, D., Karlin, R.E., 1996. A stable isotope study of pyrite formation in the Late Pleistocene and Holocene sediments of the Black Sea: Papers Originating from a Workshop on “The Formation of the Earth's Core”. Geochimica et Cosmochimica Acta 60 (7), 1261–1270.
Camoin, G., Bellion, Y., Dercourt, J., Guiraud, R., Lucas, J., Poisson, A., Ricou, L.E.a.V., 1993. Late Maastrichtian (69.5 to 65 Ma), in: Dercourt, J., Ricou, L.E., and Vrielynck B. (Eds.), Atlas Tethys Palaeoenvironmental Maps. Explanatory Notes. Gauthier-Villairs, Paris, pp. 179–196.
Campillo-Campbell, C., Gordoa, A., 2004. Physical and biological variability in the Namibian upwelling system: October 1997–October 2001. Views of Ocean Processes from the Sea-viewing Wide Field-of-view Sensor (SeaWiFS) Mission: Volume 1 51 (1–3), 147–158.
Canfield, D.E., 1989. Reactive iron in marine sediments. Geochimica et Cosmochimica Acta 53 (3), 619–632.

Canfield, D.E., 1994. Factors influencing organic carbon preservation in marine sediments. Chemical Geology 114 (3-4), 315–329.
Canfield, D.E., 2001. Biogeochemistry of Sulfur Isotopes. Reviews in Mineralogy and Geochemistry 43 (1), 607–636.
Canfield, D.E., Desmarais, D.J., 1991. Aerobic Sufate Reduction in Microbial Mats. Science 251 (5000), 1471–1473.
Canfield, D.E., Farquhar, J., Zerkle, A.L., 2010. High isotope fractionations during sulfate reduction in a low-sulfate euxinic ocean analog. Geology 38 (5), 415–418.
Canfield, D.E., Lyons, T.W., Raiswell, R., 1996. A model for iron deposition to euxinic Black Sea sediments. American Journal of Science 296 (7), 818–834.
Canfield, D.E., Raiswell, R., Bottrell, S.H., 1992. The reactivity of sedimentary iron minerals toward sulfide. American Journal of Science 292 (9), 659–683.
Canfield, D.E., Raiswell, R., Westrich, J.T., Reaves, C.M., Berner, R.A., 1986. The use of chromium reduction in the analysis of reduced inorganic sulfur in sediments and shales. Chemical Geology 54 (1-2), 149–155.
Canfield, D.E., Thamdrup, B., 1994. The production of ^{34}S-depleted sulfide during bacterial disproportionation of elemental sulfur. Science 266 (5193), 1973–1975.
Canfield, D.E., Thamdrup, B., Fleischer, S., 1998. Isotope fractionation and sulfur metabolism by pure and enrichment cultures of elemental sulfur-disproportionating bacteria. Limnology and Oceanography 43 (2), 253–264.
Caplan, M.L., Bustin, R.M., 1996. Factors governing organic matter accumulation and preservation in a marine petroleum source rock from the Upper Devonian to Lower Carboniferous Exshaw Formation, Alberta. Bulletin of Canadian Petroleum Geology 44 (3), 474–494.
Carpenter, S.J., Lohmann, K.C., 1992. Sr/Mg ratios of modern marine calcite: Empirical indicators of ocean chemistry and precipitation rate. Geochimica et Cosmochimica Acta 56 (5), 1837–1849.
Carr, M.-E., 2003. Production regimes in four eastern boundary current systems. Deep Sea Research Part II: Topical Studies in Oceanography 50, 3199–3221.
Chaillou, G., Schäfer, J., Blanc, G., Anschutz, P., 2008. Mobility of Mo, U, As, and Sb within modern turbidites. Marine Geology 254 (3–4), 171–179.
Challands, T.J., Armstrong, H.A., Maloney, D.P., Davies, J.R., Wilson, D., Owen, A.W., 2009. Organic-carbon deposition and coastal upwelling at mid-latitude during the Upper Ordovician (Late Katian): A case study from the Welsh Basin, UK. Organic-carbon-rich sediments through the Phanerozoic: Processes, progress, and perspectives 273 (3–4), 395–410.
Chamley, H., 1989. Clay sedimentology. Springer-Verlag New York, 623 pp.
Chen, B., Shan, X., Shen, D.-q., Mou, S.-f., 1997. Nature of the HCl-soluble sulfate in the sequential extraction for sulfur speciation in soils. Fresenius' Journal of Analytical Chemistry 357 (7), 941–945.
Claypool, G.E., Holser, W.T., Kaplan, I.R., Sakai, H., Zak, I., 1980. The age curves of sulfur and oxygen isotopes in marine sulfate and their mutual interpretation. Chemical Geology 28, 199–260.
Cléroux, C., Cortijo, E., Anand, P., Labeyrie, L., Bassinot, F., Caillon, N., Duplessy, J.-C., 2008. Mg/Ca and Sr/Ca ratios in planktonic foraminifera: Proxies for upper water column temperature reconstruction. Paleoceanography 23 (3).
Coale, K.H., Bruland, K.W., 1988. Copper complexation in the Northeast Pacific. Limnology and Oceanography 33 (5), 1084–1101.
Cook, A.C., Sherwood, N.R., 1991. Classification of oil shales, coals and other organic-rich rocks. Organic Geochemistry 17 (2), 211–222.
Cornwell, J.C., Morse, J.W., 1987. The characterization of iron sulfide minerals in anoxic marine sediments: IX International Symposium on the Chemistry of the Mediterranean. Marine Chemistry 22 (2-4), 193–206.
Costello, A.B., Osborne, J.W., 2007. Best Practices in Exploratory Factor Analysis: Four Recommendations for Getting the Most From Your Analysis. Practical Assessment Research & Evaluation 10 (7), 1–8.
Cowie, G., 2005. The biogeochemistry of Arabian Sea surficial sediments: A review of recent studies. The Arabian Sea of the 1990s: New Biogeochemical Understanding 65 (2–4), 260–289.
Cranston, R.E., 1983. Chromium in Cascadia Basin, northeast Pacific Ocean. Marine Chemistry 13 (2), 109–125.
Creech, J.B., Baker, J.A., Hollis, C.J., Morgans, H.E.G., Smith, E.G.C., 2010. Eocene sea temperatures for the mid-latitude southwest Pacific from Mg/Ca ratios in planktonic and benthic foraminifera. Earth and Planetary Science Letters 299 (3–4), 483–495.
Cronin, T.M., 1999. Principles of paleoclimatology. Columbia University Press, New York, xiii, 560.
Crusius, J., Thomson, J., 2000. Comparative behavior of authigenic Re, U, and Mo during reoxidation and subsequent long-term burial in marine sediments. Geochimica et Cosmochimica Acta 64 (13), 2233–2242.

Cuhel, R.L., Taylor, C.D., Jannasch, H.W., 1981. Assimilatory sulfur metabolism in marine microorganisms: characteristics and regulation of sulfate transport in Pseudomonas halodurans and Alteromonas luteo-violaceus. Journal of Bacteriology 147 (2), 340–349.
Cutter, G.A., Cutter, L.S., 1995. Behavior of dissolved antimony, arsenic, and selenium in the Atlantic Ocean. IOC Contaminants Baseline Study 49 (4), 295–306.
Cutter, G.A., Kluckhohn, R.S., 1999. The cycling of particulate carbon, nitrogen, sulfur, and sulfur species (iron monosulfide, greigite, pyrite, and organic sulfur) in the water columns of Framvaren Fjord and the Black Sea. Marine Chemistry 67 (3-4), 149–160.
Darvishzad, B., Abdolalipour, S., 2009. Campanian and Maastrichtian Biostratigraphy and Paleoenvironment in Jorband Section, North of Iran. Journal of Sciences, Islamic Republic of Iran 20 (1), 23–39.
Davis, C., Pratt, L.M., Sliter, W.V., Mompart, L., Murat, B., 1999. Factors influencing organic carbon and trace metal accumulation in the Upper Cretaceous La Luna Formation of the western Maracaibo Basin, Venezuela 332, 203–230.
Davis, S.J., Gibbs, C.F., 1975. The effect of weathering on a crude oil residue exposed at sea. Water Research 9 (3), 275–285.
de Leeuw, J.W., Sinninghe Damsté, J.S., 1990. Organic Sulfur Compounds and Other Biomarkers as Indicators of Palaeosalinity, in: , Geochemistry of Sulfur in Fossil Fuels, vol. 429. American Chemical Society, pp. 417-443.
Dean, W.E., 2007. Sediment geochemical records of productivity and oxygen depletion along the margin of western North America during the past 60,000 years: teleconnections with Greenland Ice and the Cariaco Basin. Quaternary Science Reviews 26 (1–2), 98–114.
Dean, W.E., Arthur, M.A., 1987. Inorganic and organic geochemistry of Eocene to Cretaceous strata recovered from the lower continental rise, North American Basin, Site 603, Deep Sea Drilling Project Leg 93. Initial Reports of the Deep Sea Drilling Project 93, 1093–1137.
Dean, W.E., Arthur, M.A., 1998. Geochemical expressions of cyclicity in Cretaceous pelagic limestone sequences: Niobrara Formation, Western Interior Seaway. Stratigraphy and Paleoenvironments of the Cretaceous Western Interior Seaway, USA: SEPM, Concepts in Sedimentology and Paleontology 6, 227–255.
Dean, W.E., Arthur, M.A., Claypool, G.E., 1986. Depletion of ^{13}C in Creatceous marine organic matter , source, diagenetic, or envrionmental signal? Marine Geology 70 (1-2), 119–157.
Deconinck, J.F., Chamley, H., 1995. Diversity of smectite origins in Late Cretaceous sediments: example of chalks from northern France. Clay Minerals 30 (4), 365–380.
Dehairs, F., Chesselet, R., Jedwab, J., 1980. Discrete suspended particles of barite and the barium cycle in the open ocean. Earth and Planetary Science Letters 49 (2), 528–550.
Demaison, G.J., Moore, G.T., 1980. Anoxic environments and oil source bed genesis. Organic Geochemistry 2 (1), 9–31.
Dercourt, J., Ricou, L.E., and Vrielynck B. (Eds.), 1993. Atlas Tethys Palaeoenvironmental Maps: Explanatory Notes. Gauthier-Villairs, Paris.
D'Hondt, S., Zachos, J.C., 1998. Cretaceous foraminifera and the evolutionary history of planktic photosymbiosis. Paleobiology 24 (4), 512–523.
Diaz, R., Moreira, M., Mendoza, U., Machado, W., Böttcher, M.E., Santos, H., Belém, A., Capilla, R., Escher, P., Albuquerque, A.L., 2012. Early diagenesis of sulfur in a tropical upwelling system, Cabo Frio, southeastern Brazil. Geology 40 (10), 879–882.
Diener, A., 2012. Structural Incorporation of Selenium into Pyrite and Mackinawite. Dissertation, Karlsruhe, 128 pp.
Diester-Haass, L., Schrader, H.-J., 1979. Neogene coastal upwelling history off northwest and southwest Africa. Marine Geology 29 (1-4), 39–53.
Dinur, D., Spiro, B., Aizenshtat, Z., 1980. The distribution and isotopic composition of sulfur in organic-rich sedimentary rocks. Chemical Geology 31, 37–51.
Donahue, M.A., Werne, J.P., Meile, C., Lyons, T.W., 2008. Modeling sulfur isotope fractionation and differential diffusion during sulfate reduction in sediments of the Cariaco Basin. Geochimica et Cosmochimica Acta 72 (9), 2287–2297.
Doney, S.C., Ruckelshaus, M., Emmett Duffy, J., Barry, J.P., Chan, F., English, C.A., Galindo, H.M., Grebmeier, J.M., Hollowed, A.B., Knowlton, N., Polovina, J., Rabalais, N.N., Sydeman, W.J., Talley, L.D., 2012. Climate Change Impacts on Marine Ecosystems. Annual Review of Marine Science 4 (1), 11–37.
Douglas, R., Staines-Urias, F., 2007. Dimorphism, shell Mg/Ca ratios and stable isotope content in species of Bolivina (benthic foraminifera) in the Gulf of California, Mexico. Journal of Foraminiferal Research 37 (3), 189–203.
Drews, G., 2010. Stoffwechselzyklen in Prokaryoten- Gesellschaften. Naturwissenschaftliche Rundschau 63 (6), 285–295.

Dumitrescu, M., Brassell, S.C., 2006. Compositional and isotopic characteristics of organic matter for the early Aptian Oceanic Anoxic Event at Shatsky Rise, ODP Leg 198: Causes and Consequence of Marine Organic Carbon Burial Through Time "Black Shales and Sapropels", "Organic-Carbon Burial and Rapid Climate Change". Palaeogeography, Palaeoclimatology, Palaeoecology 235 (1–3), 168–191.

Dybek, J., 1973. Zur Geochemien und Lagerstättenkunde des Urans, in: Borchert, H. (Ed.), Clausthaler Hefte zur Lagerstättenkunde und Geochemie der mineralischen Rohostoffe, vol. 1, 1st ed. Borntraeger, Berlin - Stuttgart, pp. 182.

Dyni, J.R., 2003. Geology and resources of some world oil-shale deposits. Oil Shale 20 (3), 193–252.

Dyni, J.R., 2004. Oil Shale, in: Cutler J. Cleveland (Ed.), Encyclopedia of Energy. Elsevier, New York, pp. 739–752.

Edelman-Furstenberg, Y., 2009. Cyclic upwelling facies along the Late Cretaceous southern Tethys (Israel): taphonomic and ichnofacies evidence of a high-productivity mosaic. Cretaceous Research 30 (4), 847–863.

Eggins, S., Deckker, P. de, Marshall, J., 2003. Mg/Ca variation in planktonic foraminifera tests: implications for reconstructing palaeo-seawater temperature and habitat migration. Earth and Planetary Science Letters 212 (3–4), 291–306.

Eggins, S.M., Sadekov, A., Deckker, P. de, 2004. Modulation and daily banding of Mg/Ca in Orbulina universa tests by symbiont photosynthesis and respiration: a complication for seawater thermometry? Earth and Planetary Science Letters 225 (3–4), 411–419.

Eglinton, T.I., Irvine, J.E., Vairavamurthy, A., Zhou, W., Manowitz, B., 1994. Formation and diagenesis of macromolecular organic sulfur in Peru margin sediments. Organic Geochemistry 22 (3–5), 781–799.

Eicher, D.L., Worstell, P., 1970. Cenomanian and Turonian Foraminifera from the Great Plains, United States. Micropaleontology 16 (3), 269–324.

Einsele, G., 2000. Sedimentary basins: evolution, facies, and sediment budget, 2nd ed. Springer, Berlin, New York, Heidelberg, Amsterdam.

El Beialy, Salah Y., 1995. Campanian-Maastrichtian palynomorphs from the Duwi (Phosphate) Formation of the Hamrawein and Umm El Hueitat mines, Red Sea Coast, Egypt. Review of Palaeobotany and Palynology 85 (3–4), 303–317.

El-Azabi, M.H., Farouk, S., 2011. High-resolution sequence stratigraphy of the Maastrichtian-Ypresian succession along the eastern scarp face of Kharga Oasis, southern Western Desert, Egypt. Sedimentology 58 (3), 579–617.

Elderfield, H., Bertram, C.J., Erez, J., 1996. A biomineralization model for the incorporation of trace elements into foraminiferal calcium carbonate. Earth and Planetary Science Letters 142 (3–4), 409–423.

Elderfield, H., Ganssen, G., 2000. Past temperature and $\delta^{18}O$ of surface ocean waters inferred from foraminiferal Mg/Ca ratios. Nature 405 (6785), 442–445.

El-Sabagh, S.M., Basta, J.S., Ahmed, F.S., Barakat, M.A., 2000. Characterization of Selected Egyptian Oil Shales from the Red Sea Area: Composition of Inorganic Matrix and Potential of Organic Matters. Energy Sources, Part A: Recovery, Utilization, and Environmental Effects 22 (10), 901–911.

Emeis, K.-C., Brüchert, V., Currie, B., Endler, R., Ferdelman, T., Kiessling, A., Leipe, T., Noli-Peard, K., Struck, U., Vogt, T., 2004. Shallow gas in shelf sediments of the Namibian coastal upwelling ecosystem. Continental Shelf Research 24 (6), 627–642.

Emeis, K.-C., Morse, J.W., 1990. Organic chemistry of sediments of the Peru margin: Supplement to: Emeis, Kay-Christian; Morse, John W (1990): Organic carbon, reduced sulfur, and iron relationships in sediments of the Peru margin, sites 680 and 688. In: Suess, E; von Huene, R; et al. (eds.), Proceedings of the Ocean Drilling Program, Scientific Results, College Station, TX (Ocean Drilling Program), 112, 441-453

Emeis, K.-C., Morse, J.W., 1993. Carbon and Sulphur concentrations of sediments from Peru, Oman and Benguela upwelling environments: Supplement to: Emeis, Kay-Christian; Morse, John W (1993): Zur Systematik der Kohlenstoff-Schwefel-Eisen-Verhältnisse in Auftriebssedimenten. Geologische Rundschau, 82(4), 604-618, Geologische Rundschau 82 (4), 604–618.

Emeis, K.-C., Morse, J.W., Mays, L.L., 1991. Organic carbon, reduced sulfur, and iron in Miocene to Holocene sediments from the Oman and Beguela upwelling systems: Supplement to: Emeis, Kay-Christian; Morse, John W; Mays, Linda L (1991): Organic carbon, reduced sulfur, and iron in Miocene to Holocene upwelling sediments from the Oman and Benguela upwelling systems. In: Prell, WL; Niitsuma, N; et al. (eds.), Proceedings of the Ocean Drilling Program, Scientific Results, College Station, TX (Ocean Drilling Program), 117, 517-527

Emerson, S.R., Huested, S.S., 1991. Ocean anoxia and the concentrations of molybdenum and vanadium in seawater. Marine Chemistry 34 (3–4), 177–196.

Emiliani, C., 1955. Pleistocene Temperatures. The Journal of Geology 63 (6), 538–578.

Erbacher, J., Gerth, W., Schmiedl, G., Hemleben, C., 1998. Benthic foraminiferal assemblages of late Aptian-early Albian black shale intervals in the Vocontian Basin, SE France. Cretaceous Research 19 (6), 805–826.

Erbacher, J., Nelskamp, S., 2006. Comparison of benthic foraminifera inside and outside a sulphur-oxidizing bacterial mat from the present oxygen-minimum zone off Pakistan (NE Arabian Sea). Deep Sea Research Part I: Oceanographic Research Papers 53 (5), 751–775.

Erez, J., 2003. The source of ions for biomineralization in foraminifera and their implications for paleoceanographic proxies, in: Biomineralization. Mineralogical Society of America, Washington D.C., pp. 115–149.

Eshet, Y., Almogi-Labin, A., 1996. Calcareous nannofossils as paleoproductivity indicators in Upper Cretaceous organic-rich sequences in Israel. Marine Micropaleontology 29 (1), 37–61.

Eshet, Y., Almogi-Labin, A., Bein, A., 1994. Dinoflagellate cysts, paleoproductivity and upwelling systems: A Late Cretaceous example from Israel. Marine Micropaleontology 23 (3), 231–240.

Eshet, Y., Moshkovitz, S., Habib, D., Benjamini, C., Magaritz, M., 1992. Calcareous nannofossil and dinoflagellate stratigraphy across the Cretaceous/Tertiary boundary at Hor Hahar, Israel. Marine Micropaleontology 18 (3), 199–228.

Fairbanks, R.G., Matthews, R.K., 1978. The marine oxygen isotope record in Pleistocene coral, Barbados, West Indies. Quaternary Research 10 (2), 181–196.

Falasco, E., Bona, F., Badino, G., Hoffmann, L., Ector, L., 2009. Diatom teratological forms and environmental alterations: a review. Hydrobiologia 623 (1), 1-35.

Farrimond, P., Love, G.D., Bishop, A.N., Innes, H.E., Watson, D.F., Snape, C.E., 2003. Evidence for the rapid incorporation of hopanoids into kerogen. Geochimica et Cosmochimica Acta 67 (7), 1383–1394.

Faure, G., Mensing, T.M., 2005. Isotopes: Principles and applications, 3rd ed. Wiley, Hoboken, NJ, 897 pp.

Fendorf, S., Wielinga, B.W., Hansel, C.M., 2000. Chromium Transformations in Natural Environments: The Role of Biological and Abiological Processes in Chromium(VI) Reduction. International Geology Review 42 (8), 691–701.

Ferguson, J.E., Henderson, G.M., Kucera, M., Rickaby, R.E.M., 2008. Systematic change of foraminiferal Mg/Ca ratios across a strong salinity gradient. Earth and Planetary Science Letters 265 (1-2), 153–166.

Fhlaithearta, S.N., Reichart, G.-J., Jorissen, F.J., Fontanier, C., Rohling, E.J., Thomson, J., Lange, G.J. de, 2010. Reconstructing the seafloor environment during sapropel formation using benthic foraminiferal trace metals, stable isotopes, and sediment composition. Paleoceanography 25 (4), 1–17.

Fike, D.A., Finke, N., Zha, J., Blake, G., Hoehler, T.M., Orphan, V.J., 2009. The effect of sulfate concentration on (sub)millimeter-scale sulfide $\delta^{34}S$ in hypersaline cyanobacterial mats over the diurnal cycle. Geochimica et Cosmochimica Acta 73 (20), 6187–6204.

Filley, T.R., Freeman, K.H., Wilkin, R.T., Hatcher, P.G., 2002. Biogeochemical controls on reaction of sedimentary organic matter and aqueous sulfides in holocene sediments of Mud Lake, Florida. Geochimica et Cosmochimica Acta 66 (6), 937–954.

Fischer, G., Wefer, G., 1999. Use of proxies in paleoceanography: Examples from the South Atlantic. Springer, Berlin, 735 pp.

Föllmi, K.B., 1996. The phosphorus cycle, phosphogenesis and marine phosphate-rich deposits. Earth-Science Reviews 40 (1-2), 55–124.

Fossing, H., 1990. Sulfate reduction in shelf sediments in the upwelling region off Central Peru. Continental Shelf Research 10 (4), 355–367.

Fossing, H., Gallardo, V.A., Jørgensen, B.B., Huttel, M., Nielsen, L.P., Schulz, H., Canfield, D.E., Forster, S., Glud, R., Gundersen, J., Kuver, J., Ramsing, N.B., Teske, A., Thamdrup, B., Ulloa, O., 1995. Concentration and transport of nitrate by the mat forming bacterium Thioploca. Nature 374 (6524), 713–715.

Francois, R., 1987. A study of sulphur enrichment in the humic fraction of marine sediments during early diagenesis. Geochimica et Cosmochimica Acta 51 (1), 17–27.

Friedrich, O., 2005. Climatich changes in the Late Campanian - Early Maastrichtian: Micropaleontological and stable isotopic evidence from an epicontinental sea. The Journal of Foraminiferal Research 35 (3), 228–247.

Friedrich, O., 2009. Benthic foraminifera and their role to decipher paleoenvironment during mid-Cretaceous Oceanic Anoxic Events - the "anoxic benthic foraminifera" paradox. Revue de Micropaléontologie In Press, Corrected Proof.

Friedrich, O., Erbacher, J., 2006. Benthic foraminiferal assemblages from Demerara Rise (ODP Leg 207, western tropical Atlantic): possible evidence for a progressive opening of the Equatorial Atlantic Gateway. Cretaceous Research 27 (3), 377–397.

Friedrich, O., Erbacher, J., Moriya, K., Wilson, P.A., Kuhnert, H., 2008. Warm saline intermediate waters in the Cretaceous tropical Atlantic Ocean. Nature Geoscience 1 (7), 453–457.

Friedrich, O., Norris, R.D., Erbacher, J., 2012. Evolution of mid- to Late Cretaceous oceans—A 55 million year record of Earth's temperature and carbon cycle: GSA Data Repository 2012043.

Fry, B., Jannasch, H.W., Molyneaux, S.J., Wirsen, C.O., Muramoto, J.A., King, S., 1991. Stable isotope studies of the carbon, nitrogen and sulfur cycles in the Black Sea and the Cariaco Trench: Black Sea Oceanography: Results from the 1988 Black Sea Expedition. Deep Sea Research Part A. Oceanographic Research Papers 38, Supplement 2 (0), S1003 – S1019.

Fry, B., Silva, S.R., Kendall, C., Anderson, R.K., 2002. Oxygen isotope corrections for online $\delta^{34}S$ analysis. Rapid Communications in Mass Spectrometry 16 (9), 854–858.

Füchtbauer, H., Müller, G., 1988. Sediment-Petrologie: Sedimente und Sedimentgesteine, 3rd ed. E. Schweizerbart'sche Verlagsbuchhandlung, Stuttgart, Stuttgart, 1141 pp.

Ganssen, G., Sarnthein, M., 1983. Stable isotope composition of foraminifera: the surface and bottom waters record of coastal upwelling, in: Thiede, J., Suess, E. (Eds.), Sedimentary records of ancient coastal upwelling. Plenum Press, New York, pp. 99–121.

Garcia, D., Fonteilles, M., Moutte, J., 1994. Sedimentary fractionations between Al, Ti, and Zr and the genesis of strongly peraluminous granites. The Journal of Geology, 411–422.

Garfunkel, Z., 1988. The pre-Quaternary geology of Israel. Monographiae biologicae 62, 7–34.

Garfunkel, Z., 1989. Tectonic setting of phaneroozoic magmatism in Israel. Israel journal of earth-sciences 38 (2-4), 51–74.

Garreaud, R.D., Falvey, M., 2009. The coastal winds off western subtropical South America in future climate scenarios. Int. J. Climatol. 29 (4), 543–554.

Ghourchaei, S., Ghasemi-Nejad, E., Vahidinia, M., Ashouri, A., 2014. Paleoenvironmental reconstruction of the upper Cretaceous succession (Abtalkh Formation) of the Kopeh-Dagh Basin, northeastern Iran based on foraminiferal and palynological analyses. Arabian Journal of Geosciences, 1-16.

Gilles S. Odin, 2001. The Campanian-Maastrichtian stage boundary: Characterisation at Tercis les Bains (France) and correlation with Europe and other continents, 1st ed. Elsevier, Amsterdam, New York, 881 pp.

Gilly, W.F., Beman, J.M., Litvin, S.Y., Robison, B.H., 2013. Oceanographic and Biological Effects of Shoaling of the Oxygen Minimum Zone. Annual Review of Marine Science 5 (1), 17–49.

Giraudeau, J., Bailey, G.W., Pujol, C., 2000. A high-resolution time-series analyses of particle fluxes in the Northern Benguela coastal upwelling system: carbonate record of changes in biogenic production and particle transfer processes. Deep Sea Research Part II: Topical Studies in Oceanography 47 (9–11), 1999–2028.

Glock, N., Eisenhauer, A., Liebetrau, V., Wiedenbeck, M., Hensen, C., Nehrke, G., 2012. EMP and SIMS studies on Mn/Ca and Fe/Ca systematics in benthic foraminifera from the Peruvian OMZ: a contribution to the identification of potential redox proxies and the impact of cleaning protocols. Biogeosciences 9 (1), 341–359.

Goldberg, M., 1978. Continental to marine environments in the Negev, Guidbook: Tenth Int. Congress on Sedimentology. IAS, Jerusalem, 35–110.

Gómez, J.J., Fernández-López, S., 1994. Condensation processes in shallow platforms. Sedimentary Geology 92 (3–4), 147–159.

González-Muñoz, M.T., Linares, C. de, Martínez-Ruiz, F., Morcillo, F., Martín-Ramos, D., Arias, J.M., 2008. Ca–Mg kutnahorite and struvite production by Idiomarina strains at modern seawater salinities. Chemosphere 72 (3), 465–472.

Gradstein, F.M., 1999. On the Cretaceous time scale. Neues Jahrbuch für Geologie und Paläontologie-Abhandlungen 212 (1-3), 3–14.

Grassineau, N.V., Mattey, D.P., Lowry, D., 2001. Sulfur isotope analysis of sulfide and sulfate minerals by continuous flow-isotope ratio mass spectrometry. Analytical Chemistry 73 (2), 220–225.

Griffiths, N., Müller, W., Johnson, K.G., Aguilera, O.A., 2013. Evaluation of the effect of diagenetic cements on element/Ca ratios in aragonitic Early Miocene (~16Ma) Caribbean corals: Implications for 'deep-time' palaeo-environmental reconstructions. Palaeogeography, Palaeoclimatology, Palaeoecology (369), 185–200.

Gromet, L.P., Haskin, L.A., Korotev, R.L., Dymek, R.F., 1984. The "North American shale composite": Its compilation, major and trace element characteristics. Geochimica et Cosmochimica Acta 48 (12), 2469–2482.

Groot, P.A. de (Ed.), 2004. Handbook of stable isotopes: Analytical Techniques, 1st ed. Elsevier, 1234 pp.

Gruber, N., 2006. Eddy-resolving simulation of plankton ecosystem dynamics in the California current system. Deep Sea Research Part I: Oceanographic Research Papers 53, 1483–1516.

Gruber, N., Lachkar, Z., Frenzel, H., Marchesiello, P., Munnich, M., McWilliams, J.C., Nagai, T., Plattner, G.-K., 2011. Eddy-induced reduction of biological production in eastern boundary upwelling systems. Nature Geoscience 4 (11), 787–792.

Guiraud, R., Bosworth, W., 1997. Senonian basin inversion and rejuvenation of rifting in Africa and Arabia: synthesis and implications to plate-scale tectonics. Structural Controls on Sedimentary Basin Formation 282 (1–4), 39–82.

Guiraud, R., Bosworth, W., 1999. Phanerozoic geodynamic evolution of northeastern Africa and the northwestern Arabian platform. Tectonophysics 315 (1-4), 73–104.
Guiraud, R., Bosworth, W., Thierry, J., Delplanque, A., 2005. Phanerozoic geological evolution of Northern and Central Africa: An overview: Phanerozoic Evolution of Africa. Journal of African Earth Sciences 43 (1-3), 83–143.
Gvirtzman, G., Almogi-Labin, A., Honigstein, A., Reis, Z., 1989. Upper Cretaceous high-resolution multiple stratigraphy, northern margin of the Arabian platform, central Israel. Cretaceous Research 10, 107–135.
Habicht, K.S., Canfield, D.E., 1997. Sulfur isotope fractionation during bacterial sulfate reduction in organic-rich sediments. Geochimica et Cosmochimica Acta 61 (24), 5351–5361.
Haq, B.U., 2014. Cretaceous eustasy revisited. Global and Planetary Change 113 (0), 44–58.
Haq, B.U., Hardenbol, J., Vail, P.R., 1987. Chronology of Fluctuating Sea Levels Since the Triassic. Science 235, 1156–1167.
Haq, B.U., Schutter, S.R., 2008. A Chronology of Paleozoic Sea-Level Changes. Science 322 (5898), 64–68.
Hastings, D.W., Emerson, S.R., 1996. Vanadium in foraminiferal calcite as a tracer for changes in the areal extent of reducing sediments sediments. Paleoceanography 11 (6), 665–678.
Hastings, D.W., Emerson, S.R., Erez, J., Nelson, B.K., 1996. Vanadium in foraminiferal calcite: Evaluation of a method to determine paleo-seawater vanadium concentrations. Geochimica et Cosmochimica Acta 60 (19), 3701–3715.
Hatch, J.R., Leventhal, J.S., 1992. Relationship between inferred redox potential of the depositional environment and geochemistry of the Upper Pennsylvanian (Missourian) Stark Shale Member of the Dennis Limestone, Wabaunsee County, Kansas, U.S.A: Geochemistry of Metalliferous Black Shales. Chemical Geology 99 (1-3), 65–82.
Hay, W.W., 2008. Evolving ideas about the Cretaceous climate and ocean circulation. Cretaceous Research 29, 725–753.
Hayashi, K.-I., Fujisawa, H., Holland, H.D., Ohmoto, H., 1997. Geochemistry of ~1.9 Ga sedimentary rocks from northeastern Labrador, Canada. Geochimica et Cosmochimica Acta 61 (19), 4115–4137.
Hayes, J.M., Popp, B.N., Takigiku, R., Johnson, M.W., 1989. An isotopic study of biogeochemical relationships between carbonates and organic carbon in the Greenhorn Formation. Geochimica et Cosmochimica Acta 53 (11), 2961–2972.
Helz, G.R., Miller, C.V., Charnock, J.M., Mosselmans, J.F., Pattrick, R.A., Garner, C.D., Vaughan, D.J., 1996. Mechanism of molybdenum removal from the sea and its concentration in black shales: EXAFS evidence. Geochimica et Cosmochimica Acta 60 (19), 3631–3642.
Henderson, P., Henderson, G., 2009. The Cambridge handbook of earth science data. Cambridge University Press, Cambridge, U.K, New York, 295 pp.
Henneke, E., Luther III, G.W., Lange, G.J. de, Hoefs, J., 1997. Sulphur speciation in anoxic hypersaline sediments from the eastern Mediterranean Sea. Geochimica et Cosmochimica Acta 61 (2), 307–321.
Hertelendi, E., Vetö, I., 1991. The marine photosynthetic carbon isotopic fractionation remained constant during the Early Oligocene. Palaeogeography, Palaeoclimatology, Palaeoecology 83 (4), 333–339.
Hesse, R., 1986. Diagenesis 11. Early diagenetic pore water/ sediment interaction: Modern offshore basins. Geoscience Canada 13 (3), 165–196.
Hetzel, A., Böttcher, M.E., Wortmann, U.G., Brumsack, H.-J., 2009. Paleo-redox conditions during OAE 2 reflected in Demerara Rise sediment geochemistry (ODP Leg 207). Organic-carbon-rich sediments through the Phanerozoic: Processes, progress, and perspectives 273 (3–4), 302–328.
Hodgson, G.W., Hitchon, B., Taguchi, K., Baker, B.L., Peake, E., 1968. Geochemistry of porphyrins, chlorins and polycyclic aromatics in soils, sediments and sedimentary rocks. Geochimica et Cosmochimica Acta 32 (7), 737–772.
Hoefs, J., 2009. Stable isotope geochemistry, 6th ed. Springer; Springer Berlin Heidelberg, Berlin /// Berlin, Heidelberg, 285 pp.
Hoek, R.P., Eshet, Y., Almogi-Labin, A., 1996. Dinoflagellate Cyst Zonation of Campanian-Maastrichtian Sequences in Israel. Micropaleontology 42 (2), 125–150.
Høgslund, S., Revsbech, N.P., Cedhagen, T., Nielsen, L.P., Gallardo, V.A., 2008. Denitrification, nitrate turnover, and aerobic respiration by benthic foraminiferans in the oxygen minimum zone off Chile. Journal of Experimental Marine Biology and Ecology 359 (2), 85–91.
Holleman, A.F., Wiberg, E., 1995. Lehrbuch der anorganischen Chemie. Walter de Gruyter.2149 pp.
Hoogakker, B.A.A., Klinkhammer, G.P., Elderfield, H., Rohling, E.J., Hayward, C., 2009. Mg/Ca paleothermometry in high salinity environments. Earth and Planetary Science Letters 284 (3-4), 583–589.

Hovan, S.A., Kish, S.W., Renyck, H.J., 2000. Sedimentation rate, bulk density, accumulation rate of terrigenous material and grain sizes of ODP Leg 167 sites: Supplement to: Hovan, Steven A; Kish, SW; Renyck, Heather J (2000): Late Pleistocene record of terrigenous mineral deposition along the northern California margin (Sites 1018 and 1020). In: Lyle, M; Koizumi, I; Richter, C; Moore, TC Jr (eds.) Proceedings of the Ocean Drilling Program, Scientific Results, College Station, TX (Ocean Drilling Program), 167, 1-8

Hsieh, Y.P., Shieh, Y.N., 1997. Analysis of reduced inorganic sulfur by diffusion methods: improved apparatus and evaluation for sulfur isotopic studies. Chemical Geology 137 (3-4), 255–261.

Huber, B.T., Norris, R.D., MacLeod, K.G., 2002. Deep-sea paleotemperature record of extreme warmth during the Cretaceous. Geology 30 (2), 123–126.

Huerta-Diaz, M.A., Morse, J.W., 1990. A quantitative method for determination of trace metal concentrations in sedimentary pyrite. Marine Chemistry 29, 119–144.

Huerta-Diaz, M.A., Morse, J.W., 1992. Pyritization of trace metals in anoxic marine sediments. Geochimica et Cosmochimica Acta 56 (7), 2681–2702.

Hutton, A.C., 1987. Petrographic classification of oil shales. International Journal of Coal Geology 8 (3), 203–231.

Hutton, A.C. (Ed.), 1991. Classification, organic petrography and geochemistry of oil shale, 163-172.

Ifrim, C., Götz, S., Stinnesbeck, W., 2011. Fluctuations of the oxygen minimum zone at the end of Oceanic Anoxic Event 2 reflected by benthic and planktic fossils. Geology 39 (11), 1043–1046.

Ingall, E., Jahnke, R., 1997. Influence of water-column anoxia on the elemental fractionation of carbon and phosphorus during sediment diagenesis. Marine Geology 139 (1–4), 219–229.

Inthorn, M., Wagner, T., Scheeder, G., Zabel, M., 2006. Lateral transport controls distribution, quality, and burial of organic matter along continental slopes in high-productivity areas. Geology 34 (3), 205.

Irino, T., Pedersen, T.F., 2000. (Table 1) Minor and trace element composition of ODP Hole 167-1017E sediments: Supplement to: Irino, Tomohisa; Pedersen, Thomas F (2000): Geochemical character of glacial to interglacial sediments at Site 1017, southern California margin: minor and trace elements. In: Lyle, M; Koizumi, I; Richter, C; Moore, TC Jr (eds.) Proceedings of the Ocean Drilling Program, Scientific Results, College Station, TX (Ocean Drilling Program), 167, 1-9

Iruthayaraj, M.R., Morachan, Y.B., 1978. Relationship between evaporation from different evaporimeters and meteorological parameters. Agricultural Meteorology 19 (2–3), 93–100.

Ishiwatari, R., Matsumoto, K., Seki, O., Yamamoto, S., 2000. Variations in the organic carbon isotopic composition in sediments at the site 1017 during the last 25 k.y.[1]: Supplement to: Ishiwatari, Ryoshi; Matsumoto, Kohei; Seki, Osamu; Yamamoto, Shuichi (2000): Variations in organic carbon isotopic composition in sediments at Site 1017 during the last 25 k.y. In: Lyle, M; Koizumi, I; Richter, C; Moore, TC Jr (eds.) Proceedings of the Ocean Drilling Program, Scientific Results, College Station, TX (Ocean Drilling Program), 167, 1-4, Proceedings of the Ocean Drilling Program 167 (273-276).

Issawi, B., Francis, M.H., El Hinnawi, M., Mehanna, A., El Deftar, T., 1969. Contribution to the structure and phosphate deposits of Quseir area. Paper Geological Survey of Egypt 50.

Jander, G., Blasius, E., Strähle, J., Schweda, E., Rossi, R., Jander-Blasius, 2006. Lehrbuch der analytischen und präparativen anorganischen Chemie, 16th ed. Hirzel, Stuttgart, 704 pp.

Jaraula, C.M.B., Brassell, S.C., Morgan-Kiss, R.M., Doran, P.T., Kenig, F., 2010. Origin and tentative identification of tri to pentaunsaturated ketones in sediments from Lake Fryxell, East Antarctica. Organic Geochemistry 41 (4), 386–397.

Jarvis, I., Mabrouk, A., Moody, Richard T. J., Cabrera, S.d., 2002. Late Cretaceous (Campanian) carbon isotope events, sea-level change and correlation of the Tethyan and Boreal realms. Palaeogeography, Palaeoclimatology, Palaeoecology 188 (3–4), 215–248.

Jasmund, K., 1993. Tonminerale und Tone: Struktur, Eigenschaften, Anwendungen und Einsatz in Industrie und Umwelt. Steinkopff, Darmstadt, 490 pp.

Jørgensen, B.B., 1982. Mineralization of organic matter in the sea bed - the role of sulphate reduction. Nature 296 (5858), 643–645.

Jørgensen, B.B., 1990. A Thiosulfate Shunt in the Sulfur Cycle of Marine Sediments. Science 249 (4965), 152–154.

Katz, M.E., Cramer, B.S., Franzese, A., Hoenisch, B., Miller, K.G., Rosenthal, Y., Wright, J.D., 2010. Traditional and Emerging Geochemical Proxies in Foraminifera. Journal of Foraminiferal Research 40 (2), 165–192.

Keeling, R.F., Körtzinger, A., Gruber, N., 2010. Ocean Deoxygenation in a Warming World. Annual Review of Marine Science 2 (1), 199–229.

Keller, G., Abramovich, S., 2009. Lilliput effect in late Maastrichtian planktic foraminifera: Response to environmental stress. Palaeogeography, Palaeoclimatology, Palaeoecology 1-2 (284), 47–62.

Keller, G., Pardo, A., 2004. Disaster opportunists Guembelitrinidae: index for environmental catastrophes. Marine Micropaleontology 53 (1–2), 83–116.

Kennedy, M.J., Pevear, D.R., Hill, R.J., 2002. Mineral Surface Control of Organic Carbon in Black Shale. Science 295 (5555), 657–660.
Khider, K., McQueen, K.G. (Eds.), 2005. Geochemical discrimination of weathered bedrock in the Hermidale-Byrock region of western NSW, 170-175.
Killops, S., Killops, V., 2005. Introduction to organic geochemistry, 2nd ed. Blackwell Publ, Malden, Mass, 393 pp.
Kisakürek, B., Eisenhauer, A., Böhm, F., Garbe-Schönberg, D., Erez, J., 2008. Controls on shell Mg/Ca and Sr/Ca in cultured planktonic foraminiferan, Globigerinoides ruber (white). Earth and Planetary Science Letters 273 (3-4), 260–269.
Klinkhammer, G.P., Palmer, M.R., 1991. Uranium in the oceans: Where it goes and why. Geochimica et Cosmochimica Acta 55 (7), 1799–1806.
Kniewald, G., Branica, M., 1988. Role of uranium (V) in marine sedimentary environments: a geochemical possibility. Marine Chemistry 24 (1), 1–12.
Koch, M.C., Friedrich, O., 2012. Campanian-Maastrichtian intermediate- to deep-water changes in the high latitudes: Benthic foraminiferal evidence. Paleoceanography 27 (2), 1–11.
Koepke, J., Seidel, E., Kreuzer, H., 2002. Ophiolites on the Southern Aegean islands Crete, Karpathos and Rhodes: composition, geochronology and position within the ophiolite belts of the Eastern Mediterranean. Eastern Mediterranean Ophiolites: Magmatic Processes and Geodynamic Implications, held at the 10th Meeting of the European Union of Geosciences, Strasbourg, France, 28 March-1 April, 1999 65 (1–2), 183–203.
Kohnen, M.E.L., Damsté, J.S.S., Kock-van Dalen, A.C., Haven, H.L.T., Rullkötter, J., Leeuw, J.W. de, 1990. Origin and diagenetic transformations of C25 and C30 highly branched isoprenoid sulphur compounds: Further evidence for the formation of organically bound sulphur during early diagenesis. Geochimica et Cosmochimica Acta 54 (11), 3053–3063.
Kohnen, M.E.L., Sinninghe Damsté, J.S., Haven, H.L.T., kock.-Van Dalen, A.C., Schouten, S., Leeuw, J.W. de, 1991. Identification and geochemical significance of cyclic di-and trisulphides with linear and acyclic isoprenoid carbon skeletons in immature sediments. Geochimica et Cosmochimica Acta 55 (12), 3685–3695.
Kok, M.D., Rijpstra, W.I.C., Robertson, L., Volkman, J.K., Sinninghe Damsté, J.S., 2000a. Early steroid sulfurisation in surface sediments of a permanently stratified lake (Ace Lake, Antarctica). Geochimica et Cosmochimica Acta 64 (8), 1425–1436.
Kok, M.D., Schouten, S., Sinninghe Damsté, J.S., 2000b. Formation of insoluble, nonhydrolyzable, sulfur-rich macromolecules via incorporation of inorganic sulfur species into algal carbohydrates. Geochimica et Cosmochimica Acta 64 (15), 2689–2699.
Kok, M.D., Schouten, S., Sinninghe Damsté, J.S., 2000c. Formation of insoluble, nonhydrolyzable, sulfur-rich macromolecules via incorporation of inorganic sulfur species into algal carbohydrates. Geochimica et Cosmochimica Acta 64 (15), 2689–2699.
Kolonic, S., Sinninghe Damsté, J.S., Böttcher, M.E., Kuypers, M.M.M., Kuhnt, W., Beckmann, B., Scheeder, G., Wagner, T., 2002. Geochemical charakterization of Cenomanian/ Turonian black shales frim the Tarfaya Basin (SW Morocco). Journal of Petroleum Geology 25 (3), 325–350.
Köster, J., Rospondek, M., Schouten, S., Kotarba, M., Zubrzycki, A., Sinninghe Damsté, J.S., 1998. Biomarker geochemistry of a foreland basin: the Oligocene Menilite Formation in the Flysch Carpathians of Southeast Poland. Advances in Organic Geochemistry 1997 Proceedings of the 18th International Meeting on Organic Geochemistry Part I. Petroleum Geochemistry 29 (1–3), 649–669.
Kotaś, J., Stasicka, Z., 2000. Chromium occurrence in the environment and methods of its speciation. Environmental Pollution 107 (3), 263–283.
Krenkel, E., 1924. Der Syrische Bogen. Centralbl. Mineral 9, 274–281.
Kuypers, M.M.M., 2005. From The Cover: Massive nitrogen loss from the Benguela upwelling system through anaerobic ammonium oxidation. Proceedings of the National Academy of Sciences 102 (18), 6478–6483.
La Lanza-Espino, G. de, Soto, L.A., 1999. Sedimentary geochemistry of hydrothermal vents in Guaymas Basin, Gulf of California, Mexico. Applied Geochemistry 14 (4), 499–510.
Lamy, F., Hebbeln, D., Wefer, G., 1999. High-Resolution Marine Record of Climatic Change in Mid-latitude Chile during the Last 28,000 Years Based on Terrigenous Sediment Parameters. Quaternary Research 51 (1), 83–93.
Langlet, D., Geslin, E., Baal, C., Metzger, E., Lejzerowicz, F., Riedel, B., Zuschin, M., Pawlowski, J., Stachowitsch, M., Jorissen, F.J., 2013. Foraminiferal survival after long term experimentally induced anoxia. Biogeoscience Discussions 10 (6), 9243–9284.
Langmuir, D., 1978. Uranium solution-mineral equilibria at low temperatures with applications to sedimentary ore deposits. Geochimica et Cosmochimica Acta 42 (6, Part A), 547–569.
Lea, D.W., 1999. Trace elements in foraminiferal calcite. Modern foraminifera, 259–277.

Lea, D.W., Boyle, E.A., 1991. Barium in planktonic foraminifera: The Macalpine Hills Lunar Meteorite Consortium. Geochimica et Cosmochimica Acta 55 (11), 3321–3331.
Lea, D.W., Mashiotta, T.A., Spero, H.J., 1999. Controls on magnesium and strontium uptake in planktonic foraminifera determined by live culturing. Geochimica et Cosmochimica Acta 63 (16), 2369–2379.
Lear, C.H., Rosenthal, Y., Slowey, N., 2002. Benthic foraminiferal Mg/Ca-paleothermometry: A revised core-top calibration. Geochimica et Cosmochimica Acta 66 (19), 3375–3387.
Leary, P.N., Carson, G.A., Cooper, M.K.E., Hart, M.B., Horne, D., Jarvis, I., Rosenfeld, A., Tocher, B.A., 1989. The biotic response to the late Cenomanian oceanic anoxic event; integrated evidence from Dover, SE England. Journal of Geological Society 146 (2), 311–317.
Leckie, R.M., 1987. Paleoecology of Mid-Cretaceous Planktonic Foraminifera: A Comparison of Open Ocean and Epicontinental Sea Assemblages. Micropaleontology 33 (2), 164–176.
Leggett, J.K., 1980. British Lower Palaeozoic black shales and their palaeo-oceanographic significance. Journal of Geological Society 137 (2), 139–156.
Lein, A.Y., Ivanov, M.V., 1991. On the Sulfur and Carbon Balances in the Black Sea, in: İzdar, E., Murray, J. (Eds.), Black Sea Oceanography, vol. 351. Springer Netherlands, pp. 307-318.
Leventhal, J.S., 1983. An interpretation of carbon and sulfur relationships in Black Sea sediments as indicators of environments of deposition. Geochimica et Cosmochimica Acta 47 (1), 133–137.
Leventhal, J.S., 1987. Carbon and sulfur relationships in Devonian shales from the Appalachian Basin as an indicator of environment of deposition. American Journal of Science 287 (1), 33–49.
Levin, L.A., Sibuet, M., 2012. Understanding Continental Margin Biodiversity: A New Imperative. Annual Review of Marine Science 4 (1), 79–112.
Lewan, M.D., 1984. Factors controlling the proportionality of vanadium to nickel in crude oils. Geochimica et Cosmochimica Acta 48 (11), 2231–2238.
Lewan, M.D., Henry, A.A., 2001. Gas: Oil Ratios for Source Rocks Containing Type-I, -II, -IIS, and -III Kerogens as Determined by Hydrous Pyrolysis: Prepared in cooperation with the U.S. Department of Energy–National Energy Technology Laboratory, the Gas Technology Institute, and Advanced Resources International. U.S. Department of the Interior; US Geologica Survey.
Lewan, M.D., Maynard, J.B., 1982. Factors controlling enrichment of vanadium and nickel in the bitumen of organic sedimentary rocks. Geochimica et Cosmochimica Acta 46 (12), 2547–2560.
Lewis, B.L., Landing, W.M., 1991. The biogeochemistry of manganese and iron in the Black Sea: Black Sea Oceanography: Results from the 1988 Black Sea Expedition. Deep Sea Research Part A. Oceanographic Research Papers 38, Supplement 2 (0), S773.
Li, L., Keller, G., 1999. Variability in Late Cretaceous climate and deep waters: evidence from stable isotopes. Marine Geology 161 (2-4), 171–190.
Li, L., Keller, G., Adatte, T., Stinnesbeck, W., 2000. Late Cretaceous sea-level changes in Tunisia: a multi-disciplinary approach. Journal of Geological Society 157 (2), 447–458.
Li, Y.-H., Schoonmaker, J., 2004. Chemical Composition and Mineralogy of Marine Sediments, in: Holland, H.D., Turekian, K.K. (Eds.), Treatise on geochemistry, 1st ed. Elsevier/Pergamon, Amsterdam, Boston, pp. 1–30.
Littke, R., 1993. Deposition, diagenesis and weathering of organic matter-rich sediments. Habilschrift. Springer, Berlin, 216 pp.
Louda, J.W., Baker, E.W., 1981. Geochemistry of tetrapyrrole, carotenoid, and perylene pigments in sediments from the San Miguel Gap (site 467) and Baja California borderland (site 471), deep sea drilling project Leg 63. Initial Reports of the Deep Sea Drilling Project 63, 785–818.
Lovley, D.R., 1991. Dissimilatory Fe(III) and Mn(IV) reduction. Microbiological Reviews 55 (2), 259–287.
Lovley, D.R., 1995. Microbial Reduction of Iron, Manganese, and other Metals, in: Donald L. Sparks (Ed.), Advances in Agronomy. Academic Press, pp. 175–231.
Lovley, D.R., Phillips, E., 1992. Reduction of uranium by Desulfovibrio desulfuricans. Applied and Evironmental Microbiology 58 (3), 850–856.
Lovley, D.R., Phillips, E.J.P., Gorby, Y.A., Landa, E.R., 1991. Microbial reduction of uranium. Nature 350 (6317), 413–416.
Lucas, J., Lucas-Prèvot, L., 1996. Tethyan phosphates and bioproductites: Chapter 4E, in: Nairn, A.E.M. (Ed.), The Ocean Basins and Margins; Vol. 8: The Tethys Ocean, New York, pp. 367–397.
Lückge, A., Boussafir, M., Lallier-Verges, E., Littke, R., 1996. Organic matter preservation in sediments of the Peru and Oman continental margin: Supplement to: Lückge, Andreas; Boussafir, Mohammed; Lallier-Verges, Elisabeth; Littke, Ralf (1996): Comparative study of organic matter preservation in immature sediments along the continental margins of Peru and Oman. Part I: results of petrographical and bulk geochemical data. Organic Geochemistry, 24(4), 437-451

Lückge, A., Ercegovac, M., Strauss, H., Littke, R., 1999. Early diagenetic alteration of organic matter by sulfate reduction in Quaternary sediments from the northeastern Arabian Sea. Marine Geology 158 (1–4), 1–13.

Luther, M.E., O'Brien, J.J., Prell, W.L., 1990. Variability in upwelling fields in the northwestern Indian Ocean 1. Model experiments for the past 18,000 years. Paleoceanography 5 (3), 433–445.

Lyle, M., Zahn, R., Prahl, F., Dymond, J., Collier, R., Pisias, N., Suess, E., 1992. Paleoproductivity and carbon burial across the California Current: The multitracers transect, 42°N. Paleoceanography 7 (3), 251–272.

Lyle, M.W., Mix, A.C., Ravelo, A.C., Andreasen, D., Heusser, L.E., Olivarez, A., 2000. C_{org}, $CaCO_3$, bulk densities, accumulation rates and ages of ODP Leg 167 sites and three piston cores, California margin: Supplement to: Lyle, Mitchell W; Mix, Alan C; Ravelo, Ana Christina; Andreasen, Dyke; Heusser, Linda E; Olivarez, Annette (2000): Millennial-scale CaCO3 and Corg events along the northern and central California margins: stratigraphy and origins. In: Lyle, M; Koizumi, I; Richter, C; Moore, TC Jr (eds.) Proceedings of the Ocean Drilling Program, Scientific Results, College Station, TX (Ocean Drilling Program), 167, 1-20

Lyons, T.W., Berner, R.A., 1992. Carbon-sulfur-iron systematics of the uppermost deep-water sediments of the Black Sea: Geochemistry of Metalliferous Black Shales. Chemical Geology 99 (1-3), 1–27.

Lyons, T.W., Severmann, S., 2006. A critical look at iron paleoredox proxies: New insights from modern euxinic marine basins. Geochimica et Cosmochimica Acta 70 (23), 5698–5722.

Lyons, T.W., Werne, J.P., Hollander, D.J., Murray, R.W., 2003a. (Table 1) Forms of iron, organic and inorganic carbon, aluminium, molybdenum, pyrite sulphur and its isotope composition in bottom sediments of the Cariaco Basin, ODP Site 165-1002: Supplement to: Lyons, Timothy W; Werne, Josef P; Hollander, David J; Murray, Richard W (2003): Contrasting sulfur geochemistry and Fe/Al and Mo/Al ratios across the last oxic-to-anoxic transition in the Cariaco Basin, Venezuela. Chemical Geology, 195(1-4), 131-157

Lyons, T.W., Werne, J.P., Hollander, D.J., Murray, R.W., 2003b. Contrasting sulfur geochemistry and Fe/Al and Mo/Al ratios across the last oxic-to-anoxic transition in the Cariaco Basin, Venezuela: Isotopic records of microbially mediated processes. Chemical Geology 195 (1-4), 131–157.

Mackensen, A., 2008. On the use of benthic foraminiferal $\delta^{13}C$ in palaeoceanography: constraints from primary proxy relationships, in: Austin, W.E.N., James, R.H. (Eds.), Biogeochemical controls on palaeoceanographic environmental. Geological Society; Geological Soc., London, pp. 121–133.

MacLeod, K.G., Isaza Londoño, C., Martin, E.E., Jiménez Berrocoso, Á., Basak, C., 2011. Changes in North Atlantic circulation at the end of the Cretaceous greenhouse interval. Nature Geoscience (4), 779–782.

Madigan, M.T., Martinko, J.M., 2009. Brock Mikrobiologie, 11th ed. Pearson Studium, München, 1203 pp.

Madsen, H.B., Stemmerik, L., Surlyk, F., 2010. Diagenesis of silica-rich mound-bedded chalk, the Coniacian Arnager Limestone, Denmark. Sedimentary Geology 223 (1-2), 51–60.

Mallinson, D.J., Flower, B., Hine, A., Brooks, G., Garza, R.M., 2003. Paleoclimate implications of high latitude precession-scale mineralogic fluctuations during early Oligocene Antarctic glaciation: the Great Australian Bight record. Global and Planetary Change 39 (3-4), 257–269.

Mann, K.H., Lazier, J.R.N., 2006. Dynamics of marine ecosystems: Biological-physical interactions in the oceans, 3rd ed. Blackwell Pub., Malden, MA, xii, 496pp.

Marchesiello, P., 2009. Eddy activity and mixing in upwelling systems: A comparative study of Northwest Africa and California regions. Int. J. Earth Sci. 98, 299–308.

Marchitto, T.M., 2004. Lack of a significant temperature influence on the incorporation of Cd into benthic foraminiferal tests. Geochemistry, Geophysics, Geosystems 5 (10), 1–9.

Marnette, E.C.L., van Breemen, N., Hordijk, K.A., Cappenberg, T.E., 1993. Pyrite formation in two freshwater systems in the Netherlands. Geochimica et Cosmochimica Acta 57 (17), 4165–4177.

Marshall, J.D., 1992. Climatic and oceanographic isotopic signals from the carbonate rock record and their preservation. Geological Magazine 129 (02), 143–160.

Martin, P.A., Lea, D.W., 2002. A simple evaluation of cleaning procedures on fossil benthic foraminiferal Mg/Ca. Geochem.-Geophys.-Geosyst. 3 (10), 8401.

Martin, R.E., Harris, M.S., Liddell, W.D., 1995. Taphonomy and time-averaging of foraminiferal assemblages in Holocene tidal flat sediments, Bahia la Choya, Sonora, Mexico (northern Gulf of California). Selected papers from the Fifth International Symposium of Foraminifera 26 (1–4), 187–206.

Maslin, M., Swann, G.A., 2006. Isotopes in marine Sediments, in: Leng, M. (Ed.), Isotopes in Palaeoenvironmental Research, vol. 10. Springer Netherlands, pp. 227-290.

Mason, B., Moore, C.B., 2001. Grundzüge der Geochemie. Spektrum Akademischer Verlag, Stuttgart.

Masuzawa, T., Takada, J., Matsushita, R., 1992. (Table 1) Sediment chemistry and Sulphur isotope ratios of ODP Site 127-795: Supplement to: Masuzawa, Toshiyuki; Takada, Jitsuya; Matsushita, Rokuji (1992): Trace-element geochemistry of sediments and sulfur isotope geochemistry of framboidal pyrite from Site 795, Leg 127, Japan

Sea. In: Pisciotto, K.A.; Ingle, J.C.Jr.; von Breymann, M.T.; Barron, J.; et al. (eds.), Proceedings of the Ocean Drilling Program, Scientific Results, College Station, TX (Ocean Drilling Program), 127/128(1), 705-717

Mateer, N.J., Wycisk, P., Jacobs, L.L., Brunet, M., Luger, P., Arush, M.A., Hendriks, F., Weissbrod, T., Gvirtzman, G., Mbede, E., Dina, A., Moody, Richard T. J., Weigelt, G., El-Nakhal, H.A., Hell, J., Stets, J., 1992. Correlation of nonmarine Cretaceous strata of Africa and the Middle East. Cretaceous Research 13 (3), 273–318.

Mayer, B., Krouse, H., 2004. Procedures for Sulfur Isotope Abundances Studies, in: Groot, P.A. de (Ed.), Handbook of stable isotopes. Analytical Techniques, vol. 1, 1st ed. Elsevier, pp. 539–596.

Mayer, L.M., 1994. Surface area control of organic carbon accumulation in continental shelf sediments. Geochimica et Cosmochimica Acta 58 (4), 1271–1284.

McArthur, J.M., Algeo, T. J., van de Schootbrugge, B., Li, Q., Howarth, R. J., 2008. Basinal restriction, black shales, Re-Os dating, and the Early Toarcian (Jurassic) oceanic anoxic event. Paleoceanography 23 (4), 1–22.

McCaffrey, M.A., Farrington, J.W., Repeta, D.J., 1989. Geochemical implications of the lipid composition of Thioploca spp. from the Peru upwelling region - 15°S. Organic Geochemistry 14 (1), 61–68.

McKee, E.D., 1963. Origin of the Nubian and similar sandstones. Geologische Rundschau 52 (2), 551–587.

McLennan, S.M., 1993. Earth's continental continental crust. Journal of Geology 101 (101), 295–303.

McManus, J., Berelson, W.M., Klinkhammer, G.P., Hammond, D.E., Holm, C., 2005. Authigenic uranium: Relationship to oxygen penetration depth and organic carbon rain. Geochimica et Cosmochimica Acta 69 (1), 95–108.

McManus, J., Berelson, W.M., Severmann, S., Poulson, R.L., Hammond, D.E., Klinkhammer, G.P., Holm, C., 2006. Molybdenum and uranium geochemistry in continental margin sediments: Paleoproxy potential. Geochimica et Cosmochimica Acta 70 (18), 4643–4662.

Meinecke, G., 1973. Zur Geochemie des Vanadiums, in: Borchert, H. (Ed.), Clausthaler Hefte zur Lagerstättenkunde und Geochemie der mineralischen Rohostoffe, 1st ed. Borntraeger, Berlin - Stuttgart, pp. 1–89.

Metzger, E., Langlet, D., Viollier, E., Koron, N., Riedel, B., Stachowitsch, M., Faganeli, J., Tharaud, M., Geslin, E., Jorissen, F., 2013. Artificially induced migration of redox layers in a coastal sediment from the Northern Adriatic. Biogeoscience Discussions 10 (7).

Meudt, M., 2004. Geochemie der Foraminiferenschalen: Relevanz für die Rekonstruktion von Paläoumweltbedingungen. Dissertation, Karlsruhe, 162 pp.

Meyers, P.A., 2006. Paleoceanographic and paleoclimatic similarities between Mediterranean sapropels and Cretaceous black shales: Causes and Consequence of Marine Organic Carbon Burial Through Time “Black Shales and Sapropels”, “Organic-Carbon Burial and Rapid Climate Change”. Palaeogeography, Palaeoclimatology, Palaeoecology 235 (1–3), 305–320.

Miller, K.G., Browning, J.V., Aubry, M.-P., Wade, B.S., Katz, M.E., Kulpecz, A.A., Wright, J.D., 2008. Eocene–Oligocene global climate and sea-level changes: St. Stephens Quarry, Alabama. Geological Society of America Bulletin 120 (1-2), 34–53.

Miller, K.G., Kominz, M.A., Browning, J.V., Wright, J.D., Mountain, G.S., Katz, M.E., Sugarman, P.J., Cramer, B.S., Christie-Blick, N., Pekar, S.F., 2005. The Phanerozoic Record of Global Sea-Level Change. Science 310 (5752), 1293–1298.

Miller, K.G., Sugarman, P.J., Browning, J.V., Kominz, M.A., Hernández, J.C., Olsson, R.K., Wright, J.D., Feigenson, M.D., van Sickel, W., 2003. Late Cretaceous chronology of large, rapid sea-level changes: Glacioeustasy during the greenhouse world. Geology 31 (7), 585–588.

Miller, R.G., 1988. Palaeoceanographic approach to the Kimmeridge Clay Formation. AAPG Bulletin (American Association of Petroleum Geologists);(USA) 72 (CONF-8809346--).

Minster, T., 2009. Oil Shale deposits in Israel: Jerusalem, July 2009. (In Hebrew, English abstract). update. Geological Survey of Israel. Report GSI/18/2009.

Minster, T., Miknis, F.P., 1994. Solid State ^{13}C in NMR of Israeli Oil Shales. Oil Shale 11 (4), 305–314.

Minster, T., Nathan, Y., Raveh, A., 1992. Carbon and sulfur relationships in marine Senonian organic-rich, iron-poor sediments from Israel — A case study. Chemical Geology 97 (1–2), 145–161.

Mohtadi, M., Hebbeln, D., Marchant, M., 2005. Upwelling and productivity along the Peru-Chile Current derived from faunal and isotopic compositions of planktic foraminifera in surface sediments. Marine Geology 216 (3), 107–126.

Mongenot, T., Derenne, S., Largeau, C., Tribovillard, N.-P., Lallier-Vergès, E., Dessort, D., Connan, J., 1999. Spectroscopic, kinetic and pyrolytic studies of kerogen from the dark parallel laminae facies of the sulphur-rich Orbagnoux deposit (Upper Kimmeridgian, Jura). Organic Geochemistry 30 (1), 39–56.

Mongenot, T., Tribovillard, N. (Eds.), 1996. Preservation mechanism in the different facies of organic-rich lagoonal sediments. American Chemical Society, Washington D.C., 29 pp.

Mongenot, T., Tribovillard, N.-P., Desprairies, A., Lallier-Vergès, E., Laggoun-Defarge, F., 1996. Trace elements as palaeoenvironmental markers in strongly mature hydrocarbon source rocks: the Cretaceous La Luna Formation of Venezuela. Sedimentary Geology 103 (1-2), 23–37.

Monteiro, P.M.S., Nelson, G., van der Plas, A., Mabille, E., Bailey, G.W., Klingelhoeffer, E., 2005. Internal tide—shelf topography interactions as a forcing factor governing the large-scale distribution and burial fluxes of particulate organic matter (POM) in the Benguela upwelling system. Continental Shelf Research 25 (15), 1864–1876.

Monteiro, P.M.S., Roychoudhury, A.N., 2005. Spatial characteristics of sediment trace metals in an eastern boundary upwelling retention area (St. Helena Bay, South Africa): A hydrodynamic–biological pump hypothesis. Estuarine, Coastal and Shelf Science 65 (1–2), 123–134.

Monteiro, P.M.S., van der Plas, A.K., Mélice, J.-L., Florenchie, P., 2008. Interannual hypoxia variability in a coastal upwelling system: Ocean–shelf exchange, climate and ecosystem-state implications. Deep Sea Research Part I: Oceanographic Research Papers 55 (4), 435–450.

Moodley, L., Schaub, B.E., van der Zwaan, G.J., Herman, P.M., 1998. Tolerance of benthic foraminifera (Protista: Sarcodina) to hydrogen sulphide. Marine Ecology Progress Series 169, 77–86.

Moore, D.M., Reynolds, R.C. Jr., 1989. X-ray diffraction and the identification and analysis of clay minerals. Oxford University Press (OUP), Oxford, New York, 373 pp.

Morel, F.M.M., 2003. The Biogeochemical Cycles of Trace Metals in the Oceans. Science 300 (5621), 944–947.

Morford, J.L., Emerson, S., 1999. The geochemistry of redox sensitive trace metals in sediments. Geochimica et Cosmochimica Acta 63 (11-12), 1735–1750.

Morford, J.L., Martin, W.R., Carney, C.M., 2009. Uranium diagenesis in sediments underlying bottom waters with high oxygen content. Geochimica et Cosmochimica Acta 73 (10), 2920–2937.

Morse, J.W., Berner, R.A., 1995. What determines sedimentary C/S ratios? Geochimica et Cosmochimica Acta 59 (6), 1073–1077.

Morse, J.W., Emeis, K.C., 1990. Controls on the C/S ratios in hemipelagic upwelling sedimnets. American Journal of Science 290 (10), 1117–1135.

Morse, J.W., Millero, F.J., Cornwell, J.C., Rickard, D., 1987. The chemistry of the hydrogen sulfide and iron sulfide systems in natural waters. Earth-Science Reviews 24 (1), 1–42.

Mosch, T., Sommer, S., Pfannkuche, O., Wallmann, K., 2010. Habitat mapping in the Peruvian OMZ.

Mossmann, J.-R., Aplin, A.C., Curtis, C.D., Coleman, M.L., 1990. Sulfur geochemistry at ODP Site 112-680 and 112-686: Supplement to: Mossmann, Jean-Remi; Aplin, Andrew C; Curtis, Charles D; Coleman, Max L (1990): Sulfur geochemistry. Proceedings of the Ocean Drilling Program 112, 455–464.

Mucci, A., 1987. Influence of temperature on the composition of magnesian calcite overgrowths precipitated from seawater. Geochimica et Cosmochimica Acta 51 (7), 1977–1984.

Mucci, A., Morse, J., Kaminsky, M., 1985. Auger spectroscopy analysis of magnesian calcite overgrowths precipitated from seawater and solutions of similar composition. American Journal of Science 4 (285), 289–305.

Mucci, A., Morse, J.W., 1983. The incorporation of Mg^{2+} and Sr^{2+} into calcite overgrowths: influences of growth rate and solution composition. Geochimica et Cosmochimica Acta 47 (2), 217–233.

Muñoz, P., Lange, C.B., Gutiérrez, D., Hebbeln, D., Salamanca, M.A., Dezileau, L., Reyss, J.L., Benninger, L.K., 2004. Recent sedimentation and mass accumulation rates based on 210Pb along the Peru-Chile continental margin: Oceanography in the eastern South Pacific: Part I. Deep Sea Research Part II: Topical Studies in Oceanography 51 (20-21), 2523–2541.

Murray, J.W., Yakushev, E.V., 2006. The suboxic transition zone in the Black Sea, in: Neretin, L.N. (Ed.), Past and present water column anoxia. Springer, Dordrecht, [Great Britain], pp. 105–139.

Nagender Nath, B., Bau, M., Ramalingeswara Rao, B., Rao, C.M., 1997. Trace and rare earth elemental variation in Arabian Sea sediments through a transect across the oxygen minimum zone. Geochimica et Cosmochimica Acta 61 (12), 2375–2388.

Nameroff, T.J., Balistrieri, L.S., Murray, J.W., 2002. Suboxic trace metal geochemistry in the Eastern Tropical North Pacific. Geochimica et Cosmochimica Acta 66 (7), 1139–1158.

Nasir, S., Sadeddin, W., 1989. The heavy minerals of the Kurnub Sandstone (Early Cretaceous) of Jordan. Sedimentary Geology 62 (1), 101–107.

Nathan, Y., 1969. Studies on palygorskite. Dissertation, Jerusalem, 153 pp.

Nathan, Y., Benalioulhaj, N., Prevot, L., Lucas, J., 1996. The geochemistry of cadmium in the phosphate-rich and organic-rich sediments of the Oulad-Abdoun and Timahdit basins (Morocco). Journal of African Earth Sciences 22 (1), 17–27.

Nathan, Y., Soudry, D., Levy, Y., Shitrit, D., Dorfman, E., 1997. Geochemistry of cadmium in the Negev phosphorites. Chemical Geology 142 (1-2), 87–107.

Neuendorf, K.K.E., Mehl, J.P., Jackson, Julia, A. (Eds.), 2005. Glossary of geology, 5th ed. American Geological Institute, Alexandria Va, XII, 779 pp.

Neumann, T., Rausch, N., Leipe, T., Dellwig, O., Berner, Z., Böttcher, M.E., 2005. Intense pyrite formation under low-sulfate conditions in the Achterwasser lagoon, SW Baltic Sea. Geochimica et Cosmochimica Acta 69 (14), 3619–3630.

Nguyen, T.M.P., Petrizzo, M.R., Speijer, R.P., 2009. Experimental dissolution of a fossil foraminiferal assemblage (Paleocene–Eocene Thermal Maximum, Dababiya, Egypt): Implications for paleoenvironmental reconstructions. Marine Micropaleontology 73 (3–4), 241–258.

Noe-Nygaard, N., Surlyk, F., 1985. Mound bedding in a sponge-rich Coniacian chalk, Bornholm, Denmark. Bulletin of the geological Society of Denmark 34, 237–249.

Nriagu, J.O., Soon, Y.K., 1985. Distribution and isotopic composition of sulfur in lake sediments of northern Ontario. Geochimica et Cosmochimica Acta 49 (3), 823–834.

Nürnberg, D., Bijma, J., Hemleben, C., 1996. Assessing the reliability of magnesium in foraminiferal calcite as a proxy for water mass temperatures. Geochimica et Cosmochimica Acta 60 (5), 803–814.

Obrien, G.W., Harris, JR, Milnes, A.R., Veeh, H.H., 1981. Bacterial origin of East Australian continental - margin phosphorites. Nature 294 (5840), 442–444.

Obrien, G.W., Veeh, H.H., 1980. Holocene Phosphorite on the East Australian continental margin. Nature 288 (5792), 690–692.

Okrusch, M., 2005. Mineralogie: Eine Einführung in die spezielle Mineralogie, Petrologie und Lagerstättenkunde, 7th ed. Springer-Verlag Berlin Heidelberg, Berlin, Heidelberg, 483 pp.

Oomori, T., Kaneshima, H., Maezato, Y., Kitano, Y., 1987. Distribution coefficient of Mg^{2+} ions between calcite and solution at 10–50°C. Marine Chemistry 20 (4), 327–336.

Orr, W.L., Sinninghe Damsté, J.S., 1990. Geochemistry of Sulfur in Petroleum Systems, in: Orr, W.L., White, C.M. (Eds.), Geochemistry of sulfur in fossil fuels. Developed from a symposium sponsored by the Division of Geochemistry at the 197th National Meeting of the American Chemical Society, Dallas, Texas, April 9-14, 1989, vol. 429. American Chemical Society, Washington, DC, pp. 2–29.

Oschmann, W., 1988. Kimmeridge clay sedimentation — A new cyclic model. Palaeogeography, Palaeoclimatology, Palaeoecology 65 (3–4), 217–251.

Pana, Y., Fleet, M.E., 2002. Compositions of the Apatite-Group Minerals: Substitution Mechanisms and Controlling Factors, in: Kohn, M.J., Rakovan, J., Hughes, J.M. (Eds.), Phosphates. Geochemical, geobiological, and materials importance. Mineralogical Society of America, Washington, DC, pp. 13–50.

Passey, Q.R., Bohacs, K.M., Esch, W.L., Klimentidis, R., Sinha, S. (Eds.), 2010. From oil-prone source rock to gas-producing shale reservoir-geologic and petrophysical characterization of unconventional shale gas reservoirs: This paper was prepared for presentation at the CPS/SPE International Oil & Gas Conference and Exhibition in China held in Beijing, China, 8–10 June 2010.

Paulmier, A., Ruiz-Pino, D., 2009. Oxygen minimum zones (OMZs) in the modern ocean. Progress in Oceanography 80 (3–4), 113–128.

Pedersen, T.F., Vogel, J.S., Southon, J.R., 1986. Copper and manganese in hemipelagic sediments at 21 °N, east pacific rise: Diagenetic contrasts. Geochimica et Cosmochimica Acta 50 (9), 2019–2031.

Peeters, F.J.C., Brummer, G.-J.A., Ganssen, G., 2002. The effect of upwelling on the distribution and stable isotope composition of Globigerina bulloides and Globigerinoides ruber (planktic foraminifera) in modern surface waters of the NW Arabian Sea. Global and Planetary Change 34, 269–291.

Pekar, S.F., Christie-Blick, N., Kominz, M.A., Miller, K.G., 2002. Calibration between eustatic estimates from backstripping and oxygen isotopic records for the Oligocene. Geology 30 (10), 903–906.

Pena, L.D., Calvo, E., Cacho, I., Eggins, S., Pelejero, C., 2005. Identification and removal of Mn-Mg-rich contaminant phases on foraminiferal tests: Implications for Mg/Ca past temperature reconstructions. Geochemistry, Geophysics, Geosystems 6 (9).

Pichevin, L., Bertrand, P., Boussafir, M., Disnar, J.-R., 2004. Organic matter accumulation and preservation controls in a deep sea modern environment: an example from Namibian slope sediments. Organic Geochemistry 35 (5), 543–559.

Pinet, P.R., 1992. Oceanography, an introduction to the planet Oceanus. West Pub. Co., St. Paul, xiv, 571.

Piper, D.Z., 1994. Seawater as the source of minor elements in black shales, phosphorites and other sedimentary rocks. Chemical Geology 114 (1-2), 95–114.

Piper, D.Z., Perkins, R.B., 2004. A modern vs. Permian black shale the hydrography, primary productivity, and water-column chemistry of deposition. Geochemistry of Organic-Rich Shales: New Perspectives 206 (3-4), 177–197.

Pisarzowska, A., Berner, Z.A., Racki, G., 2014. Geochemistry of Early Frasnian (Late Devonian) pyrite-ammonoid level in the Kostomłoty Basin, Poland, and a new proxy parameter for assessing the relative amount of syngenetic and diagenetic pyrite. Sedimentary Geology 308 (0), 18–31.

Pope, M.C., Steffen, J.B., 2003. Widespread, prolonged late Middle to Late Ordovician upwelling in North America: A proxy record of glaciation? Geology 31 (1), 63–66.

Poulton, S.W., Canfield, D.E., 2005. Development of a sequential extraction procedure for iron: implications for iron partitioning in continentally derived particulates. Chemical Geology 214 (3–4), 209–221.

Pratt, L.M., 1984. Influence of Paleoenvironmental Factors of the Organic Matter in the Middle Cretaceous Greenhorn Formation, Pueblo, Colorado. AAPG Bulletin (American Association of Petroleum Geologists);(USA) 68 (9), 1146–1159.

Raiswell, R., Bottrell, S.H., Al-Biatty, H.J., Tan, M.M., 1993. The influence of bottom water oxygenation and reactive iron content on sulfur incorporation into bitumens from Jurassic marine shales. American Journal of Science 293 (6), 569–596.

Raiswell, R., Buckley, F., Berner, R.A., Anderson, T.F., 1988. Degree of pyritization of iron as a paleoenvironmental indicator of bottom-water oxygenation. Journal of Sedimentary Petrology 58 (5), 812–819.

Raiswell, R., Canfield, D.E., 1996. Rates of reaction between silicate iron and dissolved sulfide in Peru Margin sediments. Geochimica et Cosmochimica Acta 60 (15), 2777–2787.

Raiswell, R., Canfield, D.E., 1998. Sources of iron for pyrite formation in marine sediments. American Journal of Science 298 (3), 219–245.

Raiswell, R., Canfield, D.E., 2012. The Iron Biogeochemical Cycle Past and Present. Geochemical Perspectives 1 (1), 1–220.

Raiswell, R., Canfield, D.E., Berner, R.A., 1994. A comparison of iron extraction methods for the determination of degree of pyritisation and the recognition of iron-limited pyrite formation. Chemical Geology 111 (1-4), 101–110.

Rakovan, J., 2002. Growth and Surface Properties of Apatite, in: Kohn, M.J., Rakovan, J., Hughes, J.M. (Eds.), Phosphates. Geochemical, geobiological, and materials importance. Mineralogical Society of America, Washington, DC, pp. 51–86.

Rathburn, A.E., Deckker, P. de, 1997. Magnesium and strontium compositions of Recent benthic foraminifera from the Coral Sea, Australia and Prydz Bay, Antarctica. Marine Micropaleontology 32 (3–4), 231–248.

Reiss, Z., Almogi-Labin, A., Honigstein, A., Lewy, Z., Lipson-Benitah, S., Moshkovitz, S., Zaks, Y., 1985. Late Cretaceous Multiple Stratigraphic Framework of Israel. Israel Journal of Earth Sciences 34, 147–166.

Rentería-Cano, M., Sánchez-Velasco, L., Shumilin, E., Lavín, M., Gómez-Gutiérrez, J., 2010. Major and Trace Elements in Zooplankton from the Northern Gulf of California During Summer. Biological Trace Element Research, 1–17.

Riboulleau, A., Baudin, F., Deconinck, J.F., Derenne, S., Largeau, C., Tribovillard, N., 2003. Depositional conditions and organic matter preservation pathways in an epicontinental environment: the Upper Jurassic Kashpir Oil Shales (Volga Basin, Russia). Palaeogeography, Palaeoclimatology, Palaeoecology 197 (3-4), 171–197.

Rice, C.A., Tuttle, M.L., Reynolds, R.L., 1993. The analysis of forms of sulfur in ancient sediments and sedimentary rocks: comments and cautions. Chemical Geology 107 (1-2), 83–95.

Rickard, D., 1995. Kinetics of FeS precipitation: Part 1. Competing reaction mechanisms. Geochimica et Cosmochimica Acta 59 (21), 4367–4379.

Rickard, D., Luther, I.G.W., 2007. Chemistry of iron sulfides. Chemical Reviews 107 (2), 514–562.

Rickard, D., Morse, J.W., 2005. Acid volatile sulfide (AVS). Marine Chemistry 97 (3-4), 141–197.

Rickard, D.T., 2012. Sulfidic sediments and sedimentary rocks. Elsevier, Amsterdam, 801 pp.

Rimmer, S.M., 2004. Geochemical paleoredox indicators in Devonian-Mississippian black shales, Central Appalachian Basin (USA): Geochemistry of Organic-Rich Shales: New Perspectives. Chemical Geology 206 (3-4), 373–391.

Roberts, J.A., Kenward, P.A., Fowle, D.A., Goldstein, R.H., González, L.A., Moore, D.S., 2013. Surface chemistry allows for abiotic precipitation of dolomite at low temperature. Proceedings of the National Academy of Sciences 110 (36), 14540–14545.

Rosenthal, Y., Boyle, E.A., Slowey, N., 1997. Temperature control on the incorporation of magnesium, strontium, fluorine, and cadmium into benthic foraminiferal shells from Little Bahama Bank: Prospects for thermocline paleoceanography. Geochimica et Cosmochimica Acta 61 (17), 3633–3643.

Rosenthal, Y., Lear, C.H., Oppo, D.W., Linsley, B.K., 2006. Temperature and carbonate ion effects on Mg/Ca and Sr/Ca ratios in benthic foraminifera: Aragonitic species Hoeglundina elegans. Paleoceanography 21 (1), 1–14.

Rosenthal, Y., Perron-Cashman, S., Lear, C.H., Bard, E., Barker, S., Billups, K., Bryan, M., Delaney, M.L., deMenocal, P.B., Dwyer, G.S., Elderfield, H., German, C.R., Greaves, M., Lea, D.W., Marchitto, T.M., Pak, D.K., Paradis, G.L., Russell, A.D., Schneider, R.R., Scheiderich, K., Stott, L., Tachikawa, K., Tappa, E., Thunell, R., Wara, M., Weldeab, S., Wilson, P.A., 2004. Interlaboratory comparison study of Mg/Ca and Sr/Ca measurements in planktonic foraminifera for paleoceanographic research. Geochemistry, Geophysics, Geosystems 5 (4), 1–29.

Rösler, H.J., Lange, H., 1972. Geochemical tables. Elsevier, Amsterdam, New York, 468 pp.

Rospondek, M.J., Köster, J., Damsté, J.S.S., 1997. Novel C26 highly branched isoprenoid thiophenes and alkane from the Menilite Formation, Outer Carpathians, SE Poland. ORGANIC GEOCHEMISTRY 26 (5–6), 295–304.

Rossi, V., 2008. Comparative study of mixing and biological activity of the Benguela and Canary upwelling systems. Geophys. Res. Lett. 35 (11), 1–5.

Rowan, C.J., Roberts, A.P., Broadbent, T., 2009. Reductive diagenesis, magnetite dissolution, greigite growth and paleomagnetic smoothing in marine sediments: A new view. Earth and Planetary Science Letters 277 (1–2), 223–235.

Rowe, H.D., Loucks, R.G., Ruppel, S.C., Rimmer, S.M., 2008. Mississippian Barnett Formation, Fort Worth Basin, Texas: Bulk geochemical inferences and Mo – TOC constraints on the severity of hydrographic restriction. Chemical Geology 257 (1–2), 16–25.

Rozanov, A.G., Volkov, I.I., Sokolov, V.S., Pushkina, Z.V., Pilipchuk, M.F., 1976. Chemical composition of sediments and interstitial waters in the Gulf of California and Eastern Pacific: Supplement to: Rozanov, Alexander G; Volkov, Igor I; Sokolov, Vassily S; Pushkina, Zinaida V; Pilipchuk, Mikhail F (1976): Redox processes in bottom sediments of the Gulf of California and adjacent part of the Pacific Ocean (iron and manganese compounds). In: Volkov, I.I. (Ed.), Biogeochemistry of Diagenesis of Ocean Sediments; Nauka Publ. (Moscow): in Russian, 96-135.

Rudnicki, M.D., Elderfield, H., Spiro, B., 2001. Fractionation of sulfur isotopes during bacterial sulfate reduction in deep ocean sediments at elevated temperatures. Geochimica et Cosmochimica Acta 65 (5), 777–789.

Rullkötter, J., Aizenshtat, Z., Spiro, B., 1984. Biological markers in bitumens and pyrolyzates of Upper Cretaceous bituminous chalks from the Ghareb Formation (Israel). Geochimica et Cosmochimica Acta 48 (1), 151–157.

Ruokolainen, M., Pantsar-Kallio, M., Haapa, A., Kairesalo, T., 2000. Leaching, runoff and speciation of arsenic in a laboratory mesocosm. Science of the Total Environement 258 (3), 139–147.

Russell, A.D., Emerson, S., Nelson, B.K., Erez, J., Lea, D.W., 1994. Uranium in foraminiferal calcite as a recorder of seawater uranium concentrations. Geochimica et Cosmochimica Acta 58 (2), 671–681.

Russell, A.D., Hönisch, B., Spero, H.J., Lea, D.W., 2004. Effects of seawater carbonate ion concentration and temperature on shell U, Mg, and Sr in cultured planktonic foraminifera. Geochimica et Cosmochimica Acta 68 (21), 4347–4361.

Ruttenberg, K.C., 2004. The Global Phosphorus Cycle, in: Holland, H.D., Turekian, K.K. (Eds.), Biogeochemistry, 1st ed. Elsevier, Amsterdam, Boston, pp. 585–643.

Sadekov, A., Eggins, S.M., 2005. Characterization of Mg/Ca distributions in planktonic foraminifera species by electron microprobe mapping. Geochemistry, Geophysics, Geosystems 12 (6).

Sælen, G., Raiswell, R., Talbot, M. R., Skei, J.M., Bottrell, S.H., 1993. Heavy sedimentary sulfur isotopes as indicators of super-anoxic bottom-water conditions. Geology 21 (12), 1091–1094.

Sageman, B.B., Lyons, T.W., 2003. Geochemistry of Fine-grained Sediments and Sedimentary Rocks, in: Heinrich D. Holland, Karl K. Turekian (Eds.), Treatise on Geochemistry. Pergamon, Oxford, pp. 115–158.

Sandler, A., Harlavan, Y., 2006. Early diagenetic illitization of illite-smectite in Cretaceous sediments (Israel): evidence from K-Ar dating. Clay Minerals 41 (2), 637–658.

Sani, R.K., Peyton, B.M., Amonette, J.E., Geesey, G.G., 2004. Reduction of uranium(VI) under sulfate-reducing conditions in the presence of Fe(III)-(hydr)oxides. Geochimica et Cosmochimica Acta 68 (12), 2639–2648.

Schäfer, A., 2010. Klastische Sedimente: Fazies und Sequenzstratigraphie, 1st ed. Spektrum Akademischer Verlag München, 416pp.

Schenau, S.J., Passier, H.F., Reichart, G.J., de Lange, G. J., 2002. Sedimentary pyrite formation in the Arabian Sea. Marine Geology 185 (3–4), 393–402.

Schiebel, R., Hemleben, C., 2005. Modern planktic foraminifera. Paläontol Z 79 (1), 135-148.

Schiebel, R., Zeltner, A., Treppke, U.F., Waniek, J.J., Bollmann, J., Rixen, T., Hemleben, C., 2004. Distribution of diatoms, coccolithophores and planktic foraminifers along a trophic gradient during SW monsoon in the Arabian Sea. Marine Micropaleontology 51 (3-4), 345–371.

Schlanger, S.O., 1988. Strontium Storage and Release During Deposition and Diagenesis of Marine Carbonates Related to Sea-Level Variations, in: Lerman, A., Meybeck, M. (Eds.), Physical and Chemical Weathering in Geochemical Cycles, vol. 251. Springer Netherlands, pp. 323–339.

Schmaljohann, R., Drews, M., Walter. S., Linke, P., von Rad, U., Imhoff, J.F., 2001. Oxygen-minimum zone sediments in the northeastern Arabian Sea off Pakistan: a habitat for the bacterium Thioploca. Marine Ecology Progress Series 211, 27–42.

Schneider-Mor, A., Alsenz, H., Ashckenazi-Polivoda, S., Illner, P., Abramovich, S., Feinstein, S., Almogi-Labin, A., Berner, Z., Püttmann, W., 2012. Paleoceanographic reconstruction of the late Cretaceous oil shale of the Negev, Israel: Integration of geochemical, and stable isotope records of the organic matter. Palaeogeography, Palaeoclimatology, Palaeoecology (319-320), 46–57.

Schön, J., 2004. Physical properties of rocks: Fundamentals and principles of petrophysic, 1st ed. Elsevier, Amsterdam, 583 pp.

Schoonen, M.A.A., Barnes, H.L., 1991a. Mechanisms of pyrite and marcasite formation from solution: III. Hydrothermal processes. Geochimica et Cosmochimica Acta 55 (12), 3491–3504.

Schoonen, M.A.A., Barnes, H.L., 1991b. Reactions forming pyrite and marcasite from solution: II. Via FeS precursors below 100°C. Geochimica et Cosmochimica Acta 55 (6), 1505–1514.

Schouten, S., Eglinton, T., Jaap, S., Sinninghe Damste, J.S., Leeuw, J.W. de, 1990. Influence of Sulphur Cross-linking on the Molecular-Size Distribution of Sulphur-Rich Macromolecules in Bitumen, in: Orr, W.L., White, C.M. (Eds.), Geochemistry of sulfur in fossil fuels. Developed from a symposium sponsored by the Division of Geochemistry at the 197th National Meeting of the American Chemical Society, Dallas, Texas, April 9-14, 1989. American Chemical Society, Washington, DC.

Schouten, S., Sinninghe Damsté, J.S., Leeuw, J.W. de, 1995. The occurrence and distribution of low-molecular-weight sulphoxides in polar fractions of sediment extracts and petroleum. Organic Geochemistry 23 (2), 129–138.

Schultz, R.B., 2004. Geochemical relationships of Late Paleozoic carbon-rich shales of the Midcontinent, USA: a compendium of results advocating changeable geochemical conditions. Geochemistry of Organic-Rich Shales: New Perspectives. Chemical Geology 206 (3-4), 347–372.

Seifert, R., Michaelis, W., 1991. Organic Compounds in Sediments and Pore Waters of Sites 723 and 724. Proceedings of the Ocean Drilling Program 117, 529–545.

Shahar, J., 1994. The Syrian arc system: an overview. Palaeogeography, Palaeoclimatology, Palaeoecology 112 (1–2), 125–142.

Shahar, Y., 1968. Type Section of the Campanian Maastrichtian Ghareb Formation in the Oron Syncline (northern Negev). Geological Survey of Israel, Stratigraphic Sections (6), 1–8.

Shazly, E.M., Krs, M., 1973. Paleogeography and paleomagnetism of the Nubian Sandstone Eastern Desert of Egypt. Geol Rundsch 62 (1), 212–225.

Shen, Y.N., Canfield, D.E., Knoll, A.H., 2002. Middle proterozoic ocean chemistry: Evidence from the McArthur Basin, northern Australia. American Journal of Science 302 (2), 81–109.

Shiller, A.M., 1983. Particulate geochemistry in an area of coastal upwelling - the Santa Barbara Basin, in: Thiede, J., Suess, E. (Eds.), Sedimentary records of ancient coastal upwelling. Plenum Press, New York, pp. 289–301.

Shoval, S., 2004a. Clay sedimentation along the southeastern Neo-Tethys margin during the oceanic convergence stage. Third Mediterranean Clay Meeting 24 (3–4), 287–298.

Shoval, S., 2004b. Deposition of volcanogenic smectite along the southeastern Neo-Tethys margin during the oceanic convergence stage. Third Mediterranean Clay Meeting 24 (3–4), 299–311.

Shpirt, M., Punanova, S., Strizhakova, Y., 2007. Trace elements in black and oil shales. Solid Fuel Chemistry 41 (2), 119–127.

Siebert, C., Nagler, T.F., Blanckenburg, F. von, Kramers, J.D., 2003. Molybdenum isotope records as a potential new proxy for paleoceanography. Earth and Planetary Science Letters 211 (1-2), 159–171.

Sim, M.S., Bosak, T., Ono, S., 2011. Large Sulfur Isotope Fractionation Does Not Require Disproportionation. Science 333 (6038), 74–77.

Sinninghe Damsté, J.S., Eglinton, T.I., Leeuw, J.W. de, Schenck, P.A., 1989. Organic sulphur in macromolecular sedimentary organic matter: I. Structure and origin of sulphur-containing moieties in kerogen, asphaltenes and coal as revealed by flash pyrolysis. Geochimica et Cosmochimica Acta 53 (4), 873–889.

Sinninghe Damsté, J.S., Kuypers, M.M.M., Pancost, R.D., Schouten, S., 2008. Carbon isotopic composition of biomarkers of Cenomanian sediments of DSDP Hole 41-367: Supplement to: Sinninghe Damsté, Jaap S; Kuypers, Marcel MM; Pancost, Richard D; Schouten, Stefan (2008): The carbon isotopic response of algae, (cyano)bacteria, archaea and higher plants to the late Cenomanian perturbation of the global carbon cycle: Insights from biomarkers in black shales from the Cape Verde Basin (DSDP Site 367). Organic Geochemistry, 39(12), 1703-1718

Sinninghe Damsté, J.S., Leeuw, J.W. de, 1990. Analysis, structure and geochemical significance of organically-bound sulphur in the geosphere: State of the art and future research: Proceedings of the 14th International Meeting on Organic Geochemistry. Organic Geochemistry 16 (4-6), 1077–1101.
Sinninghe Damsté, J.S., Rijpstra, W.I.C., Coolen, M.J.L., Schouten, S., Volkman, J.K., 2007. Rapid sulfurisation of highly branched isoprenoid (HBI) alkenes in sulfidic Holocene sediments from Ellis Fjord, Antarctica. Organic Geochemistry 38 (1), 128–139.
Sliter, W.V., 1972. Upper Cretaceous planktonic foraminiferal zoogeography and ecology—eastern Pacific margin. Palaeogeography, Palaeoclimatology, Palaeoecology 12 (1–2), 15–31.
Smillie, R.H., Hunter, K., Loutit, M., 1981. Reduction of chromium(VI) by bacterially produced hydrogen sulphide in a marine environment. Water Research 15 (12), 1351–1354.
Sohrin, Y., Matsui, M., Kawashima, M., Hojo, M., Hasegawa, H., 1997. Arsenic biogeochemistry affected by eutrophication in Lake Biwa, Japan. Environmental Science & Technology 31 (10), 2712–2720.
Soliman, M.A., Habib, M.E., Ahmed, E.A., 1986. Sedimentologic and tectonic evolution of the Upper Cretaceous-Lower Tertiary succession at Wadi Qena, Egypt. Sedimentary Geology 46 (1–2), 111–133.
Soudry, D., 1987. Ultra-fine structures and genesis of the Campanian Negev high-grade phosphorites (southern Israel). Sedimentology 34 (4), 641–660.
Soudry, D., Ehrlich, S., Yoffe, O., Nathan, Y., 2002. Uranium oxidation state and related variations in geochemistry of phosphorites from the Negev (southern Israel). Chemical Geology 189 (3–4), 213–230.
Soudry, D., Glenn, C.R., Nathan, Y., Segal, I., VonderHaar, D., 2006. Evolution of Tethyan phosphogenesis along the northern edges of the Arabian-African shield during the Cretaceous-Eocene as deduced from temporal variations of Ca and Nd isotopes and rates of P accumulation. Earth-Science Reviews 78 (1-2), 27–57.
Soudry, D., Gregor, H.J., 1997. Jodes israelii sp. nov: A huge phosphate-mineralized icacinacean fructification from the Late Cretaceous of the Negev, southern Israel. Cretaceous Research 18 (2), 161–178.
Soudry, D., Nathan, Y., Ehrlich, S., 2012. Geochemical diagenetic trends during phosphorite formation – economic implications: The case of the Negev Campanian phosphorites, Southern Israel. Sedimentology, no.
Southam, J.R., Peterson, W.H., Brass, G.W., 1982. Dynamics of anoxia: Paleogeography and Climate. Palaeogeography, Palaeoclimatology, Palaeoecology 40 (1-3), 183–198.
Speijer, R.P., Schmitz, B., 1998. A benthic foraminiferal record of Paleocene sea level and trophic/redox conditions at Gebel Aweina, Egypt. Palaeogeography, Palaeoclimatology, Palaeoecology 137 (1–2), 79–101.
Spero, H.J., Bijma, J., Lea, D.W., Bemis, B.E., 1997. Effect of seawater carbonate concentration on foraminiferal carbon and oxygen isotopes. Nature 390 (6659), 497–500.
Spiro, B., 1977. Bacterial sulphate reduction and calcite precipitation in hypersaline deposition of bituminous shales. Nature 269 (5625), 235–237.
Spiro, B., Dinur, D., Aizenshtat, Z., 1983. Evaluation of source, environments of deposition and diagenesis of some israeli "oil shales" -- N-Alkanes, fatty acids, tetrapyrroles and kerogen. Chemical Geology 39 (3-4), 189–214.
Spiro, B., Rozenson, I., 1980. Distribution of iron species in some "oil shales" of the Judea Desert, Israel. Chemical Geology 28, 41–54.
Spiro, B., Rozenson, I., 1982. Formation and properties of authigenic minerals in bituminous calcareous shales, Ghareb Formation, Israel. Canadian Mineralogist 20 (FEB), 29–40.
Stankiewicz, B.A., Kruge, M.A., Mastalerz, M., Salmon, G.L., 1996. Geochemistry of the alginite and amorphous organic matter from Type II-S kerogens. Organic Geochemistry 24 (5), 495–509.
Stein, R., 1986. Organic carbon and sedimentation rate—further evidence for anoxic deep-water conditions in the Cenomanian/Turonian Atlantic Ocean. Marine Geology 72 (3), 199–209.
Stein, R., 1990. Organic carbon content/sedimentation rate relationship and its paleoenvironmental significance for marine sediments. Geo-Marine Letters 10 (1), 37–44.
Steuber, T., Veizer, J., 2002. Phanerozoic record of plate tectonic control of seawater chemistry and carbonate sedimentation. Geology 30 (12), 1123–1126.
Stewart, R.H., 2007. Introduction to physical oceanography, 2008th ed. Texas A & M University, College Station, Texas, 313 pp.
Stille, P., 1992. Nd-Sr isotope evidence for dramatic changes of paleocurrents in the Atlantic Ocean during the past 80 m.y. Geology 20 (5), 387–390.
Stille, P., Steinmann, M., Riggs, S.R., 1996. Nd isotope evidence for the evolution of the paleocurrents in the Atlantic and Tethys Oceans during the past 180 Ma. Earth and Planetary Science Letters 144 (1–2), 9–19.
Stoll, H.M., Schrag, D.P., 1996. Evidence for Glacial Control of Rapid Sea Level Changes in the Early Cretaceous. Science (New Series) 272 (5269), 1771–1774.
Stoll, H.M., Schrag, D.P., 1998. Effects of Quaternary Sea Level Cycles on Strontium in Seawater. Geochimica et Cosmochimica Acta 62 (7), 1107–1118.

Stoll, H.M., Schrag, D.P., 2000. High-resolution stable isotope records from the Upper Cretaceous rocks of Italy and Spain: Glacial episodes in a greenhouse planet? Geological Society of America Bulletin 112 (2), 308–319.
Stoll, H.M., Schrag, D.P., 2001. Sr/Ca variations in Cretaceous carbonates: relation to productivity and sea level changes. Palaeogeography, Palaeoclimatology, Palaeoecology 168 (3–4), 311–336.
Stramma, L., Oschlies, A., Schmidtko, S., 2012. Mismatch between observed and modeled trends in dissolved upper-ocean oxygen over the last 50 yr. Biogeoscience 9 (10), 4045–4057.
Strauss, H., 1997. The isotopic composition of sedimentary sulfur through time. Palaeogeography, Palaeoclimatology, Palaeoecology 132 (1–4), 97–118.
Strauss, H., 1999. Geological evolution from isotope proxy signals — sulfur. Chemical Geology 161 (1–3), 89–101.
Strizhov, V.P., Nikolaev, S.D., Gurina, N.V., 1989. Isotope composition of sulfur, oxygen and carbon in Black Sea sediments: Supplement to: Strizhov, Valentin P; Nikolaev, Sergey D; Gurina, NV (1989): Isotope composition of sulfur, oxygen and carbon in Black Sea sediments and possible reasons for its alteration in Late Quaternary time. Oceanology, 29(6), 731-736.
Stüben, D., Kramar, U., Berner, Z., Stinnesbeck, W., Keller, G., Adatte, T., 2002. Trace elements, stable isotopes, and clay mineralogy of the Elles II K-T boundary section in Tunisia: indications for sea level fluctuations and primary productivity. Palaeogeography, Palaeoclimatology, Palaeoecology 178 (3-4), 321–345.
Stüben, D., Kramar, U., Berner, Z.A., Meudt, M., Keller, G., Abramovich, S., Adatte, T., Hambach, U., Stinnesbeck, W., 2003. Late Maastrichtian paleoclimatic and paleoceanographic changes inferred from Sr/Ca ratio and stable isotopes. Palaeogeography, Palaeoclimatology, Palaeoecology 199 (1-2), 107–127.
Suhr, D., 2009. Principal component analysis vs. exploratory factor analysis, in: SUGI 30 Proceedings.
Suits, N.S., Arthur, M.A., 2000. Sulfur diagenesis and partitioning in Holocene Peru shelf and upper slope sediments. Chemical Geology 163 (1–4), 219–234.
Summerhayes, C.P., Prell, W.L., Emeis, K.-C., 1992. Evolution of upwelling systems since the Early Miocene. Geological Society, London, Special Publications 64 (1), 1–5.
Sundby, B., Martinez, P., Gobeil, C., 2004. Comparative geochemistry of cadmium, rhenium, uranium, and molybdenum in continental margin sediments. Geochimica et Cosmochimica Acta 68 (11), 2485–2493.
Swanston, J., 2000. Thiophene, in: Ullmann's Encyclopedia of Industrial Chemistry. Wiley-VCH Verlag GmbH & Co. KGaA.
Sweeney, R.E., Kaplan, I.R., 1980. Diagenetic sulfate reduction in marine sediments. Marine Chemistry 9 (3), 165–174.
Tantawy, A.A., Keller, G., Adatte, T., Stinnesbeck, W., Kassab, A., Schulte, P., 2001. Maastrichtian to Paleocene depositional environment of the Dakhla Formation, Western Desert, Egypt: sedimentology, mineralogy, and integrated micro- and macrofossil biostratigraphies. Cretaceous Research 22 (6), 795–827.
Taylor, K.G., Macquaker, J.H.S., 2011. Iron Minerals in Marine Sediments Record Chemical Environments. Elements 7 (2), 113–118.
Temraz, M., 2005. Mineralogical and geochemical studies of carbonaceous shale deposits from Egypt. Dissertation, Berlin, 124 pp.
Thiede, J., Suess, E. (Eds.), 1983. Sedimentary records of ancient coastal upwelling. Plenum Press, New York, xiv, 610.
Thomsen, L., vanWeering, T., Gust, G., 2002. Processes in the benthic boundary layer at the Iberian continental margin and their implication for carbon mineralization. Benthic processes and dynamics at the NW Iberian Margin: resultss of the OMEX II Program 52 (2–4), 315–329.
Thunell, R.C., Pride, C.J., Tappa, E., Muller-Karger, F.E., 1994. Biogenic silica fluxes and accumulation rates in the Gulf of California. Geology 22 (4), 303–306.
Tomczak, M., Godfrey, J.S., 2003. Regional oceanography: An introduction, 2nd ed. Daya Publ. House, Delhi, 390 pp.
Totman Parrish, J., Curtis, R.L., 1982. Atmospheric circulation, upwelling, and organic-rich rocks in the Mesozoic and Cenozoic eras: Paleogeography and Climate. Palaeogeography, Palaeoclimatology, Palaeoecology 40 (1-3), 31–66.
Tribovillard, N., Algeo, T.J., Lyons, T., Riboulleau, A., 2006. Trace metals as paleoredox and paleoproductivity proxies: An update. Chemical Geology 232 (1-2), 12–32.
Tribovillard, N., Bout-Roumazeilles, V., Algeo, T., Lyons, T.W., Sionneau, T., Montero-Serrano, J.C., Riboulleau, A., Baudin, F., 2008a. Paleodepositional conditions in the Orca Basin as inferred from organic matter and trace metal contents. Marine Geology 254 (1–2), 62–72.
Tribovillard, N., Lyons, T.W., Riboulleau, A., Bout-Roumazeilles, V., 2008b. A possible capture of molybdenum during early diagenesis of dysoxic sediments. Bulletin de la Societe Geologique de France 179 (1), 3–12.

Tribovillard, N., Riboulleau, A., Lyons, T., Baudin, F.O., 2004. Enhanced trapping of molybdenum by sulfurized marine organic matter of marine origin in Mesozoic limestones and shales. Chemical Geology 213 (4), 385–401.
Turekian, K., 1968. Oceans, 1st ed. Prentice-Hall, 120 pp.
Tyson, R.V., 1987. The genesis and palynofacies characteristics of marine petroleum source rocks. Geological Society, London, Special Publications 26 (1), 47–67.
Tyson, R.V. (Ed.), 1991. Modern and ancient continental shelf anoxia: Papers presented at a Meeting of the Geological Society Marine Studies Group at Burlington House, London, May 17 - 19, 1989. Geological Society, London, 470 pp.
Tyson, R.V., 2001. Sedimentation rate, dilution, preservation and total organic carbon: some results of a modelling study. Organic Geochemistry 32 (2), 333–339.
Urban, N.R., Ernst, K., Bernasconi, S., 1999. Addition of sulfur to organic matter during early diagenesis of lake sediments. Geochimica et Cosmochimica Acta 63 (6), 837–853.
van der Veen, A., 2003. Schwefelspeziation und assoziierte Metalle in rezenten Sedimenten. Dissertation, Braunschweig, 205 pp.
van der Weijden, C.H., 2002. Pitfalls of normalization of marine geochemical data using a common divisor. Marine Geology 184 (3–4), 167–187.
van der Zwaan, G.J., Duijnstee, I. A. P, den Dulk, M., Ernst, S.R., Jannink, N.T., Kouwenhoven, T.J., 1999. Benthic foraminifers: proxies or problems?: A review of paleocological concepts. Earth-Science Reviews 46 (1–4), 213–236.
van Kaam-Peters, H.M.E., Schouten, S., Köster, J., Sinninghe Damsté, J.S., 1998. Controls on the molecular and carbon isotopic composition of organic matter deposited in a Kimmeridgian euxinic shelf sea: evidence for preservation of carbohydrates through sulfurisation. Geochimica et Cosmochimica Acta 62 (19-20), 3259–3283.
van Lith, Y., Warthmann, R., Vasconcelos, C., McKenzie, J.A., 2003. Microbial fossilization in carbonate sediments: a result of the bacterial surface involvement in dolomite precipitation. Sedimentology 50 (2), 237–245.
Vasconcelos, C., McKenzie, J.A., 1997. Microbial mediation of modern dolomite precipitation and diagenesis under anoxic conditions (Lagoa Vermelha, Rio de Janeiro, Brazil). Journal of Sedimentary Research 67 (3), 378–390.
Vasconcelos, C., McKenzie, J.A., Bernasconi, S., Grujic, D., Tiens, Albert J., 1995a. Microbial mediation as a possible mechanism for natural dolomite formation at low temperatures. Nature 377 (6546), 220–222.
Vasconcelos, C., McKenzie, Judith A., Bernasconi, S., Grujic, D., Tiens, Albert J., 1995b. Microbial mediation as a possible mechanism for natural dolomite formation at low temperatures. Nature 377 (6546), 220–222.
Voigt, S., Friedrich, O., Norris, R.D., Schönfeld, J., 2010. Campanian - Maastrichtian carbon isotope stratigraphy: shelf-ocean correlation between the European shelf sea and the tropical Pacific Ocean. Newsletter of Stratigraphy 44 (1), 57–72.
Voigt, S., Gale, A.S., Jung, C., Jenkyns, H.C., 2012. Global correlation of Upper Campanian - Maastrichtian successions using carbon-isotope stratigraphy: development of a new Maastrichtian timescale. Newsletter of Stratigraphy 45 (1), 25–53.
Volkman, J.K., Farrington, J.W., Gagosian, R.B., 1987. Marine and terrigenous lipids in coastal sediments from the Peru upwelling region at 15°S: Sterols and triterpene alcohols. Organic Geochemistry 11 (6), 463–477.
Volkov, I.I., 1984. Sulfur in oceans and seas: Supplement to: Volkov, Igor I (1984): Geokhimiya Sery v Osadkakh Okeana (Geochemistry of Sulfur in Ocean Sediments). Nauka Publ. (Moscow): in Russian, 272 pp.
Wakeham, S.G., Sinninghe Damsté, J.S., Kohnen, M.E.L., Leeuw, J.W. de, 1995. Organic sulfur compounds formed during early diagenesis in Black Sea sediments. Geochimica et Cosmochimica Acta 59 (3), 521–533.
Wang, D., Wallace, A.F., De Yoreo, James J., Dove, P.M., 2009. Carboxylated molecules regulate magnesium content of amorphous calcium carbonates during calcification. Proceedings of the National Academy of Sciences 106 (51), 21511–21516.
Ward, K.C., 1979. Nubia Formation of Central Eastern Desert, Egypt--Major Subdivisions and Depositional Setting. The American Association of Petroleum Bulletin 63 (6), 975–983.
Wedepohl, K.H., 1969-1972. Handbook of geochemistry. Springer-Verlag, Berlin, v.1, xiv, 442.
Weeks, S.J., Currie, B., Bakun, A., Peard, K.R., 2004. Hydrogen sulphide eruptions in the Atlantic Ocean off southern Africa: implications of a new view based on SeaWiFS satellite imagery. Deep Sea Research Part I: Oceanographic Research Papers 51 (2), 153–172.
Wefer, G. (Ed.), 1985. Die Verteilung stabiler Isotope in Kalkschalen mariner Organismen. E. Schweizerbart'sche Verlagsbuchhandlung, Stuttgart, 108 pp.
Weiner, S., Addadi, L., 2011. Crystallization Pathways in Biomineralization: Annual Review of Materials Research. Annu. Rev. Mater. Res 41 (1), 21–40.

Werne, J.P., 2000. A geochemical evaluation of depositional controls and paleoenvironmental reconstructions in organic rich sedimentary deposits: evidence from the modern Cariaco basin, Venezuela, and application to the Devonian Appalachian basin.
Werne, J.P., Hollander, D.J., Behrens, A., Schaeffer, P., Albrecht, P., Sinninghe Damsté, J.S., 2000. Timing of early diagenetic sulfurization of organic matter: a precursor-product relationship in Holocene sediments of the anoxic Cariaco Basin, Venezuela. Geochimica et Cosmochimica Acta 64 (10), 1741–1751.
Werne, J.P., Hollander, D.J., Lyons, T.W., Damsté, J.S.S., 2004. Organic sulfur biogeochemistry: Recent advances and future rsearch directions, in: Amend, J.P., Edwards, K.J., Lyons, T.W. (Eds.), Sulfur Biogeochemistry—Past and Present, pp. 135–150.
Werne, J.P., Lyons, T.W., Hollander, D.J., Formolo, M.J., Sinninghe Damsté, J.S., 2003. Reduced sulfur in euxinic sediments of the Cariaco Basin: sulfur isotope constraints on organic sulfur formation: Isotopic records of microbially mediated processes. Chemical Geology 195 (1-4), 159–179.
Werne, J.P., Lyons, T.W., Hollander, D.J., Schouten, S., Hopmans, E.C., Sinninghe Damsté, J.S., 2008. Investigating pathways of diagenetic organic matter sulfurization using compound-specific sulfur isotope analysis. Geochimica et Cosmochimica Acta 72 (14), 3489–3502.
Werne, J.P., Sageman, B.B., Lyons, T.W., Hollander, D.J., 2002. An integrated assessment of a “type euxinic” deposit: Evidence for multiple controls on black shale deposition in the Middle Devonian Oatka Creek Formation. American Journal of Science 302 (2), 110–143.
Westrich, J.T., Berner, R.A., 1984. The role of sedimentary organic matter in bacterial sulfate reduction: The G model tested. Limnology and Oceanography 29 (2), 236–249.
Widmark, J.G., 1997. Deep-sea benthic foraminifera from Cretaceous-Paleogene boundary strata in the South Atlantic. Scandinavian Univ. Pr., Oslo.
Wignall, P.B., Newton, R., Brookfield, M.E., 2005. Pyrite framboid evidence for oxygen-poor deposition during the Permian–Triassic crisis in Kashmir. Palaeogeography, Palaeoclimatology, Palaeoecology 216 (3–4), 183–188.
Wijsman, J.W.M., Middelburg, J.J., Heip, C.H.R., 2001a. Reactive iron in Black Sea Sediments: implications for iron cycling. Marine Geology 172 (3–4), 167–180.
Wijsman, J.W.M., Middelburg, J.J., Herman, P.M.J., Böttcher, M.E., Heip, C.H.R., 2001b. Sulfur and iron speciation in surface sediments along the northwestern margin of the Black Sea. Marine Chemistry 74 (4), 261–278.
Wilkerson, F., Dugdale, R.C., 2008. Coastal Upwelling, in: Nitrogen in the Marine Environment (2nd Edition). Academic Press, San Diego, pp. 771–807.
Wilkin, R.T., Arthur, M.A., 2001. Variations in pyrite texture, sulfur isotope composition, and iron systematics in the Black Sea: evidence for Late Pleistocene to Holocene excursions of the o2-h2s redox transition. Geochimica et Cosmochimica Acta 65 (9), 1399–1416.
Wilkin, R.T., Barnes, H.L., 1997. Formation processes of framboidal pyrite. Geochimica et Cosmochimica Acta 61 (2), 323–339.
Wilkin, R.T., Barnes, H.L., Brantley, S.L., 1996. The size distribution of framboidal pyrite in modern sediments: An indicator of redox conditions. Geochimica et Cosmochimica Acta 60 (20), 3897–3912.
Willis, K.M., Stern, R.J., Clauer, N., 1988. Age and geochemistry of Late Precambrian sediments of the Hammamat Series from the Northeastern Desert of Egypt. Precambrian Research 42 (1), 173–187.
Wilson, P.A., Norris, R.D., Cooper, M.J., 2002. Testing the Cretaceous greenhouse hypothesis using glassy foraminiferal calcite from the core of the Turonian tropics on Demerara Rise. Geology 30 (7), 607–610.
Wortmann, U.G., Bernasconi, S.M., Böttcher, M.E., 2001. Hypersulfidic deep biosphere indicates extreme sulfur isotope fractionation during single-step microbial sulfate reduction. Geology 29 (7), 647–650.
Wright, D.T., 1999. The role of sulphate-reducing bacteria and cyanobacteria in dolomite formation in distal ephemeral lakes of the Coorong region, South Australia. Sedimentary Geology 126 (1–4), 147–157.
Wright, D.T., Wacey, D., 2005. Precipitation of dolomite using sulphate-reducing bacteria from the Coorong Region, South Australia: significance and implications. Sedimentology 52 (5), 987–1008.
Yoffe, O., Nathan, Y., Wolfarth, A., Cohen, S., Shoval, S., 2002. The chemistry and mineralogy of the Negev oil shale ashes. Fuel 81 (9), 1101–1117.
Yokoyama, Y., Tanaka, K., Takahashi, Y., 2012. Differences in the immobilization of arsenite and arsenate by calcite. Geochimica et Cosmochimica Acta 91 (0), 202–219.
Youssef, M.M., 2003. Structural Setting of Central and South Egypt: An Overview. Micropaleontology 49, 1–13.
Zhabina, N.N., Volkov, I.I., 1978. A method of determination of various sulfur compounds in sea sediments and rocks, in: Environmental biogeochemistry and geomicrobiology. Vol. 3: Methods, metals and assessment. Ann arbor science publ, pp. 735–746.
Zhang, L., Sun, M., Wang, S., Yu, X., 1998. The composition of shales from the Ordos basin, China: effects of source weathering and diagenesis. Sedimentary Geology 116 (1-2), 129–141.

Zhang, Z., Metzger, P., Sachs, J.P., 2011. Co-occurrence of long chain diols, keto-ols, hydroxy acids and keto acids in recent sediments of Lake El Junco, Galápagos Islands. Organic Geochemistry 42 (7), 823–837.

Zheng, Y., Anderson, R.F., van Geen, A., Fleisher, M.Q., 2002. Preservation of particulate non-lithogenic uranium in marine sediments. Geochimica et Cosmochimica Acta 66 (17), 3085–3092.

Zheng, Y., Anderson, R.F., van Geen, A., Kuwabara, J., 2000. Authigenic molybdenum formation in marine sediments: A link to pore water sulfide in the Santa Barbara Basin. Geochimica et Cosmochimica Acta 64 (24), 4165–4178.

Zonneveld, K.A.F., Versteegh, G.J.M., Kasten, S., Eglinton, T.I., Emeis, K.-C., Huguet, C., Koch, B.P., Lange, G.J. de, Leeuw, J.W. de, Middelburg, J.J., Mollenhauer, G., Prahl, F.G., Rethemeyer, J., Wakeham, S.G., 2010. Selective preservation of organic matter in marine environments; processes and impact on the sedimentary record. Biogeoscience 7 (2), 483–511.

9. Appendix

Table 8 Main Element composition bulk sediment (WD- XRF)

Marl - Oil Shale - Phosphorite Member

Sample	Depth (m)	SiO_2 (%)	Al_2O_3 (%)	MnO (%)	Fe_2O_{3T} (%)	TiO_2 (%)	CaO (%)	MgO (%)	Na_2O (%)	K_2O (%)	P_2O_5 (%)	Sum	LOI (%)
SAM012	0	10.77	4.02	0.01	1.88	0.19	43.02	0.58	0.36	0.01	2.09	98.62	35.69
SAM009	0.6	13.34	4.84	0.01	2.31	0.24	40.69	0.68	0.37	0.01	1.92	98.68	34.27
SAM008	0.8	13.18	5.11	0.01	2.34	0.24	40.95	0.50	0.38	0.06	1.98	96.95	32.21
SAM007	1	n.d.	n.d.	n.d.	n.d.	n.d.	n.d.	n.d.	n.d.	n.d.	n.d.	n.d.	n.d.
Numbers		***3***	***3***	***3***	***3***	***3***	***3***	***3***	***3***	***3***	***3***	***3***	***3***
Average		***12.43***	***4.66***	***0.01***	***2.18***	***0.22***	***41.56***	***0.59***	***0.37***	***0.03***	***1.99***	***98.08***	***34.05***
Maximum		***13.34***	***5.11***	***0.01***	***2.34***	***0.24***	***43.02***	***0.68***	***0.38***	***0.06***	***2.09***	***98.68***	***35.69***
Minimum		***10.77***	***4.02***	***0.01***	***1.88***	***0.19***	***40.69***	***0.50***	***0.36***	***0.01***	***1.92***	***96.95***	***32.21***
Stbw		***1.17***	***0.46***	***0.00***	***0.21***	***0.02***	***1.04***	***0.08***	***0.01***	***0.03***	***0.07***	***0.80***	***1.43***
SAOS001	2.8	15.37	5.80	0.01	2.80	0.28	35.63	0.68	0.35	0.12	1.43	98.85	36.38
SAOS006	3.2	15.21	6.13	0.01	2.67	n.d.	32.05	0.69	0.49	0.19	1.24	96.06	37.38
SAOS015	5	15.46	6.33	0.01	3.03	0.30	34.79	0.75	0.51	0.25	1.16	100.98	38.38
SAOS018	5.6	19.22	8.33	0.01	3.38	0.39	27.86	0.78	0.41	0.34	1.13	96.30	34.46
SAOS021	6.2	16.67	7.22	0.01	2.95	0.34	27.01	0.72	0.38	0.38	1.25	96.31	39.38
SAOS035	9	12.93	5.06	0.01	2.47	0.23	36.37	0.67	0.35	0.07	0.93	95.91	36.82
SAOS039	9.8	9.90	3.47	0.01	1.84	0.17	38.42	0.49	0.33	0.09	0.86	96.94	41.38
SAOS045	11	11.20	3.98	0.01	2.14	0.21	37.58	0.78	0.34	0.01	1.05	95.96	38.66
SAOS050	12	10.42	3.60	0.01	1.94	0.19	39.11	0.53	0.34	0.03	0.93	96.62	39.52
SAOS060	14	13.52	4.81	0.01	2.54	0.24	36.81	0.89	0.37	0.08	1.69	98.89	37.91
SAOS062	14.4	12.73	4.82	0.01	2.38	0.24	33.38	0.96	0.36	0.11	1.56	95.17	38.62
SAOS070	16	14.29	5.31	0.01	2.65	0.27	30.67	0.75	0.36	0.34	1.73	95.40	39.01
SAOS081	18.2	13.89	5.59	0.01	2.64	0.27	27.79	0.71	0.38	0.29	1.32	95.27	42.38
SAOS090	20	12.94	4.85	0.01	2.51	0.25	35.15	0.68	0.35	0.27	1.31	95.99	37.69
SAOS105	23	14.16	5.64	0.01	2.73	0.25	34.06	0.73	0.35	0.27	1.30	96.17	36.67
SAOS106	23.2	15.01	6.17	0.01	2.93	0.29	31.64	0.83	0.41	0.24	1.40	94.72	35.79
SAOS110	24	13.34	5.09	0.01	2.22	0.25	35.08	0.72	0.43	0.27	2.11	95.95	36.43
SAOS116	25.2	8.57	2.82	0.01	2.12	0.14	35.89	0.49	0.39	0.22	1.64	96.65	44.38
SAOS120	26	8.79	2.88	0.01	1.88	0.16	39.27	0.68	0.33	0.15	1.21	95.60	40.25
SAOS125	26.9	14.91	5.92	0.01	3.06	0.27	32.39	1.02	0.50	0.23	1.55	94.88	35.01
SAOS130	28	16.56	6.85	0.01	3.59	0.29	25.24	0.82	0.37	0.49	1.83	101.42	45.38
SAOS132	28.4	14.59	5.23	0.01	2.90	0.26	32.29	0.82	0.43	0.29	1.72	95.91	37.37
SAOS135-136	29.1	14.14	5.75	0.01	3.15	0.25	24.21	0.65	0.30	0.44	1.46	96.73	46.38
SAOS136	29.2	17.76	6.76	0.01	3.91	0.32	29.57	0.94	0.42	0.45	1.73	95.00	33.13
SAOS140	30	n.d.	n.d.	n.d.	n.d.	n.d.	n.d.	n.d.	n.d.	n.d.	n.d.	n.d.	n.d.
SAOS150	32	7.03	1.71	0.01	1.47	0.11	44.22	0.88	0.35	0.19	3.80	96.11	36.34
SAOS165	35	8.40	2.37	0.01	1.56	0.13	35.36	0.83	0.32	0.07	2.57	94.58	42.96
SAOS170	36	5.61	1.15	0.01	1.20	0.09	36.03	0.78	0.29	0.14	3.07	95.74	47.38
SAOS177	37.4	n.d.	n.d.	n.d.	n.d.	n.d.	n.d.	n.d.	n.d.	n.d.	n.d.	n.d.	n.d.
SAOS180	38	4.69	0.36	0.01	0.43	0.08	42.89	0.44	0.32	0.18	3.92	95.40	42.07
SAOS185	39	5.72	0.84	0.01	0.67	0.10	37.57	0.50	0.30	0.15	3.10	94.83	45.88
SAOS190	40	13.82	5.19	0.01	2.64	0.24	29.14	0.75	0.42	0.31	1.54	101.00	46.94
OSP024	42.2	5.63	1.29	0.01	0.65	0.10	36.25	0.62	0.28	0.18	1.75	95.72	48.97
OSP022	42.6	5.91	1.13	0.01	0.68	0.10	36.48	0.49	0.29	0.13	1.93	94.88	47.73
OSP020	43	4.89	0.49	0.00	0.49	0.07	40.72	0.64	0.31	0.14	4.22	97.13	45.15
OSP016	43.8	5.82	0.89	0.01	0.68	0.09	38.29	0.78	0.30	0.19	4.15	96.46	45.26
Numbers		***34***	***34***	***34***	***34***	***33***	***34***	***34***	***34***	***34***	***34***	***34***	***34***
Average		***11.74***	***4.23***	***0.01***	***2.20***	***0.21***	***34.39***	***0.72***	***0.37***	***0.21***	***1.87***	***96.46***	***40.51***
Maximum		***19.22***	***8.33***	***0.01***	***3.91***	***0.39***	***44.22***	***1.02***	***0.51***	***0.49***	***4.22***	***101.42***	***48.97***
Minimum		***4.69***	***0.36***	***0.00***	***0.43***	***0.07***	***24.21***	***0.44***	***0.28***	***0.01***	***0.86***	***94.58***	***33.13***
Stbw.		***4.13***	***2.18***	***0.00***	***0.93***	***0.09***	***4.69***	***0.14***	***0.06***	***0.12***	***0.94***	***1.74***	***4.35***
OSP013	44.4	0.06	n.d.	0.00	0.06	0.00	28.56	0.09	0.31	0.00	11.57	100.17	59.51
OSP006	45.8	1.25	n.d.	0.01	0.24	0.03	49.81	0.48	0.36	0.01	11.25	98.82	35.38
OSP001	46.8	0.79	n.d.	0.01	0.21	0.41	32.35	0.12	0.34	0.01	17.07	98.24	46.94
SAP013	49.4	0.14	n.d.	0.00	0.07	0.00	34.92	0.20	0.37	0.00	14.18	100.26	50.38
Numbers		***4***	***n.d.***	***4***	***4***	***4***	***4***	***4***	***4***	***4***	***4***	***4***	***4***
Average		***0.56***	***n.d.***	***0.00***	***0.14***	***0.11***	***36.41***	***0.22***	***0.35***	***0.01***	***13.52***	***99.37***	***48.05***
Maximum		***1.25***	***n.d.***	***0.01***	***0.24***	***0.41***	***49.81***	***0.48***	***0.37***	***0.01***	***17.07***	***100.26***	***59.51***
Minimum		***0.06***	***n.d.***	***0.00***	***0.06***	***0.00***	***28.56***	***0.09***	***0.31***	***0.00***	***11.25***	***98.24***	***35.38***
Stbw.		***0.49***	***n.d.***	***0.00***	***0.08***	***0.17***	***8.06***	***0.16***	***0.02***	***0.00***	***2.35***	***0.87***	***8.64***

Table 9 Trace element composition bulk sediment (ED- XRF)

Marl Member 0 – 3 mbsf

Sample	Depth [m]	V (ppm)	Cr (ppm)	Ni (ppm)	Cu (ppm)	Zn (ppm)	Ga (ppm)	Rb (ppm)	Sr (ppm)	Y (ppm)
SAM012*	0	69	405	122	95	146	11	16	1506	34
SAM011	0.2	n.d.	n.d.	n.d.	n.d.	n.d.	n.d.	n.d.	n.d.	n.d.
SAM010	0.4	n.d.	n.d.	n.d.	n.d.	n.d.	n.d.	n.d.	n.d.	n.d.
SAM009*	0.6	99	416	132	83	205	12	19	1453	32
SAM008*	0.8	106	421	123	86	211	12	20	1436	33
SAM007*	1	72	322	102	57	188	12	15	1256	26
SAM006	1.2	79	398	121	82	187	12	18	1372	30
SAM006	1.2	93	400	120	81	190	13	19	1400	32
SAM005	1.4	86	433	131	78	203	12	20	1394	32
SAM004	1.6	n.d.	n.d.	n.d.	n.d.	n.d.	n.d.	n.d.	n.d.	n.d.
SAM003	1.8	87	410	131	78	216	12	18	1423	31
SAM002	2	96	410	132	75	245	12	17	1245	32
SAM001	2.2	95	444	121	98	184	10	18	1510	35
SAM001	2.2	117	443	142	92	202	14	25	1284	36
SAOS 004	2.4	89	363	109	60	206	14	21	1326	30
SAOS 003	2.6	87	376	101	88	184	13	22	1365	29
SAOS 002	2.8	106	391	102	81	227	13	21	1320	32
SAOS 001*	3	112	402	118	88	226	13	22	1291	34
Numbers		***15***	***15***	***15***	***15***	***15***	***15***	***15***	***15***	***15***
Average		***93***	***402***	***120***	***81***	***201***	***12***	***19***	***1372***	***32***
Max		***117***	***444***	***142***	***98***	***245***	***14***	***25***	***1510***	***36***
Min		***69***	***322***	***101***	***57***	***146***	***10***	***15***	***1245***	***26***
Stbw		***14***	***31***	***12***	***11***	***24***	***1***	***3***	***85***	***3***
%RSD		***5***	***2***	***2***	***3***	***1***	***2***	***1***	***1***	***3***
Detection limit		***50***	***26***	***12***	***5***	***3***	***3***	***1***	***1***	***0.4***

Table 10 Trace element composition bulk sediment (ED- XRF)

Marl Member 0 – 3 mbsf

Sample	Depth [m]	Zr (ppm)	Ba (ppm)	La (ppm)	Ce (ppm)	As (ppm)	Mo (ppm)	Cd (ppm)	U (ppm)
SAM012*	0	40	35	23	25	8	7	9	35
SAM011	0.2	n.d.	n.d.	n.d.	n.d.	n.d.	n.d.	n.d.	n.d.
SAM010	0.4	n.d.	n.d.	n.d.	n.d.	n.d.	n.d.	n.d.	n.d.
SAM009*	0.6	40	39	22	27	13	7	9	31
SAM008*	0.8	43	38	23	30	9	9	7	35
SAM007*	1	32	30	20	25	12	11	10	27
SAM006	1.2	44	35	24	29	9	7	7	32
SAM006	1.2	40	36	22	28	11	7	7	31
SAM005	1.4	42	37	23	28	11	7	9	30
SAM004	1.6	n.d.	n.d.	n.d.	n.d.	n.d.	n.d.	n.d.	n.d.
SAM003	1.8	39	36	21	26	12	9	7	33
SAM002	2	44	46	24	33	14	14	7	28
SAM001	2.2	41	36	22	27	10	9	11	36
SAM001	2.2	47	42	26	34	15	10	7	28
SAOS 004	2.4	44	37	24	28	15	12	8	23
SAOS 003	2.6	40	36	21	29	14	5	8	33
SAOS 002	2.8	45	38	22	29	17	13	12	26
SAOS 001*	3	46	38	24	30	17	11	6	28
Numbers		***15***	***15***	***15***	***15***	***15***	***15***	***15***	***15***
Average		***42***	***37***	***23***	***28***	***13***	***9***	***8***	***30***
Max		***47***	***46***	***26***	***34***	***17***	***14***	***12***	***36***
Min		***32***	***30***	***20***	***25***	***8***	***5***	***6***	***23***
Stbw		***4***	***4***	***1***	***3***	***3***	***3***	***2***	***4***
%RSD		***1***	***1***	***3***	***2***	***2***	***7***	***32***	***7***
Detection limit		***2***	***3***	***4***	***4***	***2***	***2***	***1***	***3***

Table 11 Trace element composition bulk sediment (ED- XRF)

Sample	Depth [m]	V (ppm)	Cr (ppm)	Ni (ppm)	Cu (ppm)	Zn (ppm)	Ga (ppm)	Rb (ppm)	Sr (ppm)	Y (ppm)	Zr (ppm)
SAOS005	3.2	n.d.	n.d.	n.d.	n.d.	n.d.	n.d.	n.d.	n.d.	n.d.	n.d.
SAOS 006*	3.4	121	398	124	69	180	13	24	1226	32	45
SAOS 006*	3.4	116	409	128	72	183	14	24	1239	31	48
SAOS 007	3.6	n.d.	n.d.	n.d.	n.d.	n.d.	n.d.	n.d.	n.d.	n.d.	n.d.
SAOS 008	3.8	124	412	118	73	191	15	25	1222	33	47
SAOS 009	4	133	430	119	73	190	15	27	1213	35	56
SAOS 010	4.2	151	490	120	79	205	17	29	1165	37	59
SAOS 011	4.4	122	473	150	90	215	14	23	1236	38	53
SAOS 012	4.6	136	479	149	90	213	14	24	1242	40	55
SAOS 013A	4.8	149	529	144	88	228	16	29	1117	43	61
SAOS 013B	4.8	148	537	140	91	230	16	30	1106	42	61
SAOS 014	5	121	486	146	86	216	13	23	1312	37	49
SAOS 015*	5.2	n.d.	n.d.	n.d.	n.d.	n.d.	n.d.	n.d.	n.d.	n.d.	n.d.
SAOS 016	5.4	133	491	132	84	224	15	24	1254	37	53
SAOS 017	5.6	140	494	135	81	222	16	24	1205	35	52
SAOS 018*	5.8	162	521	111	100	410	17	27	1456	38	61
SAOS 019	6	160	480	132	78	193	15	25	1161	35	58
SAOS 020	6.2	163	453	119	87	203	15	28	1174	34	54
SAOS 021*	6.4	n.d.	n.d.	n.d.	n.d.	n.d.	n.d.	n.d.	n.d.	n.d.	n.d.
SAOS 022	6.6	142	444	135	86	209	14	25	1228	32	46
SAOS 023	6.8	139	426	127	78	197	15	23	1230	32	49
SAOS 024	7	145	428	135	90	215	15	24	1233	37	49
SAOS 025	7.2	162	454	116	74	211	15	27	1140	34	54
SAOS 026	7.4	151	418	107	70	191	16	27	1154	32	53
SAOS 027	7.6	153	421	106	67	200	15	23	1205	33	49
SAOS 028	7.8	125	396	122	77	194	15	22	1226	32	48
SAOS 029	8	111	335	114	69	170	14	19	1306	32	37
SAOS 030	8.2	121	368	110	71	201	14	21	1339	29	40
SAOS 031	8.4	n.d.	n.d.	n.d.	n.d.	n.d.	n.d.	n.d.	n.d.	n.d.	n.d.
SAOS 032	8.6	101	357	129	75	195	12	16	1430	27	35
SAOS 033	8.8	89	364	136	81	199	13	14	1484	28	34
SAOS 034	9	110	367	137	78	196	14	20	1366	29	38
SAOS 035*	9.2	99	321	102	64	172	12	21	1376	28	39
SAOS 036	9.4	100	332	115	70	177	13	17	1446	27	34
SAOS 037	9.6	92	333	124	74	197	12	18	1467	28	35
SAOS 038	9.8	n.d.	n.d.	n.d.	n.d.	n.d.	n.d.	n.d.	n.d.	n.d.	n.d.
SAOS 039*	10	81	305	109	69	189	12	17	1462	25	31
SAOS 040	10.2	84	300	106	68	178	12	16	1409	26	32
SAOS 041	10.4	99	313	108	69	196	12	18	1394	28	36
SAOS 042	10.6	n.d.	n.d.	n.d.	n.d.	n.d.	n.d.	n.d.	n.d.	n.d.	n.d.
SAOS 043	10.8	102	333	124	68	170	12	18	1362	25	34
SAOS 044	11	101	365	134	78	202	12	20	1347	29	39
SAOS 045*	11.2	99	349	123	73	197	11	19	1336	29	38
SAOS 046	11.4	107	369	135	73	187	12	20	1340	29	38
SAOS 047	11.6	n.d.	n.d.	n.d.	n.d.	n.d.	n.d.	n.d.	n.d.	n.d.	n.d.
SAOS 048	11.8	102	361	140	78	195	11	20	1503	30	39
SAOS 049	12	n.d.	n.d.	n.d.	n.d.	n.d.	n.d.	n.d.	n.d.	n.d.	n.d.
SAOS 050*	12.2	92	331	119	72	158	12	18	1487	27	35
SAOS 051	12.4	97	336	123	78	200	12	17	1456	27	37
SAOS 051	12.4	103	349	120	77	207	12	16	1480	28	35
SAOS 052	12.6	114	352	120	78	199	12	17	1472	31	44
SAOS 053	12.8	104	309	105	70	163	11	16	1528	26	33
SAOS 054	13	76	279	106	66	174	11	14	1539	25	33
SAOS 055	13.2	92	263	99	62	158	11	13	1544	24	30
SAOS 056	13.4	90	292	105	71	174	11	14	1486	28	34
SAOS 057	13.6	105	313	114	72	173	11	16	1484	28	38
SAOS 058	13.8	164	470	164	99	249	12	23	1230	43	50
SAOS 059	14	163	471	155	92	263	12	25	1258	42	50
SAOS 060*	14.2	124	408	144	82	229	12	21	1281	37	44
SAOS 061	14.4	156	456	151	92	233	13	25	1251	41	46
SAOS060-061	14.6	n.d.	n.d.	n.d.	n.d.	n.d.	n.d.	n.d.	n.d.	n.d.	n.d.
SAOS 062*	14.8	136	437	153	90	240	13	22	1273	40	45
SAOS 063	15	152	451	158	92	285	13	22	1267	44	45
SAOS 064	15.2	164	475	159	99	270	12	22	1241	45	49
SAOS 065	15.4	155	484	169	98	269	14	22	1208	43	52
SAOS 066	15.6	161	469	157	99	257	13	19	1237	42	45
SAOS 067	15.8	145	432	149	91	247	12	19	1316	38	42
SAOS 069	16	146	462	157	91	287	12	22	1329	40	45

Table 12 Trace element composition bulk sediment (ED- XRF)

Oil Shale Member 16.2 – 28.6 mbsf

Sample	Depth [m]	V (ppm)	Cr (ppm)	Ni (ppm)	Cu (ppm)	Zn (ppm)	Ga (ppm)	Rb (ppm)	Sr (ppm)	Y (ppm)	Zr (ppm)
SAOS 070*	16.2	157	501	164	97	277	14	26	1215	44	50
SAOS 071	16.4	142	455	150	90	276	13	23	1257	41	47
SAOS 072	16.6	153	471	157	90	287	13	24	1222	41	50
SAOS 073	16.8	170	502	156	95	304	13	27	1216	42	51
SAOS 074	17	170	521	164	95	287	15	27	1099	46	53
SAOS 075	17.2	n.d.	n.d.	n.d.	n.d.	n.d.	n.d.	n.d.	n.d.	n.d.	n.d.
SAOS 076	17.4	n.d.	n.d.	n.d.	n.d.	n.d.	n.d.	n.d.	n.d.	n.d.	n.d.
SAOS 077	17.6	147	480	159	97	273	13	25	1235	43	50
SAOS 078	17.8	116	337	111	59	177	12	15	805	25	32
SAOS 079	18	155	513	168	93	264	14	27	1078	43	52
SAOS 080	18.2	176	539	170	99	286	14	29	1061	47	58
SAOS 081*	18.4	166	510	152	93	264	14	24	1122	38	48
SAOS 082	18.6	163	529	169	96	307	13	25	1203	40	50
SAOS 083	18.8	154	540	178	103	243	13	26	1158	44	49
SAOS 084	19	23	72	25	20	42	9	2	599	6	8
SAOS 084	19	28	76	32	18	35	8	3	611	5	10
SAOS 085	19.2	160	539	173	98	291	13	26	1163	46	49
SAOS 086	19.4	153	532	163	100	285	13	27	1226	45	48
SAOS 087	19.6	144	523	168	103	274	13	24	1265	42	45
SAOS 088	19.8	n.d.	n.d.	n.d.	n.d.	n.d.	n.d.	n.d.	n.d.	n.d.	n.d.
SAOS 089	20	159	525	185	110	350	14	24	1245	51	50
SAOS 090*	20.2	131	430	120	75	181	12	21	1271	37	42
SAOS 091	20.4	132	407	121	77	201	12	21	1281	34	42
SAOS 092	20.6	118	409	119	73	205	12	19	1321	36	40
SAOS 093	20.8	132	426	138	90	239	13	20	1250	38	42
SAOS 094	21	129	437	139	90	220	13	26	1120	42	48
SAOS094-095	21.2	n.d.	n.d.	n.d.	n.d.	n.d.	n.d.	n.d.	n.d.	n.d.	n.d.
SAOS 095*	21.2	n.d.	n.d.	n.d.	n.d.	n.d.	n.d.	n.d.	n.d.	n.d.	n.d.
SAOS 096	21.4	125	384	130	80	225	12	20	1105	36	39
SAOS 097	21.6	135	438	134	87	215	13	23	1078	43	43
SAOS 098	21.8	162	480	138	85	217	14	24	1106	46	50
SAOS 099	22	199	569	153	102	265	16	32	986	51	58
SAOS 100	22.2	n.d.	n.d.	n.d.	n.d.	n.d.	n.d.	n.d.	n.d.	n.d.	n.d.
SAOS 101	22.4	175	517	140	84	219	15	29	1029	49	54
SAOS 102	22.6	172	528	173	103	276	15	26	1093	48	51
SAOS 103	22.8	185	522	162	94	248	15	28	1077	48	56
SAOS 104	23	178	519	170	105	279	14	28	1096	46	52
SAOS 105*	23.2	136	428	120	78	187	14	23	1258	33	44
SAOS 106*	23.4	157	461	135	80	204	12	25	1172	37	50
SAOS 107	23.6	160	455	155	89	244	12	21	1245	44	42
SAOS 108	23.8	183	522	166	98	246	14	26	1152	54	47
SAOS 109	24	140	419	137	83	227	12	21	1235	42	43
SAOS 110*	24.2	176	477	149	91	249	13	23	1229	45	47
SAOS 111	24.4	n.d.	n.d.	n.d.	n.d.	n.d.	n.d.	n.d.	n.d.	n.d.	n.d.
SAOS 112	24.6	158	496	157	92	240	12	22	1159	52	44
SAOS 113	24.8	132	460	159	95	243	13	21	1257	49	42
SAOS 114	25	118	432	160	91	242	11	19	1353	41	39
SAOS 115	25.2	n.d.	n.d.	n.d.	n.d.	n.d.	n.d.	n.d.	n.d.	n.d.	n.d.
SAOS 116*	25.4	108	416	150	95	234	10	16	1408	38	31
SAOS 116-117	25.4	n.d.	n.d.	n.d.	n.d.	n.d.	n.d.	n.d.	n.d.	n.d.	n.d.
SAOS 117	25.6	89	361	128	79	175	10	14	1411	32	32
SAOS 118	25.8	91	369	124	78	214	11	14	1455	33	31
SAOS 119	26	80	359	141	85	217	11	15	1482	33	32
SAOS 120*	26.2	84	351	126	85	209	10	14	1381	32	32
SAOS 120-121	26.6	n.d.	n.d.	n.d.	n.d.	n.d.	n.d.	n.d.	n.d.	n.d.	n.d.
SAOS 121	26.6	96	363	106	73	178	11	16	1392	29	35
SAOS 122	26.8	124	419	125	80	191	12	20	1307	33	38
SAOS 123	27	139	482	149	92	233	13	21	1245	41	41
SAOS 124-125	27	n.d.	n.d.	n.d.	n.d.	n.d.	n.d.	n.d.	n.d.	n.d.	n.d.
SAOS 125*	27.2	136	462	117	79	182	14	22	1219	37	45
SAOS 126	27.4	175	551	163	102	289	15	24	1156	51	50
SAOS 126	27.4	159	535	164	105	284	15	23	1130	48	49
SAOS 127	27.6	153	494	138	88	229	15	25	1146	44	47
SAOS 128	27.8	155	457	129	83	198	14	22	1140	41	47
SAOS 129	28	145	459	127	84	197	14	21	1146	40	43
SAOS 130*	28.2	182	502	140	87	237	14	29	1032	46	53
SAOS 131	28.4	151	445	160	100	306	13	23	1212	48	48
SAOS 132*	28.6	157	441	134	84	218	13	24	1154	44	46

Table 13 Trace element composition bulk sediment (ED- XRF)

Oil Shale Member 28.8 – 38.4 mbsf

Sample	Depth [m]	V (ppm)	Cr (ppm)	Ni (ppm)	Cu (ppm)	Zn (ppm)	Ga (ppm)	Rb (ppm)	Sr (ppm)	Y (ppm)	Zr (ppm)
SAOS 133	28.8	139	457	123	85	229	14	23	1183	42	49
SAOS 134	29	167	500	154	96	246	14	28	1114	50	51
SAOS 135	29.2	n.d	n.d	n.d	n.d	n.d	n.d	n.d	n.d	n.d	n.d
SAOS 135-136*	29.2	n.d	n.d	n.d	n.d	n.d	n.d	n.d	n.d	n.d	n.d
SAOS 136*	29.4	170	482	120	80	203	15	29	1098	42	52
SAOS 137	29.6	141	433	153	94	255	13	21	1226	49	50
SAOS 138	29.8	147	450	143	86	246	13	22	1213	42	44
SAOS 139	30	155	460	150	90	267	13	21	1204	46	44
SAOS 140*	30.2	158	454	127	77	212	14	25	1195	40	50
SAOS 141	30.4	152	500	143	87	241	14	23	1169	49	51
SAOS 142	30.6	126	466	128	81	207	13	20	1181	35	41
SAOS 143	30.8	128	490	133	83	223	13	20	1154	38	44
SAOS 144	31	150	567	147	91	272	14	22	1125	39	48
SAOS 144-145	31	n.d	n.d	n.d	n.d	n.d	n.d	n.d	n.d	n.d	n.d
SAOS 145	31.2	130	512	141	90	249	12	18	1230	38	41
SAOS 146	31.4	n.d	n.d	n.d	n.d	n.d	n.d	n.d	n.d	n.d	n.d
SAOS 147	31.6	116	416	133	87	265	11	17	1267	34	39
SAOS 148	31.8	83	371	163	88	272	11	16	1317	37	35
SAOS 149	32	134	483	149	98	283	11	17	1313	42	42
SAOS 150*	32.2	124	429	125	82	211	11	15	1292	39	37
SAOS 151	32.4	125	416	125	81	188	11	17	1313	35	31
SAOS 152	32.6	154	574	173	103	324	12	20	1235	52	46
SAOS 153	32.8	184	614	162	103	295	14	21	1198	48	52
SAOS 154	33	94	378	149	89	243	10	14	1367	37	33
SAOS 155	33.2	118	410	130	89	250	12	18	1251	35	34
SAOS 156	33.4	125	416	139	91	237	12	21	1286	40	38
SAOS 157	33.6	173	493	126	81	221	14	25	1077	39	50
SAOS 158	33.8	147	486	157	94	341	13	22	1166	43	45
SAOS 159	34	132	392	113	72	206	13	21	1201	34	35
SAOS 160	34.2	138	413	140	89	256	12	19	1280	38	37
SAOS 161	34.4	97	416	160	97	259	9	15	1439	38	35
SAOS 162	34.6	106	400	152	93	256	9	14	1491	38	31
SAOS 163	34.8	107	433	178	102	291	9	14	1457	43	36
SAOS 164	35	157	495	136	91	268	11	17	1322	44	42
SAOS 165*	35.2	154	462	139	85	244	10	15	1409	44	38
SAOS 166	35.4	165	495	179	118	379	11	16	1421	49	43
SAOS 167	35.6	136	571	225	136	504	9	16	1416	70	57
SAOS 168	35.8	n.d	n.d	n.d	n.d	n.d	n.d	n.d	n.d	n.d	n.d
SAOS 169	36	146	465	168	100	296	11	15	1394	42	39
SAOS 170*	36.2	104	403	156	92	295	9	11	1497	49	36
SAOS 171	36.4	129	502	169	101	297	9	14	1448	65	43
SAOS 172	36.6	132	461	159	96	265	9	13	1463	52	38
SAOS 173	36.8	73	551	175	123	466	8	11	1412	74	62
SAOS 174	37	153	532	168	105	297	9	14	1497	47	35
SAOS 175	37.2	123	458	178	106	281	10	12	1576	46	34
SAOS 175-176	37.4	n.d	n.d	n.d	n.d	n.d	n.d	n.d	n.d	n.d	n.d
SAOS 176	37.4	119	408	170	98	319	9	11	1511	50	30
SAOS 177*	37.6	175	521	170	99	268	10	16	1409	58	54
SAOS 177	37.8	140	453	149	93	262	10	11	1478	58	42
SAOS 179	38	129	430	143	89	267	9	11	1451	54	40
SAOS 180*	38.2	123	413	169	85	404	8	8	1470	64	53
SAOS 181	38.4	148	500	159	109	367	8	9	1489	60	65

Table 14 Trace element composition bulk sediment (ED- XRF)

Oil Shale Member 38.6 – 44.2mbsf

Sample	Depth [m]	V (ppm)	Cr (ppm)	Ni (ppm)	Cu (ppm)	Zn (ppm)	Ga (ppm)	Rb (ppm)	Sr (ppm)	Y (ppm)	Zr (ppm)
SAOS 182	38.6	199	598	172	116	397	9	12	1443	69	90
SAOS 183	38.8	115	536	202	124	467	8	11	1436	54	56
SAOS 184	39	139	627	226	145	530	8	11	1412	68	56
SAOS 185-184	39.2	n.d.	n.d.	n.d.	n.d.	n.d.	n.d.	n.d.	n.d.	n.d.	n.d.
SAOS 185*	39.2	108	585	210	130	496	9	12	1470	64	60
SAOS 186	39.4	116	554	212	125	467	9	13	1436	64	65
SAOS 187	39.6	n.d.	n.d.	n.d.	n.d.	n.d.	n.d.	n.d.	n.d.	n.d.	n.d.
SAOS 188	39.8	110	584	181	117	425	8	12	1480	53	53
SAOS 189**	40	95	579	197	127	516	9	11	1511	60	70
SAOS 190*	40.2	90	566	204	127	489	9	11	1404	72	73
SAOS 191	40.4	93	527	185	112	455	8	11	1473	85	63
SAOS 192	40.6	78	484	178	110	396	8	10	1355	47	45
SAOS 193	40.8	87	575	188	121	458	8	13	1407	62	53
SAOS 194	41	92	576	194	122	432	9	11	1436	49	44
SAOS 195	41.2	86	534	192	134	445	9	12	1413	60	52
OSP030	41.4	n.d.	n.d.	n.d.	n.d.	n.d.	n.d.	n.d.	n.d.	n.d.	n.d.
OSP029	41.6	22	362	139	97	373	8	10	1408	79	41
OSP028	41.8	46	378	139	111	382	8	11	1417	116	59
OSP027	42	39	390	147	103	343	9	10	1332	70	52
OSP026	42.2	36	383	148	107	358	9	11	1371	91	47
OSP025	42.4	82	649	203	120	464	9	14	1492	50	44
OSP024*	42.6	72	630	194	119	403	9	12	1473	51	44
OSP023	42.8	100	706	204	129	451	9	15	1397	48	51
OSP022*	43	80	625	176	110	436	9	14	1428	51	49
OSP021	43.2	62	546	169	113	398	9	11	1437	52	48
OSP020*	43.4	35	373	144	107	351	9	11	1369	90	46
OSP019	43.6	42	378	123	85	345	8	9	1471	87	32
OSP018	43.8	41	399	133	86	345	8	8	1424	73	32
OSP017	44	n.d.	n.d.	n.d.	n.d.	n.d.	n.d.	n.d.	n.d.	n.d.	n.d.
OSP016d*	44.2	72	533	176	120	458	9	12	1323	79	41
Numbers		***187***	***187***	***187***	***187***	***187***	***187***	***187***	***187***	***187***	***187***
Average		***127***	***451***	***146***	***90***	***264***	***12***	***19***	***1290***	***43***	***45***
Max		***199***	***706***	***226***	***145***	***530***	***17***	***32***	***1576***	***116***	***90***
Min		***22***	***72***	***25***	***18***	***35***	***8***	***2***	***599***	***5***	***8***
Stbw		***36***	***88***	***28***	***18***	***88***	***2***	***6***	***155***	***15***	***10***
% RSD		***5***	***2***	***2***	***3***	***1***	***2***	***1***	***1***	***3***	***1***
Detection limit		***50***	***26***	***12***	***5***	***3***	***3***	***1***	***1***	***0.4***	***2***

Table 15 Trace element composition bulk sediment (ED- XRF)

Sample	Depth [m]	Ba (ppm)	La (ppm)	Ce (ppm)	As (ppm)	Mo (ppm)	Cd (ppm)	U (ppm)
SAOS005	3.2	n.d.	n.d.	n.d.	n.d.	n.d.	n.d.	n.d.
SAOS 006*	3.4	36	22	30	9	7	4	27
SAOS 006*	3.4	37	22	28	10	7	9	30
SAOS 007	3.6	n.d.	n.d.	n.d.	n.d.	n.d.	n.d.	n.d.
SAOS 008	3.8	36	22	30	10	9	8	28
SAOS 009	4	37	21	30	11	8	8	31
SAOS 010	4.2	111	22	32	11	7	6	25
SAOS 011	4.4	35	21	27	12	6	8	29
SAOS 012	4.6	36	23	30	13	7	12	28
SAOS 013A	4.8	37	24	33	16	12	6	25
SAOS 013B	4.8	37	24	32	15	13	6	25
SAOS 014	5	32	21	28	11	11	11	31
SAOS 015*	5.2	n.d.	n.d.	n.d.	n.d.	n.d.	n.d.	n.d.
SAOS 016	5.4	34	22	31	10	13	11	28
SAOS 017	5.6	38	23	31	12	9	9	23
SAOS 018*	5.8	38	21	31	13	21	10	33
SAOS 019	6	40	23	32	11	9	8	28
SAOS 020	6.2	37	22	31	9	9	6	27
SAOS 021*	6.4	n.d.	n.d.	n.d.	n.d.	n.d.	n.d.	n.d.
SAOS 022	6.6	34	21	25	8	9	9	31
SAOS 023	6.8	35	21	30	11	8	11	30
SAOS 024	7	35	22	28	11	10	7	30
SAOS 025	7.2	38	23	30	16	8	3	25
SAOS 026	7.4	37	21	31	14	7	9	25
SAOS 027	7.6	37	21	31	10	7	9	28
SAOS 028	7.8	35	21	29	13	10	12	29
SAOS 029	8	34	21	25	12	8	11	26
SAOS 030	8.2	36	19	28	12	7	12	30
SAOS 031	8.4	n.d.	n.d.	n.d.	n.d.	n.d.	n.d.	n.d.
SAOS 032	8.6	31	19	22	10	8	8	26
SAOS 033	8.8	31	18	22	11	8	10	30
SAOS 034	9	32	21	26	10	8	7	28
SAOS 035*	9.2	36	21	27	11	5	8	27
SAOS 036	9.4	32	19	25	10	10	9	23
SAOS 037	9.6	29	17	21	5	10	9	30
SAOS 038	9.8	n.d.	n.d.	n.d.	n.d.	n.d.	n.d.	n.d.
SAOS 039*	10	29	18	21	6	9	8	24
SAOS 040	10.2	30	18	20	8	11	9	27
SAOS 041	10.4	29	17	20	7	13	12	24
SAOS 042	10.6	n.d.	n.d.	n.d.	n.d.	n.d.	n.d.	n.d.
SAOS 043	10.8	28	18	21	8	10	7	25
SAOS 044	11	28	18	21	12	11	10	29
SAOS 045*	11.2	27	19	20	10	9	12	27
SAOS 046	11.4	29	18	20	10	9	8	27
SAOS 047	11.6	n.d.	n.d.	n.d.	n.d.	n.d.	n.d.	n.d.
SAOS 048	11.8	36	18	21	10	7	13	28
SAOS 049	12	n.d.	n.d.	n.d.	n.d.	n.d.	n.d.	n.d.
SAOS 050*	12.2	26	18	20	6	9	6	30
SAOS 051	12.4	26	18	20	9	10	11	26
SAOS 051	12.4	28	17	21	8	9	7	29
SAOS 052	12.6	29	18	22	10	10	9	31
SAOS 053	12.8	26	18	19	9	9	7	26
SAOS 054	13	24	15	18	9	9	8	28
SAOS 055	13.2	25	17	18	6	9	9	27
SAOS 056	13.4	28	20	20	8	9	11	30
SAOS 057	13.6	27	19	20	7	10	7	29
SAOS 058	13.8	32	21	25	11	17	5	34
SAOS 059	14	31	22	25	10	15	10	35
SAOS 060*	14.2	33	19	23	10	13	12	33
SAOS 061	14.4	32	22	25	12	15	8	37
SAOS060-061	14.6	n.d.	n.d.	n.d.	n.d.	n.d.	n.d.	n.d.
SAOS 062*	14.8	37	22	26	11	15	9	38
SAOS 063	15	30	21	25	11	14	10	38
SAOS 064	15.2	30	22	24	11	14	6	35
SAOS 065	15.4	30	21	23	14	15	11	36
SAOS 066	15.6	33	22	25	11	14	8	37
SAOS 067	15.8	28	19	21	8	12	8	35
SAOS 069	16	31	22	25	9	10	11	33

Table 16 Trace element composition bulk sediment (ED- XRF)

Sample	Depth [m]	Ba (ppm)	La (ppm)	Ce (ppm)	As (ppm)	Mo (ppm)	Cd (ppm)	U (ppm)
SAOS 070*	16.2	32	22	26	15	13	10	29
SAOS 071	16.4	33	21	27	13	11	11	33
SAOS 072	16.6	32	21	26	15	14	10	33
SAOS 073	16.8	34	23	27	15	13	8	32
SAOS 074	17	34	23	29	18	18	10	35
SAOS 075	17.2	n.d.	n.d.	n.d.	n.d.	n.d.	n.d.	n.d.
SAOS 076	17.4	n.d.	n.d.	n.d.	n.d.	n.d.	n.d.	n.d.
SAOS 077	17.6	31	21	26	17	15	9	31
SAOS 078	17.8	24	17	19	8	9	9	19
SAOS 079	18	31	21	27	18	19	9	34
SAOS 080	18.2	34	21	29	18	19	11	35
SAOS 081*	18.4	31	20	25	15	19	12	34
SAOS 082	18.6	31	21	25	12	17	10	35
SAOS 083	18.8	31	21	26	16	20	11	37
SAOS 084	19	664	9	6	1	2	8	9
SAOS 084	19	674	7	7	0	2	3	0
SAOS 085	19.2	32	22	26	16	21	12	37
SAOS 086	19.4	31	22	25	19	17	10	36
SAOS 087	19.6	31	21	23	16	13	7	34
SAOS 088	19.8	n.d.	n.d.	n.d.	n.d.	n.d.	n.d.	n.d.
SAOS 089	20	31	20	24	14	17	11	37
SAOS 090*	20.2	31	20	25	11	12	11	31
SAOS 091	20.4	30	18	20	10	12	10	27
SAOS 092	20.6	31	18	24	6	8	7	25
SAOS 093	20.8	32	20	25	10	8	7	31
SAOS 094	21	32	21	25	15	10	10	28
SAOS094-095	21.2	n.d.	n.d.	n.d.	n.d.	n.d.	n.d.	n.d.
SAOS 095*	21.2	n.d.	n.d.	n.d.	n.d.	n.d.	n.d.	n.d.
SAOS 096	21.4	29	22	24	12	8	10	24
SAOS 097	21.6	32	23	28	17	8	8	30
SAOS 098	21.8	33	23	27	15	11	9	31
SAOS 099	22	40	25	34	23	8	8	31
SAOS 100	22.2	n.d.	n.d.	n.d.	n.d.	n.d.	n.d.	n.d.
SAOS 101	22.4	40	27	33	21	11	7	30
SAOS 102	22.6	37	25	30	21	15	10	35
SAOS 103	22.8	37	24	31	22	14	8	30
SAOS 104	23	34	23	27	15	12	7	31
SAOS 105*	23.2	32	21	28	12	10	7	26
SAOS 106*	23.4	34	23	29	14	8	7	27
SAOS 107	23.6	32	21	26	13	11	7	32
SAOS 108	23.8	37	26	31	19	16	9	35
SAOS 109	24	32	22	24	14	13	9	31
SAOS 110*	24.2	32	21	25	16	15	11	33
SAOS 111	24.4	n.d.	n.d.	n.d.	n.d.	n.d.	n.d.	n.d.
SAOS 112	24.6	32	23	24	19	12	9	33
SAOS 113	24.8	31	22	25	14	13	8	30
SAOS 114	25	29	20	21	12	14	11	34
SAOS 115	25.2	n.d.	n.d.	n.d.	n.d.	n.d.	n.d.	n.d.
SAOS 116*	25.4	27	20	19	15	16	6	35
SAOS 116-117	25.4	n.d.	n.d.	n.d.	n.d.	n.d.	n.d.	n.d.
SAOS 117	25.6	24	18	18	13	13	6	30
SAOS 118	25.8	25	19	18	11	12	11	32
SAOS 119	26	24	17	17	10	13	11	31
SAOS 120*	26.2	24	18	18	10	13	9	29
SAOS 120-121	26.6	n.d.	n.d.	n.d.	n.d.	n.d.	n.d.	n.d.
SAOS 121	26.6	26	18	19	8	10	13	26
SAOS 122	26.8	28	19	23	12	12	11	33
SAOS 123	27	30	22	25	11	16	12	33
SAOS 124-125	27	n.d.	n.d.	n.d.	n.d.	n.d.	n.d.	n.d.
SAOS 125*	27.2	33	20	26	17	12	9	29
SAOS 126	27.4	32	23	28	18	17	4	35
SAOS 126	27.4	31	22	24	18	16	9	33
SAOS 127	27.6	34	22	27	19	18	7	31
SAOS 128	27.8	34	24	26	22	17	9	31
SAOS 129	28	35	22	30	20	16	7	33
SAOS 130*	28.2	36	23	29	25	21	7	32
SAOS 131	28.4	31	21	24	14	16	9	38
SAOS 132*	28.6	32	20	26	14	15	10	33

Table 17 Trace element composition bulk sediment (ED- XRF)

Sample	Depth [m]	Ba (ppm)	La (ppm)	Ce (ppm)	As (ppm)	Mo (ppm)	Cd (ppm)	U (ppm)
SAOS 133	28.8	35	23	29	18	16	9	31
SAOS 134	29	39	24	31	23	26	9	37
SAOS 135	29.2	n.d.	n.d.	n.d.	n.d.	n.d.	n.d.	n.d.
SAOS 135-136*	29.2	n.d.	n.d.	n.d.	n.d.	n.d.	n.d.	n.d.
SAOS 136*	29.4	37	23	31	20	17	5	28
SAOS 137	29.6	33	23	26	13	15	11	36
SAOS 138	29.8	33	23	25	12	12	5	32
SAOS 139	30	31	22	25	12	13	12	35
SAOS 140*	30.2	36	24	29	15	12	11	31
SAOS 141	30.4	33	24	29	14	12	5	32
SAOS 142	30.6	30	19	23	18	17	8	32
SAOS 143	30.8	29	21	23	15	16	10	35
SAOS 144	31	32	21	23	19	20	10	33
SAOS 144-145	31	n.d.	n.d.	n.d.	n.d.	n.d.	n.d.	n.d.
SAOS 145	31.2	29	20	22	16	14	9	31
SAOS 146	31.4	n.d.	n.d.	n.d.	n.d.	n.d.	n.d.	n.d.
SAOS 147	31.6	26	19	20	15	15	11	31
SAOS 148	31.8	24	18	16	15	17	7	28
SAOS 149	32	29	19	22	17	13	7	39
SAOS 150*	32.2	28	20	23	16	12	9	36
SAOS 151	32.4	27	19	22	16	13	12	37
SAOS 152	32.6	31	23	24	20	17	12	45
SAOS 153	32.8	34	23	29	20	14	9	38
SAOS 154	33	26	19	20	20	14	10	40
SAOS 155	33.2	28	20	21	13	15	13	37
SAOS 156	33.4	30	21	25	14	13	10	33
SAOS 157	33.6	37	22	28	17	14	8	31
SAOS 158	33.8	31	21	24	18	13	11	37
SAOS 159	34	33	19	25	16	11	8	31
SAOS 160	34.2	32	21	23	19	12	12	34
SAOS 161	34.4	25	17	17	18	18	13	42
SAOS 162	34.6	23	17	15	14	17	10	40
SAOS 163	34.8	22	17	13	18	20	12	48
SAOS 164	35	26	20	19	16	21	14	50
SAOS 165*	35.2	28	20	20	16	19	10	46
SAOS 166	35.4	26	19	17	22	24	14	53
SAOS 167	35.6	26	21	16	25	18	16	47
SAOS 168	35.8	n.d.	n.d.	n.d.	n.d.	n.d.	n.d.	n.d.
SAOS 169	36	27	20	18	28	22	13	45
SAOS 170*	36.2	25	22	19	19	15	8	46
SAOS 171	36.4	28	24	19	22	18	12	51
SAOS 172	36.6	24	18	20	29	17	14	44
SAOS 173	36.8	27	22	15	13	19	12	43
SAOS 174	37	25	21	18	34	19	12	43
SAOS 175	37.2	22	18	18	35	14	12	47
SAOS 175-176	37.4	n.d.	n.d.	n.d.	n.d.	n.d.	n.d.	n.d.
SAOS 176	37.4	20	17	14	33	16	15	47
SAOS 177*	37.6	27	23	20	45	19	17	47
SAOS 177	37.8	26	21	18	34	18	12	49
SAOS 179	38	25	22	19	36	21	14	48
SAOS 180*	38.2	25	22	13	20	23	22	61
SAOS 181	38.4	29	21	14	26	29	11	62

Table 18 Trace element composition bulk sediment (ED- XRF)

Sample	Depth [m]	Ba (ppm)	La (ppm)	Ce (ppm)	As (ppm)	Mo (ppm)	Cd (ppm)	U (ppm)
SAOS 182	38.6	31	22	17	32	38	19	85
SAOS 183	38.8	22	18	11	26	21	20	52
SAOS 184	39	24	21	14	28	21	18	57
SAOS 185-184	39.2	n.d.	n.d.	n.d.	n.d.	n.d.	n.d.	n.d.
SAOS 185*	39.2	27	22	15	23	20	18	56
SAOS 186	39.4	26	20	14	24	19	16	48
SAOS 187	39.6	n.d.	n.d.	n.d.	n.d.	n.d.	n.d.	n.d.
SAOS 188	39.8	26	20	14	19	23	18	45
SAOS 189**	40	25	20	13	23	18	17	48
SAOS 190*	40.2	26	22	16	29	17	16	50
SAOS 191	40.4	27	25	16	43	18	14	57
SAOS 192	40.6	22	17	15	16	21	19	34
SAOS 193	40.8	24	18	14	16	22	12	42
SAOS 194	41	21	15	13	17	20	14	39
SAOS 195	41.2	22	20	16	15	14	17	40
OSP030	41.4	n.d.	n.d.	n.d.	n.d.	n.d.	n.d.	n.d.
OSP029	41.6	23	25	15	14	8	10	35
OSP028	41.8	26	30	19	23	9	10	50
OSP027	42	25	25	16	24	13	11	35
OSP026	42.2	24	25	16	25	12	14	44
OSP025	42.4	33	19	13	16	16	14	34
OSP024*	42.6	40	18	13	16	18	19	38
OSP023	42.8	23	17	14	21	24	19	34
OSP022*	43	27	16	15	19	19	16	40
OSP021	43.2	27	18	14	18	17	12	38
OSP020*	43.4	26	28	16	27	11	10	45
OSP019	43.6	22	27	15	13	8	14	49
OSP018	43.8	24	26	19	14	8	15	41
OSP017	44	n.d.	n.d.	n.d.	n.d.	n.d.	n.d.	n.d.
OSP016d*	44.2	24	25	17	25	15	16	52
Numbers		***187***	***187***	***187***	***187***	***187***	***187***	***187***
Average		***38***	***21***	***23***	***16***	***14***	***10***	***35***
Max		***674***	***30***	***34***	***45***	***38***	***22***	***85***
Min		***20***	***7***	***6***	***0***	***2***	***3***	***0***
Stbw		***66***	***3***	***6***	***7***	***5***	***3***	***9***
% RSD		***1***	***3***	***2***	***2***	***7***	***32***	***7***
Detection limit		***3***	***4***	***4***	***2***	***2***	***1***	***3***

Table 19 Trace element composition bulk sediment (ED- XRF)

Phosphorite Member 44.4 – 49.8 mbsf

Sample	Depth [m]	Zr (ppm)	Ba (ppm)	La (ppm)	Ce (ppm)	As (ppm)	Mo (ppm)	Cd (ppm)	U (ppm)
OSP015	44.4	12	1888	19	10	5	9	17	93
OSP014	44.6	n.d.	n.d.	n.d.	n.d.	n.d.	n.d.	n.d.	n.d.
OSP013*	44.8	19	35	36	23	6	11	22	90
OSP013	44.8	13	25	16	12	0	11	68	85
OSP012	45	27	37	40	22	9	11	22	107
OSP011	45.2	17	47	21	14	4	39	89	148
OSP010	45.4	16	962	29	16	10	32	50	196
OSP009	45.6	18	647	16	10	10	57	85	107
OSP008	45.8	14	36	28	19	8	22	49	145
OSP007	46	7	72	13	11	3	34	117	40
OSP006*	46.2	11	116	13	11	6	51	151	67
OSP005	46.4	9	177	18	13	6	39	105	72
OSP004	46.6	16	247	24	17	12	69	53	126
OSP003	46.8	15	50	24	18	7	43	53	102
OSP002	47	n.d.	n.d.	n.d.	n.d.	n.d.	n.d.	n.d.	n.d.
OSP001*	47.2	n.d.	n.d.	n.d.	n.d.	n.d.	n.d.	n.d.	n.d.
SAP001	47.4	n.d.	n.d.	n.d.	n.d.	n.d.	n.d.	n.d.	n.d.
SAP002	47.6	19	40	19	12	2	22	87	106
SAP003	47.8	19	37	24	15	3	27	84	130
SAP004	48	19	36	19	13	1	25	116	118
SAP005	48.2	25	20	13	14	18	84	334	54
SAP006	48.4	12	25	19	14	1	10	92	102
SAP007	48.6	n.d.	n.d.	n.d.	n.d.	n.d.	n.d.	n.d.	n.d.
SAP008	48.8	16	53	26	19	2	13	63	118
SAP008	48.8	15	61	21	15	1	11	61	114
SAP009	49	16	109	30	21	1	11	83	147
SAP010	49.2	15	155	24	17	1	18	92	136
SAP011	49.4	18	147	28	18	2	17	95	132
SAP012	49.6	15	98	23	15	2	18	103	118
SAP013*	49.8	n.d.	n.d.	n.d.	n.d.	n.d.	n.d.	n.d.	n.d.
Numbers		***24***	***24***	***24***	***24***	***24***	***24***	***24***	***24***
Average		***16***	***213***	***23***	***15***	***5***	***29***	***87***	***111***
Max		***27***	***1888***	***40***	***23***	***18***	***84***	***334***	***196***
Min		***7***	***20***	***13***	***10***	***0***	***9***	***17***	***40***
Stbw		***4***	***418***	***7***	***4***	***4***	***20***	***62***	***34***
%RSD		***1***	***1***	***3***	***2***	***2***	***7***	***32***	***7***
Detection limit		***2***	***3***	***4***	***4***	***2***	***2***	***1***	***3***

Table 20 Correlation matrix (bulk sediment) OSM (1)

	SiO_2 [%]	TiO_2 [%]	Al_2O_3 %	$Fe_2O_{3\,(t)}$ [%]	MnO [%]	CaO [%]	S [ppm]	C_{org} [%]	P_2O_5 [%]
SiO_2 [%]	1.00	0.97	0.82	0.94	0.28	-0.96	-0.46	-0.41	-0.38
TiO_2 [%]	0.97	1.00	0.79	0.96	0.25	-0.98	-0.40	-0.35	-0.34
Al_2O_3 %	0.82	0.79	1.00	0.77	0.41	-0.74	-0.59	-0.56	-0.48
$Fe_2O_{3\,(t)}$ [%]	0.94	0.96	0.77	1.00	0.33	-0.97	-0.35	-0.30	-0.26
MnO [%]	0.28	0.25	0.41	0.33	1.00	-0.25	-0.31	-0.34	-0.14
CaO [%]	-0.96	-0.98	-0.74	-0.97	-0.25	1.00	0.33	0.29	0.27
S [ppm]	-0.46	-0.40	-0.59	-0.35	-0.31	0.33	1.00	0.91	0.86
C_{org} [%]	-0.41	-0.35	-0.56	-0.30	-0.34	0.29	0.91	1.00	0.78
P_2O_5 [%]	-0.38	-0.34	-0.48	-0.26	-0.14	0.27	0.86	0.78	1.00
V [ppm]	0.68	0.72	0.48	0.74	0.19	-0.75	0.07	0.13	0.21
Cr [ppm]	0.12	0.19	-0.10	0.20	-0.25	-0.23	0.68	0.67	0.56
Ni [ppm]	-0.30	-0.23	-0.50	-0.22	-0.41	0.18	0.87	0.84	0.72
Cu [ppm]	-0.33	-0.26	-0.48	-0.24	-0.39	0.21	0.88	0.85	0.77
Zn [ppm]	-0.41	-0.34	-0.54	-0.34	-0.43	0.30	0.88	0.87	0.79
Ga [ppm]	0.94	0.96	0.79	0.94	0.31	-0.95	-0.45	-0.40	-0.39
Rb [ppm]	0.94	0.96	0.72	0.93	0.22	-0.96	-0.33	-0.27	-0.28
Sr [ppm]	-0.74	-0.77	-0.69	-0.78	-0.31	0.79	0.20	0.16	0.11
Y [ppm]	-0.30	-0.24	-0.44	-0.20	-0.29	0.19	0.87	0.81	0.90
Zr [ppm]	0.37	0.41	0.15	0.36	-0.23	-0.41	0.33	0.28	0.32
Ba [ppm]	0.81	0.81	0.73	0.79	0.28	-0.81	-0.40	-0.37	-0.35
La [ppm]	0.42	0.45	0.22	0.46	0.00	-0.48	0.17	0.15	0.38
Ce [ppm]	0.94	0.95	0.76	0.93	0.30	-0.94	-0.44	-0.39	-0.31
Th [ppm]	0.56	0.53	0.51	0.53	0.26	-0.52	-0.24	-0.26	-0.16
As [ppm]	-0.23	-0.20	-0.36	-0.09	-0.05	0.12	0.80	0.72	0.81
Mo [ppm]	-0.28	-0.25	-0.43	-0.17	-0.19	0.17	0.77	0.74	0.67
Cd [ppm]	-0.57	-0.56	-0.61	-0.54	-0.32	0.52	0.56	0.49	0.44
U [ppm]	-0.51	-0.48	-0.62	-0.42	-0.31	0.42	0.83	0.81	0.87
Sn [ppm]	0.21	0.19	0.19	0.21	0.16	-0.17	-0.15	-0.17	-0.16
Sb [ppm]	-0.26	-0.25	-0.33	-0.22	-0.21	0.24	0.42	0.40	0.39
Cs [ppm]	0.25	0.25	0.28	0.24	0.13	-0.23	-0.20	-0.17	-0.15

Table 21 Correlation matrix (bulk sediment) OSM (2)

	V [ppm]	Cr [ppm]	Ni [ppm]	Cu [ppm]	Zn [ppm]	Ga [ppm]	Rb [ppm]	Sr [ppm]	Y [ppm]	Zr [ppm]
SiO_2 [%]	0.68	0.12	-0.30	-0.33	-0.41	0.94	0.94	-0.74	-0.30	0.37
TiO_2 [%]	0.72	0.19	-0.23	-0.26	-0.34	0.96	0.96	-0.77	-0.24	0.41
Al_2O_3 %	0.48	-0.10	-0.50	-0.48	-0.54	0.79	0.72	-0.69	-0.44	0.15
$Fe_2O_{3\,(t)}$ [%]	0.74	0.20	-0.22	-0.24	-0.34	0.94	0.93	-0.78	-0.20	0.36
MnO [%]	0.19	-0.25	-0.41	-0.39	-0.43	0.31	0.22	-0.31	-0.29	-0.23
CaO [%]	-0.75	-0.23	0.18	0.21	0.30	-0.95	-0.96	0.79	0.19	-0.41
S [ppm]	0.07	0.68	0.87	0.88	0.88	-0.45	-0.33	0.20	0.87	0.33
C_{org} [%]	0.13	0.67	0.84	0.85	0.87	-0.40	-0.27	0.16	0.81	0.28
P_2O_5 [%]	0.21	0.56	0.72	0.77	0.79	-0.39	-0.28	0.11	0.90	0.32
V [ppm]	1.00	0.50	0.18	0.16	0.09	0.64	0.74	-0.63	0.20	0.50
Cr [ppm]	0.50	1.00	0.74	0.76	0.68	0.11	0.23	-0.24	0.69	0.71
Ni [ppm]	0.18	0.74	1.00	0.92	0.86	-0.30	-0.15	0.13	0.78	0.42
Cu [ppm]	0.16	0.76	0.92	1.00	0.92	-0.33	-0.19	0.14	0.85	0.47
Zn [ppm]	0.09	0.68	0.86	0.92	1.00	-0.40	-0.27	0.19	0.87	0.43
Ga [ppm]	0.64	0.11	-0.30	-0.33	-0.40	1.00	0.91	-0.74	-0.31	0.32
Rb [ppm]	0.74	0.23	-0.15	-0.19	-0.27	0.91	1.00	-0.76	-0.19	0.42
Sr [ppm]	-0.63	-0.24	0.13	0.14	0.19	-0.74	-0.76	1.00	0.04	-0.37
Y [ppm]	0.20	0.69	0.78	0.85	0.87	-0.31	-0.19	0.04	1.00	0.51
Zr [ppm]	0.50	0.71	0.42	0.47	0.43	0.32	0.42	-0.37	0.51	1.00
Ba [ppm]	0.56	0.14	-0.27	-0.30	-0.35	0.81	0.78	-0.69	-0.23	0.38
La [ppm]	0.51	0.37	0.16	0.24	0.24	0.39	0.44	-0.49	0.49	0.58
Ce [ppm]	0.67	0.10	-0.31	-0.32	-0.39	0.93	0.92	-0.72	-0.23	0.37
Th [ppm]	0.34	0.08	-0.24	-0.18	-0.24	0.51	0.52	-0.41	-0.11	0.29
As [ppm]	0.23	0.63	0.64	0.70	0.69	-0.22	-0.16	-0.01	0.79	0.39
Mo [ppm]	0.24	0.65	0.71	0.72	0.69	-0.30	-0.17	0.13	0.63	0.29
Cd [ppm]	-0.27	0.25	0.46	0.46	0.54	-0.55	-0.52	0.47	0.43	0.05
U [ppm]	0.06	0.50	0.74	0.79	0.82	-0.53	-0.42	0.33	0.80	0.21
Sn [ppm]	0.12	-0.04	-0.15	-0.18	-0.16	0.19	0.20	-0.02	-0.19	-0.03
Sb [ppm]	0.05	0.31	0.38	0.36	0.37	-0.27	-0.24	0.22	0.40	0.13
Cs [ppm]	0.15	-0.02	-0.19	-0.18	-0.15	0.26	0.26	-0.28	-0.14	0.05

Table 22 Correlation matrix (bulk sediment) OSM (3)

	Ba [ppm]	La [ppm]	Ce [ppm]	Th [ppm]	As [ppm]	Mo [ppm]	Cd [ppm]	U [ppm]	Sn [ppm]	Sb [ppm]	Cs [ppm]
SiO_2 [%]	0.81	0.42	0.94	0.56	-0.23	-0.28	-0.57	-0.51	0.21	-0.26	0.25
TiO_2 [%]	0.81	0.45	0.95	0.53	-0.20	-0.25	-0.56	-0.48	0.19	-0.25	0.25
Al_2O_3 %	0.73	0.22	0.76	0.51	-0.36	-0.43	-0.61	-0.62	0.19	-0.33	0.28
$Fe_2O_{3\,(t)}$ [%]	0.79	0.46	0.93	0.53	-0.09	-0.17	-0.54	-0.42	0.21	-0.22	0.24
MnO [%]	0.28	0.00	0.30	0.26	-0.05	-0.19	-0.32	-0.31	0.16	-0.21	0.13
CaO [%]	-0.81	-0.48	-0.94	-0.52	0.12	0.17	0.52	0.42	-0.17	0.24	-0.23
S [ppm]	-0.40	0.17	-0.44	-0.24	0.80	0.77	0.56	0.83	-0.15	0.42	-0.20
C_{org} [%]	-0.37	0.15	-0.39	-0.26	0.72	0.74	0.49	0.81	-0.17	0.40	-0.17
P_2O_5 [%]	-0.35	0.38	-0.31	-0.16	0.81	0.67	0.44	0.87	-0.16	0.39	-0.15
V [ppm]	0.56	0.51	0.67	0.34	0.23	0.24	-0.27	0.06	0.12	0.05	0.15
Cr [ppm]	0.14	0.37	0.10	0.08	0.63	0.65	0.25	0.50	-0.04	0.31	-0.02
Ni [ppm]	-0.27	0.16	-0.31	-0.24	0.64	0.71	0.46	0.74	-0.15	0.38	-0.19
Cu [ppm]	-0.30	0.24	-0.32	-0.18	0.70	0.72	0.46	0.79	-0.18	0.36	-0.18
Zn [ppm]	-0.35	0.24	-0.39	-0.24	0.69	0.69	0.54	0.82	-0.16	0.37	-0.15
Ga [ppm]	0.81	0.39	0.93	0.51	-0.22	-0.30	-0.55	-0.53	0.19	-0.27	0.26
Rb [ppm]	0.78	0.44	0.92	0.52	-0.16	-0.17	-0.52	-0.42	0.20	-0.24	0.26
Sr [ppm]	-0.69	-0.49	-0.72	-0.41	-0.01	0.13	0.47	0.33	-0.02	0.22	-0.28
Y [ppm]	-0.23	0.49	-0.23	-0.11	0.79	0.63	0.43	0.80	-0.19	0.40	-0.14
Zr [ppm]	0.38	0.58	0.37	0.29	0.39	0.29	0.05	0.21	-0.03	0.13	0.05
Ba [ppm]	1.00	0.43	0.83	0.47	-0.19	-0.31	-0.49	-0.47	0.12	-0.30	0.32
La [ppm]	0.43	1.00	0.53	0.33	0.35	0.02	-0.17	0.16	-0.07	0.01	0.15
Ce [ppm]	0.83	0.53	1.00	0.52	-0.19	-0.33	-0.55	-0.47	0.19	-0.25	0.27
Th [ppm]	0.47	0.33	0.52	1.00	0.00	-0.16	-0.37	-0.31	0.13	-0.22	0.02
As [ppm]	-0.19	0.35	-0.19	0.00	1.00	0.68	0.39	0.69	-0.10	0.41	-0.12
Mo [ppm]	-0.31	0.02	-0.33	-0.16	0.68	1.00	0.45	0.73	-0.03	0.39	-0.14
Cd [ppm]	-0.49	-0.17	-0.55	-0.37	0.39	0.45	1.00	0.59	-0.01	0.35	-0.16
U [ppm]	-0.47	0.16	-0.47	-0.31	0.69	0.73	0.59	1.00	-0.14	0.45	-0.21
Sn [ppm]	0.12	-0.07	0.19	0.13	-0.10	-0.03	-0.01	-0.14	1.00	0.01	-0.05
Sb [ppm]	-0.30	0.01	-0.25	-0.22	0.41	0.39	0.35	0.45	0.01	1.00	-0.09
Cs [ppm]	0.32	0.15	0.27	0.02	-0.12	-0.14	-0.16	-0.21	-0.05	-0.09	1.00

Table 23carbon sulphur analysis

Sample	Depth (m)	S (%)
SAM012	0.2	0.13
SAM009	0.6	0.15
SAM008	0.8	1.00
SAM007	1	5.64
Numbers		***4***
Average		***1.73***
Maximum		***5.64***
Minimmum		***0.13***
Stbw.		***2.64***
SAOS001	2.2	0.15
SAOS015	5.2	2.39
SAOS018	5.8	1.77
SAOS021	6.4	2.18
SAOS035	9.2	1.90
SAOS039	10	1.67
SAOS045	11.2	1.85
SAOS050	12.2	1.79
SAOS060	14.2	2.48
SAOS062	14.8	2.40
SAOS070	16.2	2.78
SAOS081	18.4	2.79
SAOS090	20.2	2.05
SAOS095	21.2	2.19
SAOS105	23.2	2.26
SAOS106	23.4	2.39
SAOS110	24.2	2.26
SAOS116	25.4	2.63
SAOS120	26.2	2.18
SAOS125	27.2	2.93
SAOS130	28.2	3.13
SAOS132	28.6	2.39
SAOS136	29.4	2.98
SAOS140	30.2	2.50
SAOS150	32.2	2.17
SAOS165	35.2	2.98
SAOS166	35.4	3.19
SAOS170	36.2	2.66
SAOS177	37.6	3.08
SAOS180	38.2	2.71
SAOS185	39.2	3.53
SAOS190	40.2	3.33
OSP024	42.6	3.64
OSP022	43	3.42
OSP020	43.4	2.57
Numbers		***35***
Average		***2.50***
Maximum		***3.64***
Minimmum		***0.15***
Stbw.		***0.66***
OSP013	44.8	0.91
OSP006	46.2	0.69
OSP001	47.2	1.72
SAP013	49.8	0.64
Numbers		***4***
Average		***0.99***
Maximum		***1.72***
Minimmum		***0.64***
Stbw.		***0.50***

Table 24 Di-thionate iron

Sample	Depth (m)	F_D (%)
SAM012	0.2	0.73
SAM009	0.6	0.72
SAM008	0.8	0.69
SAM007	1	0.52
Numbers		***4***
Average		***0.67***
Maximum		***0.73***
Minimmum		***0.52***
Stbw.		***0.10***
SAOS 001	2.2	0.92
SAOS 006	3.4	0.45
SAOS 015	5.2	0.46
SAOS 018	5.8	0.77
SAOS 021	6.4	0.54
SAOS 035	9.2	0.42
SAOS 039	10	0.31
SAOS 045	11.2	0.34
SAOS 050	12.2	0.25
SAOS 060	14.2	0.49
SAOS 062	14.8	0.41
SAOS 070	16.2	0.50
SAOS 081	18.4	0.45
SAOS 090	20.2	0.49
SAOS 095	21.2	0.37
SAOS 105	23.2	0.43
SAOS 106	23.4	0.45
SAOS 110	24.2	0.26
SAOS 116	25.4	0.53
SAOS 120	26.2	0.41
SAOS 125	27.2	0.51
SAOS 130	28.2	0.62
SAOS 132	28.6	0.47
SAOS 136	29.4	0.50
SAOS 140	30.2	0.32
SAOS 150	32.2	0.37
SAOS 165	35.2	0.20
SAOS 170	36.2	0.20
SAOS 177	37.6	0.30
SAOS 180	38.2	0.06
SAOS 185	39.2	0.12
SAOS 190	40.2	0.07
OSP 024	42.6	0.07
OSP 022	43	0.06
OSP 020	43.4	0.07
Numbers		***35***
Average		***0.38***
Maximum		***0.92***
Minimmum		***0.06***
Stbw.		***0.20***
OSP 013	44.8	0.04
OSP 006	46.2	0.02
OSP 001	47.2	0.03
SAP 013	49.8	0.02
Numbers		***4***
Average		***0.03***
Maximum		***0.04***
Minimmum		***0.02***
Stbw.		***0.01***

Table 25 Different bond sulphur wet chemical extraction

Sample	Depth (m)	$S_{sulphate}$	S_{pyrite}	$S_{intramol.}$	$S_{intermol.}$	∑ S	$S_{sulphate}$	S_{pyrite}	$S_{intramol.}$	$S_{intermol.}$	∑ S
		wt. %	wt. %	wt. %	wt. %	%	rel. %	rel. %	rel. %	rel %	rel. %
SAM012	0	0.00	0.00	0.00	0.25	0.25	0.0	0.0	0.0	0.0	0
SAM009	0.6	0.00	0.00	0.00	0.14	0.14	0.0	0.0	0.0	0.0	0
SAM008	0.8	0.83	0.00	0.00	0.13	0.96	86.4	0.1	0.0	13.6	100
SAM007	1	2.70	0.00	0.00	0.25	2.95	91.6	0.0	0.0	8.4	100
Numbers		***4***	***4***	***4***	***4***	***4***	***4***	***4***	***4***	***4***	
Average		***0.88***	***0.00***	***0.00***	***0.19***	***1.07***	***44.49***	***0.01***	***0.00***	***5.50***	
Maximum		***2.70***	***0.00***	***0.00***	***0.25***	***2.95***	***91.57***	***0.05***	***0.00***	***13.56***	
Minimmum		***0.00***	***0.00***	***0.00***	***0.13***	***0.14***	***0.00***	***0.00***	***0.00***	***0.00***	
Stbw.		***1.27***	***0.00***	***0.00***	***0.06***	***1.30***	***51.42***	***0.03***	***0.00***	***6.68***	
SAOS 001	3	0.57	0.00	0.00	0.06	0.65	89.9	0.1	0.0	10.0	100
SAOS 006	3.4	0.50	0.49	0.03	0.60	1.62	30.9	30.3	1.7	37.1	100
SAOS 015	5.2	0.22	0.63	0.04	0.78	1.67	13.3	37.7	2.7	46.3	100
SAOS 018	5.8	0.36	0.34	0.04	0.63	1.35	26.2	25.0	2.6	46.2	100
SAOS 021	6.4	0.76	0.47	0.03	0.69	1.95	39.0	24.2	1.3	35.5	100
SAOS 035	9.2	0.38	0.52	0.03	0.64	1.58	24.3	33.1	1.9	40.7	100
SAOS 039	10	0.22	0.35	0.03	0.89	1.49	14.9	23.4	1.9	59.8	100
SAOS 045	11.2	0.31	0.38	0.04	0.50	1.22	25.5	30.8	3.0	40.7	100
SAOS 050	12.2	0.35	0.39	0.03	0.95	1.72	20.3	22.6	1.7	55.4	100
SAOS 060	14.2	2.32	0.28	0.03	0.97	2.17	40.9	13.1	1.3	44.8	100
SAOS 062	14.8	0.73	0.30	0.04	0.93	2.00	36.7	14.9	2.1	46.3	100
SAOS 070	16.2	2.35	0.33	0.05	0.87	2.26	45.0	14.6	2.1	38.3	100
SAOS 081	18.4	0.45	0.53	0.04	0.81	1.84	24.6	28.9	2.3	44.1	100
SAOS 090	20.2	0.28	0.10	0.02	0.83	1.24	23.0	8.4	1.7	66.9	100
SAOS 095	21.2	1.24	0.37	0.04	0.91	2.00	33.5	18.8	1.9	45.8	100
SAOS 105	23.2	0.51	0.37	0.04	0.81	1.72	29.3	21.7	2.1	46.8	100
SAOS 106	23.4	0.51	0.57	0.04	0.83	1.94	26.3	29.2	1.9	42.5	100
SAOS 110	24.2	0.52	0.68	0.04	0.77	2.01	25.7	34.0	2.2	38.1	100
SAOS 116	25.4	0.49	0.22	0.04	0.79	1.54	31.5	14.4	2.8	51.3	100
SAOS 120	26.2	0.28	0.41	0.03	1.08	1.80	15.5	22.5	1.6	60.3	100
SAOS 125	27.2	0.72	0.70	0.04	0.79	2.25	32.1	31.1	1.9	34.8	100
SAOS 130	28.2	0.42	1.01	0.05	0.70	2.18	19.1	46.5	2.5	32.0	100
SAOS 132	28.6	0.45	0.61	0.03	0.93	2.01	22.3	30.3	1.5	45.9	100
SAOS 135-136	29.2	0.61	1.03	0.05	0.68	2.37	25.8	43.4	2.0	28.8	100
SAOS 136	29.4	0.60	0.08	0.05	0.81	1.54	39.0	5.3	2.9	52.7	100
SAOS 140	30.2	0.48	1.09	0.03	1.07	2.68	19.2	39.7	1.4	39.7	100
SAOS 150	32.2	0.16	0.51	0.03	0.89	1.58	9.8	32.2	2.0	56.0	100
SAOS 165	35.2	0.79	0.38	0.05	1.00	2.21	35.5	17.1	2.2	45.2	100
SAOS 170	36.2	0.40	0.29	0.04	1.28	2.00	20.1	14.2	1.9	63.8	100
SAOS 177	37.6	0.53	0.55	0.05	1.00	2.17	22.9	28.6	2.2	46.3	100
SAOS 180	38.2	0.21	0.07	0.03	1.36	1.67	12.5	4.4	1.8	81.3	100
SAOS 185	39.2	0.42	0.15	0.07	1.33	1.97	21.2	7.8	3.4	67.6	100
SAOS 190	40.2	0.26	0.10	0.04	1.47	1.88	13.6	5.3	2.3	78.7	100
OSP 024	42.6	0.22	0.17	0.10	1.60	2.09	10.4	8.2	4.8	76.6	100
OSP022	43	0.29	0.11	0.05	1.39	1.8	15.8	5.8	2.5	75.86	100
OSP020	43.6	0.00	0.10	0.01	1.72	1.83	0.0	5.4	0.3	94.3	100
OSP016d	44.2	0.00	0.05	0.04	1.53	1.63	0.0	3.3	2.6	94.1	100
Numbers		***37***	***37***	***37***	***37***	***37***	***37***	***37***	***37***	***37***	
Average		***0.54***	***0.40***	***0.04***	***0.94***	***1.83***	***25.29***	***20.98***	***2.08***	***51.64***	
Maximum		***2.35***	***1.09***	***0.10***	***1.72***	***2.68***	***89.88***	***46.46***	***4.77***	***94.29***	
Minimmum		***0.00***	***0.00***	***0.00***	***0.06***	***0.65***	***0.00***	***0.08***	***0.00***	***10.04***	
Stbw.		***0.49***	***0.27***	***0.02***	***0.33***	***0.38***	***15.15***	***12.42***	***0.80***	***18.13***	
OSP 013	44.8	0.00	0.19	0.09	1.70	1.99	0.0	9.6	4.5	85.8	100
OSP 006	46.2	0.41	0.09	0.04	0.63	1.18	35.3	7.5	3.4	53.8	100
OSP 001	47.2	0.26	0.09	0.14	0.49	1.00	26.3	9.4	14.3	49.8	100
SAP 013	49.8	0.30	0.18	0.05	0.89	1.18	16.8	9.8	2.9	52.6	100
Numbers		***4***	***4***	***4***	***4***	***4***	***4***	***4***	***4***	***4***	
Average		***0.24***	***0.14***	***0.08***	***0.93***	***1.34***	***19.60***	***9.09***	***6.30***	***60.49***	
Maximum		***0.41***	***0.19***	***0.14***	***1.70***	***1.99***	***35.29***	***9.84***	***14.34***	***85.84***	
Minimmum		***0.00***	***0.09***	***0.04***	***0.49***	***1.00***	***0.00***	***7.51***	***2.91***	***49.76***	
Stbw.		***0.18***	***0.06***	***0.05***	***0.54***	***0.44***	***15.09***	***1.07***	***5.40***	***16.98***	

Table 26 Repeated measurements (wet chemical sulphur extraction)

Sample	Depth (m)	$S_{sulphate}$	S_{pyrite}	$S_{intramol.}$	$S_{intermol.}$	∑ S	$S_{sulphate}$	S_{pyrite}	$S_{intramol.}$	$S_{intermol.}$	∑ S
		wt. %	wt. %	wt. %	wt. %	%	rel. %	rel. %	rel. %	rel %	rel. %
SAOS 095	21.2	0.53	0.48	0.02	0.83	1.86	28.5	25.8	1.0	44.7	100
SAOS 095	21.2	0.32	0.48	0.03	0.84	1.67	19.3	28.7	1.7	50.2	100
SAOS 095	21.2	0.61	0.47	0.03	0.97	2.08	29.2	22.7	1.5	46.6	100
SAOS 095	21.2	1.10	0.53	0.03	0.98	2.62	41.9	20.0	1.0	37.2	100
SAOS 095	21.2	0.33	0.51	0.02	0.80	1.67	20.0	30.7	1.1	48.2	100
Numbers		***5***	***5***	***5***	***5***	***5***	***5***	***5***	***5***	***5***	***5***
Average		***0.58***	***0.49***	***0.02***	***0.88***	***1.98***	***27.78***	***25.60***	***1.26***	***45.37***	100
Maximum		***1.10***	***0.53***	***0.03***	***0.98***	***2.62***	***41.86***	***30.71***	***1.73***	***50.24***	100
Minimmum		***0.32***	***0.47***	***0.02***	***0.80***	***1.67***	***19.34***	***20.02***	***0.96***	***37.15***	100
Stbw.		***0.32***	***0.02***	***0.01***	***0.08***	***0.40***	***9.11***	***4.33***	***0.33***	***5.03***	
Sample	**Depth (m)**	$S_{sulphate}$	S_{pyrite}	$S_{intramol.}$	$S_{intermol.}$	∑ S	$S_{sulphate}$	S_{pyrite}	$S_{intramol.}$	$S_{intermol.}$	∑ S
		wt. %	wt. %	wt. %	wt. %	%	rel. %	rel. %	rel. %	rel %	rel. %
SAOS 140	30.2	0.38	1.65	0.03	1.53	3.59	10.6	45.9	0.9	42.5	100
SAOS 140	30.2	0.38	0.84	0.04	0.88	2.14	17.6	39.5	1.7	41.1	100
SAOS 140	30.2	0.68	0.78	0.03	0.82	2.30	29.5	33.7	1.4	35.4	100
Numbers		***3***	***3***	***3***	***3***	***3***	***3***	***3***	***3***	***3***	***3***
Average		***0.48***	***1.09***	***0.03***	***1.07***	***2.68***	***19.21***	***39.73***	***1.37***	***39.68***	100
Maximum		***0.68***	***1.65***	***0.04***	***1.53***	***3.59***	***29.48***	***45.95***	***1.74***	***42.53***	100
Minimmum		***0.38***	***0.78***	***0.03***	***0.82***	***2.14***	***10.58***	***33.70***	***0.94***	***35.39***	100
Stbw.		***0.17***	***0.49***	***0.00***	***0.40***	***0.80***	***9.55***	***6.13***	***0.41***	***3.79***	
Sample	**Depth (m)**	$S_{sulphate}$	S_{pyrite}	$S_{intramol.}$	$S_{intermol.}$	∑ S	$S_{sulphate}$	S_{pyrite}	$S_{intramol.}$	$S_{intermol.}$	∑ S
		wt. %	wt. %	wt. %	wt. %	%	rel. %	rel. %	rel. %	rel %	rel. %
SAOS 177	37.6	0.55	0.55	0.05	1.15	2.35	23.8	23.9	2.1	50.1	100
SAOS 177	37.6	0.18	0.55	0.03	0.56	1.40	13.3	41.6	2.5	42.4	100
SAOS 177	37.6	0.87	0.56	0.05	1.29	2.77	31.4	20.2	2.0	46.5	100
Numbers		***3***	***3***	***3***	***3***	***3***	***3***	***3***	***3***	***3***	***3***
Average		***0.53***	***0.55***	***0.05***	***1.00***	***2.17***	***22.86***	***28.57***	***2.20***	***46.32***	100
Maximum		***0.87***	***0.56***	***0.05***	***1.29***	***2.77***	***31.41***	***41.62***	***2.50***	***50.06***	100
Minimmum		***0.18***	***0.55***	***0.03***	***0.56***	***1.40***	***13.33***	***20.17***	***1.95***	***42.43***	100
Stbw.		***0.35***	***0.00***	***0.01***	***0.38***	***0.70***	***9.08***	***11.45***	***0.28***	***3.81***	
Sample	**Depth (m)**	$S_{sulphate}$	S_{pyrite}	$S_{intramol.}$	$S_{intermol.}$	∑ S	$S_{sulphate}$	S_{pyrite}	$S_{intramol.}$	$S_{intermol.}$	∑ S
		wt. %	wt. %	wt. %	wt. %	%	rel. %	rel. %	rel. %	rel %	rel. %
OSP022	43.0	0.35	0.06	0.00	1.74	2.15	16.3	2.7	0.1	80.9	100
OSP022	43.0	0.26	0.14	0.09	1.76	2.25	11.5	6.2	4.1	78.2	100
OSP022	43.0	0.65	0.08	0.01	0.00	0.74	88.6	10.4	1.0	0.0	100
Numbers		***3***	***3***	***3***	***3***	***3***	***3***	***3***	***3***	***3***	***3***
Average		***0.42***	***0.09***	***0.03***	***1.17***	***1.71***	***38.79***	***6.44***	***1.73***	***53.03***	100
Maximum		***0.65***	***0.14***	***0.09***	***1.76***	***2.25***	***88.58***	***10.40***	***4.06***	***80.86***	100
Minimmum		***0.26***	***0.06***	***0.00***	***0.00***	***0.74***	***11.51***	***2.74***	***0.11***	***0.00***	100
Stbw.		***0.21***	***0.04***	***0.05***	***1.01***	***0.85***	***43.18***	***3.84***	***2.06***	***45.95***	
Sample	**Depth (m)**	$S_{sulphate}$	S_{pyrite}	$S_{intramol.}$	$S_{intermol.}$	∑ S	$S_{sulphate}$	S_{pyrite}	$S_{intramol.}$	$S_{intermol.}$	∑ S
		wt. %	wt. %	wt. %	wt. %	%	rel. %	rel. %	rel. %	rel %	rel. %
SAP 013	49.8	0.38	0.01	0.00	0.00	0.39	97.8	1.7	0.4	0.0	100
SAP 013	49.8	1.08	0.00	0.00	0.00	1.08	99.8	0.3	-0.1	0.0	100
SAP 013	49.8	0.53	0.01	0.00	0.06	0.60	88.7	1.0	0.4	9.9	100
Numbers		***3***	***3***	***3***	***3***	***3***	***3***	***3***	***3***	***3***	***3***
Average		***0.66***	***0.01***	***0.00***	***0.02***	***0.69***	***95.46***	***0.97***	***0.25***	***3.31***	100
Maximum		***1.08***	***0.01***	***0.00***	***0.06***	***1.08***	***99.85***	***1.70***	***0.45***	***9.93***	100
Minimmum		***0.38***	***0.00***	***0.00***	***0.00***	***0.39***	***88.69***	***0.25***	***-0.10***	***0.00***	100
Stbw.		***0.37***	***0.00***	***0.00***	***0.03***	***0.36***	***5.95***	***0.73***	***0.30***	***5.73***	

Table 27 Sulphur isotopy (complete profile)

Sample	Depth (m)	$\delta^{34}S_{sulphate}$ [‰]	$\delta^{34}S_{pyrite}$ [‰]	$\delta^{34}S_{intramol.}$ [‰]	$\delta^{34}S_{intermol.}$ [‰]
SAM012	0.0	-1.25	n.d.	n.d.	-2.64
SAM009	0.6	-3.53	n.d.	n.d.	-2.14
SAM008	0.8	-9.41	n.d.	n.d.	n.d.
SAM007	1.0	-10.68	n.d.	n.d.	n.d.
Numbers		***4***	***n.d.***	***n.d.***	***2***
Average		***-6.22***	***n.d.***	***n.d.***	***-2.39***
Max		***-1.25***	***n.d.***	***n.d.***	***-2.14***
Min		***-10.68***	***n.d.***	***n.d.***	***-2.64***
SAOS001	3.0	3.97			-1.04
SAOS006	3.4	-4.38	-37.75	-1.54	-2.21
SAOS015	5.2	n.d.	-38.57	-2.85	-2.79
SAOS016	5.4	-8.90	n.d.	n.d.	n.d.
SAOS018	6.0	-13.47	-39.01	7.02	-2.86
SAOS018	6.0	n.d.	n.d.	n.d.	n.d.
SAOS021	6.4	-6.05	-35.81	-3.95	-2.13
SAOS035	9.2	-4.01	-37.27	-1.16	-1.64
SAOS039	10.0	-5.14	-37.83	-3.50	-2.41
SAOS045	11.2	-8.02	-38.42	-3.76	-2.68
SAOS050	12.0	-6.82	-38.33	-3.93	-2.76
SAOS060	14.2	-14.91	-42.30	-5.26	-1.79
SAOS062	14.8	-12.48	-39.14	-7.44	-1.69
SAOS070	16.2	-12.12	-38.09	-5.17	-0.69
SAOS081	18.4	-11.75	-37.02	-5.65	-2.06
SAOS090	20.2	-14.92	-39.97	-5.68	-3.26
SAOS095	21.2	-11.64	-37.59	-6.06	-4.04
SAOS105	23.2	-12.39	-38.65	-6.48	-3.77
SAOS106	23.4	-10.14	-38.41	-4.87	-3.95
SAOS110	24.2	-13.41	-39.03	-7.41	-4.75
SAOS116	25.4	-20.61	-42.33	-10.13	-5.39
SAOS120	26.2	-13.85	-40.32	-6.1	-4.83
SAOS125	27.2	-13.27	-40.00	-5.58	-4.09
SAOS130	28.2	-17.22	-39.46	-10.34	-3.77
SAOS132	28.6	-12.8	-38.62	-8.54	-4.61
SAOS135	29.2	n.d.	-39.37	n.d.	n.d.
SAOS135-136	29.2	-13.15	n.d.	-7.59	n.d.
SAOS136	29.4	-11.85	-37.31	-6.14	-3.77
SAOS140	30.2	-6.49	-39.06	-5.02	-4.3
SAOS150	32.2	-13.96	-39.70	-7.44	-4.05
SAOS165	35.2	-9.69	-34.65	-5	-1.28
SAOS170	36.0	-13.52	-36.26	-7.31	-2.64
SAOS177	37.6	-15.76	-37.88	-6.71	-1.38
SAOS180	38.2	-0.87	-34.51	-7.32	-1.97
SAOS185	39.2	-2.76	-30.49	-5.33	0.67
SAOS190	40.2	-0.07		-4.28	1.43
OSP024	42.6	-2.19	-16.18	-6.43	-0.48
OSP022	43.0	-2.09	-16.37	-7	-0.34
OSP020	43.4	-1.06	-17.61	-6.08	-3.86
OSP16d	44.2	-1.39	-24.33	-8.6	-1.68
Numbers		***37***	***35***	***36***	***36***
Average		***-9.17***	***-35.93***	***-5.52***	***-2.58***
Max		***3.97***	***-16.18***	***7.02***	***1.43***
Min		***-20.61***	***-42.33***	***-10.34***	***-5.39***
OSP013	44.80	-1.02	-32.13	n.d.	-0.87
OSP006	46.20	n.d.	n.d.	-13.98	-5.42
OSP001	47.20	3.56	-17.21	14.92	-3.00
SAP013	49.80	-5.35	-23.46	n.d.	-4.22
Numbers		***3***	***3***	***2***	***4***
Average		***-0.94***	***-24.27***	***0.47***	***-3.38***
Max		***3.56***	***-17.21***	***14.92***	***-0.87***
Min		***-5.35***	***-32.13***	***-13.98***	***-5.42***

Table 28 Concentration of trace elements in benthic foraminifera high- resolution (ICP-MS)

Sample	Depth [m]	Mg/Ca	V/Ca	Cr/Ca	Mn/Ca	Fe/Ca	Co/Ca	Ni/Ca	Cu/Ca	Zn/Ca	As/Ca	Rb/Ca	Sr/Ca	Mo/Ca	Cd/Ca	Ba/Ca	Pb/Ca	U /Ca
Benthic		µmol/l	µmol/l	µmol/l	µmol/l	µmol/l	µmol/l	µmol/l	µmol/l	µmol/l	µmol/l	µmol/l	µmol/l	µmol/l	µmol/l	µmol/l	µmol/l	µmol/l
SAM011	0.2	9355.27	86.90	135.74	67.93	241.69	0.02	8.02	4.15	67.15	0.27	0.00	833.48	0.18	0.26	3.71	0.94	0.84
SAM007	1.0	8127.99	71.49	154.13	67.97	762.66	0.14	10.20	7.45	41.00	1.16	0.30	939.90	3.27	0.81	7.18	2.37	1.14
SAOS001	3.0	9116.29	69.95	126.02	94.22	640.69	0.10	12.97	1.87	49.98	1.09	0.00	861.12	0.26	0.33	5.28	0.37	1.29
SAOS005	3.2	10735.47	77.48	121.82	97.97	1387.10	0.73	29.30	19.47	683.96	2.13	0.46	806.77	13.08	0.38	8.53	1.04	1.40
SAOS014	5.0	9660.11	71.62	132.71	91.23	4324.87	0.79	50.52	67.92	2449.26	1.86	0.31	843.53	1.85	0.66	6.36	3.31	2.01
SAOS021	6.4	7662.95	57.65	92.65	79.42	2042.04	0.56	18.07	28.06	-43.41	19.90	0.26	1010.53	0.79	0.49	6.88	3.30	1.04
SAOS022	6.6	9537.54	78.03	101.10	81.59	1912.50	0.48	19.30	23.30	106.91	3.18	0.14	866.97	3.70	0.23	41.61	0.91	1.36
SAOS035	9.2	7864.16	55.66	94.29	113.62	1929.41	1.00	18.51	18.07	-3.99	1.64	0.24	991.73	0.85	0.37	6.68	6.16	1.02
SAOS039	10.0	9412.26	76.10	124.79	92.87	3286.92	0.81	29.36	40.10	74.10	2.31	0.15	899.18	1.29	0.33	5.94	3.11	1.60
SAOS045	11.2	8846.93	70.37	133.85	120.86	3220.59	2.72	95.21	33.52	-9.99	2.36	1.03	934.23	2.86	0.38	6.38	3.22	1.32
SAOS050	12.2	9220.55	70.99	112.89	67.45	650.73	0.35	20.53	21.13	456.39	0.62	-0.06	985.83	0.33	1.80	11.53	1.95	1.31
SAOS062	14.8	9828.03	103.15	200.48	89.02	3740.88	0.75	36.34	27.78	67.59	2.33	0.35	845.74	2.05	0.82	6.67	1.79	1.54
SAOS070	16.2	11065.43	110.51	590.29	120.28	5629.39	4.13	208.21	44.87	176.65	1.95	1.28	799.58	7.79	0.54	8.15	16.11	1.84
SAOS080	18.2	11374.13	105.50	225.66	265.50	1013.36	1.35	147.64	291.16	944.04	0.31	16.27	752.41	16.89	5.01	52.79	71.15	1.47
SAOS090	20.2	9344.46	109.17	194.89	97.78	4673.04	0.98	47.71	30.56	-89.58	5.77	-0.27	874.11	1.27	0.10	9.56	1.50	1.32
SAOS095	20.4	16409.51	133.55	184.43	89.84	4398.31	1.74	88.90	63.18	-864.36	8.19	-6.28	825.15	-12.80	-0.46	-22.72	5.18	1.29
SAOS095	20.4	16538.62	132.81	154.07	96.29	4379.49	1.73	85.80	62.83	-1454.68	6.11	-5.36	828.43	-12.72	-0.45	-19.26	5.16	1.28
SAOS120	26.2	13813.30	130.19	183.31	100.57	1011.80	0.33	17.49	12.18	663.44	1.62	-0.06	662.48	0.47	0.05	4.08	1.77	1.85
SAOS125	27.2	8820.31	83.30	161.81	100.86	864.06	0.37	21.20	16.24	146.61	0.74	-0.23	877.28	0.35	0.09	2.23	1.28	0.86
SAOS130*	28.2	2954.17	131.67	158.56	223.27	14653.10	0.86	606.19	212.24	3930.73	24.46	-8.93	661.05	46.15	0.45	-12.97	2.21	1.92
SAOS132	28.6	11414.60	149.42	232.46	113.00	5014.19	1.59	142.50	105.43	2142.40	1.88	-2.47	615.48	10.99	0.83	7.85	2.37	1.18
SAOS136	29.4	8308.45	100.49	186.93	179.32	4034.13	1.29	46.89	35.10	56.80	4.60	-0.36	859.37	3.08	0.18	5.39	7.52	1.22
SAOS140*	30.2	8199.58	88.72	129.10	141.55	3132.47	1.52	133.13	19.67	62.55	3.33	-0.73	918.61	12.81	3.09	-6.93	-1.43	0.83
SAOS150	32.2	7958.12	94.83	238.16	138.98	676.16	0.62	5.05	49.65	174.77	0.58	-0.14	933.26	5.61	0.57	8.15	0.17	0.71
SAOS165	35.2	8994.32	190.34	514.41	99.07	603.59	0.44	18.47	10.24	-14.02	1.52	0.06	712.59	1.11	0.16	5.27	0.34	0.65
SAOS170	36.2	8113.77	102.31	252.04	73.28	3488.25	0.67	50.96	33.94	126.51	5.73	-0.01	934.14	2.61	0.69	5.98	1.24	0.55
SAOS180*	38.2	11666.51	77.79	3484.56	430.19	-27435.93	0.00	-3792.08	402.89	50601.25	105.15	-23.04	224.78	205.29	-350.42	-358.54	-95.05	0.00
SAOS184	39.0	7054.28	73.04	428.01	48.17	176.31	0.02	7.05	3.81	543.31	0.43	0.03	750.01	0.48	2.67	4.40	0.30	1.38
SAOS189*	40.0	549092.26	308.36	-367.03	1547.47	-21228.79	196.29	-4237.39	-982.88	106136.41	-200.71	724.04	257.43	-295.39	69.46	6064.45	926.71	-4.86
OSP030	41.4	11123.45	40.93	211.07	148.64	158.19	0.08	9.53	5.96	80.22	0.06	-0.04	805.37	0.32	0.16	3.47	0.29	0.47
OSP024	42.6	-1045.19	91.99	154.73	-30.83	1834.94	0.00	126.27	-76.63	-8354.27	28.26	2.48	850.63	278.08	3.77	-20.04	-4.09	0.00
Average		9988.47	94.07	203.38	105.22	2317.71	0.91	47.91	40.69	252.73	3.01	0.21	848.03	2.15	0.65	7.39	5.49	1.23
Stbw.		3173.80	32.41	122.14	49.45	1739.73	0.92	52.53	59.83	1814.26	6.26	3.65	94.88	53.44	1.22	14.80	13.65	0.45
%RSD		31.77	34.45	60.05	46.99	75.06	100.17	109.63	147.03	717.85	207.84	1698.22	11.19	2482.08	186.62	200.31	248.51	36.56
Detection limit		2.9	0.03	0.03	0.05	0.74	0.01	0.26	0.18	2.06	0.09	0.07	0.03	0.12	0.19	0.06	0.02	

Sample weight below 50µg*

Table 29 Concentration of trace elements in benthic foraminifera high- resolution (ICP-MS)

Sample	Depth [m]	Mg/Ca	V/Ca	Cr/Ca	Mn/Ca	Fe/Ca	Co/Ca	Ni/Ca	Cu/Ca	Zn/Ca	As/Ca	Rb/Ca	Sr/Ca	Mo/Ca	Cd/Ca	Ba/Ca	Pb/Ca	U /Ca
planktic		(µ/mol)	(µ/mol)	(µ/mol)	(µ/mol)	(µ/mol)	(µ/mol)	(µ/mol)	(µ/mol)	(µ/mol)	(µ/mol)	(µ/mol)	(µ/mol)	(µ/mol)	(µ/mol)	(µ/mol)	(µ/mol)	(µ/mol)
SAM011	0,2	11260.16	94.73	180.56	86.53	215.26	0.08	5.41	3.19	94.59	0.43	0.14	567.43	0.71	0.23	2.10	0.63	1.23
SAM007	1.0	10679.30	84.83	143.53	82.83	1570.02	0.21	17.28	5.52	-25.01	3.01	0.19	695.90	1.32	0.19	5.34	2.97	1.61
SAOS001	3.0	11533.79	79.20	116.72	99.06	1456.17	0.17	14.57	3.59	-65.84	1.92	0.26	651.43	0.27	0.40	3.95	3.29	1.81
SAOS005	3.2	36074.13	224.62	190.20	374.17	29216.60	23.04	693.91	1019.25	9549.81	23.30	61.26	433.81	-12.13	37.95	289.49	-2.81	2.44
SAOS014	5.0	12129.56	79.77	143.37	105.53	1273.93	0.54	44.75	25.02	17.15	1.52	0.16	569.06	2.36	0.16	3.46	1.93	2.85
SAOS021	6.4	18736.93	143.17	208.39	180.07	8575.04	2.73	142.30	143.73	-80.92	13.82	2.42	669.84	-2.16	1.43	17.76	9.99	1.45
SAOS035	9.2	8847.98	57.88	77.65	116.08	9901.63	2.18	65.52	113.96	-230.34	4.81	1.69	1263.54	2.76	0.07	21.76	10.44	0.91
SAOS039	10.0	12189.13	95.19	144.07	162.88	5735.22	1.41	54.25	55.34	270.51	0.00	3.65	624.40	-4.56	0.19	8.33	3.31	2.62
SAOS039	9.8	15422.66	140.79	189.19	121.00	1946.78	0.66	32.21	19.04	-211.51	0.45	0.78	675.63	0.00	0.05	16.00	0.81	1.83
SAOS045	11.2	12213.46	85.62	116.87	112.50	9673.04	0.91	57.06	72.08	285.14	5.96	1.74	778.14	1.29	0.15	13.04	27.06	1.35
SAOS050	12.2	13774.36	115.93	187.12	117.58	2425.78	0.23	59.41	8.51	1366.09	4.33	1.42	467.95	-1.27	-0.24	6.89	4.30	2.73
SAOS062	14.8	33588.42	189.29	222.52	313.11	22685.03	9.16	224.76	135.95	-342.11	0.00	43.32	452.53	282.22	6.86	44.38	39.09	5.83
SAOS070	16.2	13699.01	117.17	176.79	99.89	4245.92	0.92	41.95	24.79	-49.53	3.87	0.31	641.31	2.80	0.21	6.99	6.68	1.94
SAOS080	18.2	13391.11	139.68	276.09	271.79	4341.64	0.93	63.62	34.02	-52.43	4.68	-0.16	595.39	2.96	0.31	7.06	10.93	1.92
SAOS090	20.2	11034.03	221.36	200.74	290.85	-803.55	3.83	186.09	0.51	-970.59	0.00	-4.52	389.75	-2.01	-0.57	17.83	-1.87	2.84
SAOS106	23.4	13075.26	115.09	156.13	110.77	1398.90	0.53	25.94	31.15	83.96	2.06	0.12	587.09	0.86	0.07	3.80	0.83	1.34
SAOS116	25.4	13848.03	157.30	273.93	107.35	1367.35	0.41	35.87	22.54	-86.23	1.36	-0.51	603.65	5.90	0.09	2.93	1.40	1.92
SAOS120	26.2	8615.96	82.20	169.32	78.48	1502.39	0.59	30.46	24.17	-13.54	1.95	-0.13	916.12	1.13	0.11	4.65	10.46	1.04
SAOS130*	28.2	-1395639.65	1263.82	-4153.85	-2475.43	1161396.60	950.28	47844.61	22407.55	214100.02	3523.76	-842.40	-456.52	4002.50	284.67	-291.27	-463.32	0.00
SAOS132	28.6	12840.09	178.97	273.11	111.35	1769.84	0.81	25.75	18.72	133.10	1.65	0.02	611.63	1.00	3.92	10.30	1.80	1.23
SAOS136	29.4	15489.73	171.58	303.71	199.56	8333.57	3.56	123.80	71.65	28.30	8.64	-0.01	763.93	4.84	0.21	8.76	5.31	1.70
SAOS140	30.2	14019.38	194.64	320.62	129.55	549.48	0.95	47.73	19.35	429.22	1.79	-0.59	462.17	4.55	0.05	10.67	1.13	1.41
SAOS150	32.2	11016.57	237.35	905.03	147.62	4168.80	5.19	265.59	34.00	72.83	3.42	-1.75	493.63	5.56	0.25	1.76	1.03	1.70
SAOS170	36.2	12820.76	149.71	347.00	116.07	625.63	1.09	181.67	220.64	5821.90	5.23	13.84	529.56	16.48	4.49	39.38	15.49	0.89
SAOS184*	39.0	6297.02	164.74	338.50	163.99	43542.60	4.25	646.03	582.19	-446.52	34.52	0.49	1288.19	11.30	1.48	121710.64	10.07	1.75
Average		14621.73	137.22	231.42	153.68	5311.93	2.61	106.08	91.60	696.72	4.09	5.38	628.00	13.69	2.46	23.77	6.70	1.94
Stbw.		6744.38	52.48	162.50	81.56	7284.67	4.92	147.12	209.65	2309.62	5.25	15.39	185.15	58.75	7.94	58.96	9.65	1.04
%RSD		46.13	38.25	70.22	53.07	137.14	188.25	138.69	228.88	331.50	128.30	286.19	29.48	429.15	322.76	248.11	143.98	53.39
Detection limit		2.9	0.03	0.03	0.05	0.74	0.01	0.26	0.18	2.06	0.09	0.07	0.03	0.12	0.19	0.06	0.02	

Sample weight below 50µg*

Table 30 Correlationmatrix benthic foraminifera

	Mg*	V	Cr	Mn	Fe	Co	Ni	Cu	Zn	As	Rb	Sr	Mo	Cd	Ba	Pb	U	δ^{18}Ogavelinella (Benthic)
Mg*	1.00	0.30	0.15	0.22	0.24	0.26	0.45	0.32	0.43	-0.19	0.25	-0.59	0.33	0.02	0.36	0.23	0.44	0.14
V	0.30	1.00	0.65	0.18	0.42	0.40	0.51	0.44	0.14	0.17	-0.15	-0.49	0.56	0.12	0.20	0.06	0.08	-0.15
Cr	0.15	0.65	1.00	0.23	0.05	0.08	0.19	0.20	0.24	-0.28	-0.09	-0.61	0.19	0.15	-0.17	-0.15	-0.11	-0.29
Mn	0.22	0.18	0.23	1.00	0.05	0.51	0.29	0.24	-0.06	-0.19	-0.08	-0.18	0.42	-0.14	-0.09	0.13	-0.23	-0.23
Fe	0.24	0.42	0.05	0.05	1.00	0.78	0.75	0.68	0.00	0.67	0.05	0.03	0.48	0.09	0.24	0.57	0.40	-0.22
Co	0.26	0.40	0.08	0.51	0.78	1.00	0.83	0.68	-0.01	0.42	0.19	0.00	0.71	0.22	0.26	0.59	0.30	-0.45
Ni	0.45	0.51	0.19	0.29	0.75	0.83	1.00	0.64	0.22	0.38	0.15	-0.15	0.64	0.32	0.21	0.54	0.37	-0.32
Cu	0.32	0.44	0.20	0.24	0.68	0.68	0.64	1.00	0.35	0.23	0.15	-0.03	0.64	0.33	0.50	0.58	0.36	-0.30
Zn	0.43	0.14	0.24	-0.06	0.00	-0.01	0.22	0.35	1.00	-0.49	0.10	-0.44	0.35	0.53	0.24	0.08	0.35	0.25
As	-0.19	0.17	-0.28	-0.19	0.67	0.42	0.38	0.23	-0.49	1.00	-0.04	0.38	0.27	-0.13	0.09	0.20	0.07	-0.09
Rb	0.25	-0.15	-0.09	-0.08	0.05	0.19	0.15	0.15	0.10	-0.04	1.00	-0.08	0.18	0.16	0.34	0.46	0.59	-0.40
Sr	-0.59	-0.49	-0.61	-0.18	0.03	0.00	-0.15	-0.03	-0.44	0.38	-0.08	1.00	-0.23	-0.07	0.08	0.06	-0.27	-0.19
Mo	0.33	0.56	0.19	0.42	0.48	0.71	0.64	0.64	0.35	0.27	0.18	-0.23	1.00	0.40	0.41	0.19	0.26	-0.13
Cd	0.02	0.12	0.15	-0.14	0.09	0.22	0.32	0.33	0.53	-0.13	0.16	-0.07	0.40	1.00	0.22	0.08	0.24	-0.14
Ba	0.36	0.20	-0.17	-0.09	0.24	0.26	0.21	0.50	0.24	0.09	0.34	0.08	0.41	0.22	1.00	0.39	0.41	0.16
Pb	0.23	0.06	-0.15	0.13	0.57	0.59	0.54	0.58	0.08	0.20	0.46	0.06	0.19	0.08	0.39	1.00	0.50	-0.41
U	0.44	0.08	-0.11	-0.23	0.40	0.30	0.37	0.36	0.35	0.07	0.59	-0.27	0.26	0.24	0.41	0.50	1.00	0.00
δ^{18}Ogavelinella (Benthic)	0.14	-0.15	-0.29	-0.23	-0.22	-0.45	-0.32	-0.30	0.25	-0.09	-0.40	-0.19	-0.13	-0.14	0.16	-0.41	0.00	1.00
δ^{13}C (Benthic)	-0.18	-0.79	-0.74	-0.21	0.01	0.09	-0.12	-0.15	-0.17	0.28	0.68	0.60	-0.18	-0.06	0.21	0.54	0.39	-0.16

Benthic (final)	Factor 1	Factor 2	Factor 3
Pb	0.93	0.21	0.17
Cu	0.89	0.20	0.28
Cd	0.80	0.10	-0.08
Ba	0.78	-0.15	0.25
Mn	0.74	0.31	0.15
Co	0.04	0.97	0.07
Ni	0.31	0.88	0.26
Mg*	0.23	0.27	0.83
Sr	-0.10	-0.05	-0.88
Expl. Var	3.62	2.00	1.74
Total	0.40	0.22	0.19
Summe	**0.82**		

Communality	Factor 1	Factor 2	Factor 3	Multiple
Ni	0.10	0.87	0.94	0.94
Pb	0.86	0.91	0.94	0.92
Co	0.00	0.93	0.94	0.91
Cu	0.80	0.84	0.92	0.90
Cd	0.64	0.65	0.65	0.79
Ba	0.61	0.63	0.69	0.68
Mn	0.55	0.65	0.67	0.66
Mg*	0.05	0.12	0.81	0.64
Sr	0.01	0.01	0.78	0.45

Eigenvalue	Eigenvalue	% Total	Kumul.	Kumul.
1	4.6	50.8	4.6	50.8
2	1.6	18.0	6.2	68.8
3	1.2	12.9	7.4	81.7

labelled values are significant at level p>0.05

Table 31 Correlationmatrix planktic foraminifera

	V	Cr	Mn	Fe	Co	Ni	Cu	As	Rb	Sr	Mo	Ba	Pb
V	1.00	0.87	0.67	-0.05	0.68	0.59	0.11	0.06	-0.50	-0.49	0.34	0.34	-0.29
Cr	0.87	1.00	0.54	-0.08	0.56	0.56	0.24	0.23	-0.43	-0.45	0.55	0.22	-0.08
Mn	0.67	0.54	1.00	0.30	0.79	0.83	0.39	0.23	-0.16	-0.34	-0.04	0.55	0.05
Fe	-0.05	-0.08	0.30	1.00	0.31	0.27	0.59	0.63	0.36	0.62	-0.09	0.19	0.62
Co	0.68	0.56	0.79	0.31	1.00	0.85	0.54	0.25	-0.18	-0.14	0.16	0.54	0.14
Ni	0.59	0.56	0.83	0.27	0.85	1.00	0.54	0.42	-0.06	-0.31	0.19	0.48	0.25
Cu	0.11	0.24	0.39	0.59	0.54	0.54	1.00	0.63	0.39	0.30	0.30	0.34	0.64
As	0.06	0.23	0.23	0.63	0.25	0.42	0.63	1.00	0.34	0.36	0.28	0.33	0.70
Rb	-0.50	-0.43	-0.16	0.36	-0.18	-0.06	0.39	0.34	1.00	0.32	-0.31	0.28	0.57
Sr	-0.49	-0.45	-0.34	0.62	-0.14	-0.31	0.30	0.36	0.32	1.00	-0.07	0.04	0.57
Mo	0.34	0.55	-0.04	-0.09	0.16	0.19	0.30	0.28	-0.31	-0.07	1.00	-0.12	0.14
Ba	0.34	0.22	0.55	0.19	0.54	0.48	0.34	0.33	0.28	0.04	-0.12	1.00	0.43
Pb	-0.29	-0.08	0.05	0.62	0.14	0.25	0.64	0.70	0.57	0.57	0.14	0.43	1.00

Planktic (final)	**Factor 1**	**Factor 2**
Co	0.92	-0.02
Ni	0.91	0.31
V	0.90	-0.10
Cr	0.85	-0.05
Cu	0.21	0.94
Rb	-0.12	0.91
Ba	0.23	0.87
Pb	-0.21	0.71
Expl. Var	3.38	3.09
Total	0.42	0.39
Summe	**0.81**	

Factor 1	**Factor 2**	**Factor 3**	**Multiple**
Ba	0.05	0.82	0.96
Ni	0.83	0.93	0.96
Rb	0.02	0.84	0.96
Cr	0.73	0.73	0.94
V	0.81	0.82	0.94
Co	0.85	0.85	0.93
Cu	0.05	0.93	0.92
Pb	0.05	0.55	0.65

Eigenvalue	**Eigenvalue**	**% Total**	**Kumul.**	**Kumul.**
1	3.5	44.3	3.5	44.3
2	2.9	36.7	6.5	81.0

labelled values are significant at level p>0.05